# Targeted delivery of endosomal Toll-like receptor agonists to the tumour microenvironment for the promotion of anti-tumour immunity

Corogeanu, Diana

*Awarding institution:*
King's College London

# Targeted delivery of endosomal Toll-like receptor agonists to the tumour microenvironment for the promotion of anti-tumour immunity

***Diana Corogeanu***

**Thesis submitted for the degree of**

**Doctor of Philosophy**

**at King's College London**

**March 2020**

King's College London
Faculty of Life Sciences and Medicine
School of Cancer and Pharmaceutical Sciences
Guy's Campus, London, SE1 1UL

## Abstract

Toll-like receptors (TLRs) are pattern recognition receptors that upon detection of pathogen-associated molecular patterns activate innate immune cells. TLRs localised in the endosomal compartment are specialised in recognising nucleic acid molecules and instruct adaptive immune responses towards a Th1 phenotype with strong cytotoxic T cell effector functions. Synthetic agonists of endosomal TLRs (TLR3, TLR7/8 or TLR9) were shown to promote anti-tumour immune responses when administered to the tumour site, with imiquimod (TLR7 agonist) being approved for topical administration in basal cell carcinoma and stage zero melanoma. However, when administered systemically, endosomal TLR agonists induce broad immune activation that leads to adverse reactions, preventing their use for non-topical administration. Novel strategies for targeted delivery of TLR agonists to the tumour tissue may allow overcoming these limitations.

This study explores different methods of linking endosomal TLR agonists to Trastuzumab, a clinically used HER2-specific antibody, to achieve targeted delivery to HER2-expressing tumour tissue. We investigate the feasibility of the approach and its efficiency in promoting anti-tumour immune responses. We engineered and expressed a novel fusion antibody with the nucleic acid binding, cationic peptide LL37. To achieve this, we investigated how a variety of linkers used in fusion protein design impact folding and assembly of our fusion antibody. Additionally, we evaluated methods of biochemical conjugation of Trastuzumab to the TLR9 agonist CpG. We showed that the properties of each moiety, and the conjugation chemistry impact on the functionality of the resulting biochemical conjugates.

To characterise both conjugates and complexes and their effect on immune responses, we established and adapted a variety of physicochemical and *in vitro* assays. To evaluate the efficiency of conjugates and complexes *in vivo*, we have developed a human HER2-expressing lung tumour model in immunocompetent mice, using human HER2 transgenic B16 melanoma cells, syngeneic to the C57BL/6 background. Data so far, illustrated possible advantages, but also important limitations of each approach. Specifically, in contrast with conjugates, complexes did not persist in serum. Trastuzumab-CpG conjugates generated using site-specific conjugation technologies enhanced anti-tumour T cell responses and moderately delayed tumour growth. This was not observed for conventional conjugates, indicating that appropriate conjugation technology is required for conjugate functionality.

Due to the specific *in vivo* profile of conjugates, further investigations of their effects, suitability for combination therapy and potential in tumour immunotherapy are warranted.

## Acknowledgements

As it is the case with many PhD projects, my project was technically challenging. Luckily, learning opportunities were plentiful and the experience was, above all, formative. I would like to warmly thank a great number of people for their lessons and help, and above all, for being such an incredible support network during these formative years.

First and foremost, I would like to thank my supervisor Sandra S. Diebold for bearing with me, even at the darkest of times, with unending patience, constant good advice, and a positive attitude. Thank you for all your multifaceted support, and for challenging my insecurities. I have learned a tremendous amount from you. It was a pleasure working with you. Thank you for being such a wonderful supervisor. I am lucky to be one of your students.

This project was funded by the National Institute of Biological Standards and Control (NIBSC), where I was based for the duration of the PhD program. I want to thank my colleagues at NIBSC, most of all the Cellular Immunology section. Special thanks to Anna, Andre, Elliot, Deepa, Luisa and Sandrine for the good times, the banter on difficult lab days, the laughs, the teaching, and the help. Dear Joanne, I am much happier for knowing you. Thanks to other NIBSC colleagues as well, you are too many to name here. Thanks for being such good company.

Additionally, I would like to thank my supervisor at King's College London, James N Arnold, for his many lessons, sound advice, productive supervision, and constant encouragement. It is a pleasure to talk to you about science. Many thanks for encouraging me to attend your lab meetings. It was a wonderful setting to practice giving talks and debate my work, with the added privilege of meeting amazing colleagues. A big thanks to both current and former members of the Arnold Lab. Thanks, Jamie, for being such an excellent example to aspire to. Thank you, Meg, for your kindness, warmth and support in good days and bad. Thank you, Tamara, for sharing some of your experience with me. Thank you, Jonathan, for teaching me to speak up and argue my point. Thank you, Joanne, Dominika and Paris, for your input in lab meetings, your advice, and for keeping me in good spirits. Thank you all.

I would also like to thank my Thesis Progression Committee for their continued advice, as well as their encouragement.

Finally, I would like to thank my family for being understanding and sympathetic, even from afar. A big thanks to Raul, who turns difficulty into lessons, sees misfortune as opportunity for personal growth and believes in me with unwavering enthusiasm. You are my family too.

## Table of contents

## Index of figures

### Chapter 1



### Chapter 3

**Chapter 4**

**Supplementary file – Additional information**

## Index of tables

### Chapter 2

**Chapter 4**



**Chapter 5**

## Abbreviations

2-ME - β-Mercaptoethanol

**A**

ADCC - antibody-dependent cellular cytotoxicity

ADC – antibody-drug conjugates

APC – antigen presenting cell

Approx. - approximatively

**B**

B14.3 – ovalbumin / green fluorescent protein transgenic B16 cell

bb frag – backbone fragment

BMDC – bone marrow dendritic cells

BGG – bovine gamma globulin

bp – base pairs

**C**

CC – cyanuric chloride

cDC – conventional dendritic cells

**D**

DC – dendritic cell

dsDNA – double stranded DNA

dsRNA – double stranded RNA

**E**

EDTA – Ethylenediaminetetraacetic

ELISA - enzyme-linked immunosorbent assay

Ext time – extension time

**F**

Fc – fragment crystallisable

FCS – foetal calf serum, heat inactivated

Fig. – Figure

Flt3L – fms-like tyrosine kinase 3 ligand

FS – Free Style

FW - forward

**G**

GFP - green fluorescent protein

GM-CSF – granulocyte macrophage colony stimulating factor

**H**

HC – heavy chain

HER2 – human epidermal growth factor 2

Herc – Herceptin

HPLC - high-performance liquid chromatography

**I**

IFN – interferon

IL – interleukin

Iso – isotype

IT – intratumorally

IU – international units

IV – intravenously

**L**

LAL – limulus amoebocyte lysate

LC – light chain

LPS – lipopolysaccharide

Luc – Firefly luciferase

**M**

MFI – mean fluorescent intensity

MOI – multiplicity of infection

MW – molecular weight

**N**

NA – nucleic acid

NHS esters – N-hydroxysuccinimide

**O**

ODN - oligodeoxynucleotide

OVA - ovalbumin

**P**

PBMC - peripheral blood mononuclear cell

PCR - polymerase chain reaction

pDC – plasmacytoid dendritic cells

PIPE - polymerase incomplete primer extension

poly I:C - Polyinosinic-polycytidylic acid

polyUs21 – 21-mer single stranded phosphorothioated polyuridylic acid

**R**

$R_D$ – resolution metric

ROI – region of interest

RT – room temperature

RV – reverse

**S**

SD – standard deviation

SDS-PAGE – dodecyl sulphate and polyacrylamide gel electrophoresis

SEM – standard error of mean

SEC – size exclusion chromatography

SFM – serum-free medium

SFFV - spleen focus-forming virus

SIN – self-inactivating virus

SMCC - succinimidyl-4-(N-maleimidomethyl) cyclohexane-1-carboxylate

ssRNA – single stranded RNA

**T**

TCEP - tris(2-carboxyethyl)phosphine

TC – tissue culture

TLR – toll-like receptor

Tm – melting temperature

TNF-α – tumour necrosis factor alpha

Tr – Trastuzumab

Tr(TH) – Trastuzumab with THIOMAB mutations

Tr-LL37 – Trastuzumab-LL37 (without linker)

Tr-H2-LL37 – Trastuzumab-H2-LL37

Tr-H3-LL37 – Trastuzumab-H3-LL37

Tr-H4-LL37 – Trastuzumab-H4-LL37

Tr-MCC-CpG – Trastuzumab CpG non-specific conjugate generated with SMCC

Tr(TH)-CpG - Trastuzumab CpG site-specific conjugate using THIOMAB technology

TRP-1 - tyrosinase related protein-1

**V**

VSV – vesicular stomatitis virus

**W**

WT – wild type

# Chapter 1

# Introduction

# Chapter 1

# Introduction

## 1.1 Prologue

Immunotherapy has revolutionised the clinical management of multiple cancer types, bringing long-lasting benefits to groups of patients with tumours that were previously considered untreatable. Currently, distinct classes of immunotherapies are approved for treatment of selected tumour indications, and include immune checkpoint inhibitors, bispecific antibodies and cell-based therapies. These drugs demonstrate the potential of the immune system to control tumour growth. Despite these enormous strides in cancer treatment, there are, however, many patients whom do not benefit from immunotherapy, either due to lack of efficacy or substantial, sometimes even life-threatening adverse effects (Johnson, Chandra, and Sosman 2018; Neelapu et al. 2018; Kennedy and Salama 2020). Therefore, further research efforts are currently underway to increase response rates, and minimise adverse effects (Khalil et al. 2016; Tang et al. 2018).

Progress in the field of tumour immunology has led to the important understanding that the tumour microenvironment is immunosuppressive and hinders anti-tumour immune responses. Local immunosuppression is mediated by tumour cells, stromal cells and immune cells (Chen and Mellman 2013). Therefore, developing therapies that act on immune cells to break local tumour immunosuppression is a promising strategy for cancer treatment. Among immunomodulatory molecules, the most successful class are immune checkpoint inhibitors. These are monoclonal antibodies anti-tumour T cells, leading to tumour regression in a percentage of treated patients. Currently, multiple other immunomodulators, acting on a variety of targets in the tumour microenvironment are explored for therapy, including agonists of endosomal toll-like receptors (TLRs) (Tang et al. 2018; Tang, Shalabi, and Hubbard-Lucey 2018). Endosomal TLR agonists activate dendritic cells and other innate immune cells in the tumour microenvironment and have been shown to promote anti-tumour T cell responses and local inflammation in multiple animal models, as well as a few clinical trials (Iribarren et al. 2016; Garcia-Martinez et al. 2018).

As with other immunotherapies acting on immune cells in the tumour microenvironment, appropriate accumulation of endosomal TLR agonists to the tumour site is paramount for treatment efficacy, as well as avoiding immune activation in healthy tissues, which leads to adverse effects (Engel, Holt, and Lu 2011). Increasing evidence suggests that local

administration by topical application or direct intratumoral injection of endosomal TLRs, are promising therapeutic approaches (Marabelle et al. 2014; Smith et al. 2018; Murthy, Minehart, and Sterman 2017). With growing research interest for the approach, and to facilitate clinical development of intratumoral immunotherapy, the European Society for Medical Oncology has recently published a set of expert recommendations (Marabelle et al. 2018).

Importantly, while endosomal TLR agonists show promise for intratumoral immunotherapy, not all patients have tumours that are safely accessible to direct injection. This can be due to small dimensions of metastases, inaccessible locations or bleeding risk (Marabelle et al. 2017; Marabelle et al. 2018). To circumvent these limitations, we set out to investigate the potential of antibody-based targeted delivery systems in fostering endosomal TLR agonist-based cancer immunotherapy.

This chapter will describe endosomal TLR agonists and their potential in tumour immunotherapy, explaining the need for targeted delivery. Furthermore, we describe the use of recombinant antibodies as targeted delivery systems and our strategy in harnessing their properties to enable concentration of endosomal TLR agonists to the tumour microenvironment.

## 1.2 Endosomal toll-like receptors

Toll-like receptors (TLRs) are a family of pattern recognition receptors (PRRs) of the innate immune system, that recognize a variety of pathogen-associated molecular patterns (PAMPs) and initiate immune responses (Medzhitov 2001; Takeda, Kaisho, and Akira 2003).

All TLRs are membrane-bound proteins, and can be broadly divided in two subsets, based on cellular localization, either on the plasma membrane (TLR1, TLR2, TLR4, TLR5, TLR6, TLR10) or endosomal compartments (TLR3, TLR7, TLR8 and TLR9). In terms of PAMPs, cell surface TLRs recognize microbial membrane-bound ligands, such lipids, proteins or lipoprotein. Endosomal TLRs recognize nucleic acids (NA) of viruses and other endocytosed pathogens: double-stranded RNA (dsRNA) by TLR3, single-stranded RNA (ssRNA) by TLR7 and 8 and double-stranded DNA (dsDNA) by TLR9 (Iwasaki and Medzhitov 2004; O'Neill, Golenbock, and Bowie 2013).

TLRs are expressed by multiple immune cells including monocytes, macrophages, dendritic cells (DCs) and B cells, but select receptors are also expressed by non-immune cells including fibroblast (TLR3 and TLR4) and intestinal epithelial cells (TLR5) (Takeda and Akira 2005). Innate immune cells respond to TLR agonists by secreting proinflammatory cytokines (Medzhitov 2007). In addition to cytokine release, TLR stimulation induce maturation of dendritic cells which results in antigen presentation, TLR signaling bridges innate and adaptive immunity (Iwasaki and Medzhitov 2004). The profile of these adaptive immune responses depends on the type of PAMP and can be influenced by factors in the local environment as well (Liu 2001; Diebold 2009; Iwasaki and Medzhitov 2015). Importantly, endosomal TLRs have evolved primarily to detect viral infections and are specialized in inducing Th1 and cytotoxic T lymphocyte (CTL) responses, which are crucial for the clearance of virus-infected cells. These responses can also be exploited for the eradication of tumour cells (Iwasaki and Medzhitov 2015).

### 1.2.1 Endosomal TLR signaling

In terms of signaling, ligand binding to the endosomal leucin-rich-repeats domain of TLRs induces a conformational change in the cytoplasmatic Toll-like/IL-1 receptor (TIR) domain, which recruits adaptor molecules. TLR7, TLR8 and TLR9 use the adaptor MyD88 to initiate a signaling cascade resulting in activation of NF-κB, IRF-1, and AP-1 transcription factors, which in turn induce gene transcription of proinflammatory cytokines such as IL-12, TNF-α and IL-6 by myeloid dendritic cells (mDCs) and macrophages. IRF-5 induces production of INF-α. Additionally, in plasmacytoid dendritic cells (pDCs), MyD88 induces IRF7 as well

resulting in higher levels of secreted type I interferons. In contrast with TLRs 7, 8 and 9, TLR3 recruits the adaptor TRIF and downstream signaling ultimately activates IRF3 and IFN-β production in mDCs and macrophages. TLR3 signaling can involve NF-κB activation and production of proinflammatory cytokines as well (Blasius and Beutler 2010; O'Neill and Bowie 2007).

### 1.2.2 Immune responses induced by endosomal TLR signaling

Endosomal TLRs are expressed by a variety of cells and mediate a series of immune responses. Importantly, cell expression patterns, while largely overlapping, are distinct in the mouse and human system (Iwasaki and Medzhitov 2004). Notably, TLR8 is inactive in mice (Alexopoulou, Desnues, and Demaria 2012). Endosomal TLR expression patterns are complex, and currently incompletely defined, with subsets of immune cells regulating endosomal TLR expression depending on the local environment (Akira, Uematsu, and Takeuchi 2006).

A key feature of endosomal TLR signaling is triggering dendritic cell activation, which in turn induces adaptive immune responses (Manicassamy and Pulendran 2009; Iwasaki and Medzhitov 2015). In terms of endosomal TLR expression on DC subtypes, plasmacytoid DCs express TLR7 and 9, but not TLR3, while subtypes of myeloid DCs can express either or multiple endosomal TLR. Expression can differ between human and mouse equivalent subset of myeloid DCs (Edwards et al. 2003; Liu et al. 2002; Schreibelt et al. 2010). Upon endosomal TLR triggering, both human and mouse DCs undergo a maturation process characterized by antigen presentation of the ingested material on the major histocompatibility complex (MHC), upregulation of costimulatory molecules CD80 and CD86 and production of proinflammatory cytokines IL-12, TNF-α and IL-6. Notably, plasmacytoid dendritic cells and not myeloid DCs are the main source of IFN-α. The maturation process initiated by endosomal TLR signaling drives Th1 immune responses and the expansion of antigen-specific T cells (Diebold 2008a; Brencicova and Diebold 2013; Manicassamy and Pulendran 2009). Importantly, priming of functional cytotoxic T cell responses requires TLR triggering of DCs and interaction with helper T cells (Elgueta et al. 2009).

Both human and mouse B cell subsets express endosomal TLRs and respond to their agonists. Only low levels of TLR7 and TLR9 were detected in naïve human B cells, while activated and memory cells showed substantially higher levels (Bernasconi, Onai, and Lanzavecchia 2003; Agrawal and Gupta 2011). Mouse B cells express TLRs 3, 7 and 9, at various levels among cell subtypes. To exemplify, mouse B-1a cells express significant levels of TLR7 and TLR9

(Gururajan, Jacob, and Pulendran 2007). In both human and mouse cells, expression of endosomal TLRs is up-regulated in response to BCR signaling and type I interferons (Bourke et al. 2003; Browne 2012). Both human and mouse B cells have been shown to produce cytokines IL-6, TNF-α and IL-10 in response to either TLR7 or TLR9 agonists (Pettengill et al. 2016; du Plessis et al. 2016; Barr et al. 2007).

Endosomal TLR signaling is involved in the generation of B-cell responses, whether T-cell independent or T-cell dependent. In terms of T-cell independent responses, *in vitro* experiments showed that ligand binding to TLR7 or TLR9 induces IgM production by select mouse and human B cell subsets (Bekeredjian-Ding and Jego 2009; Rawlings et al. 2012). Mouse models of infection showed that both endosomal TLR signaling and B cell receptor (BCR) signaling are required for the generation of pathogen-specific T-cell independent IgM responses *in vivo* (Alugupalli et al. 2007; Rawlings et al. 2012).

Regarding T-cell dependent antibody responses, multiple research groups showed that TLR signaling in both B cells and dendritic cells are required for class switching to a particular heavy-chain isotype and affinity maturation (Browne 2012; Hua and Hou 2013). TLR9 and TLR7 agonists have been shown to promote IgG2a, IgG2b and IgG3 production in mouse models of viral infection or vaccination (Lin, Gerth, and Peng 2004; Bekeredjian-Ding and Jego 2009; Rookhuizen and DeFranco 2014). However, when TLR7 agonist polyUs21 was used as vaccine adjuvant *in vivo* by others, no class switch preference for a particular isotype was noticed (Rajagopal et al. 2010). An increase in antibody production with no preference of B-cell class switching was reported by others in mice treated intranasally with a TLR9 agonist (Gallotta et al. 2018). These discrepancies suggest that B-cell class switch fine-tuning is complex and might be influenced by multiple stimuli or could vary with individual endosomal TLR agonists or administration routes.

As mentioned above, endosomal TLRs engagement stimulates monocytes and macrophages as well (Barbalat et al. 2011). While expression of TLR7 is similar for mouse and human macrophages, TLR9 and TLR3 expression is characteristic to murine macrophages only, while TLR8 functionality is limited to human monocytes and macrophages (Anwar et al. 2019). Endosomal TLR signaling induces proinflammatory cytokine and chemokine production by macrophages (Blasius and Beutler 2010), as well as inducible nitric oxide synthase (iNOS) (Krieg 2002).

Direct activation of immune cells by endosomal TLR triggering induces proinflammatory cytokine production. This in turn can indirectly activate other cells or support adaptive immune

responses (Iwasaki and Medzhitov 2004). For instance, IL-12 production by dendritic cells promotes Th1 and CTL responses (Trinchieri 2003). Another good example is the activation of human NK cells by type I interferons secreted by TLR9 triggered pDCs (Marshall et al. 2006). Human macrophages can be polarized to M1 phenotype in environments dominated by high amounts of IFN-ɣ, which is produced in the context of Th1 immune responses (Murray 2017).

### 1.2.3 Agonists of endosomal TLRs

In the context of infection, upon endocytic or phagocytic uptake of viruses and bacteria, microbe degradation leads to release of nucleic acids (NAs), such as double stranded DNA (dsDNA) with unmethylated CpG motifs recognized by TLR9, viral single stranded RNA (ssRNA) recognized by TLR7 and TLR8 and double stranded RNA (dsRNA) detected by TLR3 (Blasius and Beutler 2010).

While it was originally thought that endosomal TLRs recognise microbe-specific nucleic acid sequences, it was later shown that the receptors do not distinguish between foreign and self-nucleic acids (Majer, Liu, and Barton 2017). In homeostatic conditions, self-nucleic acids do not access endosomal compartments to activate TLRs (Brencicova and Diebold 2013). Under certain conditions, however, self-nucleic acids can access the endosomes and activate endosomal TLRs. For instance, in lupus patients, which develop anti-DNA antibodies, DNA-antibody complexes are internalized via Fc-mediated endocytosis, exposing self-DNA to TLR9 and triggering further inflammation (Hurst and von Landenberg 2008). The peptide LL37, which is overexpressed in psoriatic skin and other autoimmune conditions, has been shown to bind and deliver both self-DNA and self-RNA to endosomes, triggering TLR9 or TLR7 and 8, respectively (Ganguly et al. 2009; Lande et al. 2007). Therefore, discrimination between “self” and “non-self” molecules is mediated by access of agonists to the endosomal compartment, which can be breached under pathological conditions, leading to inflammation and promoting autoimmune responses.

As mentioned above, studies have defined the nucleic acid requirements for endosomal TLR receptor binding, and this has further facilitated the development of synthetic agonists, which are of great interest for therapeutic use (O'Neill, Bryant, and Doyle 2009; Vanpouille-Box, Hoffmann, and Galluzzi 2019).

Specifically, TLR3 binds dsRNA of minimum 40 base pairs in length without stringent sequence requirements (Botos et al. 2009). In terms of synthetic molecules, TLR3 detects and is activated by polyinosine-polycytidylic acid (polyI:C) (Alexopoulou et al. 2001).

TLR7 and human TLR8 recognize single stranded RNA (ssRNA). Under physiological conditions RNA does not access the endosomal compartment. This is achieved in viral infections, with recognition of viral single-stranded RNA (ssRNA) (Lund et al. 2004; Heil et al. 2004). To deliver self-RNA to endosomes, either transfection reagents (Diebold 2008b) or LL37 (Ganguly et al. 2009) can be employed. While many RNA molecules trigger TLR7 and human TLR8, a preference for uracil repeats in RNA has been noted. This allowed for the development of the synthetic TLR7 agonist polyUs21, which is a 21 bases long uracil homopolymer (Diebold et al. 2006; Diebold et al. 2004). In terms of secondary conformation, polyU homopolymers do not form double-stranded structures (Saenger 1984). To access the endosomal compartment and activate immune cells, polyUs21 needs to be administered in complex with transfection reagents (Diebold et al. 2006).

In addition to the synthetic polyUs21, TLR7 and human TLR8 also respond to imidazoquinolines, such as imiquimod and resiquimod (R848), which are synthetic small molecules (Hemmi et al. 2002). Like all small molecules, imiquimod and resiquimod passively diffuse the cell membranes (Yang and Hinner 2015) and do not require special delivery methods to reach the endosomal compartment. The profile of immune responses, however, is distinct from polyUs21. In contrast with R848, polyUs21 induces IFN-α production by plasmacytoid DCs driving robust Th1 and CTL responses in mice (Rajagopal et al. 2010).

Regarding TLR9 activation, research has shown that the sugar backbone phosphodiester (PD) 2’ deoxyribose binds and activates TLR9 and this is enhanced by DNA bases. Conversely, the phosphorothioate (PS) modified 2’ deoxyribose backbone, which confers protection to synthesized oligodeoxynucleotides (ODN) from degradation by nucleases, binds but does not activate TLR9. Addition of CpG motifs to phosphorothioate backbones is required to induce potent TLR9 activation (Haas et al. 2008). These results explain the TLR9 activation mediated by DNA, including self-DNA (Boule et al. 2004; Blasius and Beutler 2010) and by CpG containing, phosphorothioate-modified oligodeoxynucleotides (ODN), where the CpG motifs are key to receptor activation and inversion to GpC abolishes activation almost completely (Krieg 2002). In addition to conferring resistance to degradation by nucleases, the PS backbone increases uptake of CpG-ODN into the endosomes of macrophages (Sester et al. 2000).

A wide range of CpG-ODN were developed, many specifically for use in tumour immunotherapy (Krieg 2007), and they can be broadly divided in three classes of CpG molecules. Class A CpG-ODN stimulate pDCs to produce higher levels of IFN-α, class B molecules are stronger stimulants of B cells, while class C CpG-ODN combines the effects of

the other two classes (Vollmer et al. 2004). The three classes of CpG are also distinct in terms of secondary structure. Class A CpG contain poly-G motifs which facilitate assembly in higher-ordered structures called G-tetrads. Class C CpG-ODN contain a palindrome in their sequence, resulting in assembly in duplexes. In contrast, class B CpG-ODN are reportedly monomeric under physiological conditions (Krieg 2006). These distinct structures drive differences in biological activity. Class A and class C CpG molecules, which form multimers, induce much higher levels of IFN-α in pDCs than class B molecules (Vollmer et al. 2004; Samulowitz et al. 2010; Hartmann et al. 2003).

### 1.2.4 Endosomal TLR agonists in tumour immunotherapy

Due to their specific immunomodulatory profile, synthetic agonists of endosomal TLRs have been explored as adjuvants, including for anti-tumour vaccines (Duthie et al. 2011). Importantly, endosomal TLR agonists have also been studied as drugs with potential in cancer immunotherapy (Molenkamp et al. 2007; Aranda et al. 2014; Iribarren et al. 2016).

*Vaccine adjuvants*

Regarding the use of endosomal TLR agonists as vaccine adjuvants, CpG-ODNs are presently the most successful. An abundance of studies focused on CpG molecules, due to their potency in generating antigen specific Th1 and CTL responses, as well as robust, rapid antibody responses (Bode et al. 2011). Notably, CpG 1018 is used as adjuvant in the FDA approved hepatitis B vaccine Heplisav-B™ (Campbell 2017). Data pooled from a total of four randomised controlled trials showed that 90.0-100.0% of subjects receiving the CpG-containing Heplisav-B™ developed protective antibodies, compared to 70.5%-90.2% of subjects using the original anti-hepatitis B vaccine Engerix-B (Schillie et al. 2018).

CpG was used as adjuvant within human vaccines for cancer as well. In two independent clinical trials, vaccination with NY-ESO-1 peptide, montanide and CpG induced expansion of CD4+ T cells and CD8+ T cells in NY-ESO-1-expressing melanoma patients. This finding is especially important since most vaccines do not expand T cell responses required for clearing tumour cells (Valmori et al. 2007; Fourcade et al. 2008). Interestingly, a similar vaccination approach using NY-ESO-1 peptide intradermally and topical Imiquimod induced protein specific CD4+ T cells, but no CD8+ T cells in melanoma patients (Adams et al. 2008). The reasons for this are not clear and might be due to differences in administration route or agonist potency.

Importantly, both preclinical (Nierkens et al. 2008; Maurer et al. 2002) and clinical data (Cooper et al. 2004; Campbell 2017) support the notion that antigen and adjuvant (CpG) administration at the same site massively increases antigen-specific immune responses.

As with most tumour vaccines (Guo et al. 2013), the tumour-specific cytotoxic T cells generated through vaccination with tumour proteins or peptides and endosomal TLR agonists did not generally infiltrate tumours and did not induce tumour regression (Appay et al. 2006). The potential of tumour vaccines is currently investigated in combination with other immunotherapies, such as immune checkpoint inhibitors (Hollingsworth and Jansen 2019; Guo et al. 2013).

*Tumour immunotherapies*

*a) Preclinical evidence*

An extensive body of preclinical evidence studied endosomal TLR agonists as drugs for their potential in immunotherapy. A PubMed database (https://www.ncbi.nlm.nih.gov/pubmed/) search using the keywords “polyI:C” AND “tumor” AND “immunotherapy” AND “mice” returned 112 individual journal articles. When the same search was performed using the keywords “TLR7” AND “agonist” instead of polyI:C, the sech returned 89 journal articles. Impressively, the search using “CpG” AND “tumour” AND “immunotherapy” AND “mice” returned 545 individual journal articles. Considering that these databases are not all-inclusive, the possibility of counting studies that employed two or more of the mentioned agonists and other possible biases induced by the choice of keywords, the number are not exact. These searches illustrate, however, the abundance of preclinical animal studies that employed endosomal TLR agonists for immunotherapy.

In terms of delivery systems, a great number of studies have employed intratumoral administration (IT), while others used targeted delivery approaches such as nanocarriers. The following exemplified elegant preclinical studies demonstrate the anti-tumour efficacy of endosomal TLR agonists in a variety of tumour mouse models:

TLR3 agonist poly(I:C), given IT, was efficient in reactivating pre-existing anti-tumour T cell responses which controlled tumour growth in a mouse model of mesothelioma (Currie et al. 2008). More recently, a study showed that combination therapy of IT poly(I:C) and anti-PD-1 induced T cell mediated control in a B16-OVA melanoma model, which responds poorly to immune checkpoint blockade (Nagato et al. 2014). Another study using B16-OVA melanoma tumours demonstrated the anti-tumour efficacy of intratumoral B0-122, a nanoplexed form of

poly(I:C) complexed with polyethylenimine (PEI). Dendritic cell maturation was paramount for tumour specific CD8+ T cell responses and tumour growth control. These effects further synergised with systemic anti-PD-L1 or anti-CD137 antibodies. (Aznar et al. 2019).

TLR7/8 agonist 3M-052, an imidazoquinolin, induced anti-tumour immune responses when administered intratumorally in a B16F10 melanoma mouse model (Singh et al. 2014). Similar immune-mediated delay of tumour growth was observed with another TLR7 agonist small molecule, SZU101, in a 4T1 mouse model of breast cancer (Diao et al. 2016) and with resiquimod in mouse models of pancreatic cancers (Michaelis et al. 2019). A novel TLR7/8 agonists MEDI9197, with improved retention at the injected tumour site, showed even stronger anti-tumour effects when administered intratumorally, but not subcutaneously in mouse models of melanoma (B16F10), breast cancer (4T1) and colon cancer (MC-38). Anti-tumour efficacy was further improved by combination treatment with anti-OX40 antibodies (Mullins et al. 2019). These studies illustrate anti-tumour effects can be achieved with multiple TLR7 agonists and that retention of small molecules at the tumour site might lead to improved responses, either alone or in combination with other immunotherapies.

TLR9 agonists CpG molecules were studied as well. In a mouse model of lymphoma, T cell immunity and tumour growth control has been observed with IT CpG used as monotherapy (Lonsdorf et al. 2003). Treatment with CpG in combination with *in situ* tumour destruction by cryoablation induced anti-tumour T cell immunity driving regression of B16OVA tumours. Dendritic cell maturation, which primed CD8+ CTLs driving anti-tumour effect was substantially increased when CpG was administered locally, peritumorally, compared to systemic administration (Nierkens et al. 2009). In this model, collaboration between pDCs and mDCs was essential for anti-tumour efficacy (Nierkens et al. 2011). These results are in line with studies we described above showing that co-administration of antigen and adjuvant at the same site boosts anti-tumour immunity.

The capacity of CpG molecules to induce anti-tumour T cell responses, provided a strong rational for combination treatment with immune checkpoint inhibitors. In mouse models of colon carcinoma (CT26 and MCA38) and breast adenocarcinoma (TSA), which respond poorly to anti-PD-1 therapy, treatment with IT CpG reversed this resistance. When only one tumour site was treated IT with CpG and systemic anti-PD-1 in mice bearing two subcutaneous tumour nodules, tumour rejection was also observed at untreated sites in a percentage of mice (Wang et al. 2016). Another group showed similar anti-tumour efficacy of intratumoral CpG in combination with another immune checkpoint inhibitor, anti-OX40. Again, the treatment promoted anti-tumour immune responses in multiple mouse models (Sagiv-Barfi et al. 2018).

To summarise, for each of the endosomal TLRs, there is converging preclinical evidence illustrating the anti-tumour efficacy of their agonists, either alone, or in combination with other therapies. This was shown for multiple transplantable tumour mouse models. The anti-tumour effect was mediated by local activation of antigen presenting cells, promoting CTL responses. These studies suggest that administration of endosomal TLR agonist at the tumour site promote and even induce anti-tumour immune responses that control tumour growth.

*b) Clinical trials*

The success of multiple endosomal TLR agonists in preclinical settings supported their evaluation as cancer immunotherapies in the clinical setting in combination with other agents.

Historically, agonists of endosomal TLRs have been investigated in clinical trials for systemic administration and showed no therapeutic benefit to patients. Furthermore, a plethora of immune-mediated adverse effects was observed (Schmidt 2007; Weber et al. 2009; Hirsh et al. 2011). As described above, preclinical advances have led to the understanding that local administration of endosomal TLR agonists underpins anti-tumour immune responses (Nierkens et al. 2009). In subsequent studies, where TLR agonists were administered intratumorally, these drugs showed promise, reigniting research efforts (Anwar et al. 2019). These results from clinical trials support the notion that accumulation of endosomal TLR agonists at the tumour site is paramount for anti-tumour effects and systemic administration does not achieve this.

Local administration of endosomal TLR agonists shows promising anti-tumour responses in patients. Notably, topical administration of the lipophilic Imiquimod is approved for treatment of superficial skin tumours such as basal cell carcinoma (NICE NG14, 2015). Direct injection of the CpG molecule SD-101 into the tumour itself, in combination with local low-dose radiation resulted in infiltration of cytotoxic T cells into the injected tumour microenvironment which was associated favourable clinical responses in patients with indolent lymphoma. Moreover, tumour regression was observed at treated sites (26 out of 29 patients) and at distant, non-treated sites (24 out of 29 patients) (Frank et al. 2018). Intratumoral therapy with SD-101 in addition to systemic PD-1 blockade was safe in patients with metastatic melanoma and induced local anti-tumour immune responses (Ribas et al. 2018). Studies have shown that that intratumoral injection of CpG class B activates both pDCs and mDCs in the sentinel lymph node in patients with melanoma (Molenkamp et al. 2007; Koster et al. 2017). Moreover, treatment with CpG class B offered protection against melanoma recurrence (Koster et al.

2017). Many more clinical studies evaluating endosomal TLR agonists for intratumoral immunotherapy are underway, with (Anwar et al. 2019) providing a comprehensive list.

This current landscape of clinical studies involving endosomal TLR agonists for cancer immunotherapy illustrates the need for appropriate delivery methods to the tumour tissue. Intratumoral immunotherapy is gaining clinical momentum, since such approaches show promise in priming local tumour specific immunity, while limiting the access of immunotherapies to healthy tissue, thus minimising adverse effects (Marabelle et al. 2014; Murthy, Minehart, and Sterman 2017; Hamid, Ismail, and Puzanov 2019). While interest in this approach is increasing, not all patients can benefit from it, since not all tumour are safely accessible to direct injection, due to location, small dimensions or importantly, bleeding risk (Marabelle et al. 2018; Marabelle et al. 2017). These limitations could be circumvented by alternative drug administration methods that lead to predominant accumulation of therapies at the tumour site, while sparing healthy tissue.

## 1.3 Targeted delivery

Targeted drug delivery defines the concentration of a drug, independently of administration route into targeted sites, for instance tumour lesions, while sparring healthy tissues. While some authors include local administration under targeted drug delivery methods (Torchilin 2000), others distinguish it from targeted drug delivery (Murthy, Minehart, and Sterman 2017). Specialised targeted drug delivery systems are of significant interest for cancer therapy. Representatives are nanocarriers, for instance liposomes, microspheres and nanoparticles and antibody-based systems, where monoclonal antibodies recognising tumour tissue antigens are used as vehicles to transport and concentrate other drugs to the tumour tissue (Mitragotri, Burke, and Langer 2014; Schrama, Reisfeld, and Becker 2006; Rosenblum et al. 2018). The use of liposomes and other nanocarrier technologies for delivery of CpG and other endosomal TLRs does not fall under the scope of this work and was described elsewhere (Engel, Holt, and Lu 2011; Zhuang et al. 2019). Here, we only focus on the use of antibodies as vehicles for targeted drug delivery to the tumour tissue.

Monoclonal antibodies targeting membrane-bound tumour associated antigens have been developed for tumour therapy, with several agents approved for clinical use including Trastuzumab (anti-HER2), Cetuximab (anti-EGFR), Rituximab (anti-CD19) and Alemtuzumab (anti-CD52) (Weiner, Dhodapkar, and Ferrone 2009; Levene, Singh, and Palmieri 2005). One intrinsic property of anti-tumour antibodies is to concentrate into the tumour tissue. Positron emission tomography (PET) or PET/CT studies using labelled anti-tumour antibodies administered to tumour patients enable visualisation of antibody accumulation into tumour tissues (Menke-van der Houven van Oordt et al. 2015; Mortimer et al. 2014; Mortimer et al. 2018). Another useful property of anti-tumour monoclonal antibodies is the extended half-life of several days characteristic to all IgG antibodies (Keizer et al. 2010). Importantly, full-length anti-tumour monoclonal antibodies interact with immune cells and complement fractions mediating effector functions (Weiner, Dhodapkar, and Ferrone 2009).

### 1.3.1 Anti-tumour antibodies interact with immune cells in the tumour microenvironment

Anti-tumour monoclonal antibodies typically interact with tumour cells via the antigen binding site and with Fc receptors on immune cells via the antibody Fc domain. The antigen binding site mediates homing to tumour cells and inhibits tumour growth and survival signals for antibodies such as Trastuzumab and Cetuximab which are specific for the growth factor receptors HER-2 and EGFR, respectively (Weiner, Dhodapkar, and Ferrone 2009; Marcucci

et al. 2013). Monoclonal antibodies targeting tumour associated antigens are typically of the human IgG1 isotype. It was shown that both the amino acid sequence of the Ig Fc domain and the Fc-associated glycan structure determine the interactions with Fcγ receptors (FcγRs) on immune cells and impact on the evoked effector responses (Shields et al. 2001; Lazar et al. 2006; Bournazos and Ravetch 2015).

Among IgG subclasses, human IgG1 antibodies have the highest affinity for activating FcγRs, and therefore exhibit the highest cytotoxic activity *in vivo.* Induced responses include antibody-dependent cytotoxicity (ADCC) mediated mostly by NK cells and antibody-dependent phagocytosis (ADCP) mediated by a variety of cells including macrophages (Shi et al. 2015; Petricevic et al. 2013; Bournazos and Ravetch 2017). DCs express FcγRs and efficiently take up antibody coated tumour cells (Dhodapkar and Dhodapkar 2005). A complex regulatory system which can be influenced by immunomodulatory molecules in the local environment determine if FcγR mediated uptake results in immunogenic or tolerogenic responses (Dhodapkar, Dhodapkar, and Palucka 2008). It has been shown that in some patients with HER2-positive breast cancer, treatment with Trastuzumab can induce anti-HER2 CD4+ T cell responses and augment anti-HER2 B cell responses (Taylor et al. 2007; Knutson et al. 2016). The effector functions mediated via Fc-FcγRs have been shown to play an important role in the therapeutic activity of anti-tumour monoclonal antibodies such as Trastuzumab (Weiner, Dhodapkar, and Ferrone 2009; Bianchini and Gianni 2014).

The aforementioned clinically used antibodies, and others, have been explored as "vehicles" for targeted delivery to tumours of a variety of molecules with low efficacy to toxicity ratio (Schrama, Reisfeld, and Becker 2006). Antibody-based targeted delivery systems are typically generated via antibody engineering to generate fusion antibodies with other proteins or peptides, or through biochemical conjugation.

### 1.3.2 Fusion antibodies

Antibody engineering technologies have been employed to fuse other protein moieties to antibodies or antibody fragments targeting accessible tumour antigens. The scope was to facilitate accumulation of other proteins or peptides to the tumour tissue. This strategy was employed for the delivery of potent protein molecules such as cytokines to generate antibody-cytokine fusion proteins, also named immunocytokines. Antibody-fusion cytokines have been developed with a variety of cytokines and using different antibody formats, such as full-length antibodies or antibody fragments (Kontermann 2012; Young, Morrison, and Timmerman 2014), with ample literature describing their efficacy in preclinical tumour models. The

clinical development of antibody-fusion cytokines is only starting to accelerate and their efficacy in cancer treatment remains to be determined (Hutmacher and Neri 2019; Murer and Neri 2019).

### 1.3.3 Antibody conjugates

In contrast with antibody engineering technologies that allow for fusion of peptides and proteins to anti-tumour antibodies, biochemical conjugation enables binding of a variety of molecular structures. Antibody conjugates were generated with chemotherapeutic drugs (Diamantis and Banerji 2016), radioisotopes (Smaglo, Aldeghaither, and Weiner 2014) and enzymes (Sharma and Bagshawe 2017).

The term antibody-drug conjugates (ADC) typically refers to antibody conjugates with small molecules, most often chemotherapeutic drugs, that due to high toxicity are not safe for systemic administration. In terms of generating and characterising antibody conjugates most of the knowledge and expertise are derived from the expanding field of antibody-drug conjugates, which are of great interest for cancer therapy (Zolot, Basu, and Million 2013; Chau, Steeg, and Figg 2019).

The typical mechanism of action of ADCs involves three steps. First, the ADC recognises antigens on the surface of tumour cells via the antibody moiety. Then, the ADC is internalised, and the payload is released from the antibody. Once the payload is released, it can exert its cytotoxic function. Most payloads in clinical development are small molecules, and therefore able to pass through membranes once released from the ADC and access different cellular compartments (Bakhtiar 2016; Hoffmann et al. 2018).

Generally, antibody conjugates are formed of an antibody or antibody fragment, linker and payload, each of them determining the properties of the conjugate. Ideally, the antibody would recognise with high affinity a target tumour antigen with high expression levels on tumour cells but not healthy tissues (Thomas, Teicher, and Hassan 2016). Many ADCs are directed against tumour associated antigens such as HER2, CD20, CD19, CD79b, using antibodies such as Trastuzumab and Rituximab. However, most membrane-bound tumour associated antigens currently described are not exclusive to tumour cells, but are also expressed on healthy tissues, which leads to adverse effects of the ADC (McCombs and Owen 2015; Smaglo, Aldeghaither, and Weiner 2014). Moreover, targets such as HER2 are slow internalising (Hommelgaard, Lerdrup, and van Deurs 2004; Wallberg and Orlova 2008), which likely limits delivery of high amounts of cytotoxic drug. To circumvent these issues, ample

research is underway to define more suitable ADC targets and generate targeting antibodies (Damelin et al. 2015).

Aside from target selection, the antibody format should be considered as well. Full-length antibodies of the IgG1 isotype have higher half-life and mediate effector functions such as ADCC and ADCP, which can be transferred to the ADC, provided that the conjugation chemistry does not alter these properties. For instance, the approved ADC trastuzumab-emtansine (Kadcyla®) is ADCC competent (Barok et al. 2011; Phillips et al. 2014). In addition to mediating effector functions, Fc-FcγR interactions have the potential to mediate internalisation of ADCs into immune cells, inducing off-target toxicity. To exemplify, uptake of trastuzumab-emtansine (Kadcyla®) though Fc interactions into megakaryocytes has been proposed as mechanism of action for the induced thrombocytopenia (Uppal et al. 2015; Zhao et al. 2017). In contrast, antibody fragments have much shorter half-life and no effector functions. Multiple studies using ADCs generated with antibody fragments showed poor *in vitro* efficacy (Richards 2018).

In terms of suitable payloads for ADC generation, the requirements are solubility, serum stability and importantly, amenability to conjugation without loss of function (McCombs and Owen 2015).

Ample research studied developed various conjugation chemistries and linkers for the generation of ADCs. Linkers, also named cross-likers by some authors, are typically heterobifunctional, with two individual groups reacting with discrete functional groups on the antibody and payload (Mattson et al. 1993). Two broad categories of linkers exist, cleavable and non-cleavable. Pertaining to their name, cleavable linkers can be degraded by biochemical cues. Based on the mechanism, they can be further divided into acid-label linker, protease sensitive linkers and reducible (disulphide) linkers. Conversely, non-cleavable linkers rely on the degradation of the antibody for release of the payload (Jain et al. 2015; Bakhtiar 2016). While cleavable linkers seem to release the cytotoxic small molecule more easily, they are also less stable in serum. In contrast, non-cleavable linkers have no effect on neighbouring tumour cells that do not express the antigen but have higher stability in serum. In the context of solid tumours, this has been shown to contribute to higher efficacy (Parslow et al. 2016). For instance, trastuzumab-emtansine generated using the non-cleavable heterobifunctional cross-linker succinimidyl-4-(N-maleimidomethyl)cyclohexane-1-carboxylate (SMCC) showed higher serum persistence, and was more efficient than counterparts generated with reducible linkers (Lewis Phillips et al. 2008).

The properties of the resulting conjugate depend on the conjugation chemistry as well. Conjugation chemistries are typically described in literature as non-specific, to native amino acid residues on the antibody surface and site-specific, where conjugation is limited to selected site in the antibody (Chau, Steeg, and Figg 2019).

Non-specific conjugation occurs to reactive side chains such as amino groups of lysine or thiol groups of cysteine on the surface of IgG antibodies. An extensive body of evidence shows that these preparations are heterogenous, containing a spectrum of species, from antibodies with no payload to antibodies with a degree of conjugation that impairs antibody activity (Behrens and Liu 2014; McCombs and Owen 2015). For antibodies incorporating maleimide-thiol bonds, and additional issue of serum stability was reported, due to transfer of the payload to 34-cysteine in serum albumin (Alley et al. 2008). Naturally, this results in reduced efficacy and higher adverse effects mediated by non-targeted release of drug. The phenomenon was shown for SMCC-generated conjugates as well (Dere et al. 2013). To circumvent these problems, the field is moving towards generating site-specific conjugates. Some publications name non-specific conjugation techniques “conventional”, to distinguish them from novel generation technologies (Dan et al. 2018; Sochaj, Swiderska, and Otlewski 2015). These include, but are not limited to engineering amino acids in the antibody structure and conjugating payloads to antibody glycans (Behrens and Liu 2014; Deonarain et al. 2015). Importantly, such conjugates showed improved performance in animal models and are currently under clinical investigation (Beck et al. 2017). One of the big questions is to what extent can novel ADCs improve upon the low therapeutic benefit of currently approved ADCs such as trastuzumab-emtansine (Kadcyla®).

## 1.4. LL37 peptide and endosomal TLR signaling

### 1.4.1 LL37 peptide function and implication in autoimmune diseases

As described in section 1.2.3, endosomal TLR receptors do not distinguish between self and foreign nucleic acids. Triggering of TLR agonists is therefore controlled through access to the endosomal compartment. Self-nucleic acids such as DNA and RNA released from cells do not access the endosomal compartment under physiological conditions. Responsible mechanisms include degradation by DNases and RNases and sequestration of nucleic acids via association with other cellular components (Brencicova and Diebold 2013). It is now accepted that in autoimmune diseases such as psoriasis and systemic lupus erythematosus (SLE), access of self-DNA or self-RNA to the endosomes, contributes to development and exacerbation of autoimmunity (Blasius and Beutler 2010; Barbalat et al. 2011; Roers, Hiller, and Hornung 2016). One method of translocating self-nucleic acids to the endosomal compartment to access TLRs involves complex formation with LL37, a cationic peptide, which is the C-terminal fragment of hCAP18, the only human cathelicidin (Durr, Sudheendra, and Ramamoorthy 2006).

Initially, LL37 was described as an antimicrobial peptide produced by proteolytic cleavage of hCAP18 in response to microbial infection. LL37 expression was described for cells that form part of barrier tissues: epithelial cells in the gastro-intestinal tract and skin, as well as specific immune cells (neutrophils, monocytes mast cells, macrophages, dendritic cells and NK cells) (Xhindoli et al. 2016). Due to its cationic and amphipathic properties, LL37 can form pores in membranes of bacteria and viruses, acting as an antimicrobial. Cholesterol in mammalian cell membranes hinders the pore-forming activity of LL37, impairing cytotoxicity. However, it is unclear whether the protective effect of cholesterol can be overcome by increased doses of LL37, or the peptide can regulate cell-death in discrete cell populations (Kahlenberg and Kaplan 2013).

While expression of LL37 is tightly regulated under normal condition, psoriatic skin and SLE cutaneous lesions show upregulated LL37 levels. Genetic predisposition and local inflammation have been proposed to cause this increased LL37 expression (Kahlenberg and Kaplan 2013). At these sites, the cationic LL37 can form complexes with both self-DNA (Lande et al. 2007) and self-RNA (Ganguly et al. 2009) released from injured cells. LL37 has been shown to protect self-nucleic acids from degradation by endonucleases and transport them to the endosomal compartment of monocytes and pDCs, where they interact with TLR7 and TLR9, triggering inflammation. An important hallmark of LL37 induced inflammation is

IFN-I produced by pDCs, which in turn, boosts antigen presentation by mDC (Ganguly et al. 2009), and augments NK cell function as well (Pinegin et al. 2015). LL37 was shown to play a role in the progression of psoriasis and SLE (Ganguly et al. 2009; Lande et al. 2007). Importantly, there are other mechanisms that can transport self-nucleic acids to endosomes in the context of autoimmune diseases. Notably, SLE is characterized by the presence of anti-nuclear antibodies. These antibodies form circulating antibody-nucleic acid immune complexes, which gain access to endosomes via FcγRIII-mediated endocytosis (Barrat et al. 2005; Means et al. 2005).

In addition to immune-mediated effects, LL37 has other biological functions. Among them, the cationic nature of LL37 allows for binding and neutralization of LPS. Additionally, LL37 promotes wound healing of chronic ulcers via incompletely described mechanisms (Suzuki et al. 2016; Hu et al. 2016). A substantial number of studies investigated the direct effect of LL37 on cancer cell proliferation and biology. Interestingly, LL37 can promote growth of some tumours or induce direct tumour cell death in a variety of cancer cells and tumour mouse models. These effects were tumour-specific (Chen et al. 2018; Piktel et al. 2016; Kuroda et al. 2015). Studies attempting to define LL37 receptors on tumour cells and how they mediate LL37 function are still in infancy and technically challenging, as LL37 associates with membranes as a result of amphipathicity.

### 1.4.2 LL37 in immunotherapy

In terms of therapeutic use, LL37 remains under investigation for a variety of its functional properties such as its direct anti-tumour effect, its immunomodulatory activity, its antimicrobial function and its wound healing properties. The immunostimulatory activity of LL37 complexed with nucleic acids, if efficiently harnessed, could improve anti-tumour immune responses, by triggering endosomal TLRs. Research exploring this is relatively sparse. We include here a description of relevant data so far.

Pre-clinical data demonstrated that LL37 binds also to synthetic nucleic acids such as CpG and poly(I:C), mediating DC activation (Ganguly et al. 2009). This includes CpG molecules with phosphodiester backbone, which in free form are prone to degradation by endonucleases and, therefore, difficult to apply for therapeutic use (Hurtado and Peh 2010). Adding LL37 to differentiation media, led to monocyte derived DCs with superior function in promoting Th1 responses *in vitro* (Davidson et al. 2004). A recent study showed that treatment with LL37 and nucleic acid TLR agonists increased the functionality of DCs in promoting anti-tumour T cell responses both *in vitro* and *in vivo* (Findlay et al. 2019).

Only very few studies tested the benefit of LL37-induced inflammation in tumour models. In a mouse model of ovarian carcinoma, LL37 boosted anti-tumour immune responses induced by CpG (Chuang et al. 2009). In a mouse model of melanoma, LL37 injected into the tumour tissue binds DNA released from dying cells and delivers it to the endosomes of tumour associated pDCs, enhancing anti-tumour immunity through TLR signaling (Gillet et al. 2012).

The approach of LL37 for intra-tumoral injections has been investigated in a phase I clinical trial for melanoma patients with cutaneous metastases (NCT02225366). The major limitation of the study was the low number of participants enrolled (only 4). A case report has been published, highlighting the severe dermatological toxicity at tumour-free sites observed with intratumoral LL37 therapy in a patient with good clinical response (Dolkar et al. 2018). While this confirms the proinflammatory effect of LL37 linked with clinical response, the report also emphasises that similarly with other immunotherapies, LL37 also induces inflammation in tumour-free tissues, leading to adverse effects.

Current literature highlights the rational for exploring LL37, alone or complexed with nucleic TLR agonists for the promotion of anti-tumour immunity. As with other TLR signaling approaches, LL37 needs to reach the tumour tissue, whether alone, to enable the immunostimulatory activity of self-nucleic acids, or complexed with TLR agonists. Conversely, LL37 has additional biological function, which include anti-tumour, but also pro-tumour properties. These effects seem to be tumour specific. Awareness of additional functions of LL37 is important, as they might be playing a role in individual experimental settings.

## 1.5 Expected effects of antibodies and endosomal TLR agonists in the tumour microenvironment

Anti-tumour monoclonal antibodies were shown to concentrate and efficiently deliver other molecules into the tumour tissue (Parslow et al. 2016; Teicher and Chari 2011). For this study we explore delivery of endosomal TLR agonists to the tumour tissue and their effects on the tumour microenvironment. At the tumour tissue, antibodies interact with tumour cells, through the antigen-binding site and with immune cells, via the Fc region. Dendritic cells were shown to take up antibody-coated tumour cells (Dhodapkar, Dhodapkar, and Palucka 2008). Addition of endosomal TLR agonists at the site of this interaction will enhance maturation of DCs and presentation of tumour-specific antigens. Antibody-dependent phagocytosis mediated by an antibody linked to endosomal TLR agonists may lead to activation of other cells such as macrophages. At the tumour site, endosomal TLR agonists were shown to switch of macrophages from a M2 protumorigenic to a M1 tumoricidal phenotype and control tumour growth in mice (Rodell et al. 2018; Liu et al. 2016; Vidyarthi et al. 2018).

Previous studies showed that Fc-mediated effects such as antibody-dependent cytotoxicity contribute to tumour cell death, also making tumour antigens available for recognition by the immune system (Weiner, Dhodapkar, and Ferrone 2009). In this context as well, the availability of endosomal TLR agonists at the tumour tissue would be of advantage, triggering DC maturation and ultimately boosting anti-tumour T cell responses.

The immune activation profile of endosomal TLR agonists and the intrinsic property of antibodies to bridge tumour and immune cells provide a strong rationale for the generation of an antibody-based targeted delivery system to boost anti-tumour immune responses.

## 1.6 Hypothesis, experimental setup and objectives

Our hypothesis is that antibodies can be exploited as vehicles for targeted delivery of endosomal TLR agonists to the tumour tissue and will result in promotion of anti-tumour immunity. We ask if this approach is feasible and efficient in inducing anti-tumour responses in a proof of principle study.

As a model antibody, we use Trastuzumab, a monoclonal human IgG1 antibody, clinically used for treatment of HER2-positive breast (Hudis 2007) and gastric cancers (Gunturu et al. 2013). Starting with this antibody we explored two individual strategies of targeted delivery (Fig. 1.1). One is to generate a fusion antibody with the nucleic acid peptide LL37 (Fig.1.1 A), which complexes nucleic acid endosomal TLR agonists and facilitates delivery to the endosome (Lande et al. 2007; Ganguly et al. 2009). The other approach is to use conjugation chemistries developed in the field of antibody-drug conjugates to generate Trastuzumab conjugates with endosomal TLR agonists (Fig. 1.1 B).

To enable evaluation of Trastuzumab based fusion antibodies and conjugates, an ideal mouse model would offer both selective human HER2 expression on tumour cells and an intact immune system. This would allow us to explore antibody engineering and conjugation techniques using Trastuzumab rather than an equivalent mouse antibody. Importantly, human IgG1 antibodies interact with Fc receptors on mouse cells as well, and the pattern of binding and effector functions is comparable to mouse IgG2a/c, which is the most active mouse antibody in terms of antibody-mediated immune effects (Overdijk et al. 2012). Considering all this, we set out to generate human HER2-transgenic B16 melanoma cells and explore their growth into syngeneic C57/BL6 mice.

To summarise, our main objectives for this proof of principle study are:

a) To establish a mouse model using human HER2-transgenic B16 melanoma cells;

b) To explore fusion of LL37 to Trastuzumab and evaluate if the resulting fusion antibody forms complexes with nucleic acid endosomal TLR agonists and delivers them to the tumour tissue;

c) To explore biochemical conjugation of Trastuzumab with endosomal TLR agonists and assess their capacity to promote anti-tumour immune responses.

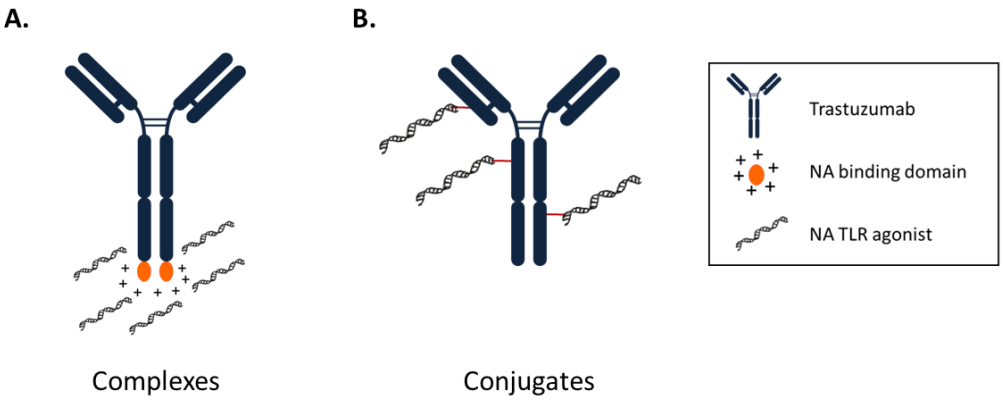


**Fig. 1.1.** Proposed strategies to link nuclei acid TLR agonists to antibodies. **A.** Complex formation of nucleic acid TLR agonists with the cationic peptide LL37 fused with Trastuzumab. **B.** Biochemical conjugation of Trastuzumab to NA TLR agonists using cross-linkers. NA – nucleic acid. TLR – toll-like receptor.

# Chapter 2

# Materials and Methods

## 2.1 Cell culture

*Tissue culture (TC) general reagents:*

RPMI 1640 [+] Glutamine (Gibco)
PBS: 1x DPBS [-] $CaCl_2$, [-] $MgCl_2$ (Gibco)
Fetal calf serum (FCS), heat inactivated (Biosera)
Penicillin 10000 U/ml + Streptomycin 10mg/ml (Gibco)
Ethylenediaminetetraacetic acid 0.5M (EDTA) (Sigma)
Trypsin-EDTA Solution 0.25% (Sigma-Aldrich)
β-Mercaptoethanol 50mM (2-ME) (Gibco)
Tripan Blue 0.4% (Gibco)
Neubauer counting chamber (Fisher Scientific)

*Cell lines and cell culture conditions:*

All adherent cell lines, either mouse (Table 2.1) or human (Table 2.2) were cultured in RPMI 1640 with Glutamine (Gibco) supplemented with 10% FCS and 100U/ml penicillin and 100μg/ml streptomycin (hence referred to as complete R10). Cells were passaged every 2-3 days, depending on doubling time. B16 and derived cell lines were detached using pre-warmed PBS + 0.5mM EDTA (hence called PBS-EDTA), while all other cell lines were detached using Trypsin-EDTA (Sigma-Aldrich). All adherent cells were cultured at 37ºC, 5% $CO_2$ in a tissue culture incubator.

| Mouse cell line | Description | Source |
|---|---|---|
| B16 | Melanoma | CRUK Cell services |
| B14.3 | B16 cells transduced with GFP-OVA encoding retrovirus | Generated by Sandra S. Diebold |
| B14.3 luciferase | B14.3 cells transduced with luciferase* encoding lentivirus | Generated by Sandra S. Diebold |
| RAW 264.7 | Abelson Murine Leukemia Virus-Induced Macrophage Tumor | CRUK Cell services |

**Table 2.1**. Cell lines of mouse origin. OVA - ovalbumin; GFP - green fluorescent protein; * Rinella luciferase

| Human cell line | Type | Source |
|---|---|---|
| BT-474 | Breast ductal carcinoma | kind gift from Sandra Prior, NIBSC |
| OE-19 | Gastro-esophageal adenocarcinoma | kind gift from Ross Hawkins, NIBSC |
| SKBr3 | Breast adenocarcinoma | NIBSC cell bank |
| SKOV3 | Ovarian adenocarcinoma | ATCC®-HTB-74 |
| JIMT-1 | Breast carcinoma | DSMZ – ACC589 |
| T47D | Breast ductal carcinoma | kind gift from James N. Arnold, King's College London |
| MCF-7 | Breast adenocarcinoma | kind gift from James N. Arnold, King's College London |
| MDA-MB-231 | Breast adenocarcinoma | kind gift from Ross Hawkins, NIBSC |
| MDA-MB-468 | Breast adenocarcinoma | kind gift from Sophie Papa, King's College London |

**Table 2.2.** Tumour cell lines of human origin.

Primary cells of either mouse or human origin including murine bone-marrow derived dendritic cells (BMDCs) and human monocyte-derived dendritic cells were cultured using complete R10 supplemented with 50μM β-Mercaptoethanol.

For antibody-dependent cellular cytotoxicity (ADCC) assays, the Human Natural Killer Cell Line No-GFP-CD16.NK-92 cell line (high affinity; 176V) was purchased from ATCC® (code PTA-6967) and cultured in MyeloCult H5100 media (STEMCELL Technologies) supplemented with 100 IU/ml fresh human IL-2 (tissue culture grade, Miltenyi Biotech) at 37ºC, 7% $CO_2$.

For lentivirus production, HEK293T cells were generously provided by Mary Collins, cultured in complete R10 at 37ºC, 5% $CO_2$, dissociated using PBS-EDTA and passaged every other day.

For recombinant antibody production, suspension cell lines FreeStyle 293™ (Life technologies) or ExpiCHO™ (Life Technologies) cells were cultured in their respective media purchased from the manufacturer (FreeStyle™ 293 expression medium and ExpiCHO™ medium, respectively), maintained at 37ºC, 8% $CO_2$, and 125-150 rotations per minute (rpm) in a tissue culture incubator and passaged every 2-3 days at a density of 0.2x $10^6$ cells/ml.

All cells were regularly tested for Mycoplasma by PCR (EZ-PCR Mycoplasma Test Kit, Geneflow Limited). Most of the Mycoplasma testing assays were performed by Miltiades Stylianou, NIBSC.

## 2.2 Polymerase Incomplete Primer Extension (PIPE) cloning

*Materials:*

Q5® High Fidelity polymerase (New England BioLabs)
Q5® Reaction Buffer (New England BioLabs)
Q5® High GC Enhancer (New England BioLabs)
Nucleotide mix dNTP (New England BioLabs)
DpnI (New England BioLabs)
CutSmart buffer (New England BioLabs)
Agarose, electrophoresis grade (Life Technologies)
Low melting point agarose (SeaKem GTG Agarose from Lonza)
Quick-Load® Purple 1 kb Plus DNA Ladder (New England BioLabs)
Gel Loading Dye, Purple (6X) (New England BioLabs)
SYBR Safe DNA Dye (Invitrogen)
Wizard SV gel and PCR clean-up system (Promega)
QIAquick PCR Purification Kit (Qiagen)
Hygromycin 100mg/ml (Invivogen)
Ampicillin (Sigma-Aldrich)
XL-1 Blue Competent bacteria (for routine cloning), $\geq 1 \times 10^8$ transformants/µg (Agilent Genomics)

*Plasmids – see appendices for full sequence and annotations:*

pVITRO-Trastuzumab-IgG1/κ (Addgene plasmid # 61883; http://n2t.net/addgene:61883; RRID:Addgene_61883) were purchased from Addgene; originally generated in Andrew Beavil's laboratory at King's College London.

pVITRO-397-LL37 plasmid was generated by Sandra S. Diebold, NIBSC.

pcDNA3-HER2WT was purchased from Addgene (Addgene plasmid # 16257; http://n2t.net/addgene:16257; RRID:Addgene_16257); originally generated in Mien-Chie Hung's laboratory.

pSIN-SFFV-luc2 was a gift from Kam Zaki, NIBSC.

*Sequencing primers:*

| Primer | Primer sequence 5'→ 3' | Use |
|---|---|---|
| FW SFFV | AGCTCTATAAAAGAGCTCAC | pSIN-SFFV plasmid; to sequence the insert, downstream of the SFFV promoter |
| pSINins_end RV | AGGCATGCAAGCTTGATATCA | pSIN-SFFV plasmid; to sequence from the end of the insert in reverse |
| pVITRO-FcF4 (RV) | CAAACCACAACTAGAATGCAGT | pVITRO-Trastuzumab and derived plasmids; to sequence from the end of the heavy chain or heavy chain fusion protein in reverse |
| pVITRO-F1 (FW) | TTTTGAGCGGAGCTAATTCTCGGG | pVITRO-Trastuzumab and Isotype control; to sequence the variable region of the heavy chain |
| pVITRO-F2 (FW) | GAGGCTAATTCTCAAGCCTCT | pVITRO-Trastuzumab and Isotype control; to sequence the variable region of the light chain |
| pVITRO2R.RV | CTGGTCTTTCCAGGTCTAGA | pVITRO-Trastuzumab-THIOMAB; to sequence from the end of the light chain in reverse |

**Table 2.3.** Sequencing primers verification of plasmid sequences. FW - forward; RV – reverse.

### 2.2.1 Description of PIPE cloning method:

PIPE cloning primer pairs (Tables 2.3, 2.4 and 2.5) were designed for the amplification of the insert and backbone fragments for each pVITRO plasmids as previously described (Dodev et al. 2014). Each primer contained a 5'-end of minimum 10 base pairs (bp) overlapping with the adjacent fragment. All sequences for reverse primers shown in tables were reversed and complemented before ordering. PCR fragments containing 5' overhangs were amplified using Q5 high fidelity DNA polymerase (New England BioLabs).

PCR reactions included 35 cycles of:

- denaturation for 10 sec
- annealing for 30 sec at temperatures depending on the primer pair and
- extension at 72ºC for 30-150 sec depending on the size of the generated fragment (~30 sec per 1kb of sequence), followed by
- a final extension step at 72ºC for 5 min and cooldown at 8ºC.

PCR products were cleaned up using QIAquick PCR Purification Kit (Qiagen) according to the manufacturer's specifications and were eluted in $H_2O$. Subsequently, PCR products were treated for one hour with 20U DpnI enzyme in CutSmart Buffer (New England Biolabs) to digest the templates. Fragments of at least 300bp were run on 1% low melting point agarose gels, while PCR fragments smaller than 300 bp were run on 2% agarose gels. The desired

bands were excised, purified with Wizard SV gel and PCR clean-up system (Promega) and eluted in $H_2O$.

For transformation, 100ng of insert fragment was incubated for 30 min with 100ng of each of the pVITRO backbone fragments and then transformed into 70µl XL-1 Blue competent bacteria (Agilent Genomics) pre-incubated on ice with 1.2µl 1.42M 2-ME using the heat-shock method. Bacteria were incubated for 2 min at 42°C, 630µl SOCS medium was added and suspensions were incubated for 1 h at 37°C in a Thermomixer shaking at 750rpm. Upon incubation, the bacterial suspension was briefly spun and 500µl supernatant was removed. The bacterial pellet was resuspended in the remaining 200µl and the transformed bacteria were plated on Luria Broth Agar plates either containing 100µg/ml Hygromycin or 50µg/ml Ampicillin as appropriate. The Agar plates were incubated over night at 37°C in a bacterial incubator. The next day, antibiotic-resistant clones were picked and expanded in 5ml LB broth containing the appropriate antibiotic. Plasmid was isolated from 3ml bacterial suspension by alkaline lysis (see Section 2.3). Optionally, plasmid DNA was analysed for the presence of insert, either by PCR or digestion with restriction enzymes cleaving sites present in the insert only. Plasmids expressing the insert or untested plasmids were sent for sequencing to Eurofin Genomics using appropriate primers (Table 2.3) to verify correct assembly of the fragments and identify possible point mutations.

### 2.2.2 Generation of pSIN-SFFV-HER2WT

In order to produce a lentivirus encoding human HER2 (hence referred to as HER2), the sequence for HER2 was subcloned from the pcDNA3-HER2WT vector into the transgene pSIN-SFFV vector using the steps for PIPE cloning described in section 2.2.1. Conditions for PCR reactions depending on the optimal melting temperature of primers (Tm) or size of the generated fragment (extension time) are shown in Table 2.4.

| Fragment | Primer | Primer sequence 5'→ 3' | Tm PCR | Extension time |
|---|---|---|---|---|
| HER2 | pSIN-HER2_fw | CTGAGTCGCCCGGGGGATGGAGCTGGCGGC CTTGTGCC | 69°C (GC enh) | 120 sec |
| | pSIN-HER2_rv | CTGGGTCTGGACGTGCCAGTGTGAGCGGCC GCGACTCTAG | | |
| pSIN bb frag A | pSINSFFV_fw | ACGTCCAGGCACGTATTGTGATGAGCGA | 69°C (GC enh) | 150 sec |
| | pSIN-fusion_rv | ACAGACTGAGTCGCCCGGGGG | | |
| pSIN bb frag B | pSIN-fusion_fw | GCGGCCGCGACTCTAGAGTCGA | 69°C (GC enh) | 150 sec |
| | pSINSFFV_rv | ACGTCCAGGCACGTATTGT | | |

**Table 2.4.** List of primers designed and used for PIPE cloning of pSIN-SFFV-HER2. pcDNA3-HER2WT plasmid was used as template to clone the HER2 fragment. pSIN-SFFV-luc2 plasmid was the template used to generate pSIN bb frag A and B. (rv) bp – base pairs; bb frag – backbone fragment; fw – forward; rv-reverse; GC enh – high GC enhancer was used.

These three generated PCR fragments were used for cloning as described above. Plasmid preparations from expanded single bacterial colonies were evaluated for the presence of human HER2 by digestion with 10U/μg DNA of restriction enzymes EcoRI (in NEBuffer EcoRI) and separately KpnI (in NEBuffer 1). Digested plasmid was mixed with gel loading dye and analysed on a 1% agarose gel stained with SYBR Safe DNA Stain (Invitrogen). Plasmids showing bands migrating as expected compared to the DNA ladder on the gel were sequenced (Eurofin Genomics) using appropriate primers described in Table 2.3.

### 2.2.3 Generation of pVITRO-Trastuzumab-LL37 IgG1/κ

The LL37 insert was cloned from the pVITRO-397-LL37 plasmid into the pVITO-Trastuzuman-IgG1/κ plasmid by PIPE cloning as described before (See Table 2.5 for primers and PCR conditions; see Appendix E for pVITRO vector map, Appendix F for annotated sequence and appendix G for nucleotide sequence of LL37). LL37 was inserted after the sequence of the heavy chain of Trastuzumab and before the stop codon to be expressed as a fusion protein.

| Fragment | Primer | Primer sequence 5'→ 3' | Tm PCR | Extension time |
|---|---|---|---|---|
| LL37 | IgG1-LL37CC.fw | CCTGTCTCCGGGTAAACTGCTGGGTGATTTCTTCC | 69°C | 120 sec |
| | distLL37.rv | CTTGGAGCGAACGACCTAC | | |
| pVITRO bb frag A | ratIgG-bb.fw | TATCCCTAATACCTGCCACCCCACTC | 68°C (GC enh) | 120 sec |
| | IgG1_fusion.rv | AGCCTCTCCCTGTCTCCGGGTAAA | | |
| pVITRO bb frag B | IgGBBfrB_ fw | CTTGGAGCGAACGACCTAC | 64°C | 120 sec |
| | ratIgG-bb.rv | TATCCCTAATACCTGCCACC | | |

**Table 2.5.** Primers designed for PIPE cloning of LL37 in pVITRO-Trastuzumab IgG1/κ. The LL37 fragment was cloned using pcDNA3-LL37 template. pVITRO bb frag A and B were generated using pVITRO-Trastuzumab IgG1/κ plasmind template. bp – base pairs; bb frag – backbone fragment; fw – forward; rv-reverse; GC enh – high GC enhancer was used. LL37 sequence is underlined.

To verify insertion of LL37 in plasmid preparations generated from Hygromycin-resistant bacterial colonies, primers specific for the LL37 insert were used in a PCR reaction with the following cycling conditions:

| | | |
|---|---|---|
| 1x | 98°C | 30 sec |
| 30x | 98°C | 10 sec |
| | 54°C | 30 sec |
| | 72°C | 30 sec |
| 1x | 72˚C | 5 min |
| | 8°C | forever |

| Primer | Primer sequence 5'→ 3' |
|---|---|
| LL37_FW | GAAAGCTTGAATTCCTGCTGGGTGATTTCTTCCGG |
| LL37_RV | ACTCGAGGATCCGGACTCTGTCCTGGGTACAAGAT |

**Table 2.6.** Primers for screening of the generated clones, with sequence specific for LL37 underlined.

PCR samples were analysed by agarose gel electrophoresis (1.5% gel). Plasmids encoding LL37 were sequenced using the pVITRO-FcF4 primer to confirm the identity of the sequence.

*Inserting linkers between the C-terminus of Trastuzumab heavy chain and the LL37 peptide*

*Long oligos (Extremers):*

H3 sense oligo: CTGGAGGCCGAGGCCGCCGCCAAGGAGGCCGCCGCCAAGGAGG CCGCCGCCAAGCTGGAG
H3 antisense: CTCCAGCTTGGCGGCGGCCTCCTTGGCGGCGGCCTCCTTGGCGGCG GCCTCGGCCTCCAG
H4 sense: CTGGAAGCAGAGGCGGCTGCAAAGGAGGCTGCAGCCAAAGAGGCCGC TGCTAAAGAAGCCGCCGCCAAGGCCCTCGAA
H4 antisense: TTCGAGGGCCTTGGCGGCGGCTTCTTTAGCAGCGGCCTCTTTGGCTG CAGCCTCCTTTGCAGCCGCCTCTGCTTCCAG

The sequences for an array of linkers, either natural (hinge region of IgG2) or empirical, with different flexibility determined by secondary structure and number of amino acid residues were introduced between the C-terminus of the heavy chain and the N-terminus of LL37. The codons used to encode the amino acid sequences of the linkers were chosen for optimal expression in mammalian cells (optimization GENEius Tool from Eurofin Genomics). For PIPE cloning of most linker sequences, we generated two PCR amplicons with 5'-end overlapping regions. Briefly, primers specific to the beginning of the LL37 sequence or to the end of the heavy chain sequence were designed with 5' overhangs that included part of the linker sequence. The 5' overhangs encoding the linker sequence, contained at least 7 nucleotides overlapping with the adjacent primer. Cloning workflow was performed as described above.

The codon sequences for H3 and H4 were too long to include in the 5'-ends of primers and were ordered as long oligos (Extremers) from Eurofin Genomics, which we used as templates for PCR reactions to generate the H3 or H4 insert. Sense and antisense oligos were mixed at molar ratio 1:1 and diluted to 25ng/ml. 1µl of the stock was used as template in PCR reactions. Primer pairs were designed to amplify the backbone fragments of the pVITRO-Trastuzumab-LL37 plasmid (Table 2.7). Full amino-acid and nucleotide sequences for all linkers are shown in appendix G.

PCR reactions were performed as described in section 2.2.1 with conditions mentioned in Table 2.7. Fragment purification and bacterial transformation were performed as mentioned in section 2.1.1. At least 5 different clones from each construct were verified by Sanger sequencing (Eurofin Genomics). Cloning for the (G4S)x3 linker was performed by Dr. Sandra S. Diebold.

| Linker name | Fragment | Primer | Primer sequence 5'→ 3' | Tm PCR | Ext time |
|---|---|---|---|---|---|
| G4S | A | hIgG1_G4S.fw | GGAGGTGGAGGTTGTCTGCTGGGTGATTTCTTC | 68°C (GC enh) | 150 sec |
| | | ratIgGbb_modif.rv | ATCCCTAATACCTGCCACC | | |
| | B | hIgG1_G4S.rv | TCTCCCTGTCTCCGGGTAAAGGAGGTGGA | 68°C (GC enh) | 150 sec |
| | | ratIgG-bb.fw | TATCCCTAATACCTGCCACCCCACTC | | |
| (G4S)x2 | C | hIgG1_G4Sx2.fw | GGTGGAGGCGGTTCAGGCGGAGGTGGCTCTCTGCTGGGTGATTTCTTC | 68°C (GC enh) | 150 sec |
| | | ratIgGbb_modif.rv | ATCCCTAATACCTGCCACC | | |
| | D | hIgG1_G4Sx2.rv | TCTCCCTGTCTCCGGGTAAAGGTGGAGGCGGTTCAGGCGGAGGT | 68°C (GC enh) | 150 sec |
| | | ratIgG-bb.fw | TATCCCTAATACCTGCCACCCCACTC | | |
| (G4S)x3 | (G4S)x3 A | IgG1-GS-LL37.fw | GGCGGAGGTGGCTCTGGCGGTGGCGGATCGCTGCTGGGTGATTTCTTCCG | 64°C | 150 sec |
| | | ratIgG-bb.rv | TATCCCTAATACCTGCCACC | | |
| | (G4S)x3 B | IgG1x-bb.fw | TATCCCTAATACCTGCCACCCCACT | 66°C | 150 sec |
| | | IgG1-GS-LL37.rv | TCCCTGTCTCCGGGTAAAGGTGGAGGCGGTTCAGGCGGAGGTGGCTCT | | |

Table 2.7a. Primers designed to clone flexible glycine-serine linkers between the Fc terminus of Trastuzumab heavy chain and LL37. Sequence encoding part of each linker is underlined. For all the PCR reactions, pVITRO-Trastuzumab-LL37 plasmid was used as the template. fw - forward; rv – reverse; ext time – extension time; GC enh – GC enhancer.

| Linker name | Fragment | Primer | Primer sequence 5'→ 3' | Tm PCR | Ext time |
|---|---|---|---|---|---|
| H1 * | E | hIgG1_H1.fw | AGCGGCCAAGGCCCTTGAGCTGCTGGGTGATTTCTTCCGGAAATCTA | 68°C (GC enh) | 150 sec |
| | | ratIgGbb_modif.rv | ATCCCTAATACCTGCCACC | | |
| | F | hIgG1_H1.rv | TCTCCCTGTCTCCGGGTAAACTGGAAGCTGAGGCAGCGGCCAAGGCCCTTGAG | 68°C (GC enh) | 150 sec |
| | | ratIgG-bb.fw | TATCCCTAATACCTGCCACCCCACTC | | |
| H2 * | G | hIgG1_H2.fw | GGCCAAGGAAGCTGCAGCCAAGGCCCTTGAGCTGCTGGGTGATTTCTTCCG | 68°C (GC enh) | 150 sec |
| | | ratIgGbb_modif.rv | ATCCCTAATACCTGCCACC | | |
| | H | hIgG1_H2. rv | TCTCCCTGTCTCCGGGTAAACTGGAAGCTGAGGCAGCGGCCAAGGAAGCTGC | 68°C (GC enh) | 150 sec |
| | | ratIgG-bb.fw | TATCCCTAATACCTGCCACCCCACTC | | |
| H3 ** | H3 insert | H3.fw | CCTGTCTCCGGGTAAACTGGAGGCCGAGGCCGC | 69°C (GC enh) | 30 sec |
| | | H3.rv | CCGCCGCCAAGCTGGAGCTGCTGGGTGATTTCTTCC | | |
| | Ante-linker | ratIgG-bb.fw | TATCCCTAATACCTGCCACCCCACTC | 68°C (GC enh) | 150 sec |
| | | IgG1_fusion.rv | AGCCTCTCCCTGTCTCCGGGTAAA | | |
| | Post-linker | LL37fusion.fw | CTGCTGGGTGATTTCTTCC | 63°C | 45sec |
| | | ratIgG-bb.rv | TATCCCTAATACCTGCCACC | | |
| H4 ** | H4 insert | H4.fw | CCTGTCTCCGGGTAAACTGGAAGCAGAGGCGGCTGCAA | 68°C (GC enh) | 45sec |
| | | H4.rv | CCGCCAAGGCCCTCGAACTGCTGGGTGATTTCTTCC | | |
| | Backbone fragments used are the same one described above: Ante-linker and post-linker | | | | |
| Hinge of human IgG2 isotype * | IgG2hinge_FW | IgG2h.fw | ACCGTGCCCAGCACCACCTGTGGCAGGACCGCTGCTGGGTGATTTCTTC | 60°C | 150sec |
| | | ratIgGbb.rv | TATCCCTAATACCTGCCACC | | |
| | IgG2hinge_RV | ratIgG-bb.fw | TATCCCTAATACCTGCCACCCCACTC | 68°C (GC enh) | 150 sec |
| | | IgG2h.rv | AGCCTCTCCCTGTCTCCGGGTAAAGAGCGCAAATGTTGTGTCGAGTGCCCACCGTGCCCA | | |

Table 2.7b. Primers designed to clone rigid alanine-based linkers or natural linkers between the Fc terminus of Trastuzumab heavy chain and LL37. Sequence encoding part of each linker is underlined. The following templates were used for the PCRs: * pVITRO-Trastuzumab-LL37; ** H3 Extremer; *** H4 Extremer. fw-forward; rv – reverse.

### 2.2.4 Generation of pVITRO-Trastuzumab THIOMAB

To use the ThioMAb technology for site-specific conjugation of TLR agonists to Trastuzumab, we exchanged the nucleotides encoding valine (codon GTC) at position 205 (Kabat numbering) in the constant region of the light chain with nucleotides encoding cysteine (codon TGT). The mutation in the sequence is illustrated in appendix F. For this single amino-acid mutation (V205C) in the sequence of Trastuzumab we employed PIPE cloning as described above, with the following modifications:

- the exchanged codon (TGT) was introduced in 2 primers (one forward, one reverse) with 5'-overlapping ends – highlighted in grey in table 2.8
- extension time for each PCR reaction was shortened by 10% of the calculated value for fragment length to enable incomplete extension
- the 5 min final extension step at 72ºC (see section 2.2.1) after the 35 PCR cycles was dropped.

PCR fragments were processed, and subsequent steps were performed as described in section 2.2.1.

| Fragment | Primer | Primer sequence 5'→ 3' | Tm PCR | Extension time |
|---|---|---|---|---|
| anteV205C | pVITRO F1 | C TTTTGAGCGGAGCTAATTCTCGGG | 69°C | 90 sec |
| | LV205C.rv01 | ATCAGGGCCTGAGCTCGCCCTGTACAAA | | |
| postV205C | LV205C.fw01 | GCCCTGTACAAAGAGCTTCAACAG | 63°C | 130 sec |
| | ratIgG2bmodif .rv | ATCCCTAATACCTGCCACC | | |
| Fragment C | ratIgG2b.fw | TATCCCTAATACCTGCCACCCCACTC | 68°C | 36 sec |
| | pVITROrvF1 | CTTGAGTTTTGAGCGGAGCTAATTCT | | |

Table 2.8. PCR primers designed to generate the THIOMAB V205C using PIPE cloning. Codon encoding cysteine is highlighted in grey. pVITRO-Trastuzumab IgG1/κ was used as template for all PCR reactions. fw – forward; rv – reverse.

### 2.2.5 Generation of isotype controls

Isotype controls of human IgG1 isotype were generated for Trastuzumab (Tr), Trastuzumab-H3-LL37 (Tr-LL37) and Trastuzumab-ThioMab (Tr(TH)) by exchanging the variable regions (both the heavy and light chain) from each of the mentioned antibodies with sequences of variable regions of in-house generated isotype control antibodies of mouse or rat isotypes (see appendix F for sequence and annotation of variable regions of Trastuzumab IgG1 and appendix H for isotype control variable regions). Cloning, protein purification and validation of all isotype controls were performed by Dr. Sandra S. Diebold.

## 2.3 Plasmid preparations

### 2.3.1 Minipreparations by alkaline lysis

*Materials:*

Rnase A (Sigma R4642)
Buffer 1 – GET solution: 50mM glucose, 10mM EDTA, 25mM Tris-HCl pH 8.0
Buffer 2 – NaOH/SDS solution: 0.2N NaOH, 1% SDS
Buffer 3 – Kac solution: 3M potassium acetate, 11.5% acetic acid (w/w)
Resuspension buffer: Rnase A diluted 1:3000 in TE buffer (e.g. from Quiagen kits)

To generate plasmid minipreparations, bacteria was grown overnight in 5ml Luria Broth and selection antibiotic. The next day, 1.5-2ml of culture was pelleted by centrifugation for 3 min at 10 000x g. Pellets were resuspended in 100µl ice-cold Buffer 1 and incubated on the bench for 5 min. 200µl of Buffer 2 (freshly prepared before use) were added, mixed and incubated for another 5 min at room temperature (RT). 150µl ice-cold Buffer 3 were added. Samples were vortexed and incubated for 5 min on ice. Afterwards, samples were centrifuged for 5 min at 14 500x g and 400µl supernatant was carefully transferred into sterile Eppendorf tubes, to which 800µl of 96% ethanol were added. Samples were centrifuged for 5 min at 14 500x g. Supernatant was removed and pellets were washed with 500µl of 70% ethanol. Samples were centrifuged again for 5 min at 14 500x g and pellets were dried. Subsequently, pelleted DNA was dissolved in 35-50µl resuspension buffer and stored at -20ºC until further use.

### 2.3.2 Midi- and maxipreparations

*Materials:*

NucleoBond Xtra Midi / Maxi EF kits (Macherey-Nagel)
Isopropanol ≥ 99.5% (Sigma)
Ethanol 96% (Hayman Group)
NanoDrop 1000 spectrophotometer (Thermo Scientific)
Avanti J-26S, high-speed centrifuge (Beckman Coulter)

In order to generate large quantities of endotoxin-free, transfection-compatible plasmid preparations, we used the NucleoBond Xtra Midi / Maxi EF kits from Macherey-Nagel and performed the High-copy plasmid purification protocols (midi or maxi) using the manufacturer's instructions supplied with the kit. Briefly, bacterial cultures were centrifuged at 6 000x g, 15 min, 4ºC. Pellets were resuspended in resuspension buffer. Bacteria were lysed by adding lysis buffer followed by neutralization with neutralization buffer. Lysates were loaded onto columns, washed as recommended and plasmid DNA was eluted using elution buffer. Plasmid DNA was precipitated in isopropanol. Pellets were washed in 70% ethanol, dried on the bench and resuspended in endotoxin-free water. Plasmid DNA yield was assessed by measuring absorption at 260nm, adjusted to 1-2μg/μl and stored at -20ºC until further use.

## 2.4 Lentivirus vector production by three-plasmid transient transfection

*Plasmids:*

pSIN-SFFV-HER2 (transgene plasmid generated as described above)
p8.91 - 2nd generation HIV-derived packaging plasmid (Plasmid Factory)
pMD.G - plasmid encoding VSV-G envelope (Plasmid Factory)

*Materials:*

Opti-MEM (Gibco)
FuGENE transfection reagent (Promega)
Optima L-90K Ultracentrifuge (Beckman Coulter)
DNA Easy Blood & Tissue Kit (Qiagen)
QuantiTect buffer (Quiagen)
PBS: 1x DPBS [-] $CaCl_2$, [-] $MgCl_2$ (Gibco)

HEK293T cells were transiently co-transfected with plasmids pSIN-SFFV-HER2, p8.91 and pMD.G at 1.5:1:1 ratio. Plasmids were diluted in Opti-MEM (Gibco) and incubated with FuGENE (Promega) transfection reagent also pre-diluted in Opti-MEM for 15 min at RT before adding dropwise to HEK293T cells. Supernatants containing lentivirus were harvested after 48 and 72 h, filtered through a 0.45μm syringe filter and concentrated 200-fold by ultra-centrifugation at 64 000x g, 2 h, 4°C. Viral pellets were re-suspended in ice-cold DPBS (hence called PBS) incubated on ice for 1 h, then aliquoted and stored at -80ºC until use.

For lentivirus quantification, $2x10^5$ HEK293T cells were transduced with 5μl lentivirus. Genomic DNA was extracted using DNA Easy Blood & Tissue Kit (Qiagen), following the manufacturer's instructions. Quantitative PCR was used to quantify integrated lentivirus using primers for long terminal repeat regions flanking the transgene: forward primer GT 248 (5'-TGTGTGCCCGTCTGTTGTGT-3'), reverse primer GT 249 (5'-GAGTCCTGCGTCGAGAGAGC-3'), TaqMan probe 5'-FAM-CAGTGGCGCCCGAACAGGGA-TAMRA-3' in QuantiTect buffer (Qiagen). Untransduced cells were used as negative control and values were calculated using a standard curve (the genomic DNA for the standard curve was provided by Kam Zaki).

PCR program used included:

- denaturation at 95ºC 15 min,
- 40 cycles of:

95ºC 15 sec

60ºC 30 sec

72ºC 30 sec

- followed by cool-down at 4ºC.

## 2.5 Generation of HER2 positive B16 cell lines

B16, B14.3 (B16 OVA-GFP) and B14.3 Luciferase (B14.3 Luc) cell lines were harvested and seeded in an appropriate volume of R10 at a density equal to the virus titer (IU) in 1 µl. After incubating at 37ºC, 5% $CO_2$ for 3 h, cells were transduced with human HER2-ecoding lentivirus at increasing multiplicity of infection (MOI). 293T cells were treated in the same way and transduced with the same lentivirus batch at MOI 1 only, for positive control. R10 medium was added the next day to double the original volume. Cells were passaged when confluent.

At day 7 post-transduction, cells were stained for HER2 expression and analysed by flow cytometry. For staining protocol and the antibodies used, see section 2.7. Cell samples showing a distinct HER2 positive population were subjected to fluorescence activated cell sorting (FACS) using BD FACS Aria II (100uM nozzle 4-laser, 13-color). After gating for cells and exclusion of doublets, a gate was placed on HER2 expressing cells and single cells were sorted into 96-well plates containing 200µl R10. Single-cell clones that grew well in plates were further expanded and aliquots of cells were frozen for later use and selection.

## 2.6 *In vitro* Bioluminescent Assays

*Materials:*

White flat bottom tissue culture treated 96 well plate (3917, Costar)
XenoLight D-Luciferin, Potassium Salt (PerkinElmer)
0.22μm syringe filter, 33mm (Merck Millipore)
MicroBeta 2® Microplate Counter (Perkin Elmer)
In Vivo Imaging System - IVIS Spectrum® (Perkin Elmer)

B14.3 Luc HER2 positive monoclonal cell lines were harvested and plated into white flat bottom tissue culture-treated 96-well plates at 1x $10^5$, 2x $10^5$ and 4x $10^5$ cells/well in 100μl R10. Either duplicates or triplicates were used. To compare among higher numbers of monoclonal cell lines, only the 1x $10^5$ cell density was used. The B14.3 Luc parent cell line and B14.3 HER2 clone E5 cell line were included in each assay as positive and negative controls, respectively. Cells were incubated at 37ºC, 5% $CO_2$ for 2-3 h. Luciferase substrate, XenoLight D-Luciferin, was reconstituted in 1x DPBS at 15mg/ml and sterile filtered using a 0.22μm syringe filter. 100μl of luciferin substrate was added to each well. Cells were incubated for 5 min at 37ºC, 5% $CO_2$ and bio-luminescence intensity were measured using a MicroBeta 2® Microplate Counter for 10 seconds with a 3 minute start delay.

When the IVIS Spectrum was used instead, substrate was added 10 min prior to imaging and the cells were left on the heated (37ºC) platform of the IVIS chamber until imaging.

## 2.7 Flow Cytometry

*Materials*:

FACS tubes (BD)
96-well U-plates, sterile, non-TC treated (3788, Costar)
LIVE/DEAD Fixable Violet Dead Cell Stain Kit (Thermo Fisher Scientific)
Streck Cell Preservative (Alpha Laboratories)
Paraformaldehyde (PFA) (VWR)
FACS buffer: PBS, 1% heat-inactivated FCS, 5mM EDTA, 0.02% $NaN_3$
Intracellular buffer: FACS buffer supplemented with 0.1% saponin
OneComp eBeads™ Compensation Beads (eBioscience)
FACS Canto II flow cytometer (BD) – 3-lasers (blue, red and violet) 8-colour (4-2-2)
LSR Fortessa flow cytometer (BD) - 3-lasers (blue, red and violet) 14-colour (5-3-6)
FACS Aria II (BD) - 4-lasers (blue, red, violet, yellow) 13-colour (3-2-5-3)
FlowJo v10 software (FlowJo, LLC)

### 2.7.1 Staining for surface markers

Cultured cells or single cells suspensions were stained with 1-3µl LIVE/DEAD Fixable Violet Dead Cell Stain (Thermo Fisher Scientific) diluted in 1ml DPBS for 30 min on ice, protected from light, then washed once in PBS and centrifuged at 500x g. Cells were either directly stained for surface markers or were fixed in 50% v/v of Streck. Cell Preservative for at least 30 min. When either fresh or fixed murine cells were used, Fc receptors were blocked with 1µg anti-mouse CD16/CD32 (BD) for 30 min on ice. To stain for surface markers, cells were washed once in FACS buffer, then incubated for 30 min with antibodies diluted in FACS buffer, either on ice (live cells) or at 4ºC (fixed cells). Cells were washed 3x times with FACS buffer. Subsequently, cells were either stored at 4ºC until acquisition or stained with secondary antibodies for another 30 min on ice (live cells) or 4ºC (fixed cells) and then washed 3x times in FACS buffer. Cells were resuspended in 200µl of FACS buffer for analysis by flow cytometry and were stored at 4ºC until samples were acquired.

Data was expressed as percent positive cells or geometric mean fluorescence (MFI) or as resolution metric ($R_D$), as appropriate for each experiment. $R_D$ was calculated by subtracting the MFI of isotype control from the MFI of stained cells and dividing the difference by the sum of standard deviations. $R_D = \frac{MFI\ (stained) - MFI\ (isotype)}{SD(stained) + SD(isotype)}$

| Antibody specificity | Dilution | Fluorophore | Isotype | Source | Identifier (clone) |
|---|---|---|---|---|---|
| CD16/CD32 | 1:100 | - | Rat IgG2b, κ | BD | 2.4G2 |
| CD45 | 1:100 | APC, APC-Cy7, FITC, PE-Cy7 | Mouse IgG2a, κ | BD | 104 |
| CD3 | 1:100 | FITC, APC, | Hamster IgG1, κ | BD | 145-2C11 |
| CD3 | 1:100 | APC-eFluor 780 | Rat IgG2b, κ | eBioscience | 17A2 |
| CD4 | 1:100 | APC, Pacific Blue | Rat IgG2a, κ | BD | RM4-5 |
| CD4 | 1:100 | APC-Cy7 | Rat IgG2b, κ | BD | GK1.5 |
| CD8α | 1:100 | APC, V500, Pacific Blue, PerCP-Cy5.5 | Rat IgG2a, κ | BD | 53-6.7 |
| CD44 | 1:100 | PE, PerCP-Cy5.5 | Rat IgG2b, κ | BD | IM7 |
| CD62L | 1:40 | FITC | Rat IgG2a, κ | BD | MEL-14 |
| NK1.1 | 1:100 | APC, PE | Mouse IgG2a, κ | BD | PK136 |
| B220 | 1:100 | PE, PerCP-Cy5.5, PE-Cy7 | Rat IgG2a, κ | BD | RA3-6B2 |
| CD11c | 1:100 | APC, PE-Cy7 | Hamster IgG1, λ2 | BD | HL3 |
| CD11b | 1:100 | V500 | Rat IgG2b, κ | BD | M1/70 |
| CD24 | 1:100 | FITC | Rat IgG2b, κ | BD | M1/69 |
| Granzyme 1 | 1:100 | FITC | Rat IgG2b, κ | BD | RB6-8C5 |
| CD86 | 1:100 | PE | Rat IgG2a, κ | BD | GL1 |
| MHC II (I-A/I-E) | 1:100 | PE | Rat BN x LEW IgG2b, κ | BD | M5/114.15-2 |
| MHC II ($I\text{-}A^b$) | 1:100 | PE | Mouse IgG2a | BD | AF6-120.1 |
| MHC II ($I\text{-}A^b$) | 1:100 | BV786 | Mouse IgG2a | BD | 25-9-17 |
| IFN-ɣ | 1:100 | PE, APC | Rat IgG1, κ | BD | XMG1.2 |
| TNF-α | 1:100 | PE | Rat IgG1, κ | BD | MP6-XT22 |
| Anti-TRP1 | 1:200 | - | Mouse IgG2a | Novus Biologicals | SPM456 |
| Anti-mouse IgG2a | 1:100 | FITC | Rat LOU IgG1 | BD | R19-15 |
| Isotype control | 1:100 | PE, PerCP-Cy5.5 | Mouse IgG2a, κ | BD | G155-178 |
| Isotype control | 1:100 | FITC, PE | Mouse IgG2b, κ | BD | MPC-11 |
| Isotype control | 1:100 | FITC, PE, APC | Rat IgG2a, κ | BD | R35-95 |
| Isotype control | 1:100 | FITC, APC, APC-Cy7 | Rat IgG2b, κ | BD | A95-1 |
| Isotype control | 1:100 | PE | Rat IgG1, κ | BD | R3-34 |
| Isotype control | 1:100 | APC | Hamster IgG1, κ | BD | A19-3 |
| Isotype control | 1:10 | PE | Mouse IgG1, κ | Miltenyi | IS5-21F5 |
| H-2kb-SIINFEKL-pentamer | 10µl/test | PE | - | ProImmune | Pro5 MHC Pentamer |

**Table 2.9a**. List of antibodies used to stain for mouse cell markers for flow cytometry analysis throughout the study.

| Antibody specificity | Dilution | Fluorophore | Isotype | Source | Identifier (clone) |
|---|---|---|---|---|---|
| Trastuzumab | 0.5µg/test 100µl buffer | - | Human IgG1, κ | Either Herceptin (Roche) or produced in house | NA |
| Isotype control | 0.5µg/test 100µl buffer | - | Human IgG1, κ | BioLegend | QA16A12 |
| Human IgG (secondary antibody) | 3µl/test in 100µl buffer | PE | Mouse IgG2a, κ | BioLegend | HP6017 |
| Human IgG (secondary antibody, Fab fragment) | 1:200 | APC | Goat | Jackson Immuno Research | 109-136-098 |
| Anti-HER2 | 1:200 | APC | Mouse IgG1 | Sino Biological | 10004-MM03 |
| CD14 | 1:100 | FITC, Pacific Blue | Mouse IgG2a, κ | Invitrogen | M5E2 |
| HLA-DR | 1:10 | APC-Cy7 | Mouse IgG2a, κ | BioLegend | L243 |
| CD3 | 1:100 | PerCP-Cy5.5 | Mouse IgG1, κ | BioLegend | SK7 |
| CD19 | 1:100 | PE-Cy7 | Mouse IgG1, κ | BD | HIB19 |
| BDCA-1 | 1:10 | PE | Mouse IgG2a | Miltenyi | AD5-8E7 |
| BDCA-2 | 1:10 | FITC | Mouse IgG1, κ | Miltenyi | AC144 |
| BDCA-3 | 1:10 | APC | Mouse IgG1 | Miltenyi | AD5-14H12 |

**Table 2.9b.** List of flow cytometry antibodies used throughout the study to stain human cell surface markers. Secondary antibodies are specified as such.

### 2.7.2 Staining with pentamers

Splenocytes from mice treated with antibodies or conjugates were first stained in FACS tubes with 1µl LIVE/DEAD fixable Violet stain (Thermo Fisher Scientific) in 1ml PBS for 30 min on ice, protected from light. Then cells were washed once in PBS and fixed overnight in Streck. Cells were subsequently stained with 10µl/test of Pro5 H-2kb-SIINFEKL-pentamer (Proimmune) in a total of 60µl FACS buffer volume for 30 min at RT in the dark. Cells were washed twice with 1ml FACS buffer, then stained 30 min at 4ºC in the dark in 100µl FACS buffer for CD8α with APC-conjugated antibody. Cells were washed 3 times and stored in FACS buffer in the fridge until acquisition.

### 2.7.3 Staining for intracellular markers

For intracellular staining, cells were stained for live/dead-cell discrimination as described in 2.7.1 and the directly stained for surface markers with antibodies diluted in FACS buffer for 30 min on ice. Cells were washed twice in FACS buffer then fixed in 4% paraformaldehyde (PFA) for 15 min. Subsequently, cells were washed twice in intracellular buffer, then

incubated with the respective antibodies diluted in intracellular buffer for 30 min on ice, protected from light. Cells were washed twice with intracellular buffer, then resuspended in 200µl FACS buffer and stored at 4ºC until acquisition on the flow cytometer.

### 2.7.4 Fluorescence activated cell sorting (FACS)

When cells were stained for sorting, FACS buffer without NaN3 was used in all steps of the protocol. 1-2 million B16 and B16-derived cell lines, either transduced at MOI 10-20 with a lentivirus for human HER2 expression or parental controls, were stained in FACS tubes with 0.5µg Trastuzumab IgG1 in 100µl FACS buffer for 60 min on ice and then washed thrice in 1ml FACS buffer. Afterwards, cells were stained with 3µl anti-human IgG-PE (BioLegend) diluted in 100µl FACS buffer for 30 min on ice, in the dark. Cells were washed thrice and resuspended in FACS buffer. SKBr3 (human HER2 overexpressing) cells were harvested and stained in parallel with the B16 cells and used as positive controls. Cells were analysed and sorted using FACS Aria II (100uM nozzle 4-laser, 13-color (3-2-5-3) 20psi). Human HER2 positive single cells were sorted immediately in wells of TC-grade 96-well plates containing 200µl R10.

### 2.7.5 Serum cytokine multiplex

*Materials:*

LEGENDplex™ Mouse Th1 panel (5-plex) with V-bottom Plate V02 (740745, BioLegend)
96-well V plate (740379, BioLegend)
LEGENDplex™ data Analysis Software v8.0 (BioLegend)

Blood harvested from tumour-bearing mice was harvested at different time-points after treatment. Blood was allowed to clot for 30 min at RT, then centrifuged for 10 min, 4ºC, 1500x g. Serum was collected and stored in sterile conditions at -80ºC until assayed.

To analyse levels of IFN-γ, TNF-α, IL-2, IL-6, IL-10 in serum of mice treated with Trastuzumab-CpG or controls, the LEGENDplex kit was used according to the manufacturer's protocol. Briefly, samples were thawed on ice, mixed and centrifuged 5min at 10 000x g to remove particulates. Samples were diluted 1:2 in assay buffer, then 1:2.5 in Matrix B, to a final dilution of 1:5. 25µl diluted sample were plated in duplicates in wells containing 25µl assay buffer. The standard curve was diluted 1:4 in assay buffer, then each dilution was plated in duplicate in wells containing 25µl matrix B. Beads were diluted 1:13 and mixed together, then 25µl/well were added. The plate was incubated for 2 h RT in the dark on a platform

shaking at 800x rpm. Afterwards, the plate was washed twice with washing buffer. Subsequently, 25µl/well of detection antibodies were added and plate was incubated 1 h RT 800x rpm in the dark. In a following step, 25µl Streptavidin-PE were added to each well, without washing the plate and incubated 30 min RT 800x rpm in the dark. Samples were washed twice in washing buffer. Samples were resuspended in 150µl and stored in the fridge until acquiring on BD Canto II cytometer.

Data was analysed using the LEGENDplex™ data Analysis Software. Cytokine levels in serum were measured on their respective standard curve.

### 2.7.6 Mouse antibody isotyping multiplex

*Materials:*

LEGENDplex™ Mouse Immunoglobulin Isotyping Panel (6-plex) with V-bottom Plate V02 (740493, BioLegend)
96-well V plate (740379, BioLegend)
LEGENDplex™ data Analysis Software v8.0 (BioLegend)

Blood was harvested before or after treatment from tumour-bearing mice or from tumour-free mice. After leaving 30 min at RT to clot, blood was centrifuged at 1500x g, 4ºC for 10 min. Serum was collected and stored in sterile conditions at -80ºC until assayed. Samples were analysed according to the protocol provided with the kit. Briefly, serum samples were diluted 1:50 000 in assay buffer. 25µl sample were incubated in duplicates with 25µl beads and incubated for 2 hours while rotating at 800 rpm. The plates were washed twice in wash buffer, then 25µl/well detection antibody cocktail was added and further incubated for 1 h, RT, 800 rpm. After 2 subsequent washes, samples were incubated for 30 min with 25µl/well of streptavidin-PE. The plates were washed twice before resuspending in 150µl and stored in the fridge until acquiring on BD Canto II cytometer. Data was analysed using the LEGENDplex™ data Analysis Software. Specific antibody isotype levels in serum were measured on their respective standard curve.

## 2.8 Enzyme-linked immunosorbent assay (ELISA)

### 2.8.1 ELISA for detection of antibodies or cytokines

*Materials:*

Nunc Maxisorp Immunoplates, 96-well (Nunc 4-39454, Thermo Scientific)
Flexiplates: Serocluster™ 96-well "U" bottom Plate, non-treated, vinyl (2797, Costar)
Lid for flexible plate (BD)
Coating buffer: 0.1M NaHCO3, pH 8.2
PBS-Tween: PBS containing 0.05% Tween
Blocking buffer 1: PBS containing 2.5% FCS and 0.02% $NaN_3$
ExtrAvidin®-AP: Steptavidin-Alkaline phosphatase (Sigma)
ELISA substrate: SIGMAFAST™ p-Nitrophenyl phosphate tablets (Sigma)
FreeStyle™ Expression Medium (Invitrogen)
R10: RPMI 1640, 2mM glutamine, 10% FCS and 100 U/ml penicillin, 100µg/ml streptomycin, 50µM 2-ME
PBS: 1x DPBS [-] $CaCl_2$, [-] $MgCl_2$ (Gibco)
SpectraMax M5 96 well plate reader (Molecular Devices)

Immunoplates were coated with 50µl per well of the relevant antibody raised against mouse or human cytokines or human IgG1, diluted as specified (Table 10a) in coating buffer. Plates were incubated overnight at 4ºC in a humid chamber.

The next day, plates were washed 3 times with 300µl PBS-Tween per well and patted dry on paper towels. Next, 150µl of blocking buffer 1 was added per well and incubated for 2 h at RT. instead. After 2 h, plates were washed with 300µl PBS-Tween per well, 4x times. Samples and standard dilutions were prepared in Flexiplates before adding to the ELISA plates. Cell culture supernatant analysed for cytokine detection was diluted in R10. Cell culture supernatant from FS 293 cells was diluted in FreeStyle™ Expression Medium. Relevant dilutions for standard curves were prepared in the same way. Starting concentrations for standards are shown in Table 10. Samples and standard were added in triplicates (or duplicates for mouse serum only), 50µl/well and incubated in a humid chamber either 4 h at RT or overnight at 4ºC.

Subsequently, plates were washed with 300µl PBS-Tween per well, 4x times and the specific biotinylated secondary antibody for the detected molecule was diluted in blocking buffer 1

and 100µl was added to the wells. Plates were incubated 1 hour at RT in a humid chamber, then washed again with 300µl PBS-Tween per well, 4x times. When a 3-step detection protocol was required, as for mouse IFN-α ELISA, wells were first incubated with the antibody detecting the cytokine, washed, then incubated again with the biotinylated secondary antibody specific for the detection antibody and washed once more. Streptavidin-Alkaline Phosphatase was diluted 1:10 000 in blocking buffer and added 100µl to the wells. After 1h incubation and 4 washes with 300µl PBS-Tween per well, 100µl ELISA substrate were added per well. To prepare the ELISA substrate stock solution, to make stock 1 buffer tablet + 1 substrate tablet from the SIGMAFAST kit were diluted in 20ml $H_2O$. Plates were incubated for 30 min to 1 hour at RT, in a humid chamber, protected from light.

Absorption at 405nm was measured using the plate reader. The OD405 values of the standard dilutions were plotted against the concentrations of the diluted standards to obtain standard curves. Sample concentrations were determined using the linear part of the standard curve, for which the goodness of fit (R squared was >0.992).

| Detected molecule | Coating reagent | Dilution | Source | Identifier | Detection antibody | Dilution | Source | Identifier |
|---|---|---|---|---|---|---|---|---|
| Human IgG1 (Trastuzumab or isotype) | Mouse anti-human IgG1, purified | 2.5µg/ml | BD | G17-1 | Mouse anti-human IgG, Biotin | 1µg/ml | BD | G18-145 |
| Human IL-12p40 | Mouse anti-human IL-12/p40 | 5µg/ml | BD | C8.3 | Mouse anti-human IL-12, Biotin | 2.5µg/ml | BD | C8.6 |
| Human IL-6 | Rat anti-human IL-6 | 4µg/ml | BD | MQ2-13A5 | Rat anti-human IL-6, Biotin | 2.5µg/ml | BD | MQ2-39C3 |
| Mouse IL-12p40 | Rat anti-mouse IL-12/p40 | 5µg/ml | BD | C15.6 | Rat anti-mouse IL-12/p40, Biotin | 1µg/ml | BD | C17.8 |
| Mouse IL-6 | Rat anti-mouse IL-6 | 4µg/ml | BD | MP5-20F3 | Rat anti-mouse IL-6, Biotin | 1.5µg/ml | BD | SXC-1 |
| Mouse IFNα | Anti-mouse IFNα | 1:100 | Hycult Biotech | mAb F18 | Rabbit polyclonal anti-mouse IFNα | 1:2000 | PBL Medical Laboratories | 32100-1 |
| | | | | | Mouse anti-rabbit biotin | 1:1000 | Jackson ImmunoResearch | 211-065-109 |

Table 2.10a. List of antibodies and recombinant proteins used throughout the study for coating or detection in ELISA.

| Standard | Starting concentration | Serial dilution | Source | Identifier |
|---|---|---|---|---|
| Human IgG1, recombinant | 1µg/ml | 1:2 | BioLegend | QA16A12 |
| Human IL-12, recombinant | 20ng/ml | 1:3 | BD | 554633 |
| Human IL-6, recombinant | 5ng/ml | 1:3 | BD | 550071 |
| Mouse IL-12, recombinant | 16.7 ng/ml | 1:3 | R&D | 419-ML |
| Mouse IL-6, recombinant | 50ng/ml | 1:3 | R&D | 406-ML |
| Mouse IFNα, recombinant | 10 000U/ml | 1:3 | Hycult Biotech | HC 1040b |

Table 2.10b. List of standards used in ELISA (antibodies and recombinant proteins) used throughout the study.

### 2.8.2 Antibody binding assay

*Materials:*

ERBB2, Human protein, recombinant, hIgG1-Fc Tag (1004-H02H, Sino Biological)
EGFR, Human protein, recombinant, hIgG1-Fc Tag (10001-H02H, Sino Biological)
Blocking buffer 2: PBS containing 3% BSA
PBS-BSA: PBS containing 0.5% BSA
Horse-radish peroxidase (HRP) anti-human kappa light chain (A7164, Sigma)
3,3′,5,5′-Tetramethylbenzidine (TMB) substrate: 1 TMB tablet (T3405, Sigma) to 10ml 0.05 M phosphate-citrate buffer, 0.006% $H_2O_2$
Stop solution: 2 M $H_2SO_4$
SpectraMax M5 96 well plate reader (Molecular Devices)

To compare the binding properties of Trastuzumab-based conjugates and complexes with the relevant parent antibody, human HER2 (Sino Biological) was immobilised to the ELISA plate at 0.5µg/ml, diluted in DPBS, 50µl/well. To analyse binding properties of Cetuximab-CpG alongside the parent antibody Cetuximab, plates were coated with 1µg/ml EGFR, diluted in DPBS, 50µl/well. All the following steps were performed in the same way. Plates were incubated overnight at 4ºC in a humidified chamber.

The next day, plates were washer 3 times with 300µl PBS-Tween per well then incubated for 2 h at RT with 150µl ELISA blocking buffer 2. Samples (antibodies and conjugates or complexes) were diluted 1:2 in PBS-BSA from a top concentration of 500ng/ml in Flexiplates in triplicates before adding 50µl per well to the ELISA plate. These were incubated 4 h at RT or overnight at 4ºC in a humid chamber.

ELISA was developed the next day using either the ExtrAvidin-AP system as described in section 2.8.1 for ELISAs, or the HRP system. To achieve the later, plates were washed 4x times with 300µl PBS-Tween per well, before being incubated for 1 hour with 100µl of HRP anti-human kappa light chain antibody diluted 1:5000 in PBS. Plates were washed again (300µl PBS-Tween per well, 4 times) and 100µl freshly prepared TMB substrate were added. 2-10 min later (when top concentrations on the plate turned a rich blue), 50µl stop solution were added per well.

Plates were measured for absorption at 450nm using the plate reader. The OD405 values were plotted against antibody concentration (nM) and data was analysed using nonlinear regression function (variable slope) of GraphPad Prism. To describe the similarity of binding curves, the

difference in upper and lower asymptotes and the fitted slope factors were compared. The goodness of fit of the equation chosen for nonlinear regression was verified by R squared. Parameters were extracted for further analysis when R squared was >0.992.

### 2.8.3 Determining of serum concentration of Tr and Tr-derived conjugates and complexes

Mice were treated IV with either one dose or three of Trastuzumab and derived conjugates and complexes as described in section 2.18.6. To determine serum availability of treatments, blood was harvested at different time-point depending on the regimen. Blood was stored at RT for 30 min to clot. Blood was centrifuged 10 min, 4ºC, 1500x g. Serum was collected and stored in sterile conditions at -80ºC until assayed. Serum samples were thawed on ice, diluted in PBS-BSA and analysed in duplicates by ELISA with immobilized human HER2 and developed using anti-human IgG1 biotinylated antibody (clone G18-145) and the ExtrAvidin-AP system. ELISA was performed and developed as described for antibody binding assay in section 2.8.2. For each antibody, conjugate or complex, the respective standard of known concentrations was included in the assay. Serum antibody / conjugate / complexes concentration were calculated using the linear part of the respective standard curve.

### 2.8.4 Determining tumour-specific antibody responses in mouse serum

*Materials:*

ERBB2, Human protein, recombinant, hIgG1-Fc Tag (1004-H02H, Sino Biological)
Ovalbumin, endotoxin-free (321000, Hyglos)
Anti-OVA antibody, mouse IgG1 (clone 14, Sigma-Aldrich)
Anti-mouse IgG1, biotinylated (clone A85-1, BD)
Anti-mouse IgG2a/IgG2c, biotinylated (clone R19-15, BD)
Anti-mouse IgM, biotinylated (clone R6-60.2, BD)
PBS-BSA: PBS containing 0.5% BSA
Blocking buffer 2: PBS containing 3% BSA
ExtrAvidin®-AP: Steptavidin-Alkaline phosphatase (Sigma)
ELISA substrate: SIGMAFAST™ p-Nitrophenyl phosphate tablets (Sigma)
SpectraMax M5 96 well plate reader (Molecular Devices)

Serum from mice was harvested as described above and stored at -80°C until use. Serum samples from 2-5 mice were pooled together and analysed as one sample. The assay was performed using the method described for antibody binding assay in section 2.8.2. Briefly,

serum was diluted in PBS-BSA and then incubated with ELISA plates pre-coated overnight with either 0.5μg/ml human HER2 or 10μg/ml OVA. The next day, mouse IgG1, IgG2c and IgM were detected by incubating individual plates with the specific biotinylated antibody, streptavidin and substrate. Plates were measured for absorption at 450nm using the plate reader. The OD450 values were plotted against serum dilution.

## 2.9 *In vitro* cell proliferation assays

### 2.9.1 Trypan Blue exclusion method

*Materials:*

Trypan Blue 0.4% (Gibco)
Neubauer counting chamber (Fisher Scientific)
TC treated 6-well plates (353046, Costar)

B16, B16 HER2, B14.3 Luc and B14.3 Luc HER2 cells were detached using PBS-EDTA and seeded 50 000 cells per well in 3ml R10 in 6-well TC-treated plates in duplicates. At days 1-3 after seeding, cells were harvested, and an aliquot was mixed with Trypan Blue pre-diluted 1:5 in PBS. Live cells excluding Trypan Blue were counted under the microscope.

### 2.9.2 MTS assay

*Materials:*

96 Well Tissue culture treated, round bottom plates (3799 Costar)
CellTiter 96® AQueous One Solution Cell Proliferation Assay (Promega)
SpectraMax M5 96 well plate reader (Molecular Devices)

Human HER2 positive or negative cell lines and B16 or B16-derived cell lines were used in this assay. Cells were harvested and seeded 10 000 cells per well in 50µl R10 in TC treated 96-well plates. Cells were incubated at 37ºC, 5% $CO_2$ for 3-4 h. Serial dilutions of vehicle (PBS), isotype control, derived conjugates or complexes, Herceptin, Trastuzumab or Trastuzumab-derived conjugates and complexes were performed in R10 and 50µl were added per well. Cells were incubated at 37ºC, 5% $CO_2$ for 48 h in a TC incubator. Subsequently, 20µl of the CellTiter 96® AQueous One Solution Reagent containing the MTS (3-(4,5-dimethylthiazol-2-yl)-5-(3-carboxymethoxyphenyl)-2-(4-sulfophenyl)-2H-tetrazolium, inner salt) compound were added per well. Plates were left at 37ºC, 5% $CO_2$ for 30 min for the MTS substrate to be converted by metabolically active cells into a coloured product detected using a 96-well plate reader to measure absorption at 490nm. OD490 of vehicle-treated cells was considered 100% proliferation in the conditions of the assay. Proliferation of treated cells was expressed as percent of vehicle-treated cells.

## 2.10 Recombinant antibody production

### 2.10.1 Expression of antibodies in mammalian cell lines

*Expression using the FreeStyle™ MAX 293 Expression System*

*Materials:*

FreeStyle™ 293-F cells (Invitrogen)
FreeStyle™ Expression Medium (Invitrogen)
FreeStyle™ MAX reagent (Invitrogen)
OptiPRO™ serum-free medium (SFM) (Invitrogen)
Midi- or maxipreparations of pVITRO plasmids
Erlenmeyer flask, flat bottom, vented cap either 125ml, 250ml or 500ml (Costar)
Stericup® 0.45μm PVDF membrane (Millipore)

FreeStyle™ 293-F cells were maintained according to the manufacturer's instructions (described in section 2.1) and used for transfections starting with passage 5 and not exceeding passage 30. Cells were harvested, counted and seeded 0.5x $10^6$ cells/ml of FreeStyle™ Expression Medium the day before transfection (day -1). On transfection day (day 0), cells were diluted if necessary, to 1x $10^6$ cells/ml. OptiPRO™ SFM (1/25 of cell culture volume) was used to form complexes of plasmid/MAX Reagent. Both FreeStyle™ MAX reagent and plasmid were used at 0.8μg/ml of cell culture volume) and diluted separately in OptiPRO™ SFM. Diluted plasmid and MAX reagent were mixed together and incubated for 10 min at RT. Complexes were added dropwise to the cells while swirling the flask. Cells were incubated at 37ºC, 8% $CO_2$. On day 7 post-transfection, cells were centrifuged at 500x g, 10 min, RT. Supernatant was filtered through a 0.45μm Polyvinylidene difluoride (PVDF) membrane and stored at 4ºC until further use. To evaluate relative antibody expression levels to Trastuzumab in cell supernatant, a human IgG1 ELISA was performed as described in section 2.8.

*Expression using the ExpiCHO™ Expression System*

*Materials:*

ExpiCHO-S™ cells (Gibco)
ExpiCHO™ Expression Medium (Gibco)
ExpiFectamine™ CHO Transfection Kit (Gibco)
OptiPRO™ serum-free medium (SFM) (Invitrogen)
Midi- or maxipreparations of pVITRO plasmids

Erlenmeyer flask, flat bottom, vented cap either 125ml, 250ml or 500ml (Costar)
Stericup® 0.22 µm and 0.45 µm PVDF membrane (Millipore)

ExpiCHO-S™ cells cells were maintained according to the manufacturer's instructions (as described in section 2.1) and only used for transfections experiments starting with passage 3 and only up to 30 passages. One the day before transfection (day -1) cells were seeded 3.5x $10^6$ cells/ml ExpiCHO™ Expression Medium. On transfection day (day 0), cells were diluted, if necessary, to 7-10x $10^6$ cells/ml. Complexes of plasmid/ExpiFectamine™ CHO were formed in OptiPRO™ SFM (1/25 of cell culture volume). Plasmid DNA was used at 1µg per ml of culture volume and diluted in OptiPRO™ SFM. ExpiFectamine™ CHO was used at 2µg per ml of culture volume and diluted in OptiPRO™ SFM. Plasmid and ExpiFectamine™ CHO were mixed together and incubated for 4 min at RT. Complexes were added dropwise to the cells while swirling the flask. Cells were incubated at 37ºC, 8% $CO_2$. On day 1 post-transfection, ExpiCHO™ Enhancer (1/6000 of culture volume) and ExpiCHO™ Feed (1/4 of culture volume), corresponding to the standard protocol in the product instruction manual. Supernatant was harvested on day 8 post-transfection by centrifugation at 500xg, 10 min, RT. Supernatant was filtered through a 0.45µm (PVDF) membrane and stored at -20ºC until further use. When thawed, supernatant was clarified by passing through a 0.22µm PVDF membrane. To evaluate antibody expression levels, human IgG1 ELISA was performed as described in section 2.8.

### 2.10.2 Purification of recombinant antibodies

*Materials:*

AKTA Start 29022094 and Unicorn Start 1.0 software (GE Healthcare)
HiTrap MabSelect SuRe (protein A) column, 5ml (GE Healthcare)
HiTrap Protein G column, 5ml (GE Healthcare)
Stericup® 0.22 μm and 0.45 μm PVDF membrane (Millipore)
Fractionation tubes 3 ml (300500, DeltaLab)
Amicon Ultra centrifugal filter units 2-15ml with either 10kDa or 100kDa cut-off (Merck-Millipore)
Spin-X centrifuge tube filter 0.22μm (8160 Costar)
NanoDrop 1000 spectrophotometer (Thermo Scientific)
Cleaning solution: 1M NaOH
10x DPBS [-] $CaCl_2$, [-] $MgCl_2$ (Gibco)
Sterile non-pyrogenic water (Baxter)
Column storage solution: 70% ethanol
Neutralisation buffer: 1M Tris-HCl, pH 9.0
Buffers for protein A column only:
Binding buffer A: 20mM sodium phosphate, 0.15M NaCl, pH 7.2
Elution buffer A: 0.1M sodium citrate, pH=3.2, 50mM NaCl
Column cleaning in place (CIP) solution: 0.2M NaOH
Buffers for protein G column only:
Binding buffer G: 20mM sodium phosphate, pH 7.2
Elution buffer G: 0.1M glycine-HCl, pH2.7
1x DPBS [-] $CaCl_2$, [-] $MgCl_2$ (Gibco)

All antibodies, weather Trastuzumab, Isotype control, ThioMab or fusion antibodies with LL37, were purified by affinity chromatography using either a protein A or a protein G column. All buffers were made up with sterile endotoxin-free water and sterile filtered through a 0.22μm membrane prior to use. Throughout the purification process, only pyrogen-free materials were used. During the run, the Unicorn software was used to monitor pressure in the system (which was always kept under 0.22MPa), absorbance at 280nm and conductivity.

The AKTA start system was cleaned, first with 1M NaOH, followed by 1x PBS and 70% ethanol using a flow rate of 5ml/min. All tubing used in the purification process (line A, line

B, sample line, waste tube, fractionation tube) were cleaned for at least 8 min with each solution.

After cleaning the machine, a flow rate of 1ml/min was set up while running 70% ethanol and the column was inserted. 5-7ml ethanol were run through the column at 1ml/min before equilibrating the column with minimum 5x column volumes of binding buffer (A for the protein A column and G for the protein G column) at 3ml/min flow rate. AutoZero of the UV detector was performed while running binding buffer. Cell supernatant was loaded onto the column through the sample line at 3ml/min. Unbound material was washed with 6 column volumes of binding buffer. Flow-through was collected into a sterile plastic flask, sterile filtered through a 0.22µm membrane and stored at 4ºC. Elution was performed with the respective buffer at 3ml/min with fractionation of 2ml in tubes pre-filled with 200µl neutralization buffer. The fractions containing eluted antibody (according to the UV trace) and a few adjacent fractions were analysed by NanoDrop for absorbance at 280nm. Fractions containing antibody were pooled. Buffer exchange and sample concentration were performed simultaneously using Amicon Ultra centrifugation filters with either 10kDa or 100kDa cut-off. Filters were spun at maximum speed of the centrifuge (800xg) for 20-25 min, topping up the filter 5x times with cold PBS. Concentrated antibody preparation was sterile filtered through a 0.22µm membrane and stored at 4ºC until further use.

While performing buffer exchange of the antibody, the column was regenerated with 30ml elution buffer at 3ml/min, followed by 6x column volumes of binding buffer. Only when the MabSelect Sure protein A column was used, cleaning in place (CIP) was performed with 0.2M NaOH run at 3ml/min for 15 min. Column was re-equilibrated with 6x column volumes of binding buffer and then used to purify another batch of antibody or stored. For storage, either of the columns were washed at 2ml/min with 5 column volumes of 70% ethanol. Columns were stored at 4ºC between runs.

### 2.10.3 Quantification of antibody yield

***BCA assay***

*Materials:*

Polypropylene tubes of plates
BCA assay kit (Pierce)
Bovine gamma globulin (BGG) standard (Thermo Scientific)
Assay plate, non-treated, round bottom, 96 well (Costar)
SpectraMax M5 96 well plate reader (Molecular Devices)

BCA assays were performed according to the manufacturer's instructions. A standard curve was prepared using the BGG standard and used to determine antibody concentration of all purified antibodies or fusion antibodies, but also of antibody conjugates. Standard curve (triplicates) and samples (duplicates) were diluted in PBS to 25µl per well, to which 200µl substrate was added. The plate was incubated for 10 min at RT in the dark, then absorption at 595nm was measured with a plate reader.

***Spectrophotometry***

*Materials:*

NanoDrop 1000 spectrophotometer (Thermo Scientific)
PBS: 1x DPBS [-] $CaCl_2$, [-] $MgCl_2$ (Gibco)

2µl of antibody suspension in PBS was used to measure absorption at 280nm against the blank (PBS). For measurements, we have used the reported extinction of Herceptin, ε280nm = 225,000 $M^{-1}$ $cm^{-1}$.

***Calculating total antibody yield from transfection experiments***

To calculate the total antibody yield generated via transient transfection, purified antibody c% was measured by BCA. The following formulas were applied:

Mass of purified antibody (mg) = c% of purified batch (mg/ml) * volume (ml)

Total antibody yield (mg/L) = mass of purified antibody (mg) / volume of supernatant it was purified from (L).

## 2.11 Organ isolation and cell cultures

### 2.11.1 Generation of GM-CSF-derived bone marrow dendritic cells (BMDC)

*Materials:*

R10: RPMI 1640, 2mM glutamine, 10% FCS and 100 U/ml penicillin, 100µg/ml streptomycin, 50µM 2-ME
GM-CSF, recombinant, murine (Peprotech)
1ml syringe, 23G needle
70µm strainer (BD)

Femur and tibia of C57BL/6 mouse hind legs were removed using sterile instruments. The bone marrow cells were flushed out with R10 using a 23 G needle and syringe. Cells were placed in a 10 cm TC dish and incubated for 30 min at 37ºC, 5% $CO_2$. Afterwards, non-adherent cells were harvested and passed through a 70µm strainer, then centrifuged 5 min at 300xg, RT. Cells were cultured at 1.3x $10^6$ cells/ml in 10cm TC dishes in 12ml R10 supplemented with 20ng/ml GM-CSF, as described previously (Inaba et al. 1992). The day cells are placed in culture was counted as day 0. On day 2, 10ml of the culture medium were carefully removed without disturbing the cells and replaced with 12ml of fresh R10 supplemented with 20ng/ml GM-CSF. On day 3, medium and non-adherent cells were discarded. Adherent cells were gently washed with R10 and further cultured in 12ml R10 containing 20ng/ml GM-CSF. Non-adherent and loosely adherent cells were harvested in R10 and used in assays on day 5 or 6. Differentiation of bone marrow cells into dendritic cells was verified by flow cytometry, specifically through analysis of surface markers CD11c, Gr-1 (common epitope on Ly-6G and Ly-6C), CD86 and MHC class II.

### 2.11.2 Generation of Flt3L-derived bone marrow dendritic cells (BMDC)

*Materials:*

R10: RPMI 1640, 2mM glutamine, 10% FCS and 100U/ml penicillin, 100µg/ml streptomycin, 50µM 2-ME

Flt3-ligand, recombinant, murine (Flt3L) (R&D Systems)

1ml syringe, 23G needle

70µm strainer (BD)

C56BL/6 mice were culled and using sterile instrument, the femur and tibia of hind legs were removed. Bone marrow cells were flushed out with R10 using a needle and syringe and differentiated into dendritic cells following previously published protocols (Gilliet et al. 2002; Brawand et al. 2002). Cells were passed through a 70µm strainer and cultured in 5ml per well of R10 supplemented with 50ng/ml Flt3L in 6-well TC treated plates at a density of $1.5x10^6$ cell/ml. On day 5, 4.5ml medium were exchanged for 5ml of R10 + 50ng/ml Flt3L. similarly, on day 7, 4.7ml medium were exchanged for 5ml of R10 + 50ng/ml Flt3L. Only non-adherent and loosely adherent cells were used for *in vitro* assays on day 10 of culture. Differentiation into dendritic cells was verified by staining the cells for surface cell markers CD11c, B220, CD24 and CD11b.

### 2.11.3 Generating single cell suspensions from mouse lung

*Materials:*

R0: RPMI 1640 (no supplementation)

R10: RPMI 1640, 2mM glutamine, 10% FCS and 100 U/ml penicillin, 100µg/ml streptomycin, 50µM 2-ME

Cell-wash buffer: 1x DPBS [-] $CaCl_2$, [-] $MgCl_2$ (Gibco) + 1% FCS + 5mM EDTA

gentleMACS Dissociator (Miltenyi Biotec)

gentleMACS (TM) C tubes (Miltenyi Biotec)

Collagenase D solution (Roche #11 088 866 001)

DNase I solution (Roche #1 284 932)

100µm cell strainer (Thermo Fisher)

Red blood cell (RBC) lysis buffer (10x): 1.5M NH4Cl, 100mM $NaHCO_3$, 5mM EDTA

Mouse lungs were harvested in sterile conditions, for some samples after *in situ* lung perfusion with 20ml DPBS. Lung tissue was carefully dissected from adjacent organs and connective tissue and rinsed in R0. Each mouse lung was injected with 2.5ml R0 containing 1mg/ml collagenase D and 0.1mg/ml DNase I. The lung and media placed into gentleMACS C tubes were processed with the gentleMACS Dissociator using the program m_impTumor_02. Subsequently lungs were incubated for 40 min at 37°C, gently inverting the tubes every 5-10 min. Tissue was processed again by running the m_impTumour_03 program of the gentleMACS Dissociator. Samples were passed through 100µm cell strainer and washed with cell-wash buffer. Cells were centrifuged 5 min, RT at 500x g. Red blood cell lysis was performed for 7 min at RT, then cells were washed, centrifuged and strained again, then resuspended either in R10 or PBS, depending on application.

### 2.11.4 Preparation of splenocytes

*Materials:*

R0: RPMI 1640 (no supplementation)
PBS-EDTA: PBS-EDTA: 1x DPBS [-] $CaCl_2$, [-] $MgCl_2$ (Gibco) + 5mM EDTA
R10: RPMI 1640, 2mM glutamine, 10% FCS and 100 U/ml penicillin, 100µg/ml streptomycin, 50µM 2-ME
Collagenase D solution (11 088 866 001, Roche)
DNase I solution (1 284 932, Roche)
70µm strainer (BD)
Red blood cell (RBC) lysis buffer 10x: 1.5M $NH_4Cl$, 100mM $NaHCO_3$, 5mM EDTA

Spleens were harvested from C57BL/6 mice using sterile instruments and aseptic technique. Enzymes were diluted in R0 to 1mg/ml collagenase and 200µg/ml DNase I. Each spleen was injected with 1ml of diluted enzymatic cocktail and incubated for 30 min at 37ºC. Spleens were filtered through a 70µm strainer and washed in PBS-EDTA. Cells were centrifuged 5 min at 300x g, 4ºC. Subsequently, cells were either filtered one more time, centrifuged and resuspended in R10 for *in vitro* activation assays, or subjected to RBC lysis.

To lyse RBC, the 10x buffer was diluted 1:10 in TC grade sterile water and 1ml was used per spleen, incubated 7 min on the bench. Afterwards, 20ml PBS-EDTA were added to the tube. Cells were centrifuged and filtered again through a 70µm strainer. Cells were either resuspended in FACS buffer and stained or resuspended in R10 and incubated *ex vivo* 37ºC, 5% $CO_2$ with either tumour-specific peptides for 72 h, or with 5µg/ml Brefeldin A (3 h) for intracellular staining. Incubated cells were filtered again after harvesting to prevent clogging of the cytometer, stained with their respective antibody panels and analysed by flow-cytometry.

### 2.11.5 *Ex vivo* restimulation of splenocytes

*Materials:*

R10: RPMI 1640, 2mM glutamine, 10% FCS and 100 U/ml penicillin, 100µg/ml streptomycin, 50µM 2-ME
24-well plates, TC treated (353047, Corning Incorporated)
SIINFEKL peptide (CRUK, London)
TRP-1 and TRP-2 peptides (Thermo Fisher Scientific)
Recombinant human HER2 (10004-H08H, SinoBiological)

Streck Cell Preservative (Alpha Laboratories)

| Peptide | Protein | MHC class restriction | Sequence |
|---|---|---|---|
| SIINFEKL | OVA $_{257-264}$ | I | SIINFEKL |
| TRP-1 a | TRP-1 | I | TWHRYHLLC |
| TRP-1 b | TRP-1 | I | TAYRYHLLC |
| TRP-1 IIa | TRP-1 | II | LFLMLFYQVWAQFPREC |
| TRP-1 IIb | TRP-1 | II | TCRPGWRGAACNQKILT |
| TRP-1 IIc | TRP-1 | II | RRLEDILGPDGNTPQFE |
| TRP-2 | TRP-2 $_{180-188}$ | I | SVYDFFVWLC |
| TRP-2 IIa | TRP-2 | II | GCKFGWTGPDCNRKKPA |
| TRP-2 IIb | TRP-2 | II | VLNKECCPPLGPEATNI |
| TRP-2 IIb | TRP-2 | II | KCTGNFAGYNCGGCKFG |

Table 2.11. Peptides, either MHC class I of class II-restricted, used for *ex vivo* stimulation of treated tumour bearing mice.

Splenocytes isolated from tumour-bearing mice on day 7 post-treatment with either vehicle, antibodies or conjugates were stained with 2μM CFSE. For CFSE labelling, cells were taken up in PBS containing diluted CFSE and incubated 10 min at 37ºC. Afterwards, 50% v/v FCS was added and cells were incubated for 1 min at RT. Cells were washed twice before incubating 1-2x $10^6$ splenocytes in R10 with 2-4x $10^5$ GM-CSF derived BMDC (harvested on day 4 of culture) and 0.03μM of the following: recombinant human HER2, SIINFEKL (OVA class I-restricted peptide), TRP-1 and TRP-2 peptides shown in Table 2.11. The bulk of cells were harvested after 72 h, stained for live/dead-cell discrimination (see section 2.7.1) and fixed in Streck. Subsequently, cells were stained for CD3, CD4, CD8 and the number of proliferating cells diluting CFSE was analysed by flow cytometry.

Alternatively, 1-2x$10^6$ splenocytes were stimulated with SIINFEKL only (final concentration 0.66μM) in the presence of 2-4x$10^5$ GM-CSF derived BMDC for 72 h. Cells were harvested, stained for live/dead-cell discrimination and then fixed with Streck. Cells were stained with H-2Kb-SIINFEKL pentamers (PE-labelled) and anti-CD8α antibodies and analysed by flow cytometry (for staining details see section 2.7.2).

## 2.12 Cell culture with human primary cells

### 2.12.1 Isolation of peripheral blood mononuclear cells (PBMCs)

*Materials:*

PBS: 1x DPBS [-] $CaCl_2$, [-] $MgCl_2$ (Gibco)
Heparin Sodium (5000 IU/ml, Wockhardt)
Lymphocyte separation medium (LSM 1077, GE Healthcare)
50ml centrifuge tubes (Greiner)

Leukocyte cones (product NC24) were ordered from NHS Blood and Transplant (HTA Research Licence 12321, NIBSC HuMAC ethical approval 18/02/AN). Blood from 1 cone was diluted 1:2 with PBS. 10IU heparin/ml were added to the tubes to prevent coagulation. 50ml tubes were pre-filled with 15ml lymphocyte separation medium. 30ml diluted blood was carefully overlaid on top of the separation medium, without mixing the two. Cells were centrifuged at 1200 rpm for 20 min RT without brake. The interphase of white blood cells (buffy coat) containing PBMCs was harvested. Cells were washed twice in PBS with centrifugation at 1200rpm, 10 min, with brake. Cells were either processed in assays or resuspended 5-10x $10^7$ cells in 900µl FCS, to which 100µl DMSO were added dropwise and cells were frozen at -80ºC until further use. Stored PBMCs were logged under HTA Research Licence no.12321 at NIBSC.

### 2.12.2 Enrichment of pan dendritic cells from PBMC

*Materials:*

Enrichment buffer: 1x DPBS [-] $CaCl_2$, [-] $MgCl_2$, 2% FCS, 1mM EDTA
EasySep® Human panDC Enrichment Kit (StemCell Technologies)
EasySep® "The Big Easy" Silver Magnet (StemCell Technologies)
15ml centrifuge tubes (Starstedt)

Dendritic cells (DC) were enriched from freshly isolated PBMCs using the human panDC enrichment kit (StemCell) following the manufacturer's protocol. Cells were stained in enrichment buffer at a density of 5x $10^7$ cells/ml with reagents from the kit. First, cells were incubated with 30µl/ml of sample Fc Blocker for 10 min RT. Then 50 µl/ml of sample Enrichment cocktail were added, and cells were incubated 30mi RT. Next, magnetic particles were added 100µl/ml of sample and incubated 10 min RT. If necessary, enrichment buffer was

added to a reach a total volume of 3.5 ml when starting with < 1x $10^8$ cells, or 6.5ml when starting with > 1x $10^8$ cells. The tube was placed in the EasySep Silver Magnet for 5 min. Subsequently, the tube was inverted while placed in the magnet to collect the enriched panDCs. To characterise the DC populations in the enriched PBMCs, cells were stained either with the myeloid DC (mDC) panel or the plasmacytoid DC (pDC) panel. The mDC panel contained antibodies against the following human markers: CD14 (FITC / Pacific Blue), HLA-DR (APC-CY7), CD3 (PerCP-Cy5.5), CD19 (PE-Cy7), BDCA-1 (PE) and BDCA-3 (APC). The pDC panel contained antibodies against BDCA-2 (FITC), HLA-DR (APC-CY7), CD3 (PerCP-Cy5.5), CD19 (PE-Cy7).

### 2.12.3 Generation of monocyte-derived dendritic cells from human PBMCs

*Materials:*

R10: RPMI 1640 containing 10% heat-inactivated FCS, glutamine, 100 U/ml penicillin/streptomycin and 50µM β-Mercaptoethanol
Human GM-CSF (200-04, Peprotech)
Human IL-4 (300-03, Peprotech)
Enrichment buffer: 1x DPBS [-] $CaCl_2$, [-] $MgCl_2$, 2% FCS, 1mM EDTA
EasySep Negative Selection, Human Monocyte Enrichment Kit (19059, StemCell)
EasySep® "The Big Easy" Silver Magnet (StemCell Technologies)
15ml centrifuge tubes (Starstedt)

For this protocol we used PBMCs isolated from cones as per protocol 2.12.1. Monocytes were enriched by negative selection using "The big easy" Silver EasySep Magnet and the EasySep Negative Selection, Human Monocyte Enrichment Kit as per manufacturer instructions. Enriched monocytes were washed once and resuspended in R10 at 3x $10^6$cells/ml. Cells were seeded in TC treated 6-well plates, 3ml per well and cultured in the presence of 20ng/ml human GM-CSF and IL-4. At day 2 and day 5, 0.5ml R10 containing sufficient GM-CSF and IL-4 to achieve a concentration of 20ng/ml in the entire volume were added to each well. Cells were used on day 6 or 7 from the start of culture.

## 2.13 *In vitro* immune activation assays

*Materials:*

R10: RPMI 1640, 2mM glutamine, 10% FCS and 100 U/ml penicillin, 100µg/ml streptomycin, 50µM 2-ME

96-well plates, TC-treated, flat bottom (353072, Corning)

DOTAP (Roche Diagnostics)

LL37 (Invivogen)

CpG various types (synthesised by Eurofin Genomics)

HEPES buffer: 20mM HEPES, 150mM NaCl, pH=7.1-7.3

The immune activation profile of nucleic acid endosomal TLR agonists used in this study (listed in Table 2.12), either soluble, conjugated or in the form of complexes were evaluated *in vitro* using either human PBMCs, enriched human panDCs, mouse splenocytes, mouse GM-CSF derived BMDCs or Flt3L-derived BMDCs. 1-5x $10^5$ cells were cultured in 100µl complete R10 in flat bottomed TC-treated 96-well plates. For GM-CSF differentiated BMDCs, R10 was also supplemented with 40ng/ml GM-CSF. Similarly, when Flt3L derived BMDCs were stimulated *in vitro*, R10 was supplemented with 100ng/ml Flt3L. TLR agonists or controls were diluted to 100µl /replicate with R10 before adding to the wells. The final volume in each well was kept constant at 200µl. Each dilution of TLR agonist, control or vehicle was performed in triplicate. When complexes were formed with either DOTAP (20µl/sample), LL37 synthetic peptide or fusion antibodies, these were added to CpG or polyUs21 in HEPES buffer, in a final volume of 80µl. The wells containing 100µl cells were topped up with 75µl R10 and 25µl of complexes were added per well. Plates were incubated overnight at 37ºC, 5% $CO_2$ in the tissue culture incubator. The following day, plates were frozen at -20ºC or -80ºC. The read-out of the assay was cytokine production (typically IL-6 and IL-12p40) measured by ELISA, as described in section 2.8.

| Name of Oligo | Modification | Backbone | Reported TLR specificity | Class of CpG | Sequence 5'→3' |
|---|---|---|---|---|---|
| CpG 1668 | - | PTO | Mouse | B | TCC ATG A**CG** TTC CTG ATG CT |
| CpG 1668-SH | 3'-C3-thiol | | | | |
| CpG 1668-C6-NH3 | 3'-C6-NH3 | | | | |
| CpG 1668-FITC | 3'-FITC | | | | |
| TAMRA CpG 1668-SH | 3'-C3-thiol, 5'-TAMRA | | | | |
| TAMRA CpG 1668-SH | 3'- C6-NH3, 5'-TAMRA | | | | |
| GpC 1668 | - | PTO | Negative control | - | TCC ATG A**GC** TTC CTG ATG CT |
| GpC 1668-SH | 3'-C3-thiol | | | | |
| CpG 2006 | - | PTO | Human | B | T**CG**T**CG**TTTTGT**CG**TTTTGT**CG**TT |
| CpG 2006-C6-NH3 | 3'-C6-NH3 | | | | |
| CpG 2216 | - | PTO / pde | Human | A | **GG**ggga**cg**a:t**cg**tcGGGGGG |
| CpG M362 | - | PTO | Human/murine | C | TCGTCGTCGTTC:GAACGACGTTGAT |
| CpG C274 | - | PTO | Human | C | T**CG**T**CG**AA**CG**TT**CG**AGATGAT |
| CpG C274-SH | 3'-C3-thiol | | | | |
| polyUs21 | - | PTO | Human/mouse TLR7 | N/A | UUUUUUUUUUUUUUUUUUUU |

Table 2.12. List of oligonucleotides, either endosomal TLR agonists. PTO – phosphorothioate backbone of bases are shown in capital letters; pde – phosphodiester backbone of bases shown in lower case; CpG or GpC motifs are highlighted in grey; CpG oligos are TLR9 agonists, while polyUs21 is a TLR7 agonist.

## 2.14 Calcein-release antibody-dependent cytotoxicity (ADCC) assays

*Materials:*

Targets: BT474 cells
Effectors: PBMC – isolated and frozen at -80
R0, R5, R10, no beta-mercaptoethanol
Assay plate: 96-well plates, TC-treated, flat bottom (353072, Corning)
Read-out plate: 96-well, sterile white bottomed plate (3917, Corning)
Flexiplates: Serocluster™ 96-well "U" bottom Plate, non-treated, vinyl (2797, Costar)
Calcein (65-0853-39, eBioscience)
10x Lysis buffer: Triton-X-100 9%
SpectraMax M5 96 well plate reader (Molecular Devices)

BT474 cells were used as targets cells. BT474 cells were labelled with 11.2µM calcein in R5 for 30 min at 37°C, then washed twice, resuspended at 1.6x $10^5$ cells/ml of R10 and 50µl were plated per well in the assay plate. Trastuzumab, conjugates or controls were diluted in R10 and added on top of BT474 cells in 50µl per well, in triplicates. Target cells were incubated with antibody, conjugate or control for 30 min at 37°C.

PBMCs were used for effector cells. Frozen PBMCs were rapidly thawed the day before the assay and rested overnight in R10. On the day of the assay, cells were washed twice in RPMI 1640 and resuspended in R10 and diluted to 2x $10^6$ cells/ml. 100µl PBMCs were plated per well to achieve an effector to target ratio of 25. For the spontaneous release controls, R10 was added to targets pre-incubated with Trastuzumab or conjugate. The plate was centrifuged for 1 min at 100x g and incubated at 37°C overnight. Each assay contained the following controls: no antibody control, antibody / conjugate induced spontaneous release, spontaneous release control (no antibody), maximum release control.

After 14-16 hours incubation of targets with effectors, 10ul of 10x lysis buffer were added to the wells containing the maximum release control. The plate was incubated for 30 min before centrifuging 5 min at 300x g. Cell supernatant was carefully collected and added to the read-out white bottomed plate. Fluorescence was read using excitation at 494nm and emission at 517nm in a spectrophotometer.

A dose response corrected for spontaneous calcein release from target cells was calculated:
% cytotoxicity = (experimental value – target cell spontaneous control) / (target cell maximal release – target cell spontaneous control).

## 2.15 Conjugate preparation

### 2.15.1 Stochastic conjugation using SMCC

*Materials:*

Trastuzumab or Herceptin (Roche)
UltraLeaf Human IgG1, κ isotype control (QA16A12, BioLegend)
CpG 1668-SH (CpG 1668-thiol) (synthesised by Eurofin Genomics)
CpG C274-SH (CpG C274-thiol) (synthesised by Eurofin Genomics)
Succinimidyl 4-(N-maleimidomethyl) cyclohexane-1-carboxylate (SMCC) (Thermo Scientific)
Dimethylsulfoxide, anhydrous (DMSO) (Life technologies)
Dithiothreitol (DTT) (Sigma)
Endotoxin Free (EF) water (Macherey Nagel)
Borate buffer 0.05M, 150mM NaCl, pH=8.9-9.1
Conjugation buffer: PBS + 2mM EDTA, pH=7.1-7.3
0.5ml Amicon Ultra centrifugal filter units with 100kDa cut-off (Merck-Millipore)
Micro Bio-Spin™ 6 Chromatography Columns (Bio-Rad)
ThermoMixer (Eppendorf)

Firstly, antibodies were concentrated when necessary to 9mg/ml in PBS, or for some samples in borate buffer using 0.5ml Amicon Ultra filters. A range of 250-1000µg were used per conjugation batch. SMCC was purchased as 1mg one-use tubes. One vial was reconstituted in 150µl DMSO. Then, SMCC was added to the antibody, 5-30 molar excess. Most experiments were performed with 10x molar excess of SMCC. The mixture was incubated at 22ºC for 1 h on the Thermoblock rotating at 300 rpm. Then, the samples were purified from excess unreacted SMCC by ultracentrifugation using 0.5ml Amicon Ultra filters. Samples were topped up to 500µl PBS and centrifuged at 14 000x g RT. The same was repeated 3x times but using conjugation buffer instead. Samples were recovered in a small volume (30-50µl) by inverting the column and centrifuging 2 min, 1000x g, RT.

While activating the antibody with SMCC, CpG-thiol was reduced in 50mM DTT (freshly reconstituted in EF water), for 1 h at 22ºC on the Thermoblock rotating at 300 rpm. Afterwards, CpG was purified from DTT using Micro Bio-Spin™ 6 Chromatography Columns. Just before use, columns were washed 3x times with 500µl conjugation buffer (centrifugation at 1000x g, 2 min, RT) follower by an additional centrifugation step to empty the column from excess

fluid. Then the column was moved into a clean tube and the CpG was purified and buffer exchanged by centrifuging 4 min at 1000x g, RT.

Reduced and purified CpG was added 3-10 molar excess to SMCC-activated antibody (depending on the experiment) and incubated for 2 h at 22ºC on the Thermoblock rotating at 300 rpm. Antibody-conjugates were purified from unreacted CpG by ultrafiltration using Amicon filters with 100kDa cut-off, by washing 5x times with PBS (10 min centrifugation at 14000x g, RT). Samples were recovered in a small volume, then the volume was topped with DPBS to 50µl if necessary. Finally, the conjugates were sterile filtered through a 0.22µm membrane and stored at 4ºC until further use.

### 2.15.2 Stochastic conjugation using CC

*Materials:*

Trastuzumab or Herceptin (Roche)
CpG 1668-SH (CpG 1668-thiol) (synthesised by Eurofin Genomics)
polyUs21
Cyanuric chloride (CC) (from Ram Abuknesha)
Borate buffer 0.05M, pH=9-9.5
Acetone (VWR)
Diethyl ether (Sigma)
Glass vials, 0.5ml (JG Finneran)
0.5ml Amicon Ultra centrifugal filter units with 100kDa cut-off (Merck-Millipore)
Spin-X centrifuge tube filter 0.22µm (8160 Costar)

Cyanuric chloride (CC) was weighed and dissolved at 2mg/ml in ice-cold acetone. 150µl of the solution was transferred into a glass vial and the acetone was evaporated by fumigating with $N_2$.

Either CpG or polyUs21 were diluted in borate buffer to 1mg/ml and added 300µg (300µl) to the glass vial with the dried CC. A tint magnetic flea was added to the glass tube and the solution was stirred at RT for 90 min. Afterwards, excess unreacted CC was removed using Diethyl ether. 2ml were added to the glass vial and mixed thoroughly. After 1-2 min the two phases separate and the upper one was removed. This was repeated 2x more times.

In a subsequent step, Trastuzumab was diluted to 2mg/ml in borate buffer and 150µl were added to the CC-activated CpG or polyUs21. This mixture was incubated at 37ºC overnight. The next day, samples were purified from unreacted oligo and buffered exchanged in DPBS

by ultrafiltration using 0.5ml Amicon Ultra filters. Samples were topped up to 500µl DPBS and centrifuged at 14000x g RT. This was repeated 5 times, then samples were recovered in a small volume in an Eppendorf by inverting the column and centrifuging for 2 min at 1000x g RT. Finally, samples were diluted to 50µl if necessary and sterile filtered through an 0.22µm membrane. CC conjugates were stored in the fridge until further use.

### 2.15.3 Site-specific conjugation of THIOMABs

*Materials:*

Tris(2-carboxyethyl)phosphine hydrochloride (TCEP) (C4706-10G, Sigma)
(L)-Dehydroascorbic acid (dhAA) (Sigma)
PBS-TH: 12mM sodium phosphates, 140mM sodium chloride, pH = 7.4
PBS: 1x DPBS [-] $CaCl_2$, [-] $MgCl_2$ (Gibco)
CpG 1668-$C_6$-$NH_3$ (amino-CpG) (synthesised by Eurofin Genomics)
DyLight488™-maleimide (Thermo Scientific)
Succinimidyl 4-(N-maleimidomethyl) cyclohexane-1-carboxylate (SMCC) (Thermo Scientific)
Dimethylsulfoxide, anhydrous (DMSO) (Life technologies)
0.5ml Amicon Ultra centrifugal filter units with 100kDa cut-off (Merck-Millipore)
VIVACON 500, 10kDA MWCO / 50kDA MWCO (Sartorius)
Spin-X centrifuge tube filter 0.22µm (8160 Costar)
Micro Bio-Spin™ 6 Chromatography Columns (Bio-Rad)
ThermoMixer (Eppendorf)

Trastuzumab-ThioMab (Tr-TH) with engineered cysteines (LC-V205C) as described in section 2.2.4 was further expressed in FS293 cells and purified on a protein A column (see section 2.10). Tr-TH was conjugated to CpG 1668 synthesised with a 3'-terminal amino (-$C_6$-$NH_3^+$) group (amino-CpG) using a modified version of the original ThioMab conjugation protocol (Junutula et al. 2008). Tr-TH (25µM) was reduced in 1mM TCEP for 1 h at 23ºC on the ThermoMixer rotating at 300 rpm. Next, the reduced antibody was purified from TCEP by ultrafiltration on VIVACON 10kDA columns (5x washes, 15 min centrifugation at 14 000x g). Reduced Tr-TH was recovered in a small volume (minimum concentration 6.73µM) by placing the column upside-down in a sterile Eppendorf and further subjected to accelerated re-oxidation with 400x molar excess of dhAA (freshly reconstituted in DMSO), for 3 h at 23ºC and mild agitation (300 rpm). Tr-TH was once more purified from dhAA by ultracentrifugation

using either VIVACON 50kDA columns or Amicon Ultra 100kDa columns (2x washes with PBS-TH, 10 min centrifugation at 14 000x g).

To generate CpG conjugates, amino-CpG was activated with SMCC. This conjugation was timed to the end of the antibody re-oxidation process. CpG was buffer exchanged in PBS-TH (150µM) and conjugated for 30 min at 23ºC with 20x molar excess of SMCC (1mg freshly reconstituted in 150µL DMSO), then purified from excess cross-linker using Micro Bio-Spin columns in PBS-TH. Then, the antibody was incubated with either 10x molar excess SMCC-activated amino-CpG or DyLight-488-maleimide overnight at 4ºC. The next morning, the conjugate was purified, and buffer exchanged into 1x PBS by ultracentrifugation using either VIVACON 50kDA cut-off or 0.5ml Amicon 100kDA cut-off. Conjugates were sterile filtered through a 0.22µm membrane and stored in the fridge until further use.

## 2.16 Conjugate characterization

### 2.16.1 Quantification of nucleic acid content of biochemical conjugates

*Materials:*

NanoDrop 1000 spectrophotometer (Thermo Scientific)
PBS: 1x DPBS [-] $CaCl_2$, [-] $MgCl_2$ (Gibco)
Trastuzumab
UltraLeaf Human IgG1, κ isotype control (QA16A12, BioLegend)
CpG various types (synthesised by Eurofin Genomics)
GpC 1668 (synthesised by Eurofin Genomics)
polyUs21 (synthesised by ThermoFisher Scientific)

A standard curve was generated containing 0.5µg/µl of human IgG1 antibody (either Trastuzumab or isotype control) in all samples and 1:5 dilution of the conjugated oligonucleotide (either CpG, GpC or polyUs21) from a starting concentration of 200ng/µl in PBS. Using the NanoDrop blanked with PBS absorbance at 260nm was measured in the SSDNA-33 channel for the standard curve in triplicates. Conjugate samples were first measured in a BCA assay to determine the antibody concentration, then were diluted to 0.5µg/µl antibody. Absorption at 260nm was measured for conjugates in duplicates. The concentration of nucleic acid was calculated against the standard curve.

### 2.16.2 Ellman's test

*Materials:*

Reaction buffer: DPBS (Ca and Mg free, Gibco) + 2mM EDTA, pH=7.1
Cysteine (44889, Thermo Scientific)
Ellman's reagent solution (DTNB) (22582, Thermo Fisher)
Assay plate: 96-well, round bottom plates (3799 Costar)
SpectraMax M5 96 well plate reader (Molecular Devices)

Cysteine was reconstituted in reaction buffer. A standard curve was built using 1:2 dilutions in reaction buffer starting from a top concentration of 1.5mM cysteine. In the assay plate, 125µl/well reaction buffer were added. Then, 25µL standard or appropriate diluted sample were added in triplicates. 1mM DTNB solution was added 50µL/well. The plate was incubated for 3-5 min at RT, then absorption at 412nm was measured using the plate reader. Cysteine concentration in the sample was measured against the standard curve.

### 2.16.3 SDS-PAGE analysis

*Materials:*

Gel electrophoresis chamber (Thermo Fischer Scientific)
Novex Wedge 4-20% Electrophoresis Gels, 1.5mm (Life Technologies)
Bolt™ 4-12% Bis-Tris Plus Gels, 10-well (Invitrogen)
Running buffer (10x): 250mM Tris base, 2.5 M glycine, 1%SDS (pH 8.3)
Non-Reducing Sample buffer (2x): 100nM Tris base, 4% SDS, 20% glycerol, spatula tip of bromophenol blue
β-Mercaptoethanol 50mM (2-ME) (Gibco)
ThermoMixer (Eppendorf)
ColorPlus prestained Protein Standard 10-230 kDa (NEB BioLabs)
Mark12 Unstained Standard 2.5–200 kDa (Invitrogen)
Ethidium Bromide (Fisher Scientific)
SYBR Gold Nucleic acid gel stain, 10 000x concentrate (Invitrogen)
SymplyBlue SafeStain (Invitrogen)
20% NaCl solution
Syngene PXi image analysis system (Syngene)
GeneTools software (Syngene)

Samples were normalized for antibody concentration and prepared in 2x non-reducing sample buffer. When sample were reduced prior to analysis, 20% 2-ME was added in the final volume and the sample was boiled for 5 min at 96ºC on the Thermoblock. To help with gel orientation, 5µl of ColorPlus pre-stained Protein Standard were consistently loaded on the first lane, followed by 7µl of Mark12 Unstained Standard and antibody samples. The gel was run at 25 min at 230V (constant voltage) in 1x running buffer diluted in ultrapure water.

To analyse oligonucleotide-containing biochemical conjugates, the gel was first stained for nucleic acid with 2µg/ml Ethidium Bromide in 50ml ultrapure water for 30 min. The gel was destained in 100ml ultrapure water for 2h, changing the water every 30 min. A subset of gels was stained instead with SYBR Gold diluted 1:10 000 in 50ml ultrapure water for 20 min and imaged without destaining.

When the gel contained fluorescently labelled antibodies or was stained for nucleic acid with either SYBR Gold or Ethidium bromide, the gel was imaged using the appropriate excitation/emission settings of the fluorophore on the Syngene PXi System. Subsequently, the

gel was washed for 10min in 100ml water and stained for protein for 1 h in 20ml of SymplyBlue SafeStain. The gel was either destained for 1 h in water or overnight in 2% NaCl and imaged using the Coomasie Blue channel with the Syngene PXi System. Images were analysed with GeneTools from Syngene software.

### 2.16.4 Size exclusion chromatography (HPLC)

*Materials:*

TSK G4000SWXL (7.8 x 300 mm, 8µm pores) column (TOSOH, code 808542)
Guard column TSK gel Guard SW XL (TOSOH, product code 808543)
Mobile Phase: 0.2 M Sodium Phosphate, 0.1 M Sodium Sulphate pH 6.0, filtered (0.22 µm), degassed
Tr and Tr-MCC-GpC conjugate
Dionex Ultimate 3000 (Thermo Fisher) controlled by Chromeleon 7.2

10µg of either Tr or Tr-MCC-GpC were diluted in mobile phase and left at 6°C for 30 min to allow equilibration between monomeric and dimeric material. The column was equilibrated in mobile phase and maintained at 25ºC and constant pressure (14 bar). 10µl water were run to establish baseline. Then, prediluted analytes were injected. Flow rate was 0.4ml/min and run time was 60 min.

### 2.16.5 Limulus Amoebocyte Lysate (LAL) assay

To test for bacterial endotoxins in our antibody/conjugate preparations, the gel-clot method of the LAL assay was performed using Endosafe lysate from Charles River Laboratories and the 3rd WHO International Standard (10/178). The semi-quantitative assay was performed following the protocol described as Method B in the European Pharmacopoeia Section 2.6.14. Concentrated samples were diluted to either 0.4mg/ml or 1:20 prior to testing. LAL assays were performed by Janet Sutherland, Trusha Desai or Sophie Myhill NIBSC.

## 2.17 Complex formation and visualisation

### 2.17.1 Complex formation

*Materials:*

1x DPBS [-] $CaCl_2$, [-] $MgCl_2$ (Gibco)
HEPES buffer: 20mM HEPES, 150mM NaCl, pH=7.1-7.3
LL37 (Invivogen)
CpG 1668 (synthesised by Eurofin Genomics)
polyUs21 - (synthesised by ThermoFisher Scientific)
Trastuzumab-linker-LL37, Isotype-H3-LL37

For complex formation, Trastuzumab-LL37 or Isotype-LL37 were diluted in PBS or HEPES buffer for some experiments at 0.6-1mg/ml. Endosomal TLR agonist (CpG or polyUs21), was also diluted in either PBS or HEPES buffer at 0.2-0.5mg/ml. The two dilutions were mixed together to achieve 1:1 oligo to LL37 molar ratio and incubated for 2-10 min RT. For some experiments, the molar ratio of oligo to LL37 moiety varied from 1:2 to 1:20. When further dilutions were required, complexes were subsequently diluted in HEPES, DPBS or R10.

### 2.17.2 Visualising complexes

*Materials:*

1x DPBS [-] $CaCl_2$, [-] $MgCl_2$ (Gibco)
CpG 1668 (synthesised by Eurofin Genomics)
polyUs21 - (synthesised by ThermoFisher Scientific)
Trastuzumab-H3-LL37
96-well U-plates, sterile, non-TC treated (3788, Costar)
SpectraMax M5 96 well plate reader (Molecular Devices)

Complex formation was visualised with the naked eye as clouding of the solution upon addition of CpG or polyUs21 to Tr-H3-LL37 or Iso-H3-LL37.

Complexes were formed as described in 2.17.1 and plated in triplicates in 96-well clear plates. Tr-H3-LL37, CpG and PBS were plated as well. Absorbance at 405nm and 600nm was measured at 1, 5, 10 and 30 min after complex formation.

## 2.18 B16 HER2 pseudo-metastasis mouse model

### 2.18.1 Mice

Seven-eight weeks old female C57BL/6 mice weighing a minimum 18g were obtained from Envigo and were acclimated in the Mouse Facility at NIBSC for at least 5 days before commencing experiments. All experiments were conducted in accordance to the Animal Scientific Procedures Act 1986 under the project license 70/8831. Animals were randomly allocated into treatment groups. NIBSC personnel administering the treatment were blinded to allocation during experiments or tissue harvest.

### 2.18.2 Preparation of tumour cells

*Materials:*

PBS: 1x DPBS [-] $CaCl_2$, [-] $MgCl_2$ (Gibco)
PBS-EDTA: 1x DPBS [-] $CaCl_2$, [-] $MgCl_2$ (Gibco) + 5mM EDTA
R10: RPMI 1640, 2mM glutamine, 10% FCS and 100U/ml penicillin, 100µg/ml streptomycin, 50µM 2-ME

B16 and B16-derived tumour cell lines were seeded the day before *in vivo* experiments at 1.5-2x $10^6$ cells per 145$cm^2$ TC dishes in complete R10. The next day, cells were detached using PBS-EDTA and centrifuged 300x g, 5 min, 4ºC. Cells were resuspended in ice-cold PBS, counted using Tripan Blue exclusion, adjusted to the concentration required for the respective cell line and experiment and injected intravenously (IV) in mice within 40 min from harvesting.

### 2.18.3 Tumour growth profiles

*Materials:*

PBS: 1x DPBS [-] CaCl2, [-] MgCl2 (Gibco)
Fekete solution: 70% EtOH, 3.7% PFA, 0.75M glacial acetic acid

Mice received on day 0 intravenous injections (IV) in the tail vein with 0.5-0.9x $10^5$ B16 and B16-derived cell lines in 150µl PBS. IV injections were performed by Alan Haynes, NIBSC. To asses tumour burden, *in vivo* imaging was performed at different time-points (see below in section 2.18.5). 15-18 days after tumour inoculation, mice were euthanized with 200mg/kg Pentobarbital by intraperitoneal (IP) route; for tumour growth profile, the lungs were harvested, washed in PBS and imaged using the IVIS Spectrum. Then, lungs placed in Fekete

solution and fixed for at least 24 h. Subsequently, lungs were weighed, and pulmonary nodules were counted under Olympus S2X10 microscope (DF PLAPO 1x-4 lens) at zoom magnification setting 0.63. Representative images of the lungs were acquired using Olympus SC30 camera connected to an Olympus S2X10 microscope (DF PLAPO 1x-4 lens) at zoom magnification setting 0.63 and processed with CellSens Entry 1.5 software.

### 2.18.4 *In vivo* imaging

*Materials:*

In Vivo Imaging System - IVIS Spectrum® (Perkin Elmer)
Living Image® 4.7.2 (Caliper Life Sciences)
XenoLight D-Luciferin, Potassium Salt (PerkinElmer)

Mice were weighed and subsequently injected IP with 150mg/kg XenoLight D-Luciferin substrate by NIBSC animal technicians. After 10 min, mice were imaged under anaesthesia with 2% isoflurane using IVIS Spectrum® (Perkin Elmer) and the Living Image® 4.7.2 (Caliper Life Sciences) software. Acquisition was performed using a 22.5cm field of view (FOV) and excitation and emission filters open. A group of mice with expected high signal was imaged first to optimize additional acquisition settings (time, lens aperture (F), binning). Acquisition parameters were optimized for at the beginning of each imaging timepoint and kept constant among groups of mice. A minimum of two luciferase-free mice (injected with B16 tumours) were included in each experiment. In some experiments, mice were dissected, major organs harvested and imaged *ex vivo* to verify the source of the bioluminescent signal. Data were analysed using Living Image software. Regions of interest (ROI) of 2.647cm diameter were placed to measure luminesce signal in the thorax area. Data were expressed as luminescence intensity in the ROI area (photons/sec). To compare the growth profiles, the CGGC permutation test (http://bioinf.wehi.edu.au/software/compareCurves) with 10 000 permutations was used (Elso et al. 2004).

### 2.18.5 Treatment with conjugates and complexes

*One-dose regimen*

Mice were injected IV, on day -11, with 0.6x $10^5$ B14.3 Luc HER2 bright cells in 100µl PBS. Ten days later (day -1), mice were injected IP with 150mg/kg XenoLight D-Luciferin and imaged 10 min later using the IVIS System to confirm tumour burden. Tumour-bearing mice were treated IV on day 0 with Trastuzumab or Trastuzumab-derived conjugates and complexes. Each treatment sample contained 270pmoles of antibody per mouse in 100µl PBS.

Pyrogen-free materials were used for all dilutions. Blood samples were harvested at day 1, 4 and 7 post-treatment. Blood was allowed to clot for 30 min at RT, then centrifuged for 10 min, 4ºC, 1500x g. Serum was collected and stored in sterile conditions at -80ºC until assayed.

*Three-dose regimen*

Mice received either 0.5-0.6x $10^5$ B16 cells or 0-9x $10^5$ B14.3 Luc HER2 bright cells (clone H2) IV in 150µl PBS (day 0). Mice were treated with 270pmoles of either isotype control, Trastuzumab, conjugates or complexes on days 4, 8 and 11. Blood samples were harvested on day 1 (pre-treatment), day 14 (day 3 post-treatment) and day 18 (day 7 post-treatment). *In vivo* imaging was performed on days 3, 7, 10, 15 and 18 post-tumour inoculation. Mice were culled on day 18, or earlier if starting to develop symptoms. Lungs were harvested and imaged *ex vivo* using IVIS. Subsequently, lungs were fixed in Fekete solution for minimum 24 h, then weighed and tumour nodules counted.

## 2.19 Statistical analysis

GraphPad Prism was used to depict data and for statistical analyses. Data are shown as mean ± standard deviation (SD) or as mean ± standard error of mean (SEM) in the case of tumour growth profiles. Luminescence intensity data from *in vivo* imaging experiments was analysed using the CGGC test (Elso et al. 2004) online platform at 10 000 permutations: http://bioinf.wehi.edu.au/software/compareCurves/. The rest of data was analysed in GraphPad Prism 8.1 (GraphPad; La Jolla, CA, USA), using appropriate statistical tests for each data set, as described separately for each figure. All t tests were two-tailed. Differences were considered significant when $p \leq 0.05$. Stars of significance are: *p<0.05, **p<0.01, ***p<0.001, ****p<0.0001.

# Chapter 3 - Results

## Developing a tumour model using human HER2-transgenic cell lines in immunocompetent mice

# Chapter 3: Developing a tumour model using human HER2-transgenic cell lines in immunocompetent mice

## Introduction

For our proof-of-concept study, a relevant mouse model is required. We work with the clinically available anti-human HER2 antibody Trastuzumab and investigate whether it is suitable for delivery of nucleic acid adjuvants such as CpG to the tumour tissue. Trastuzumab is a recombinant antibody recognising human HER2 and does not bind to the mouse homolog (Massicano, Marquez-Nostra, and Lapi 2018; Park et al. 2017). Our aim was to investigate Trastuzumab-mediated delivery of adjuvants to the tumour tissue in a HER2-expressing tumour mouse model. Since endosomal TLR agonists such as CpG promote T cell and B cell responses, we required an immunocompetent mouse model.

Transplantable tumour mouse models have been extensively employed in testing novel immunotherapies and demonstrated their use, especially in proof-of-principle studies (Dranoff 2011). Since transplantable tumour models allow for fast experimental turn-over and cell modifications with reporters such as luciferase or model antigens such as ovalbumin (OVA) (Dranoff 2011), we decided to use a transplantable mouse model for our initial experiments.

Our lab has experience in working with the B16 pseudo-metastasis mouse model. This model involves injecting B16 melanoma cells IV in syngeneic C57/BL6 mice to generate pulmonary (pseudo-metastatic) nodules. Moreover, a B16-OVA cell line was developed in our lab as well and has previously proven useful when investigating OVA antigen-specific T cell responses (Kreutz et al. 2012; Rajagopal et al. 2010). An important characteristic of B16 tumours is that they are poorly immunogenic. These tumours are void of T cell infiltration and only partially responsive to immune checkpoint blockade therapy, rendering them a relevant model for evaluating novel immunotherapeutic approaches (Dranoff 2011; Lechner et al. 2013). Moreover, our lab has shown that B16 cells do no express TLR7 or TLR9 themselves (Appendix I), making them useful for testing TLR7 or TLR9 agonist-based immunotherapies.

Considering the advantages of the model and our experience with it, we used the B16 melanoma cells as a starting point in developing a human-HER2 tumour model in immunocompetent mice.

## 3.1 Overview of workflow

Human HER2 transgenic B16 cells have been previously described and used to test immunotherapies (Wang et al. 2012). However, these cells were generated by transfection, as we wished to work with transduced cells and avoid the use of antibiotics to maintain transgene expression.

We established a pipeline to generate and characterise human HER2-transgenic B16 melanoma monoclonal cell lines (Fig. 3.1). We began with the production of a lentivirus encoding the sequence of human HER2. Then, 3 different cell lines were transduced for human HER2 expression: B16 melanoma cell line, B14.3 cells which are B16 cells expressing OVA-GFP and B14.3 luciferase (Luc) cells which express both OVA-GFP and Firefly luciferase in an independent manner. Transduced cells were stained with Trastuzumab to evaluate human HER2 expression. HER2 positive single cells were isolated by fluorescence activated cellular sorting (FACS) and expanded. 7-14 monoclonal cell lines were derived from each of the three parental cell lines, and human HER2 expression was confirmed by flow cytometry. Then, specific clones were chosen for further tests based on their human HER2 expression levels. Human HER2 positive daughter cell lines derived from B14.3 Luc cells were also evaluated for luciferase expression using an *in vitro* bioluminescence assay. B16 HER2 and B14.3 Luc HER2 monoclonal cell lines with suitable *in vitro* profiles were further assessed for their ability to generate pulmonary tumours upon IV administration in C57/BL6 mice (Fig. 3.1).

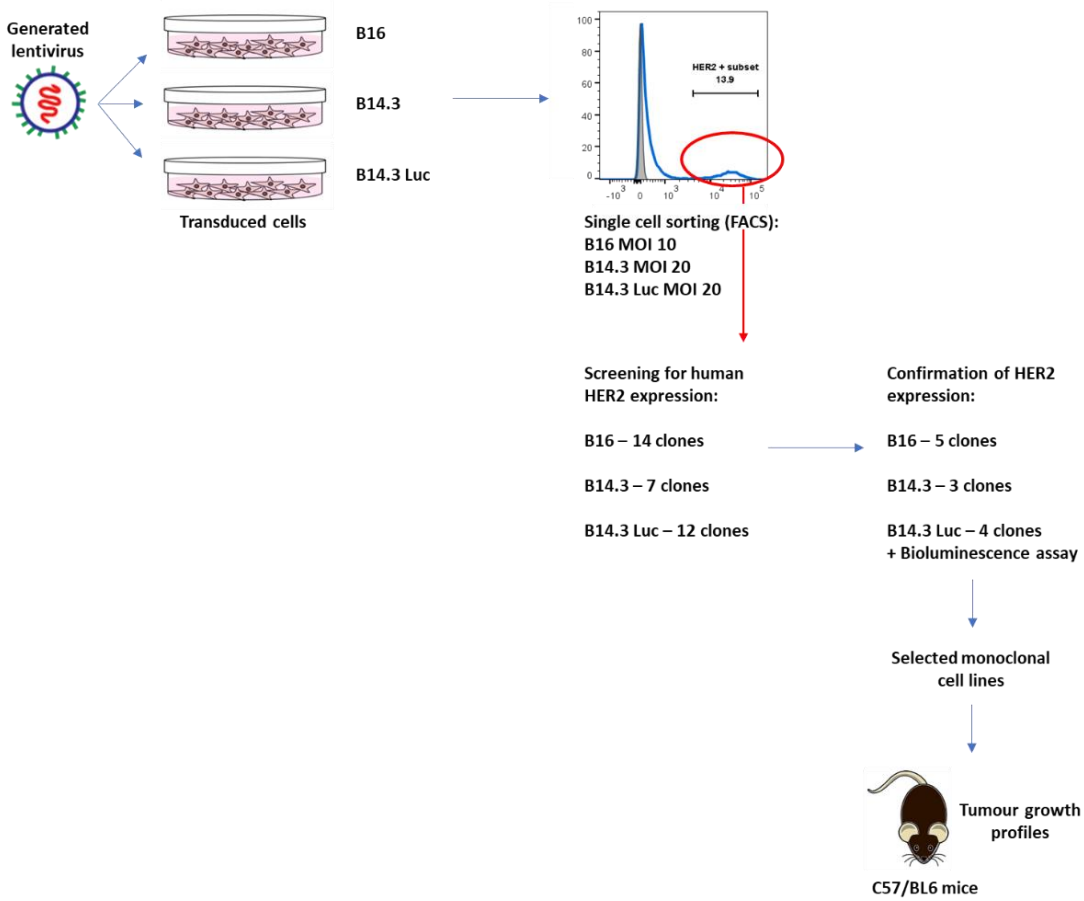


**Figure 3.1.** Overview of workflow for the generation and characterisation of immunocompetent mouse model using a human HER2-transgenic murine melanoma cell line. B14.3 – B16 OVA-GFP transgenic cells; Luc – Firefly luciferase.

## 3.2 Lentivirus production

To generate a lentivirus encoding human HER2, we began by cloning the sequence of human HER2 from the pcDNA3 plasmid from Addgene into the pSIN-SFFV-transgene plasmid (sequences in appendices A and B, respectively). The pSIN-SFFV lentiviral vector had no restriction sites suitable for the insertion of the human HER2 transgene. Therefore, we used the restriction enzyme independent Polymerase Incomplete Primer Extension (PIPE) cloning technique. Primers were designed with overlapping 5'-overhangs for amplification of HER2 sequence and 2 backbone fragments of pSIN-SFFV fragment. PCR amplified fragments were purified and transformed in competent *E. coli* cells (Fig. 3.2). Then single bacterial colonies were expanded, and plasmid minipreparations were generated. The introduced sequence of human HER2 contained 2 EcoRI and 2 KpnI restriction enzyme sites, which are not present in the pSIN-SFFV vector. Plasmid preparations were digested separately with each of these enzymes and run on a 1% agarose gel to identify plasmid containing the HER2 insert (Fig. 3.3). These were sequenced (Eurofin Genomics) to confirm the correct position of human HER2 in the plasmid and identify base pair mutations. One plasmid preparation was stored as glycerol stock and used in all subsequent experiments.

The lentivirus encoding human HER2 was produced by transient co-transfection of HEK293T cells with plasmids pSIN-SFFV-HER2, p8.91 (2nd generation HIV-derived packaging plasmid, Plasmid Factory) and pMD.G (encoding VSV-G envelope, Plasmid Factory). Virus was purified from cell supernatant by ultracentrifugation, then lentivirus titre was determined. For lentivirus quantification, HEK293T cells were transduced with the purified lentivirus, and the number of integrated lentiviral copies in extracted genomic DNA was determined by qPCR. The titre of our lentivirus preparation was $2.79 \times 10^7$ IU/ml, and this batch was sufficient to transduce all three cell lines.

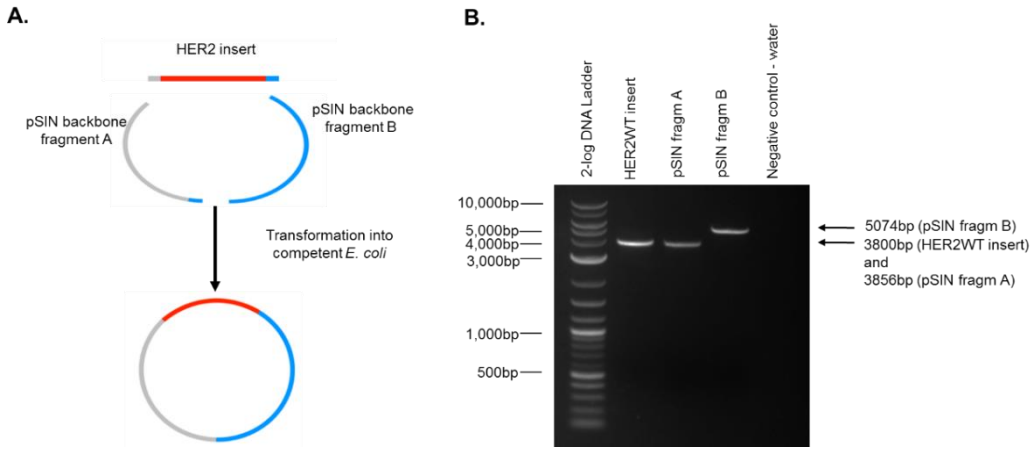


**Figure 3.2** PIPE cloning to introduce human HER2 sequence in the pSIN-SFFV plasmid for lentiviral vector production. **A.** Schematic representation of PIPE cloning strategy to introduce the sequence of human HER2 in the pSIN-SFFV plasmid. **B.** 1% agarose gel electrophoresis of purified PCR amplified fragments transformed in XL-1 blue competent bacteria for the generation of pSIN-SFFV-HER2WT plasmid. WT – wild type.

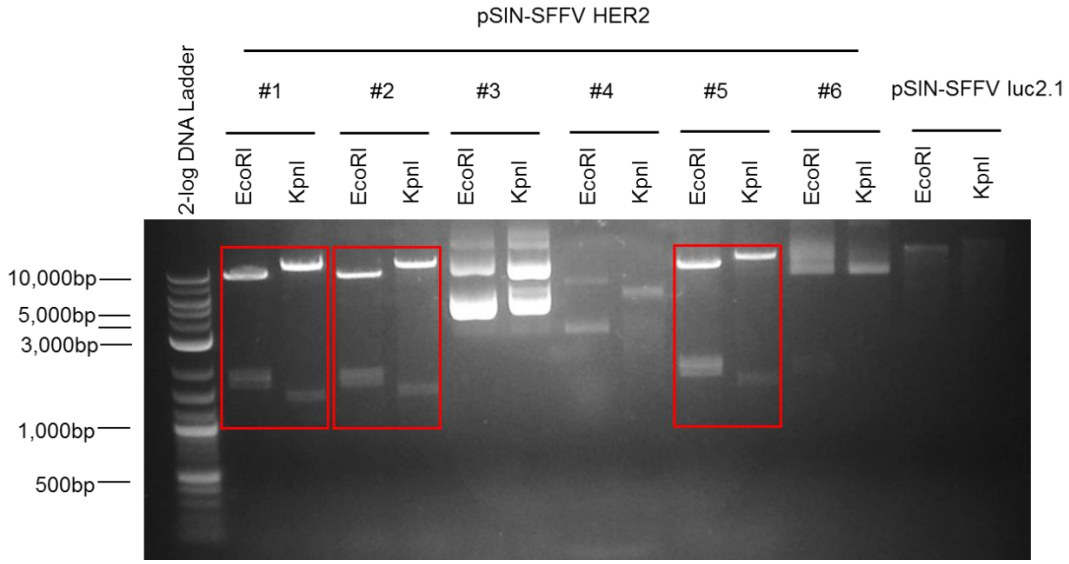


**Figure 3.3.** Representative 1% agarose gel electrophoresis of single bacterial colony plasmid minipreparations of pSIN-SFFV-HER2WT. Plasmid preparations were separately digested with EcoRI or KpnI and run on a gel. Highlighted in red boxes are plasmids with bands of the expected size (9266bp, 1816bp and 1622bp for EcoRI; 11321bp and 1383bp for KpnI), signifying the HER2 insert.

### 3.3 Generation of HER2 positive B16 cell lines

B16, B14.3 and B14.3 Luc melanoma cell lines were transduced with the produced lentivirus encoding human HER2 at MOI 1, MOI 10 and MOI 20. At day 7 post-transduction, cells were stained with Trastuzumab to detect HER2 expression and analysed by flow cytometry. Transduction efficiency curves showed an approximate proportional relation between number of lentivirus particles per cell and human HER2 florescent signal for all transduced cell lines. Transduction at MOI 1 only resulted in less than 1% of HER2 positive cells, while transduction at MOI 10, generated 6.5-8.3% HER2 positive cells. Increasing the MOI to 20 achieved even higher percentages (11.2-13.4%) of HER2 positive cells for all three B16 cell lines (Fig. 3.4).

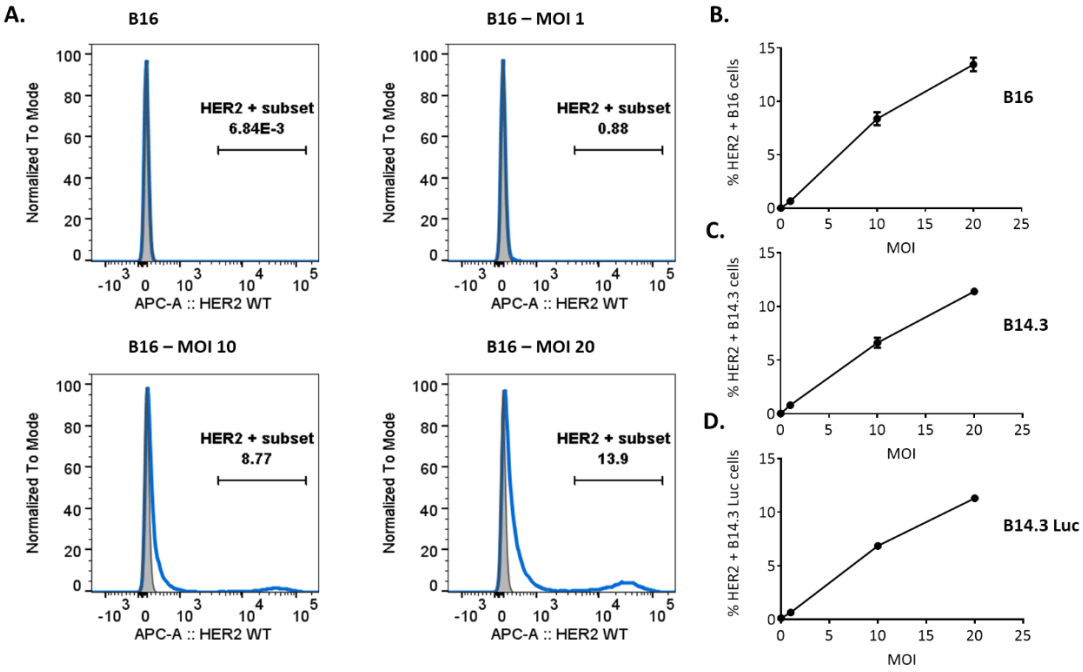


**Figure 3.4.** Evaluating HER2 expression on transduced cells. Cells were transduced with lentivirus encoding human HER2 at different MOI and then stained for human HER2 expression and analysed by flow cytometry. **A** Representative flow cytometry data of B16 cells transduced at different MOI and stained either for HER2 expression with Trastuzumab (blue) or with isotype control (solid grey histograms). Data is representative of three independent acquisitions by flow cytometry. **B-D** Percent of HER2 positive cells is shown as mean ±SD in relation to MOI for B16 cells (B), B14.3 cells (C), and B14.3 Luc cells(D). Data was pooled from 2 independent experiments and shown as mean ± SD. WT = wild type.

As illustrated in Figure 3.1, B16 cells transduced at MOI 10, B14.3 cells MOI 20 and B14.3 Luc cells MOI 20 were used for sorting of single human HER2 positive cells by FACS. These single cell clones were expanded and human HER2 expression was confirmed by flow cytometry. Fluorescence intensity data was converted to resolution metric (R) to describe the degree of separation between Trastuzumab-stained and isotype control-stained cells. The metric corrects for the spread of each population and allows pooling of data from experiments acquired on separate days (Erdbrugger et al. 2014; Yoo et al. 2015). Evaluated cells lines showed highly variable human HER2 expression levels, as exemplified for B14.3 Luc HER2 cells (Fig. 3.5 A). Hence, cells with higher HER2 expression, with $R_D$ around 2 were named HER2 bright, while the ones with lower expression levels were labelled HER2 dim (Fig. 3.5 B).

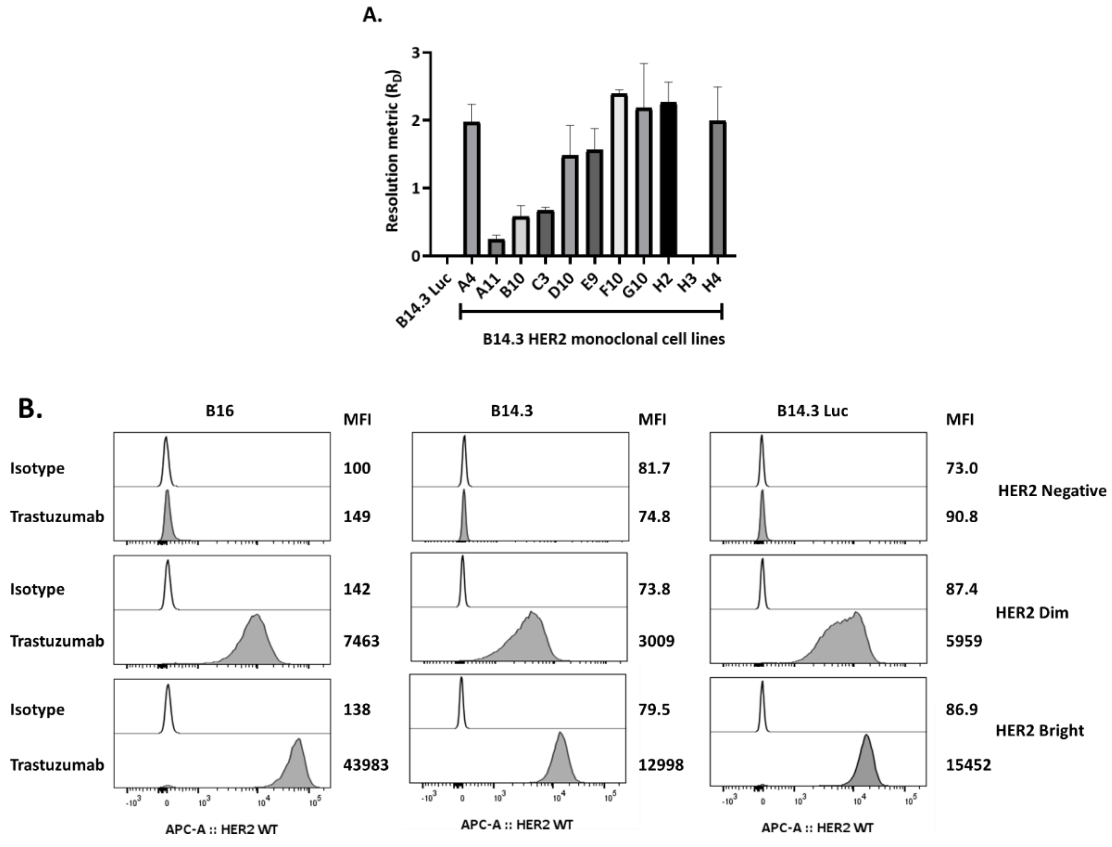


**Figure 3.5.** Evaluating surface expression of human HER2 of generated monoclonal cell lines. Cells were stained with either Trastuzumab or Isotype control, followed by an APC-conjugated secondary antibody and analysis by flow cytometry. **A**. Resolution metric ($R_D$) of B14.3 Luc HER2 monoclonal cell lines. Resolution metric ($R_D$) is calculated as the MFI of Trastuzumab minus the MFI of the isotype control corrected by the sum of standard deviations of the analysed populations in the APC channel. Data is shown as mean±SD of 2 independent experiments. **B.** Representative flow cytometry histograms and MFI of cell lines considered HER2 dim or HER2 bright. Cells were stained with either isotype control (white) or Trastuzumab (grey). Data is representative of 2 independent experiments for B14.3 cells and minimum 3 independent experiments for B16 and B14.3 Luc cells.

For the purposes of the project, we preferred HER2 bright cells for *in vivo* work, to enable efficient concentration of Tr and Tr-derived conjugates and complexes at the tumour tissue. Therefore, we focused our efforts in characterising HER2 bright monoclonal cell lines and only included one HER2 dim cell line for comparison in selected downstream assays.

Next, we verified that human HER2 transduced B14.3 and B14.3 Luc cells maintain OVA-GFP expression of the parent cell lines by flow cytometry (Fig. 3.6 A, B, respectively). We also verified luciferase activity of human HER2 bright B14.3 Luc monoclonal cell lines *in vitro* (Fig. 3.6 C). Members of the retroviral family have distinct patterns of preferred integration sites (Gabriel, Schmidt, and von Kalle 2012). These preferred integration sites might be reused upon subsequent transduction with the same or even similar virus encoding other transgenes, changing expression levels of the previously introduced transgenes. The OVA-GFP transgene was introduced using a retrovirus into B16 cells by Dr. Sandra S. Diebold, to generate the B14.3 monoclonal cell line. Upon subsequent transduction with the HER2 encoding lentivirus, most B14.3 HER2 single cell clones showed comparable OVA-GFP signal relative to parental cells (Fig. 3.6 A). The same was observed for B14.3 Luc HER2 cells, with one out of 10 cell lines showing a clear drop in OVA-GFP signal (Fig. 3.6 B). In terms of Firefly luciferase, this transgene was introduced via lentiviral transduction. Relative to the parental cell line, some of the B14.3 Luc HER2 single cell clones with unaltered GFP signal, such as F10 and G10 showed reduced (F10) or even abolished (G10) luciferase activity, as measured by luminescence intensity in an *in vitro* assay (Fig. 3.6 C). Together, these data confirm that upon subsequent transduction, previously introduced transgenes may dampen or lose expression and monoclonal cell lines must be verified in this respect to identify suitable clones.

To establish how human HER2 expression by lentivirus integration changes the tumour growth profile of B16 cells, we went on to evaluate B16 HER2 bright (clone E5) and B16 HER2 dim (clone H5) *in vivo*. As we wished to make use of the luciferase reporter as well as the OVA-GFP antigen, we chose to further evaluate B14.3 Luc HER2 bright cells and not B14.3 HER2 cells in mice. In terms of B14.3 Luc HER2 cells, monoclonal cell lines A4, H2 and H4 expressed high levels of human HER2 and OVA-GFP, as well as similar levels of luminescence activity to their parental cell line and were chosen for further evaluation in mice.

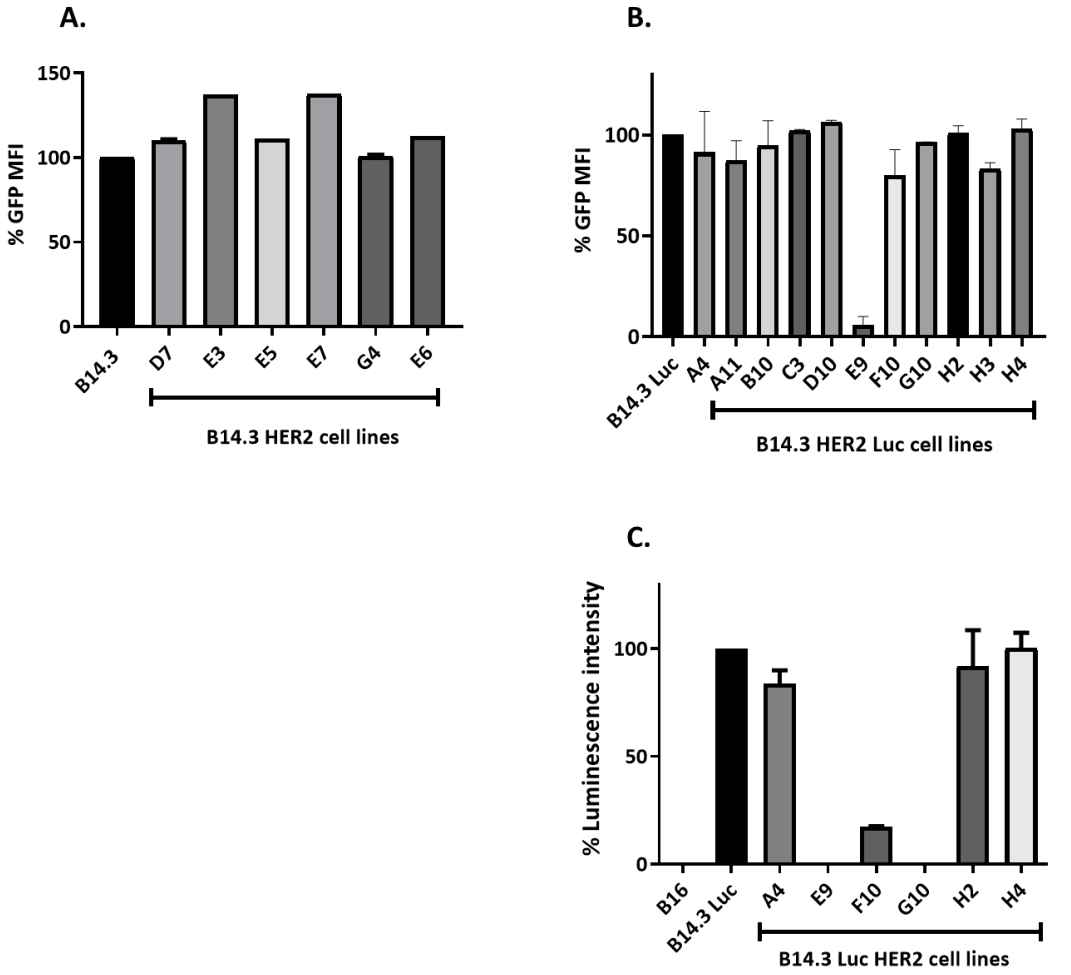


**Figure 3.6.** Evaluating maintenance of OVA-GFP and luciferase transgenes in B14.3 and B14.3 Luc human HER2 expressing monoclonal cell lines. For OVA-GFP expression, cells were analysed by flow cytometry. **A.** OVA-GFP MFI of daughter HER2 cell lines was expressed as percent of OVA-GFP MFI of the B14.3 parental cell line. Data representative of one experiment, except for B14.3 and derived clones D7, E5 and G4, which were tested twice (mean ± SD). **B.** OVA-GFP MFI of daughter HER2 cell lines was expressed as percentage of the OVA-GFP MFI of parental B14.3 Luc cells. Data is shown as mean±SD of 2 independent experiments. **C.** Evaluating luciferase activity of B14.3 Luc HER2 monoclonal cell lines. Cells were plated in triplicates and incubated with an equal volume of luciferase substrate. Luminescence intensity was measured as corrected counts per second and expressed relative to the luminescence levels of the parental B14.3 Luc cells, which was set to 100%. Mean ± SD of 3 technical replicates. Data for B16, B14.3 Luc and daughter cell lines H2 and H4 were pooled from 2 independent experiments.

## 3.4 *In vivo* profile of tumours generated with B16 HER2 cells

### 3.4.1. Growth kinetics of B16 HER2 tumours compared to B16 tumours

To establish the growth profile of B16 HER2 cells in the pseudo-metastasis model, mice were injected IV with 5x $10^5$ of either B16, B16 HER2 dim (clone H5) or B16 HER2 bright (clone E5) cells. Mice were culled 15 days later, and lung tissue was collected and weighed (Fig. 3.7 A). Afterwards, lungs were fixed for minimum 12 h in Fekete solution, transferred to PBS and lung nodules were counted. Mice injected with B16 cells showed over 200 lung tumour nodules at day 15 endpoint (Fig. 3.7 C). This significant tumour burden almost doubled the weight of lungs as compared to tumour free lungs of age-matched mice (Fig. 3.7 D). In comparison, B16 HER2 bright cells generated fewer tumour numbers with high variability between animals. Lungs with B16 HER2 bright tumours still weighed significantly more ($p<0.05$) than tumour free lungs, although the difference was not as striking. Notably, 2 mice that received B16 HER2 dim cells only developed 2-3 tumour nodules (Fig. 3.7 C), and this minimal tumour burden did not increase the weight of the lungs over tumour free control (Fig. 3.7 C). In terms of morphology, B16 HER2 bright tumours were of lighter colour, indicative of less melanin content, than B16 tumours, but were similar to these in terms of nodules size and distribution. B16 HER2 dim tumour nodules, however, were both paler and larger (Fig. 3.7 B). Together, these data show that different human HER2 expressing monoclonal cell lines generate tumours with distinct profiles.

Although lower than for B16 cells, B16 HER2 bright cells also generated relatively high tumour burden in mice. The growth profile was much more favourable than for B16 HER2 dim cells. Therefore, we continued to use B16 HER2 cells for future experiments.

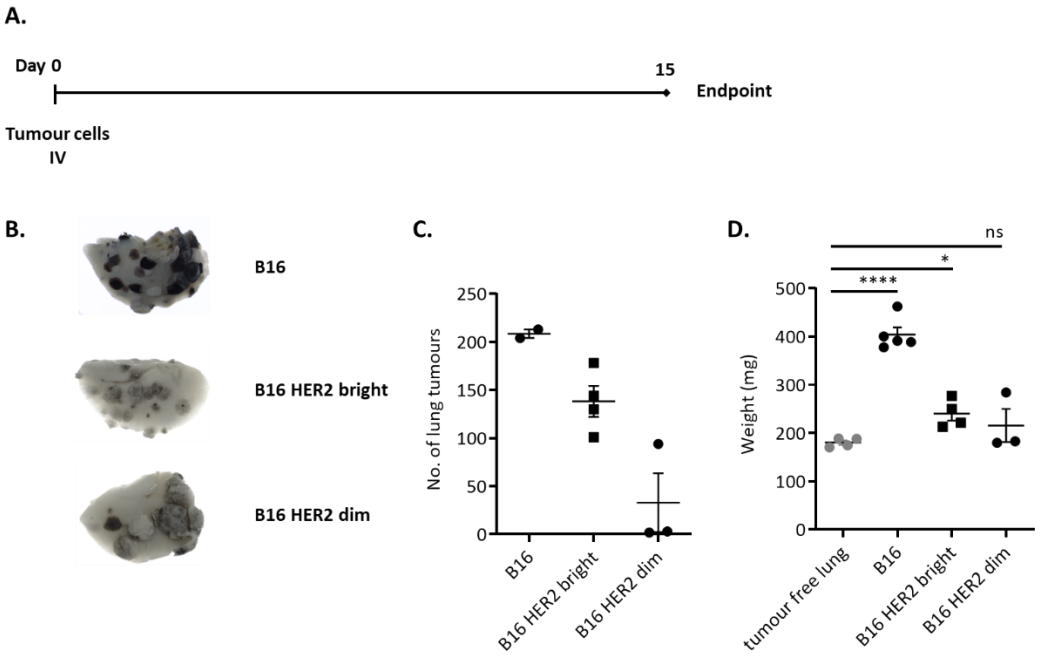


**Figure 3.7.** Tumour growth profiles of B16 HER2 cells. **A.** Mice were injected with 5x $10^5$ tumour cells. Tumour burden was measured 15 days later. **B.** Representative images of lungs with B16 and B16 HER2 bright and dim tumours after fixation in Fekete solution. Images of B16 and B16 HER2 bright are representative of three independent experiments. Tumour burden measured as weight of lungs (**B**) or as number of tumour nodules (**C**) counted after fixing the lungs in Fekete solution. Data from one experiment with minimum n=3. Each symbol represents a mouse, with mean ± SEM depicted by lines in **C** and **D**. Data for the B16 group in **D** was collected in two independent experiments. **D.** Data was analysed using Welch's t test.

### 3.4.2 Response of B16 HER2 bright tumours to treatment with Trastuzumab

To investigate the proliferation of B16 HER2 bright cells (clone E5) treated with Trastuzumab (Tr) *in vitro*, MTS assays were performed as previously described (Zhang et al. 2011). Multiple studies illustrated that HER2 signalling drives tumour growth and proliferation of HER2 overexpressing human tumour cell lines, which can be stunted by treatment with Trastuzumab (Mittendorf et al. 2010; Yu and Hung 2000; Milano et al. 2010). This, however, is unknown for ectopic expression of the human HER2 transgene in mouse tumour cell lines. In line with the publications mentioned above, we replicated *in vitro* proliferation assays showing that HER2 overexpressing human tumour cell lines such as BT474 and OE19 show a dose-dependent decrease in proliferation upon treatment with Trastuzumab, but not with isotype control (Fig. 3.8 A, B). Impairment of tumour growth was observed for recombinant Trastuzumab produced in our laboratory and the clinical-grade Herceptin®. No change in proliferation was observed for the MDA-MB-231 cell line, which expresses HER2 at minimal levels (Fig. 3.8 C) or with B16 cells, which are of mouse origin (Figure 3.8 D). The proliferation of B16 HER2 bright cells was not influenced by treatment with Trastuzumab, either the recombinant antibody produced in our laboratory or in the form of commercially available Herceptin (Fig. 3.8 E). The results are not surprising since B16 cells grow robustly in cell culture in the absence of human HER2. Moreover, B16 cells are also mouse HER2 negative (Ueno et al. 2008; Yan et al. 2012) and do not require HER2 signalling for growth.

Mice with B16 HER2 bright (clone E5) pulmonary nodules were treated 3 days after tumour inoculation ($6x10^5$ cells IV) with either vehicle or different doses of Tr (5µg, 10µg or 30µg) and tumour burden was measured after culling the mice on day 15 by weighing the lungs (Fig. 3.9 A). The weight of lungs from mice treated with vehicle had a mean of 260.2±57.62 mg, which was significantly higher than the weight of tumour free lungs. Mice treated with either 5µg, 10µg or 30µg Trastuzumab had lower lung weights (means of 212.4±30.53 mg, 308.6±151.2 mg and 201.8±21.95 mg respectively). Comparing treatment groups among themselves and with vehicle did not reach statistical difference. Importantly, there was no statistically significant difference between the weights of Tr treated tumour-bearing and tumour free lungs for the doses of 5µg and 30µg. When tumour nodules were counted (Fig. 3.9 C), we observed that the method is inaccurate, since many nodules are very pale. In this data set, the variability was high, and we do not have sufficient numbers for statistical analyses. Crucially, tumour burden was very low for most mice in the Tr treated groups (Fig. 3.9 C). This has substantial implications when it comes to testing novel Tr-derived immunotherapies

in this model. The B16 HER2 bright E5 cell line is not suitable for such experiments, as there is no difference between the weight of Tr-treated groups and tumour-free lungs.

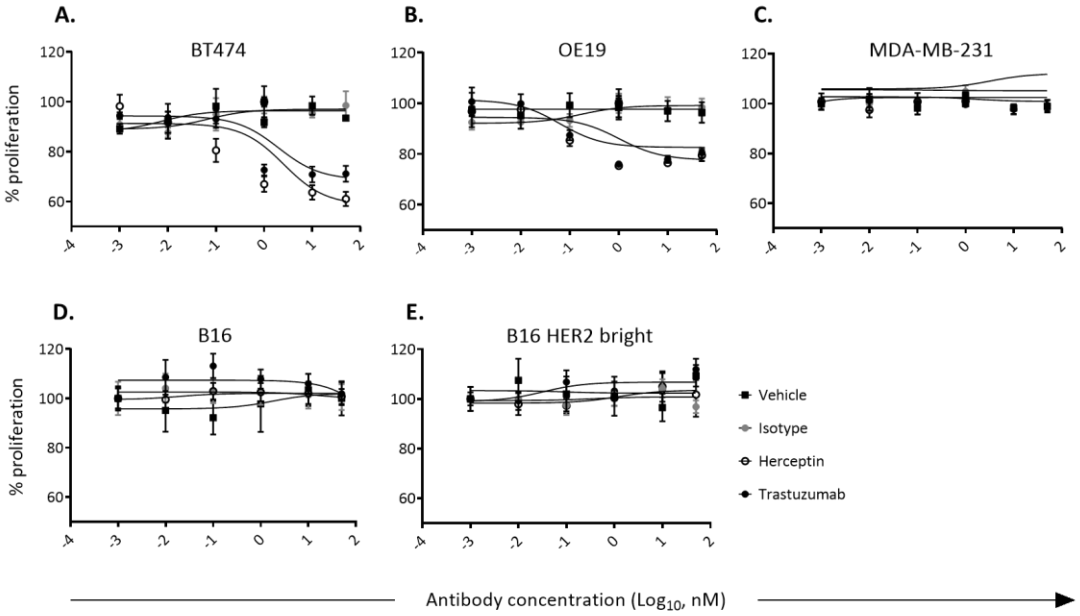


**Figure 3.8.** *In vitro* proliferation of HER2 positive and negative cell lines upon treatment with Trastuzumab measured using the MTS assay. Cells were plated in triplicates and treated with Trastuzumab or isotype 4 h later. MTS reagent was added after 48 h. BT474 (**A**) and OE-19 (**B**) are Trastuzumab sensitive HER2 overexpressing human cancer cell lines. MDA-MB-231 shows minimal HER2 expression (**C**). B16 cells are of mouse origin (**D**). B16 HER2 bright (**E**) cells do not respond to treatment with Trastuzumab *in vitro*. Data were normalised against non-treated cells and is shown as mean ± SEM of technical triplicates. Dose-response curves generated with the non-linear fit equation in GraphPad. Data is representative of 2 independent experiments.

Together, the data so far illustrate the following important observations. For one, individual HER2 expressing monoclonal cell lines generated different growth profiles. This implies that more monoclonal cell lines should be evaluated *in vivo*. We observed high variability among groups. This indicates that high numbers of mice will be required for experiments and power calculations would be valuable. It also became apparent that using lung weight alone as a measure of tumour burden may or may not be accurate, and different methods of assessing tumour burden should be employed.

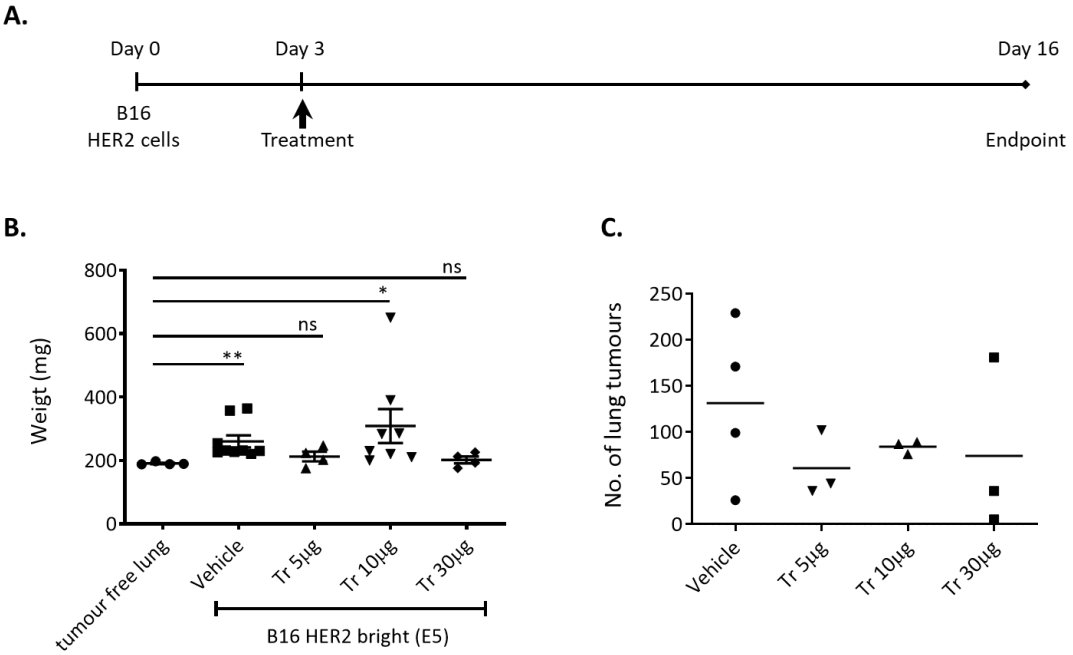


**Figure 3.9.** *In vivo* response of B16 HER2 bright tumours to treatment with Trastuzumab (Tr). **A.** Mice were injected with 6x $10^5$ tumour cells or left tumour free. 16 days later, lungs were extracted and then weighed (**B**). Data points from 2 independent experiments are shown as mean ± SEM. Number of mice per group: tumour free lung – 4; vehicle – 9; Tr 5µg – 4; Tr 10µg – 8; Tr 30µg-4. Kruskal-Wallis test with Dunn post-hoc test, **p<0.005, *p<0.05, ns – not significant. **C**. In one of the 2 experiments, lungs were fixed in Fekete solution and lung tumours were counted. Number of mice was 3 for all groups, except vehicle group, where n=4. Each symbol represents a mouse with a line showing mean.

## 3.5 *In vivo* profile of tumours generated with B14.3 Luc HER2 cells

### 3.5.1 Evaluating B14.3 Luc HER2 H2 tumour burden

To better understand the kinetics of tumour growth in immunocompetent mice, we decided to evaluate 3 monoclonal B14.3 Luc HER2 bright cell lines (A4, H2 and H4) *in vivo* and employ *in vivo* imaging to monitor tumour burden at multiple time-points post-tumour inoculation by measuring bioluminescence intensity (Fig. 3.10 A). Pulmonary tumour growth of B14.3 Luc HER2 tumours was compared to B16 cells tumours. Since we observed that HER2-transgenic cells generate lesser tumour burden in mice, we increased the dose of B14.3 Luc HER bright cells for IV injections to 9x $10^5$ cells. This dose was chosen, as it was successfully used before with B14.3 cells in our lab (Rajagopal et al. 2010). The dose of B16 cells was kept to 6x $10^5$ cells per mouse.

At day 18 post tumour-inoculation, all 3 tested B14.3 Luc HER2 bright cell lines generated dark, melanin-rich pulmonary tumours with identic morphology to B16 pulmonary nodules (Fig. 3.10 B). We assessed tumour burden at day 18 by weighing lungs (Fig. 3.10 C) and counting tumour nodules (Fig. 3.10 D). B16 cells generated substantial lung tumour burden, with more than 250 pulmonary tumour nodules (Fig. 3.10 D), which significantly increased the weight of the lungs within the tested 18-day period (Fig. 3.10 C). In contrast, none of the three tested clones of B14.3 Luc HER2 bright cells (clones A4, H2 and H4) increased the weight of the lungs significantly over lungs of tumour-free mice (Fig. 3.10 C). Numbers of tumour nodules were lower than in mice with B16 tumours, despite injecting more B14.3 Luc HER2 bright cells (Fig. 3.10 D). Among tested cell lines, B14.3 Luc HER2 bright H2 generated the highest number of tumour nodules. Clone A4 yielded much lower numbers of tumour nodules than H2 and H4 (Fig. 3.10 D). Since B14.3 Luc HER2 cells did not significantly increase the weight of the lungs, we stopped using this measurement in future experiments.

*In vivo* luminescence intensity of mouse lungs measured at day 18 reflected the number of tumour nodules for B14.3 Luc HER2 bright H2 and H4 tumours. Lungs with low numbers of tumours showed lower luminescence intensity and vice versa. In contrast, luminescence intensity of A4 tumours did not relate to the number of lung nodules (Fig. 3.10 E). Here, the luminescence levels are comparable with other cell lines, but the number of nodules was much lower. We observed that some of the lung nodules were larger in volume, and others lost melanin pigmentation and were more difficult to count accurately, which might contribute to the discrepancy.

*In vivo* imaging enabled us to assess tumour growth of these mice at multiple time-points (Fig. 3.10 F-J). Mice inoculated with B16 cells developed luciferase-free lung tumours and were used to establish the background levels. For all tested B14.3 Luc HER2 cell lines, luminescence intensity increased progressively after tumour inoculation to reach maximum values at day 18. Among the tested cell lines, clone B14.3 Luc HER2 H2 generated tumours with highest levels of luciferase activity (Fig. 3.10 I). When plotting the luminescent data for individual mice with H2 tumours (Fig. 3.10 E), it became evident that after day 7, some mice control tumour growth without any further increase in luminesce signal after this time-point. The same was observed for mice bearing B14.3 Luc HER2 tumours generated with clone H4 (data not shown). We cannot rely on results for A4 tumours, as luminescence activity did not relate to tumour burden for these tumours.

Together, these data illustrate that *in vivo* imaging showed an appropriate representation of tumour burden for 2 out of 3 tested luciferase-expressing cell lines and enabled us to visualise that tumour growth was stunted in some mice after day 7 from tumour inoculation. Among the tested cell lines, B14.3 Luc HER2 bright H2 showed the most favourable *in vivo* profile, and we proceeded to characterise these tumours further.

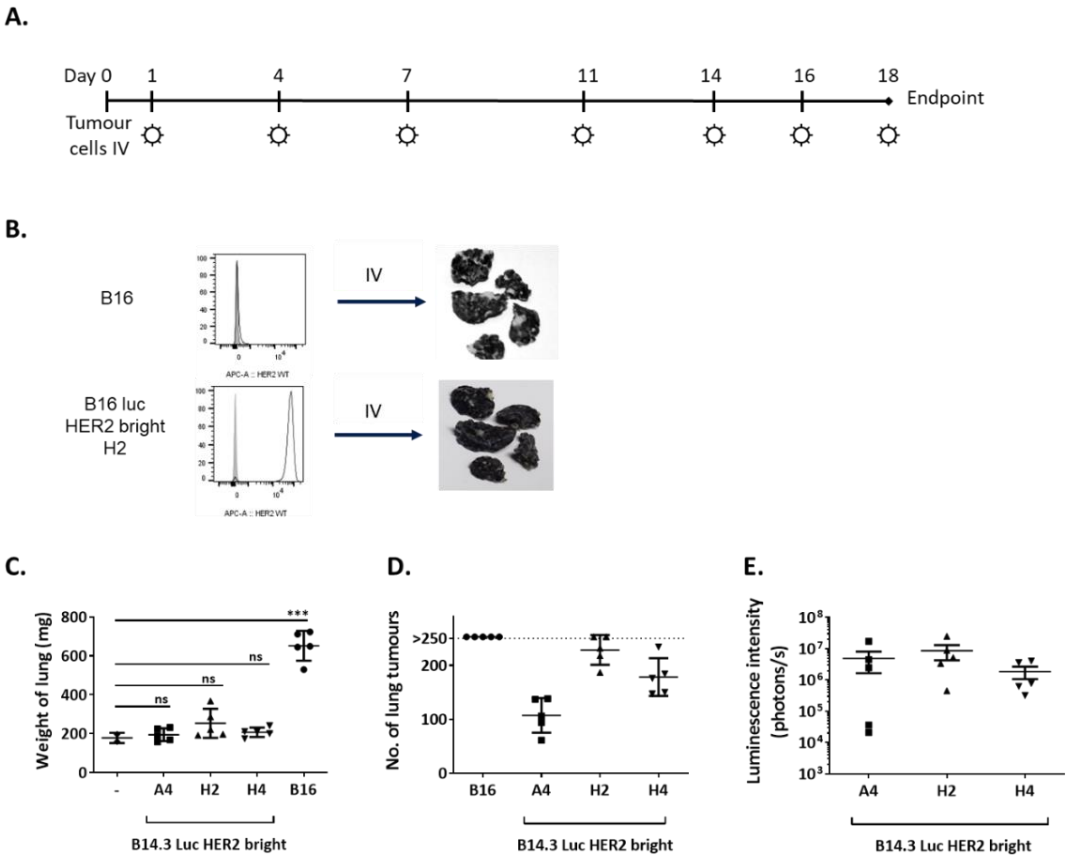

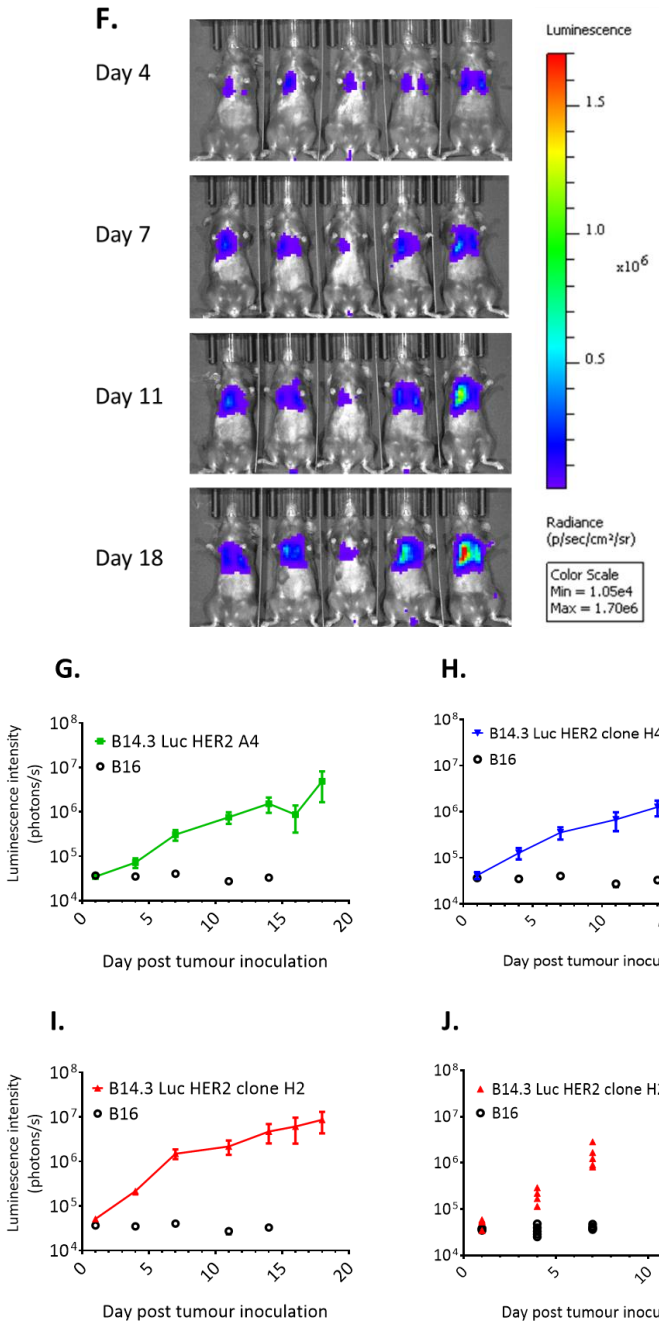


**Figure 3.10.** Tumour growth profiles of B14.3 Luc HER2 bright tumours. **A**. Time-line for monitoring tumour burden. Mice (n=5 per group) were injected IP with 150mg/kg XenoLight D-Luciferin substrate and imaged (☼) 10 minutes later. Regions of interest (ROI) with 2.647cm diameter were placed over the anterior thorax of each mouse to capture luminescence signal of pulmonary tumours (photons/s). **B.** Representative images of lung tumours generated B16 cells (top) and B14.3 Luc HER2 bright H2 cells (bottom). **C.** Weight of tumour-bearing lungs compared to tumour-free lungs. Mean ± SD. Student's t test, ***p<0.001. **D.** Number of tumour nodules counted on the surface of lungs fixed in Fekete solution. Mean ± SD. **E.** *In vivo* luminescence intensity of luciferase-expressing tumours at day 18. Each data point represents one mouse with mean ± SEM depicted by lines for each group. **F.** Representative images of luminescence signal measured *in vivo*. **G-I.** Luminescence intensity of lung tumours over time. Data from one experiment shown as mean ± SEM of total flux (photons/s) of n=5 mice bearing either B16 tumours (open) or B14.3 Luc HER2 tumours clone A4 (green), H2 (red) or H4 (blue). **J.** Luminesce signal of each mouse bearing B14.3 Luc HER2 clone H2 tumours.

## 3.6 Characterising the B14.3 Luc HER2 bright clone H2

The human HER2-transgenic B14.3 Luc cell clone H2 showed high expression levels of human HER2 and expresses the GFP-OVA and the Firefly luciferase transgenes at comparable levels to the parental B14.3 Luc cell line (see section 3.3). Importantly, this cell line generated a significant amount of tumour burden *in vivo*, higher than the other tested monoclonal cell lines, including the luciferase-negative HER2 transgenic lines. We were able to assess tumour burden both at endpoint, by counting tumour lung nodules and additionally by measuring luciferase activity using *in vivo* imaging at different time points throughout the experiment. As H2 was the cell line generating the most promising *in vivo* profile, we have further characterised it *in vitro* and *in vivo*.

### 3.6.1 *In vitro* growth kinetics

B14.3 Luc HER2 bright H2 cells generated lesser tumour burden in mice compared to the parent B16 cells (Fig. 3.10). We verified whether this difference in tumour growth was due to changes in cell proliferation generated through repeated transduction and multiple transgene expression. To test this, we compared the growth kinetics of B14.3 Luc HER2 bright H2 cells with B16 cells *in vitro* (Fig. 3.11). Both cell lines proliferated *in vitro* with comparable kinetics (Fig. 3.11).

Together with data from tumour growth profiles, these results suggest that the control in growth of B14.3 Luc HER2 H2 tumours we have observed in some mice is mediated by the host immune responses and not by changes in the growth rate of tumour cells themselves.

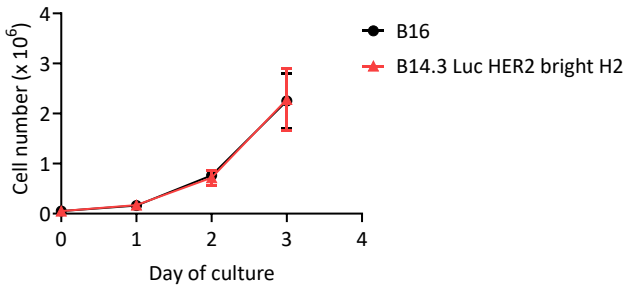


**Figure 3.11.** *In vitro* growth kinetics of B14.3 Luc HER2 bright H2 cells. 50 000 cells were plated in duplicates in 6-well plates. Each day, duplicate cell samples were harvested, and live cells were counted using Tripan Blue exclusion. Data from 2 independent experiments are shown as mean ± SD.

### 3.6.2 HER2 expression analysis of cultured cells

To evaluate expression of human HER2 on B14.3 Luc HER2 bright cell line H2 in comparison with cell lines derived from patient tumours often used for cancer research, cells were stained with Trastuzumab and analysed by flow cytometry (Fig. 3.12). For our analysis, we used the resolution metric ($R_D$), which accounts for separation between HER2 signal and control as well as the spread of data, to rank cell lines based on intensity of HER2-staining signal. As negative controls, we included HER2 negative MDA-MB-468 and the mouse B16 cells in the analysis. Reportedly, the Trastuzumab resistant JIMT-1 cells express human HER2 at robust, but moderate levels, lower than other human HER2 positive cell lines such as BT474 (Tanner et al. 2004) and OE-19 which are HER2-high (Wainberg et al. 2010). Corresponding to previous reports, JIMT-1 cells showed lower HER2 relative expression than BT474 or OE-19 cells, but higher levels than the low HER2 expressing cell line MDA-MB-231. B14.3 Luc HER2 bright H2 cell line showed similar resolution metric (1.75 ± 0.03) to JIMT-1 cells (1.77 ± 0.08) (Fig. 3.12).

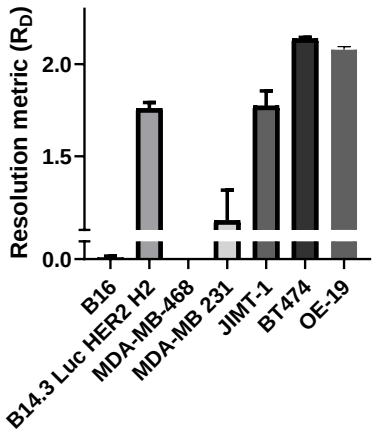


**Figure 3.12.** Evaluating human HER2 expression on cancer cell lines by flow cytometry. Comparing human HER2 expression of B14.3 Luc HER2 bright H2 cells with other cancer lines by flow cytometry. Cells were stained with Trastuzumab or isotype control. The resolution metric was calculated by subtracting the MFI of the isotype antibody control from the MFI of Trastuzumab and dividing the difference by the sum of standard deviations. Data were pooled from two independent experiments and shown as mean ± SD.

### 3.6.3 B14.3 Luc HER2 H2 lung tumours express human HER2 *in vivo*

Using flow cytometry, we evaluated HER2 expression of tumours generated with either B16 or B14.3 Luc HER2 clone H2 cells in C57BL/6 mice. Mice were injected IV with 9x $10^5$ B14.3 Luc HER2 H2 tumour cells or 6x $10^5$ B16 lung cells and lung tissue was harvested 15 days later. Single cell suspensions were generated from lung tissue. Cells were stained for live/dead discrimination, then fixed in Streck. Cells were stained after fixation and then analysed by flow cytometry alongside the cultured tumour cells. The tyrosinase related protein-1 (TRP-1) is a crucial component of the melanosome's membrane involved in melanin production and therefore specific melanocyte marker (Rosenberg 1997). In our lung single cell suspensions, only B16 or -derived tumours cells contain melanosomes and TRP-1. Both B16 and B14.3 Luc HER2 H2 tumours are black, melanin-containing tumours (Fig. 3.10 B). Hence, tumour cells were defined as CD45 negative and TRP-1 positive cells (Fig. 3.13 A). HER2 expression was analysed on gated tumour cells using a commercial anti-human HER2 antibody that binds a different epitope than Trastuzumab (data not shown). B16 cells were negative for HER2 staining. Compared to cultured cells used for tumour inoculation (Fig. 3.13 B), B14.3 Luc HER2 H2 tumours showed dimmer HER2 staining (Fig. 3.13 C). The MFI of HER2 positive cells was variable among animals inoculated with B14.3 Luc HER2 H2 cells, ranging from 1225 to 1514. Interestingly, tumour cells showed heterogeneous HER2 expression, as demonstrated by the width of the histograms. Whether HER2 expression differs among tumour lung nodules or among tumour cells of the same nodule remains to be established by future immunohistochemical studies.

Data indicate that HER2 expression of H2 cells is dimmed *in vivo* to a variable extent among individual mice. Further experiments including more mice are required to confirm the reproducibility of our results and better define the extent of this variability.

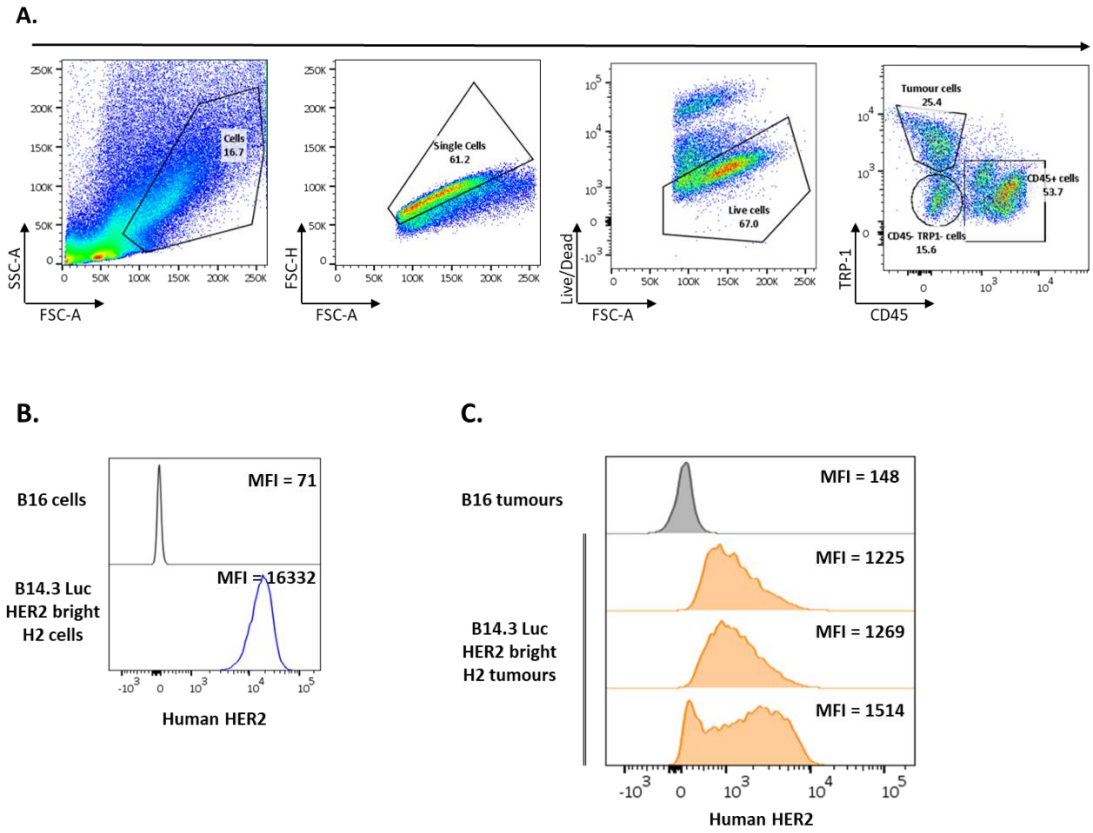


**Figure 3.13**. Evaluating human HER2 expression of B14.3 Luc HER2 H2 pulmonary tumours. Mice were injected with 6x $10^5$ cells and culled 15 days later. Single cell suspensions were generated from lung tissue and cells were stained for surface markers and analysed by flow cytometry. **A.** Gating strategy. **B.** HER2 expression on B16 (grey open histogram) and B14.3 Luc HER2 bright H2 (blue) cultured cells. **C.** Human HER2 expression on B16 (filled grey) and B14.3 Luc HER2 bright H2 (orange) tumour cells. Data collected in one experiment.

### 3.6.4 B14.3 Luc HER2 H2 tumours do not respond to treatment with Trastuzumab

To investigate the direct response of B14.3 Luc HER2 bright cells to treatment with Trastuzumab, we performed MTS assays. The controls for this assay, showing that Trastuzumab inhibits *in vitro* proliferation of HER2 over-expressing human cancer cell lines, but not of HER2 negative or low-expressing cells are shown in Fig. 3.8. As expected, similarly to B16 HER2 cells (Fig. 3.8), the proliferation of B14.3 Luc HER2 bright cells clone H2 is not influenced by treatment with Trastuzumab (Tr), either produced in our lab or the clinical grade Herceptin® (Fig. 3.14).

Next, we investigated the response of B14.3 Luc HER2 bright H2 tumours to treatment with Tr *in vivo* (Fig. 3.15). Mice inoculated IV with $9x10^5$ B14.3 Luc HER2 bright cells were treated 4, 8 and 11 days later with either vehicle or 40µg Trastuzumab equalling a dose of approx. 2mg/kg body weight. Tumour burden was monitored using *in vivo* imaging by quantifying luminesce intensity of the bioreporter luciferase, and additionally on day 18, by enumeration of lung nodules (Fig. 3.15 A). Luminescence intensity of Trastuzumab treated mice was only slightly higher than for the vehicle treated group at days 10 and 15, but there was no difference in luminescence intensity at earlier time points (Fig. 3.15 B). At day 18, vehicle treated mice had 173.0 ± 73.79 tumour nodules, while Tr treated mice showed 186.0 ± 53.87 tumour nodules, with no statistically significant difference between the groups (Figure 3.13 C).

Together, these results show that B14.3 Luc HER2 bright H2 pulmonary tumours are resistant to treatment with Trastuzumab. While the *in vitro* assay investigated a wide range of doses and excludes a direct growth inhibiting effect of the therapeutic antibody on the tumour cells, we did not titrate Tr *in vivo*. Therefore, it cannot be entirely excluded that higher doses of Trastuzumab may influence tumour burden. Future experiments are required to investigate human HER2 expression on tumours treated with Tr. So far, the model shows significant tumour burden despite repeated treatment with robust doses of Trastuzumab and was deemed suitable for investigating the effects of Trastuzumab-based conjugates and complexes. Consequently, all subsequent animal experiments performed for this study used the B14.3 Luc HER2 bright clone H2 cell line.

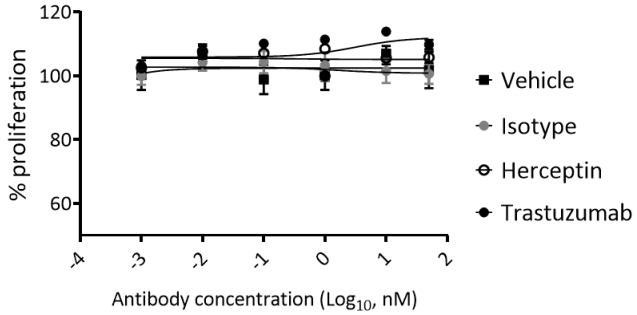


**Figure 3.14.** Treatment with Trastuzumab does not impact proliferation of B14.3 Luc HER2 bright H2 cells *in vitro*. Cells were treated for 48 hours with increasing concentrations of Tr or Herceptin or isotype control and MTS assay was performed. Controls for this assay are shown in Figure 3.7. Data are mean ± SEM of three technical replicates and is representative of 2 independent experiments.

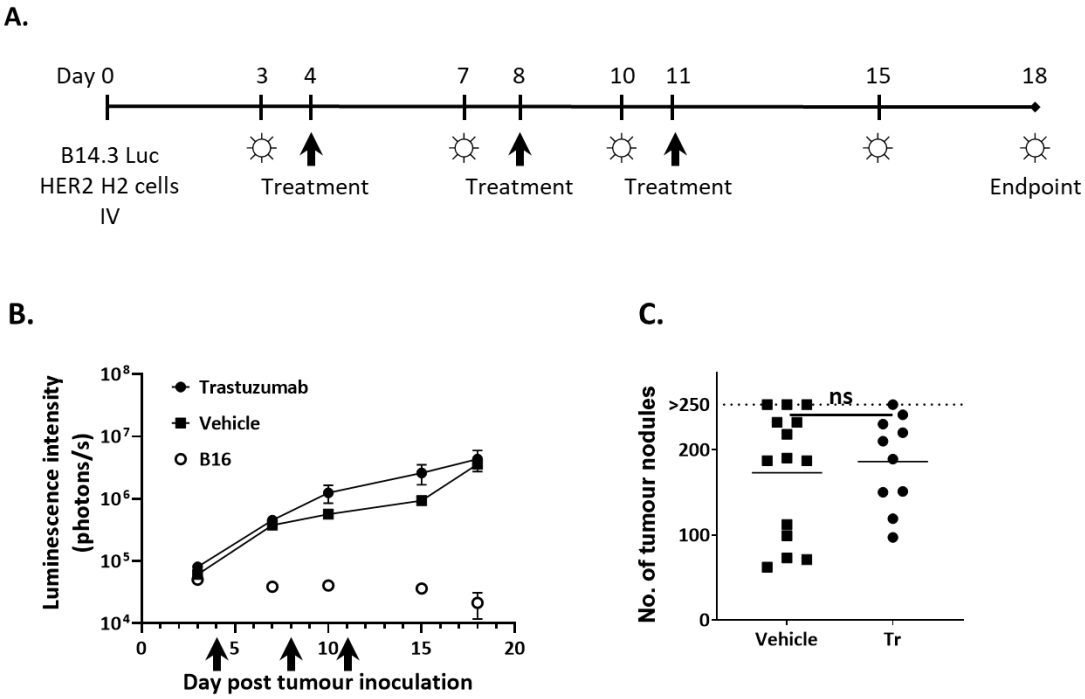


**Figure 3.15.** Response of B14.3 Luc HER2 bright H2 lung tumours to *in vivo* treatment with Trastuzumab. **A**. Mice were injected with tumour cells at day 0. At days 4, 8 and 11, mice were treated with 2mg/kg Trastuzumab IV. N=14 for vehicle group and n=10 for Tr group. **B.** Tumour burden was monitored using *in vivo* imaging. Data are mean ± SEM of values pooled from 3 independent experiments. Groups were compared using CGGC permutation test with 10 000 permutations. **C.** At day 18 mice were culled, lung tissue was fixed in Fekete solution, and pulmonary nodules were enumerated. Each symbol represents an individual mouse, and the mean is shown by a bar. Mann-Whitney t test, ns – not significant.

## 3.7 Generating subcutaneous tumours with B14.3 Luc HER2 H2 cells

### 3.7.1 Tumour growth profile of subcutaneous B14.3 Luc HER2 H2 tumours

Upon intravenous administration of any drug, the first reached capillary bed is in the lung (Chao et al. 2010; Kutscher et al. 2010). We were interested in comparing treatment efficacy between Tr-CpG conjugates, for targeted delivery of CpG to the lung tumours and free, unconjugated Tr + CpG. In our mouse model of lung tumours, it is likely that upon IV administration, both treatments would distribute to the lung first and this effect could potentially skew our results. To expand our options in terms of mouse models, we investigated the tumour growth profile of subcutaneous B14.3 Luc HER2 bright H2 tumours.

Mice were injected subcutaneously with B16 cells in the left flank and B14.3 Luc HER2 bright H2 in the right flank (Fig. 3.16). Since we knew from the IV inoculation model that larger numbers of B14.3 Luc HER2 bright H2 cells are required to increase tumour burden, we increased the numbers relative to B16 cells in this experiment as well. Tumour burden was measured regularly, and mice were culled when the cumulative tumour volume from both flanks reached 1000 $mm^3$. Tumours generated with 1x $10^5$ B16 cells (Fig. 3.16 A) reached maximum volume at day 18, later than tumours generated with 2x $10^5$ B16 cells (Fig. 3.16 C). B14.3 Luc HER2 bright H2 tumours, however, grew much less, with very little tumour burden achieved with either cell numbers. When growth of B14.3 Luc HER2 bright H2 tumours was visualised separately for each mouse, independently of dose (Fig. 3.16 B and Fig 3.16 D), it became apparent that all mice developed tumours and many of them rejected them, with drops in tumour burden at days 8-11. Tumour control was not observed with B16 cells, suggesting that expression of human HER2 and/or luciferase acts as a novel antigen in these immunocompetent mice and enables immune recognition and control of the tumour. These data show that B14.3 Luc HER2 bright H2 cells generated subcutaneous tumours and some of the mice rejected these tumours.

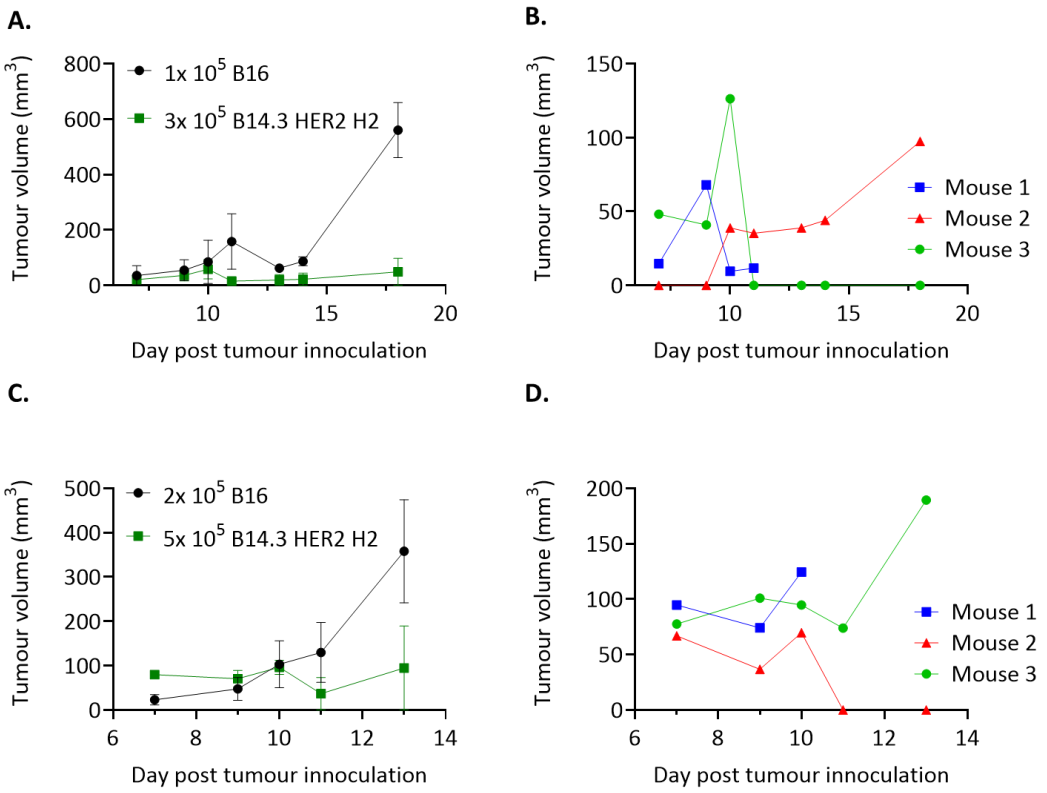


**Figure 3.16.** Tumour growth profile of subcutaneous B14.3 Luc HER2 bright H2 tumours. Mice were inoculated subcutaneously with B16 cells in the left flank and B14.3 Luc HER2 bright H2 cells in the right flank in 0.05ml PBS. Tumour growth was followed over time and mice were culled when cumulative volume of both tumours reached 1000 $mm^3$. **A.** Growth profile of subcutaneous tumours generated using 1x $10^5$ B16 cells and 3x $10^5$ B14.3 Luc HER2 bright H2 cells. Mean ± SEM of data from 3 mice. **B.** Growth profile of tumours generated with 3x $10^5$ B14.3 Luc HER2 bright H2 cells. Data from A is shown separately for individual mice. **C.** Growth profile of subcutaneous tumours generated using 2x $10^5$ B16 cells and 5x $10^5$ B14.3 Luc HER2 bright H2 cells. Mean ± SEM of data from 3 mice. **D.** Growth profile of tumours generated with 3x $10^5$ B14.3 Luc HER2 bright H2 cells. Data from C is shown separately for individual mice. Data was collected in one experiment.

### 3.7.2 Human HER2 expression of subcutaneous B14.3 Luc HER2 H2 tumours

Human HER2 expression of subcutaneous B14.3 Luc HER2 bright H2 cells was analysed by flow cytometry (Fig. 3.17). Single cell suspensions were generated from excised tumours. Cells were stained for live dead discrimination and immediately fixed in Streck. Fixed cells were stained for CD45, TRP-1 and human HER2 expression. Gating was performed as shown in Fig. 3.13. Tumour cells were defined as CD45 negative and TRP-1 positive cells. Human HER2 expression was analysed on gated tumour cells (Fig. 3.17 A). As expected, B16 tumour cells were negative for human HER2. B14.3 Luc HER2 bright H2 subcutaneous tumour cells maintained a degree of HER2 expression, which was lower than on cultured cells used for tumour inoculation and varied between animals.

Together, data in section 3.7 illustrate that B14.3 Luc HER2 bright H2 cells generate variable tumour burden and that some mice completely eliminate the tumour cells within 11 days. Human HER2 expression of tumours persisting beyond day 11 was diminished and variable between animals. Overall, tumour rejection seemed more pronounced for the subcutaneous model than for the IV model, where none of the mice rejected tumours completely. Hence, experiments using the subcutaneous model would require very large numbers of mice and careful selection of mice that do not reject these tumours. Therefore, we only used IV inoculation in subsequent experiments.

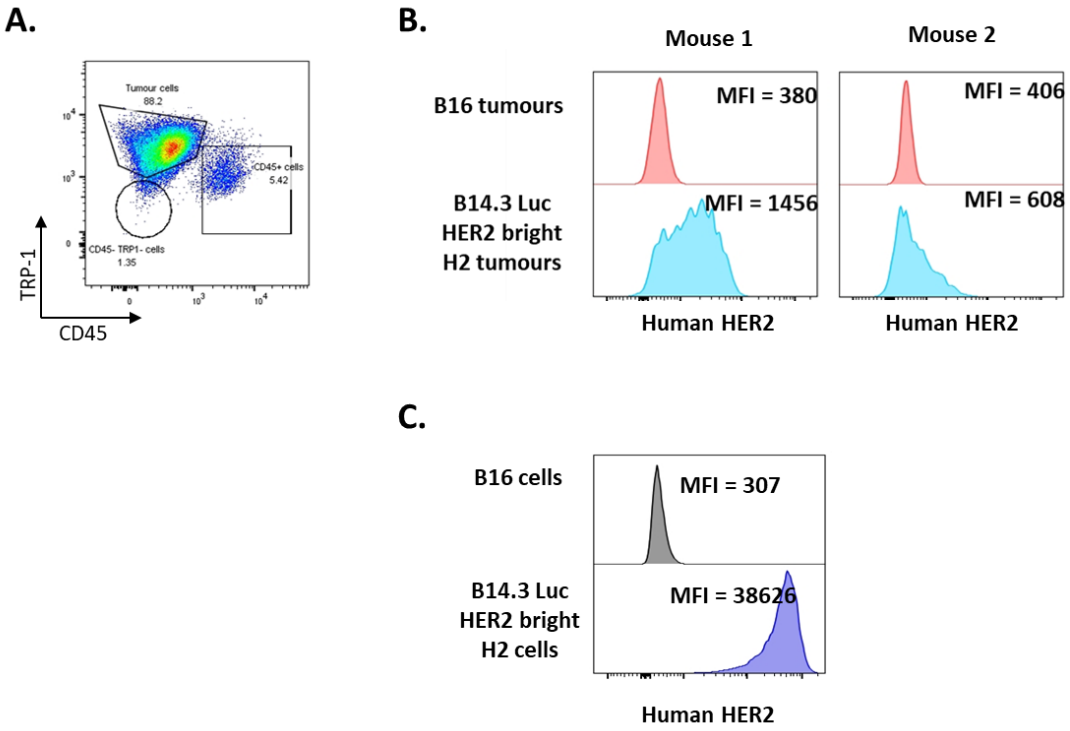


**Figure 3.17.** Human HER2 expression of subcutaneous B14.3 Luc HER2 bright H2 tumours. **A.** Representative plot showing gating on subcutaneous tumour cells. **B.** Histograms depicting human HER2 staining of tumours harvested from 2 individual mice. **C.** Human HER2 expression of cells used to generate the above analysed tumours. Data obtained in one experiment.

## Discussion

Our aim was to generate a transplantable mouse model using human HER2-transgenic cells in immunocompetent mice. Human HER2 expression was achieved via lentiviral transduction of B16 melanoma cells (Fig. 3.5). Upon IV administration, compared to B16 cells, all B16 HER2-expressing cell lines tested induced fewer lung tumour nodules. *In vivo* evaluation of several monoclonal cell lines was required to identify one that reliably generated sufficient tumour burden. In order to achieve this, increasing cell numbers for IV inoculation were necessary compared to the parental cell line.

Among tested cell lines, we identified B14.3 Luc HER2 bright H2 cells to reproducibly generate pulmonary tumours (Fig. 3.10), which maintained heterogeneous levels of human HER2 expression (Fig. 3.13). The mechanisms responsible for diminished human HER2 expression are yet unknown. Cleavage of the extracellular domain of human HER2 by metalloproteinases has been demonstrated in patients (Codony-Servat et al. 1999) and might be a possible explanation. Anti-human HER2 mouse immune responses driving immune evasion might be implicated as well. B14.3 Luc HER2 H2 tumours did not respond to treatment with 3 doses of 2 mg/kg body weight Trastuzumab, doses which are in the clinical range (Fig. 3.15). In patients, intratumoral HER2 heterogeneity correlates with poor responses to Trastuzumab therapy and poor prognosis (Hosonaga et al. 2018; Muller, Marotti, and Tafe 2019; Motoshima et al. 2018; Kaito et al. 2019). Our mouse model reflects several tumour characteristics of this group of patients with a great need for novel therapies.

B14.3 Luc HER2 bright H2 cells proliferated *in vitro* at the same rate with B16 cell (Fig. 3.11) but generated lesser tumour burden *in vivo* (Fig. 3.10). These cells express Firefly luciferase independently of human HER2 and luciferase activity measured by *in vivo* imaging related well to the number of lung tumour nodules (Fig. 3.10). This imaging technique enabled us to observe that starting 7 days after tumour inoculation, some of the mice controlled tumour growth and this resulted in decreased and variable tumour burden. The timing corresponds to the generation of adaptive immune responses in mice. Previous studies have demonstrated that dying cells are intrinsically immunogenic, releasing damage-associated molecular patterns (DAMPs) as well as exposing antigens (Hou et al. 2013; Krysko et al. 2012). Considering that each preparation of cells for inoculum may contain a few dying cells and injections themselves can damage cells, the generation of immune responses cannot be excluded. It is, therefore, possible that in some mice, B14.3 Luc HER2 H2 tumour growth is controlled by immune responses. The impact of such immune responses on immunotherapy experiments as planned

for this study is unknown. Multiple assays investigating anti-tumour immune responses were performed for untreated, but also treated mice and are discussed together in Chapter 5.

In summary, we generated a Trastuzumab-resistant, human HER2-expressing transplantable tumour mouse model which facilitates rapid immunotherapy studies, with a turn-over of 18 days. The B14.3 Luc HER2 bright H2 cells used for inoculum express luciferase, which enables monitoring of lung tumour burden via *in vivo* imaging. Among limitations of the model, diminished and heterogeneous human HER2 expression implies limited access of Trastuzumab-derived therapy to the tumour tissue. Moreover, tumour burden is controlled in some mice, possibly by the immune system, resulting in variability within groups of mice. While incomplete, data so far justify further evaluation of the model and its potential usefulness for *in vivo* evaluation of our Trastuzumab-based targeted delivery approaches of endosomal TLR agonists. However, other *in vivo* models, for instance, xenograft tumours in humanised mice may ultimately be required to evaluate the targeted delivery of Trastuzumab-CpG conjugates.

# Chapter 4

## Trastuzumab-LL37 fusion antibodies

## for targeted delivery of endosomal TLR agonists

# Chapter 4: Trastuzumab-LL37 fusion antibodies for targeted delivery of endosomal TLR agonists

## Introduction

This work investigates the use of monoclonal antibodies against tumour associated antigens in generating vehicles for targeted delivery of endosomal TLR agonists to the tumour tissue. As a model antibody, we use Trastuzumab, which is a clinically approved anti-human HER2 IgG1 antibody for the treatment of HER2 overexpressing breast (Hudis 2007) and gastric cancer (Palle et al. 2020). Since the encoding sequence of Trastuzumab is available to us in a pVITRO plasmid (Dodev et al. 2014), we can express the recombinant antibody and even further modify the sequence to facilitate linking to endosomal TLR agonists.

In this chapter we explore fusion of Trastuzumab with LL37. As described in section 1.4, LL37 is a cationic peptide that has been shown to bind various nucleic acids, including synthetic endosomal TLR agonists due to their intrinsic opposite polarity (Ganguly et al. 2009; Singh, Vaughan, and Kao 2014). Here we describe the generation of Trastuzumab-LL37 fusion antibodies and investigate their capacity to enhance local anti-tumour immune responses through delivery of endosomal TLR agonists to the HER2-expressing tumour tissue.

## 4.1 Expression and purification of antibodies

### 4.1.1 Description of workflow

For this study it is crucial to express and purify recombinant Trastuzumab (Tr), with or without modifications to the antibody structure in our lab. An overview of the workflow used to generate antibodies is shown in Figure 4.1. Briefly, the PCR-based cloning technique PIPE (Polymerase Incomplete Primer Extension) was used to modify the antibody sequence and to generate recombinant antibodies with additional heavy chain C-terminal moieties resulting in so called "fusion antibodies". This technique involves generating fragments of plasmid DNA by PCR with 5'-overlapping overhangs, which are transformed into competent bacteria, which assemble the fragments into the intended plasmid. This method does not require the use of a ligation step prior to transformation.

For the expression of unmodified and modified Trastuzumab, we used the pVITRO-Trastuzumab IgG1/κ from Addgene (Dodev et al. 2014). Hygromycin-resistant single bacterial colonies were screened for the presence of plasmid with the desired modifications. Screening methods included PCR, digesting the plasmid with restriction enzymes and evaluating the generated bands or Sanger sequencing (by Eurofin Genomics) and are described separately for each cloning strategy. Bacteria containing plasmid with the correct sequence were expanded, plasmid was isolated and sequenced (by Eurofin Genomics) to verify for point mutations. Between two and five clones were compared for recombinant antibody expression using the FreeStyleTM 293 (FS 293) expression system. Supernatants from transiently transfected cultures were harvested day 5-7 post transfection. Expression levels were determined by human IgG1 ELISA. To develop this ELISA, we used a detection antibody recognising the Fc of human IgG1. In select instances, we performed a second ELISA, using the same capture antibody and a different detection antibody, recognising the light κ chain. The clone generating the highest expression levels was used in subsequent experiments.

Antibodies were purified on Protein G or Protein A columns using FPLC. Human IgG1 was detected in the flow-through by human IgG1 ELISA, to verify efficiency of purification. Eluted antibody was desalted using Amicon Ultra centrifugal units with various MW cut-off and further characterised appropriately for their purpose.

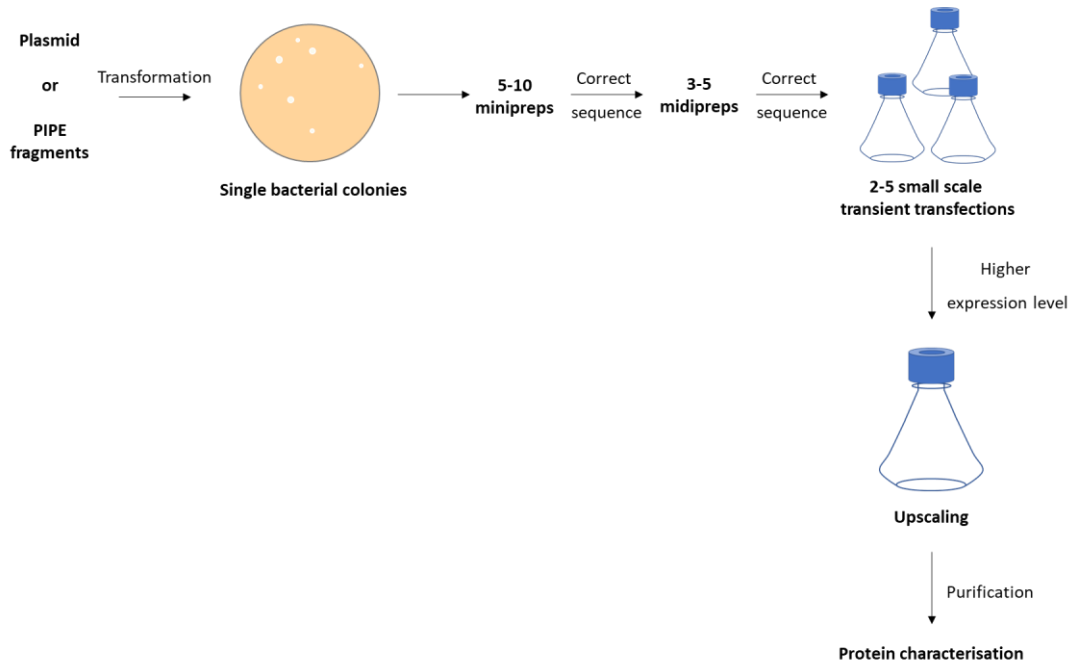


**Figure 4.1.** Schematic representation of workflow used to express and purify recombinant antibodies or fusion antibodies, starting with either plasmid or PIPE cloning fragments.

### 4.1.2 Validation of recombinant Trastuzumab

For validation of our antibody preparations, Trastuzumab (Tr) expressed and purified with our workflow (Figure 4.1) was compared to the clinical grade Trastuzumab produced by Roche, Herceptin® (Herc) in several *in vitro* assays.

First, antibodies were analysed by SDS-PAGE under non-reducing conditions (Figure 4.2 A). Both antibodies migrated on the gel corresponding to their expected molecular weight of approx. 150kDa. Additionally, very faint bands of higher molecular weight corresponding to multimers and very faint bands migrating faster, representing antibody fragments (blue arrows) were observed. These bands were slightly more visible for some preparations of Tr than for Herc and not present in every batch of purified antibody.

Binding of Tr to human HER2 was investigated using two methods, namely by ELISA with immobilised human HER2 and by staining of human HER2-expressing cells and analysis by flow cytometry. Both Herc and Tr bound immobilised human HER2, generating comparable curves (Figure 4.2 B). Furthermore, flow cytometry assays confirmed specific binding of both antibodies to cell-associated membrane-bound human HER2 (Figure 4.2 C). Additionally, both Tr and Herc inhibit *in vitro* proliferation of human HER2 overexpressing cell lines, but not HER2 minimal cell line MDA-MB-231, as shown in Figure 3.7.

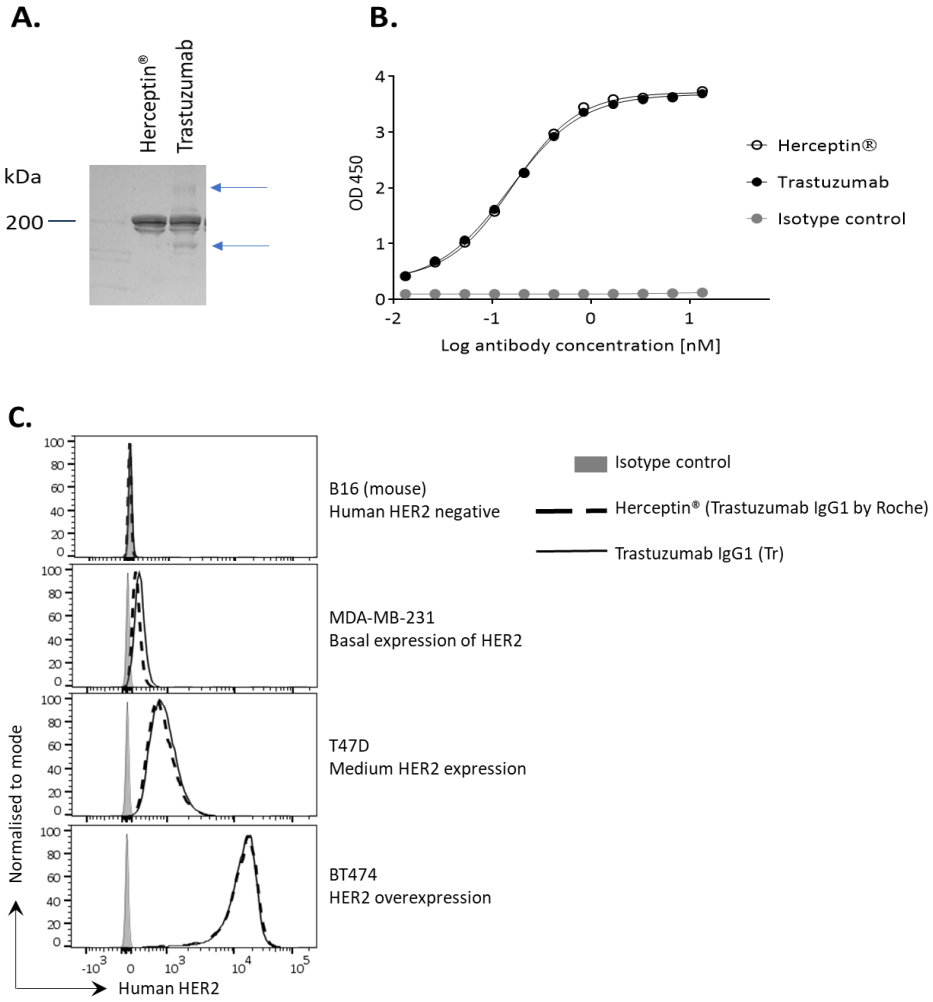


**Figure 4.2.** Validation of Trastuzumab IgG1 expressed and purified in our laboratory. A. SDS-PAGE analysis under non-reducing conditions Trastuzumab produced with our workflow and clinical grade Herceptin. B. ELISA with immobilised human HER2 was performed to compare binding properties of Trastuzumab (closed black) with Herceptin (open black) and isotype control (grey). The data was fitted with a four-parameter logistic model in GraphPad Prism C. Cell lines with different expression levels of human HER2 were stained with either isotype control (grey histogram), Herceptin (open black dotted histogram) or Trastuzumab (open black histogram) and an anti-human IgG secondary antibody (APC) before analysis by flow cytometry. Data are representative of minimum three independent experiments.

## 4.2 Generation of Trastuzumab-LL37 fusion antibody

### 4.2.1. Fusion of LL37 at the C-terminus of Trastuzumab heavy chain hinders expression of the resulting fusion antibody

Trastuzumab-LL37 (Tr-LL37) fusion antibody contains two LL37 domains per Trastuzumab IgG1 (Tr) molecule, which are fused at the C-terminus of Tr heavy chain (Figure 4.3A). We have opted for this fusion antibody architecture, as we wanted to maintain the original properties of the full-length Tr and orient the cationic peptide LL37 away from the antigen binding site. The role of fused LL37 is to form complexes with nucleic acid (NA) TLR agonists and deliver them to human HER2 overexpressing tumour tissue targeted by Tr.

To generate Tr-LL37 fusion antibody, we started with the dual cassette pVITRO plasmid encoding the heavy and light chain of Tr. The pVITRO vector map is shown in Appendix E, while the full sequence with annotations are shown in Appendix F. The sequence for LL37 (Appendix G), cloned by Dr. Sandra S. Diebold from human neutrophils, was introduced in the pVITRO vector immediately after the sequence for the heavy chain of Tr (Figure 4.3B) using Polymerase Incomplete Primer Extension (PIPE) cloning technique. The sequence for LL37 was amplified by PCR from the pVITRO-397-LL37 plasmid to generate the LL37 insert with 5' overlapping regions with the pVITRO vector. Two PCR fragments were amplified that covered the pVITRO vector backbone including the Trastuzumab antibody heavy and light chain sequences and transformed together with the LL37 insert into competent bacteria (Figure 4.3C). Plasmid preparations containing Tr-LL37 from single bacterial colonies were analysed for the LL37 insert by PCR using LL37 specific primers. Out of 10 analysed plasmid minipreparations, 9 contained the LL37 insert (Figure 4.3 D). We sequenced 5 midipreparations to confirm LL37 presence and verify for point mutations at the cloning site, then used the plasmids to transiently transfect FS 293 cells.

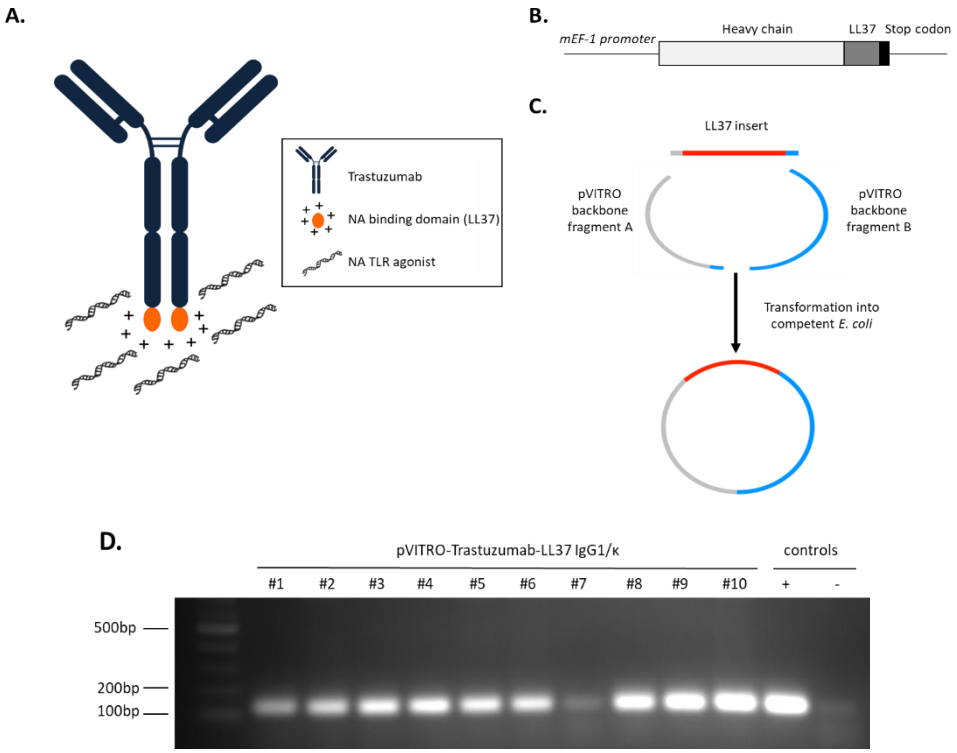


**Figure 4.3.** Generation of Trastuzumab-LL37 fusion antibody**. A.** Schematic representation of Trastuzumab-LL37 (Tr-LL37) fusion antibody and complex formation with nucleic acid TLR agonists. NA - nucleic acid. **B.** Schematic representation of pVITRO vector highlighting LL37 in relation with the sequence for Tr heavy chain. **C.** PIPE cloning strategy for introducing the sequence of LL37 into the pVITRO-Trastuzumab IgG1 mammalian expression vector. LL37 insert and pVITRO backbone fragments were generated with single stranded 5'-ends, containing overlapping sequences. When mixed, the sequences anneal, while nicks and gaps in the sequence are repaired in vivo by competent bacteria. **D.** 1.5% agarose gel analysis of PCR amplification of LL37 sequence in plasmid minipreparations (#1-#10) of pVITRO-Trastuzumab-LL37 IgG1/κ generated by PIPE cloning. pVITRO-397-LL37 was used for positive control, pVITRO-Trastuzumab IgG1/κ was used for negative control.

Expression levels of Tr-LL37 fusion antibody were approx. 10-fold lower than for the parent antibody Tr when measured using either an anti-Fc monoclonal detection antibody (Figure 4.4 A) or an anti-κ light chain polyclonal antibody (Figure 4.4 B). When we upscaled the transfection and purified Tr-LL37 on a protein G from 300ml supernatant, only 27.8µg Tr-LL37 were obtained. This was approx. 15x times lower than the yield we obtained from 300ml unmodified Tr (312µg). For both Tr and Tr-LL37, purification was efficient, as verified by measuring antibody levels in the flow-through by human IgG1 ELISA (data not shown).

Upon analysis by SDS-PAGE (Figure 4.4 D), only a fraction of the purified Tr-LL37 migrated corresponding to the expected MW of ~ 160kDa. In terms of purity, multiple bands of various molecular weights were observed, which was in contrast with integrity and purity of Tr. This suggests that folding and assembly of Tr-LL37 is probably suboptimal, leading to antibody fragments and aggregation. However, the nature of the additional bands observed on SDS-

PAGE was not further investigated by Western blot to confirm the presence of heavy chain and/or light chain fragments. The minute expression levels of Tr-LL37 in this system rendered a more extensive evaluation of the fusion antibody unfeasible within manageable laboratory costs.

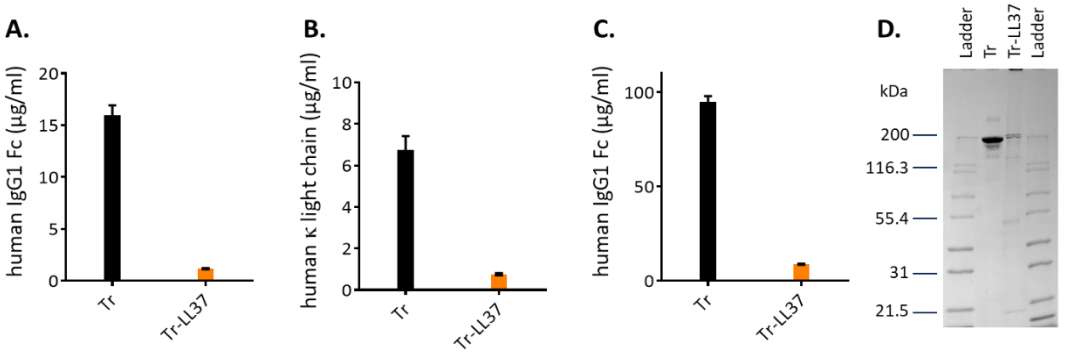


**Figure 4.4.** Expression levels of Trastuzumab-LL37 (Tr-LL37) compared to the parent antibody Tr. Human IgG1 ELISA using a recombinant anti-Fc detection antibody (**A** and **C**) or a polyclonal anti-kappa chain detection antibody (**B**) to assess antibody levels in supernatant of transiently transfected FS-293 cells (**A** and **B**) or ExpiCHO cells (**C**). Data is representative of 4 (**A** and **B**), or 2 (**C**) independent transfection experiments and ELISAs. Mean values ± SD of technical triplicates. Commercial human IgG1 (Ultra-LEAF from BioLegend) was used as standard in all assays. **D.** SDS-PAGE analysis of purified Tr and Tr-LL37 with Simply Blue staining. Both antibodies were expressed in FS-293 cells. 2µg of each sample were loaded.

In order to boost expression levels of the fusion antibody, the ExpiCHO™ expression system (Life Technologies) was tested. At day 4 post-transfection, expression levels of the parent antibody Tr were 10-fold higher for the ExpiCHO™ expression system compared to the FS 293 expression system. However, expression levels of Tr-LL37 were also reduced by approximately 10-fold as compared to Tr when ExpiCHO cells were used (Figure 4.4 C). Viability of both FS 293 cells and ExpiCHO cells was comparable when transiently transfected with pVITRO-Tr or pVITRO-Tr-LL37 (data not shown).

Taken together, expression levels of Tr-LL37 were drastically reduced across expression systems. Low purity and poor integrity of the Tr-LL37 indicates that LL37 might interfere with antibody folding and assembly, resulting in a drastic dip in expression levels.

### 4.2.2 Rigid alpha-helical linkers separating LL37 and the C-terminus of Tr heavy chain facilitate expression of Tr-LL37 fusion antibody

In order to evaluate the potential use of Trastuzumab-LL37 for targeted delivery of TLR agonists, it is essential to generate sufficient amounts of fusion antibody for both *in vitro* and *in vivo* characterisation.

It has been demonstrated that folding and assembly of IgG isotype antibodies consisting of light and heavy chains is a complex post-translational process. Assembly of most IgG antibodies, including human IgG1, is guided by obligate homo-dimerization of the $C_H3$ domains, an interaction mediated by non-covalent bonds (Feige, Hendershot, and Buchner 2010). While LL37 is a cationic peptide with strong polarity, we hypothesised that its direct proximity to the $C_H3$ domain of the antibody interferes with $C_H3$ homo-dimerization and thereby disturbs antibody assembly, hindering expression. Hence, we decided to investigate whether the introduction of a linker which spatially separates LL37 from the $C_H3$ domain of Tr would improve or even restore expression levels.

To identify linkers suitable for our purposes, we decided to compare the effect of various linkers used in fusion protein engineering (Table 4.1) for their ability to rescue expression levels of Trastuzumab-LL37. The sequence for each linker was introduced between the C-terminus of the $C_H3$ domain and LL37 (Figure 4.5A), using PIPE cloning. Using PCR reactions, we generated PIPE fragments with single stranded 5'-ends, overlapping by minimum 7 nucleotides, containing the sequence of shorter linkers (Figure 4.5B). Nucleotide sequences of linkers H3 and H4, were too long for this strategy and were ordered as long oligos from Eurofin Genomics instead. The H3 and H4 long oligos were used as PCR templates to generate the H3 and H4 inserts. These were introduced into the pVITRO vector using the PIPE cloning strategy we employed for cloning of LL37 (see Figure 4.3 C above). For protein expression experiments, at least two clones with confirmed sequence were compared and one was chosen for subsequent experiments.

| Linker | Type | Secondary structure | No. of amino acid residues | Amino acid sequence (single letter code) |
|---|---|---|---|---|
| Hinge human IgG2 | Natural, rigid | Rod-like | 19 | ERKCCVECPPCPAPPVAGP |
| G4S | Empirical, flexible | Coil | 5 | GGGGS |
| (G4S)x2 | Empirical, flexible | Coil | 10 | (GGGGS)x2 |
| (G4S)x3 | Empirical, flexible | Coil | 15 | (GGGGS)x3 |
| H1 | Empirical, rigid | α-helix | 11 | LEA**(EAAAK)**ALE |
| H2 | Empirical, rigid | α-helix | 16 | LEA**(EAAAK)$_2$**ALE |
| H3 | Empirical, rigid | α-helix | 21 | LEA**(EAAAK)$_3$**ALE |
| H4 | Empirical, rigid | α-helix | 26 | LEA**(EAAAK)$_4$**ALE |

**Table 4.1.** List of linkers used to generate Trastuzumab-liker-LL37 IgG1 fusion proteins. Amino acids determining the α-helix secondary structure are shown in bold.

Expression levels of Tr-liker-LL37 fusion antibodies generated with several linkers were analysed by human IgG1 ELISA. Hinge regions of human IgG isotype function as linkers between the Fab and Fc regions of antibodies. The hinge from human IgG2 is the shortest and is more rigid than other hinges due to the proline content (Table 4.1), which causes the restricted flexibility of the IgG2 isotype (Vidarsson, Dekkers, and Rispens 2014). We considered it reasonable to assume that this sequence might be suitable to spatially separate LL37 from the CH3 domain. However, using the hinge region of human IgG2 as a linker did not improve expression levels of Tr-LL37 (Figure 4.6).

Several studies report improved function of fusion proteins built with glycine-serine (G4S) linkers, with linkers containing fewer G4S repeats providing better separation between domains (Gillies et al. 2002; Zhao et al. 2008; Chen, Zaro, and Shen 2013; Silacci et al. 2014). In our hands, the introduction of flexible G4S linkers did not impact expression levels of Tr-(G4S)n-LL37 fusion antibodies irrespective of the linker length (Figure 4.6).

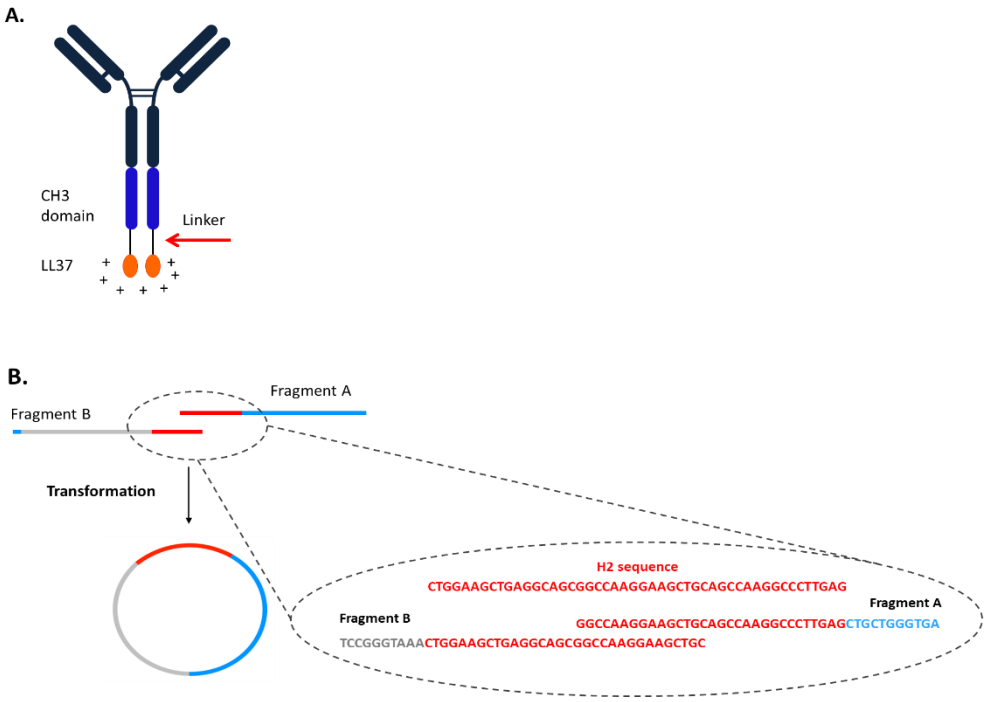


**Figure 4.5.** Generation of Trastuzumab-linker-LL37. **A.** Schematic depiction of Trastuzumab-linker-LL37 fusion antibodies. **B.** Schematic depiction of PIPE cloning strategy for cloning different linkers into the pVITRO-Trastuzumab-LL37 vector. Annealing of overlapping single stranded 5'-ends is exemplified for the H2 linker. For introduction of longer linkers such as H3 and H4, a separate insert fragment enclosing the linker region was generated and introduced into the plasmid by PIPE cloning as described.

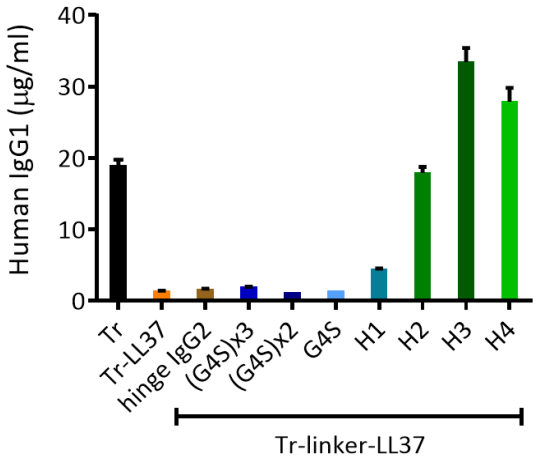


**Figure 4.6.** Impact of linker engineering on expression levels of Trastuzumab-linker-LL37 in FS 293 cell supernatant. Plasmids encoding Tr, Tr-LL37 or Tr-linker-LL37 were transiently transfected in FS 293 cells. At day 5 post-transfection human IgG1 levels were measured in supernatant by ELISA against a standard curve of purified commercial human IgG1. Representative data from 2 independent transfection experiments are shown. Mean ± SD of three technical replicates are shown. Sequence and properties of linkers are described in Table 4.1.

Linkers with the sequence (EAAAK)n have been shown to form rigid alpha helix-structures. Independent studies demonstrated that these linkers can provide efficient spacing between

protein domains and thereby increase expression yields and improve the function of various fusion proteins (Arai et al. 2001; Bai and Shen 2006; Amet, Lee, and Shen 2009). We evaluated the impact of α-helical linkers with 1-4 repeats of the EAAAK domain on expression of Tr-LL37 fusion antibodies (see Table 4.1). The helical linker with one EAAAK repeat, H1, minimally improved expression levels compared with Tr-LL37 (no linker). Introducing H2 in the structure of Tr-LL37 rescued the expression to comparable levels with the parent antibody Tr. Expression levels of Tr-H3-LL37 and Tr-H4-LL37 exceeded those of Tr by approx. 1.8-fold and 1.4-fold, respectively (Figure 4.6). These data confirm our hypothesis that efficient spatial separation of LL37 from the $C_H3$ domain of the antibody heavy chain, facilitates expression of Tr-LL37 fusion antibody.

Since expression levels were satisfying for Tr-linker-LL37 fusion antibodies generated with linkers H2, H3 and H4, we expressed and purified all three for further comparison. Expression levels in day 7 supernatant showed the same pattern with day 5 supernatant (Figure 4.7 A). Antibodies in day 7 supernatants were purified by affinity chromatography on a protein A column (MabSelect Sure, GE Healthcare). Antibody concentration was measured by ELISA in the FS 293 cell supernatant before and after purification. Post-purification, the supernatant flow-through was consistently depleted of antibody, suggesting that purification efficiency was similar for Tr and fusion antibodies (Figure 4.7 A).

An isotype control antibody was built by exchanging the variable regions in Trastuzumab with isotype control variable regions. The cloning and the validation of the isotype control antibody was performed by Dr. Sandra S. Diebold. The heavy chain variable region is from the rat IgG1 antibody 1F6, which was generated to bind mouse DNGR1, but when tested did not bind any mouse antigens. The light chain variable region is from the rat IgG1 antibody Mac49 recognising a plant protein. Full sequences of the isotype control variable regions are shown in Appendix H. The isotype control 1F6/Mac was validated by flow cytometry (see Appendix J). Subsequently, an isotype control-H3-LL37 (Iso-H3-LL37) fusion antibody was generated by Dr. Sandra S. Diebold, by introducing the H3-LL37 sequence of Tr-H3-LL37 after the heavy chain sequence of the 1F6/Mac isotype control (Iso) plasmid. Fusion of H3-LL37 at the C-terminus of the isotype control increased expression levels of the fusion antibody in FS 293 cell supernatant by approx. 2x fold over the parent antibody (Figure 4.7 B), showing the same trend as observed for Tr-H3-LL37 (Figure 4.7 A). Expression of Tr and Iso was always evaluated in separate ELISA assays and, therefore, cannot be directly compared. Further transfection experiments would be required to compare expression of Iso to Tr and Iso-H3-LL37 to Tr-H3-LL37.

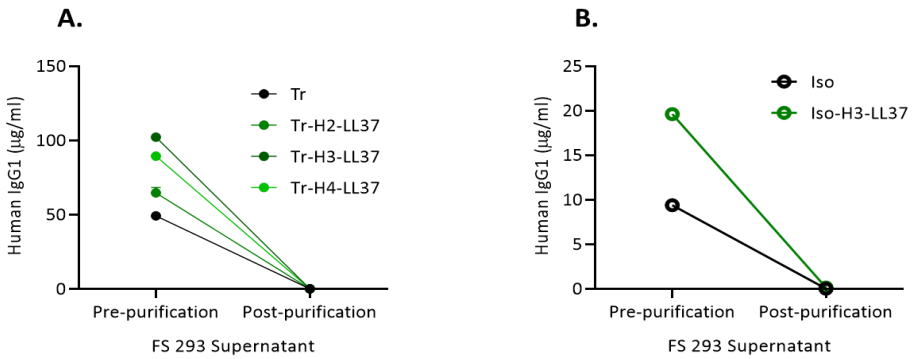


**Figure 4.7.** Efficiency of purification by affinity chromatography of Tr, Iso and derived fusion antibodies. Human IgG1 was detected by ELISA on day 7 FS 293 cell supernatant measured before and after purification of antibodies by affinity chromatography. **A.** Tr and Tr-linker-LL37 day 7 supernatant pre- and post-purification. **B.** Direct comparison of Iso and Iso-H3-LL37 levels in day 7 supernatant pre- and post-purification. Mean ± SD of three technical replicates. Data representative of at least two independent transfections.

SDS-PAGE analysis was used to investigate the composition of purified antibodies. Purified Tr and Tr-linker-LL37 antibodies were desalted and concentrated using Amicon Ultra centrifugal units with MW cut-off of 10kDa (Figure 4.8 A). While eluted Tr (control) showed a main band under native electrophoresis conditions, which migrated corresponding to an approx. 150kDa antibody, eluted Tr-linker-LL37, where the linker was either H2, H3 or H4, contained multiple additional bands migrating faster. This suggests that fusion antibody fragments are also present in tissue culture supernatant and are purified alongside the fully assembled form. It is possible that the fusion antibody fragments were also detected in the ELISA set-up we used to measure expression levels in FS 293 cell supernatant (Figure 4.6), falsely increasing levels for Tr-H2-LL37, Tr-H3-LL37 and Tr-H4-LL37. When we desalted all antibodies using filters with 100kDa MW cut-off, we were able to purify the fully assembled fusion antibodies almost completely from the fragments (Figure 4.8 B). When analysed in reduced conditions, the heavy chains (red arrow) of all three Tr-linker-LL37 (H2, H3 and H4) migrated slower than Tr heavy chain (MW of 50kDa), corresponding to increased MW of 62-66kDa, due to fusion of linker and LL37. Light chains of all antibodies had the expected mobility and apparent MW of 25kDa (grey arrow) (Figure 4.8 A, B).

Purified 1F6/Mac (Iso) and 1F6/Mac-H3-LL37 (Iso-H3-LL37), which had been desalted using 100kDa MW cut-off filters, migrated on gels corresponding to their expected MW under native or reduced conditions (Figure 4.8 C). SDS-PAGE analysis shows increased MW of the Tr-linker-LL37 and Iso-H3-LL37 heavy chains, and indicates successful purification using 100kDa cut-off filters.

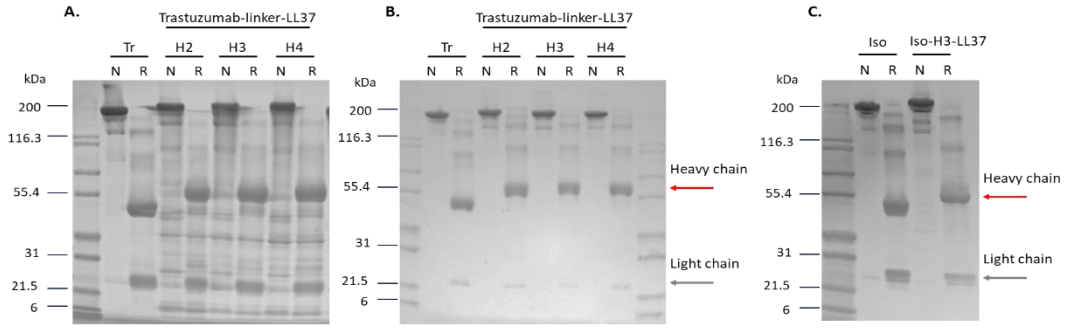


**Figure 4.8.** SDS-PAGE analysis of purified antibody and antibody-linker-LL37 desalted using filters with MW cut-off of 10kDa (**A**) or 100kDa (**B, C**). 4µg (**A, C**) or 3µg (**B**) of each antibody were analysed in native (N) or reduced (R) conditions on 4-20% gradient polyacrylamide gels stained with Simply Blue (Life Technologies). Tr-linker-LL37 (**A, B**) and Iso-H3-LL37 were analysed alongside the parent antibody. Arrows highlight the heavy (red) and light chain (grey). Data representative of one (**A**) or two (**B** and **C**) independent experiments.

To assess the purified antibody yield, we started by measuring protein concentration using BCA assay against a bovine gamma globulin (BGG) standard and additionally by spectrophotometric determination, using absorbance at 280nm (A280) and the reported extinction coefficient for Trastuzumab. Antibody concentration and the volume of purified antibody were used to calculate the mass (mg) of purified antibody obtained per L of tissue culture supernatant. Purified antibody yields were comparable when concentration was determined using either the BCA assay (Figure 4.9 A) or A280 spectrophotometry (Figure 4.9 B). The purified antibody yield was higher for Tr (1.69±0.33 mg/L) than for Tr-H2-LL37 (0.70±0.19 mg/L), Tr-H3-LL37 (1.13±0.15 mg/L) or Tr-H4-LL37 (0.96±0.10 mg/L). Among fusion antibodies, Tr-H3-LL37 consistently showed the highest yield, which only amounted for approx. 2/3 of the Tr levels (Figure 4.9). While the expression levels of Tr-H3-LL37 were 2x fold higher than for Tr in supernatant, the total purified yield was lower, despite successful purification (Figure 4.7 A). This discrepancy may be attributable to Tr-H3-LL37 fragments in present in cell supernatant (Figure 4.8A) but purified in downstream processing by ultracentrifugation (Figure 4.8 B).

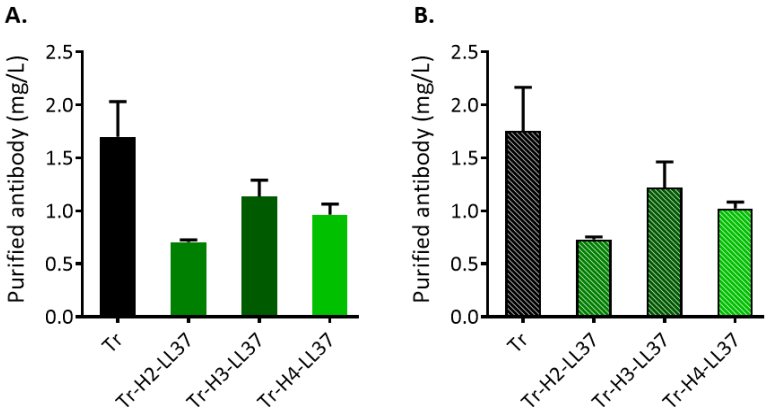


**Figure 4.9.** Purified antibody yield (mg) per L of cell culture supernatant of FS 293 cells. Purified antibody preparations were measured for protein concentration using BCA assay (**A**) or absorbance at 280nm (**B**). Total mass of antibody generated from the preparation was normalised against the volume of supernatant it was purified from. Mean ± SD of minimum three independent experiments are shown. Data representative of at least two independent experiments.

The antibody yields of fusion antibodies expressed using the FS 293 cells, while acceptable for the needs of the project, leave room for improvement. To explore this, we used the ExpiCHO™ expression system (Life Technologies), with reportedly superior performance. Tr and Tr-H2-LL37 were expressed in ExpiCHO cells and further purified by affinity chromatography on a protein A column, as described in section 2.1. At day 7, the supernatant from ExpiCHO cells contained approx. 7.6-fold higher levels of Tr compared to supernatant from FS 293 cells. Expression levels of Tr-H2-LL37 were higher using ExpiCHO cells as well, but only approx. 4-fold compared to FS 293 (Figure 4.10 A).

When analysed by SDS-PAGE, we observed that purified Tr expressed in ExpiCHO cells has increased mobility compared to Tr expressed in FS 293 cells. When analysed in reducing conditions, the band corresponding to the light chain (blue arrow) was absent in the ExpiCHO-expressed antibody, but not in the FS 293 antibody, accounting for the faster migration pattern of the antibody analysed in native conditions. Similar results were obtained with Tr-H2-LL37 as well (data not shown), suggesting that while the heavy chain is expressed by ExpiCHO cells (of mouse origin) at high levels, expression of the light chain is suboptimal. This discrepancy has not been observed in FS 293 cells, of human origin, when using the same bicistronic pVITRO plasmid (Figure 4.8). This suggests that differences in either promoters, enhancers or promoter-enhancer combination (see Appendix E) for the two transcription units in the pVITRO plasmid determine differential expression of heavy and light chains in the two host cells.

Despite the lower expression levels, we continued to use the FS 293 cells. In order to make use of the ExpiCHO expression system, cloning the light and heavy chain in two individual

plasmids would have been required, followed by experiments identifying the appropriate plasmid ratio to be used for ExpiCHO cell transfection.

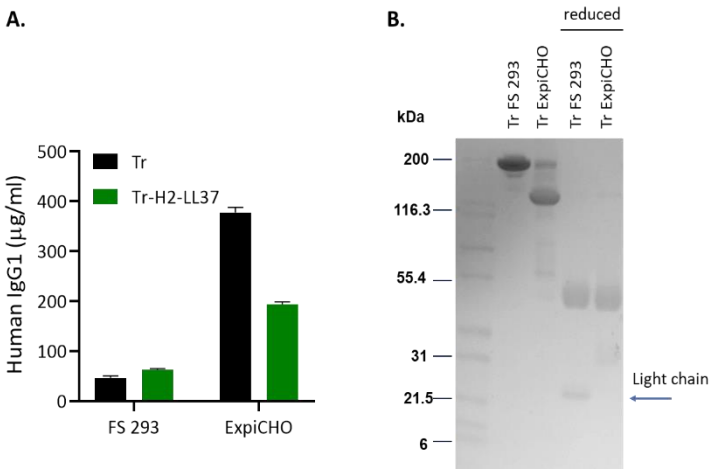


**Figure 4.10.** Expression of Tr and Tr-H2-LL37 in FS 293 and ExpiCHO cells. **A.** Expression levels in day 7 cell supernatant measured using human IgG1 ELISA with anti-Fc region monoclonal detection antibody. **B.** Purity and composition of Tr expressed in the two cell lines assessed by SDS-PAGE in native and reduced form. The data is representative of two independent experiments.

The main goal of the project is to evaluate the efficiency of treatment with Tr-linker-LL37 complexed with NA TLR agonists *in vivo*. It is thus important for the project to ensure that the immune activation which we might observe is triggered by NA TLR agonists and not by possible endotoxin contamination in the antibody preparations. The protein A column we used (MabSelect Sure, GE Healthcare) is resistant to alkaline treatment, which we employed between purification runs to maintain the column and purified material endotoxin-free. Purified antibody batches consistently showed minimum levels of endotoxin, as measured by the limulus amoebocyte lysate (LAL) gel-clot assay (Table 4.2). For the assay, antibodies were diluted to 0.5mg/ml in PBS. We have tested the purified antibodies at this dilution, as preliminary *in vivo* experiments with Tr (see Chapter 3) suggested that the final concentration of injected antibody will likely be smaller or equal to 0.5mg/ml. Most batches of antibody tested only had minute amounts of endotoxin, below 0.05 IU/ml, many of them under the detection limit of the assay of 0.025-0.03. Notably, exceptions were noticed with Tr preparations purified on a protein G column (data not shown), which we have not used since. The threshold levels of endotoxin of IV administered products, as defined by the European Pharmacopoeia 10.0 (Council of Europe 2019) is 5.0 IU per kilogram body weight. As there are no recommendations for preparations used in preclinical research, we used this value from the European Pharmacopoeia 10.0 as endotoxin limit for our experiments. We intend to evaluate recombinant antibodies in mice of approx. 20g body weight, for which the appropriate volume for IV injections is 0.1 ml. Hence, we limited the maximal endotoxin level of

antibodies to less than 0.1 IU (5.0 IU/kg) in 0.1 ml, or 1 IU/ml. Since the results we obtained from the gel-clot LAL assay were well below threshold values, we considered our expression and purification workflow endotoxin-free and suitable for *in vivo* experiments.

| Antibody | Endotoxin level (IU/ml) in diluted sample | | |
|---|---|---|---|
| | Batch 1 | Batch 2 | Batch 3 |
| Tr | <0.05 | 0.03-0.3 | <0.3 |
| Tr-H3-LL37 | 0.03-0.3 | <0.3 | <0.03 |

**Table 4.2.** Endotoxin levels of purified antibodies diluted to 0.5mg/ml. LAL gel-clot assays were performed by Janet Sutherland or Sophie Myhill.

### 4.3 Trastuzumab-linker-LL37 form complexes with nucleic acid TLR agonists

For this project, we were interested in targeting TLR3, TLR7 and TLR9 agonists to the tumour microenvironment and comparing them for their anti-tumour potential. We are therefore interested in forming complexes with various nucleic acid agonists: poly(I:C) (TLR3 agonist), polyUs21 (TLR7 agonist) and CpG (TLR9 agonist). Poly(I:C) is a polymer of large (1.5-8 kilobases), undefined molecular weight (Kato et al. 2008), and may cause issues with steric hindrance. In our experiments, depending on assay requirements and question to be answered, we used either polyUs21 or CpG 1668, which are oligonucleotides of 21 and 20 bases, respectively, of defined MW of approx. 6.5kDa.

Tr-H3-LL37 (theoretical MW=161.4 kDa) has two molecules of LL37 (MW=4.5kDa) per molecule of Tr. Complexes were formed with either CpG 1668 or polyUs21 to achieve LL37 to oligonucleotide molar ratio of 1:1. Importantly, in our hands, complexes adhered to filters of ultracentrifugation devices. Therefore, we could not establish if all added oligonucleotide was complexed by LL37 or purify the unbound fraction.

#### 4.3.1 Detecting complex formation

Previous publications demonstrated that synthetic LL37 peptide condenses and aggregates both self-DNA (Lande et al. 2007) and self-RNA (Ganguly et al. 2009), forming complexes. When polyUs21 was added to concentrated LL37 peptide or Tr-LL37, complex formation was visible with the naked eye as clouding of the suspension, or even presence of particulates, which sedimented at the bottom of the tube. This was observed for complex formation with CpG 1668 as well (data not shown).

UV-visible spectrophotometry is typically used to detect aggregates or other particulates with a hydrodynamic radius of more than 200nm in protein preparations by measuring absorption at wavelengths 320nm (Raynal et al. 2014). Here, we measured absorption at 405nm (A405) and 600nm (A600) of Tr-H3-LL37, CpG, Tr-H3-LL37+CpG complexes and their buffer (PBS) (Fig. 4.15). Spectrophotometry showed increased 405nm absorbance for Tr-H3-LL37+CpG complexes compared to Tr-H3-LL37, CpG or PBS alone. This was observed as soon as the components were mixed and decreased slightly with time (Fig. 4.11 A). In this experiment we formed complexes at 1:1 molar ratio, and it is presently unclear if other molar ratios would influence absorbance levels. A similar trend, with lower values was obtained for A600 readings (Fig. 4.11 B). Together, these data demonstrate immediate complex formation of CpG with Tr-H3-LL37, with generation of particulates visible with the naked eye and likely larger than 200nm.

This assay, however, is limited in terms of sensitivity and does not give information relating to the size of the complexes. To establish this and investigate how different complex formation conditions (e.g. concentration, molar ratio) influence the hydrodynamic radius of complexes, additional experiments are required in the future, such as dynamic light scattering measurements or imaging by scanning electron microscopy.

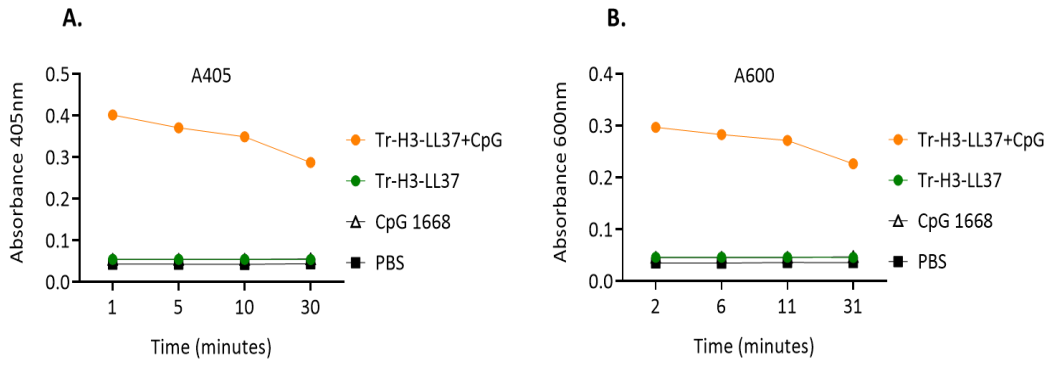


**Figure 4.11.** Visualising complex formation of Tr-H3-LL37 with CpG using UV-visible spectrophotometry. Complexes (orange) were formed by mixing Tr-H3-LL37 (0.6mg/ml) with CpG (0.5mg/ml) in PBS to achieve CpG to LL37 molar ratio of 1:1. Absorbance at 405nm (**A**) and 600nm (**B**) were read immediately, and different time-points. Each component of complexes, Tr-H3-LL37, CpG and PBS were measured as well. Mean ± SD of three technical replicates. Data representative of 2 independent experiments.

### 4.3.2 Trastuzumab-linker-LL37 complexes activate dendritic cells

Literature reports that the synthetic peptide LL37 complexes self-RNA, protects it from degradation by RNases and mediates TLR7 triggering and DC activation (Ganguly et al. 2009). In our lab we work with polyUs21, a synthetic single stranded RNA (ssRNA) oligonucleotide, synthesised to mimic self-RNA activation of DCs through TLR7 (Diebold et al. 2006). Flt3L-derived BMDCs (Flt3L-DCs) contain mouse pDCs (Appendix L), which express TLR7 and hence we used these cells for *in vitro* activation assays. However, cytokine production (IL-12p40) by Flt3L-DCs in response to polyUs21 can still be observed when polyUs21 is added to the cells in non-complexed form (Fig. 4.12 B). IL-12p40 secretion in response to polyUs21 was boosted by complex formation with either LL37, or the cationic lipid DOTAP. A typical bell-shaped dose response was observed. Notably, Flt3L-DC stimulated with only 3µg polyUs21 complexed with LL37 (1:1 molar ratio) produced similar levels of IL-12p40 as 30µg of polyUs21 alone and increasing the LL37 to polyUs21 molar ratio to 5:1 did not significantly ($p=0.2811$) increase cytokine production over the 1:1 molar ratio (Figure 4.12 C). Interestingly, polyUs21-DOTAP complexes induce higher cytokine levels by Flt3L-DCs than polyUs21-LL37 complexes (Fig. 4.12 B). At the highest concentration used for complex formation, LL37 peptide in the absence of TLR7 agonists only

induces minimal amounts of IL-12p40. Similarly, for the liposome-forming cationic lipid DOTAP low level of cytokine production was observed in the absence of polyUs21.

When GM-CSF derived BMDCs, which do not express TLR7 were used for the in vitro DC activation assay, no cytokine production was observed in response to polyUs21 complexes (data not shown). Taken together these data illustrate that the LL37 synthetic peptide enhanced polyUs21activation of Flt3L-DCs via TLR7, but with lower activity than DOTAP.

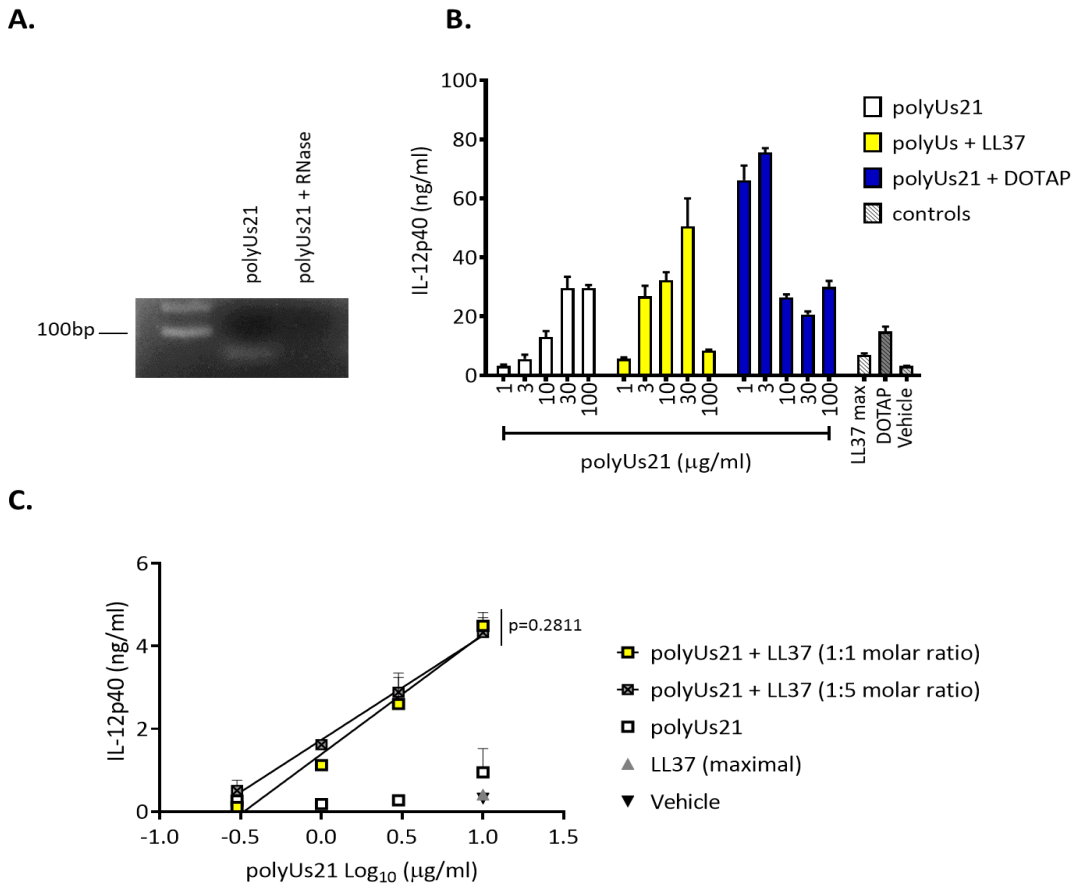


**Figure 4.12.** *In vitro* activation of Flt3L-DC by polyUS21 is mediated by complex formation. **A.** 10μg polyUs21 was incubated for 1h at 37°C in PBS or 50μg/ml RNase, then analysed on a 2% agarose gel stained with SYBR Safe. **B.** 2x $10^3$ Flt3L-DCs were incubated overnight with increasing concentrations of polyUs21, alone or complexed with either LL37 (1:1 molar ratio) or 20μg DOTAP. Cytokine levels were measured in the supernatant by ELISA. **C.** 1x $10^3$ Flt3L-DCs were incubated overnight with increasing concentrations of polyUs21, alone or complexed at either 1:1 or 1:5 molar ratio with LL37. Data are mean ± SD of three technical replicates (**B, C**). To compare between polyUs21 to LL37 molar ratios, data was analysed by linear regression (**C**). All data representative of 2 independent experiments.

Having established that complex formation with synthetic LL37 enhanced immunostimulatory activity of polyUs21 when complex at 1:1 molar ratio, we went on to evaluate weather LL37 fused to Trastuzumab showed similar activity. Since pDCs in the composition of Flt3L derived BMDCs also produce IFN-α in response to TLR7 agonists (Swiecki and Colonna 2015), we

investigated this cytokine as well. Conversely, conventional DCs do not produce IFN-α. When complexed with polyUs21, but not alone, Tr-linker-LL37, where the linker is H2, H3 or H4 and Iso-H3-LL37 induced activation of Flt3L-DCs, measured as production of cytokines IL-12p40 (Fig. 4.13 A), IL-6 (Fig. 4.13 B) and IFN-α (Fig. 4.13 C). Production of all three cytokines was similar for all mentioned antibody-LL37 fusion antibodies and was comparable to synthetic LL37 peptide activity.

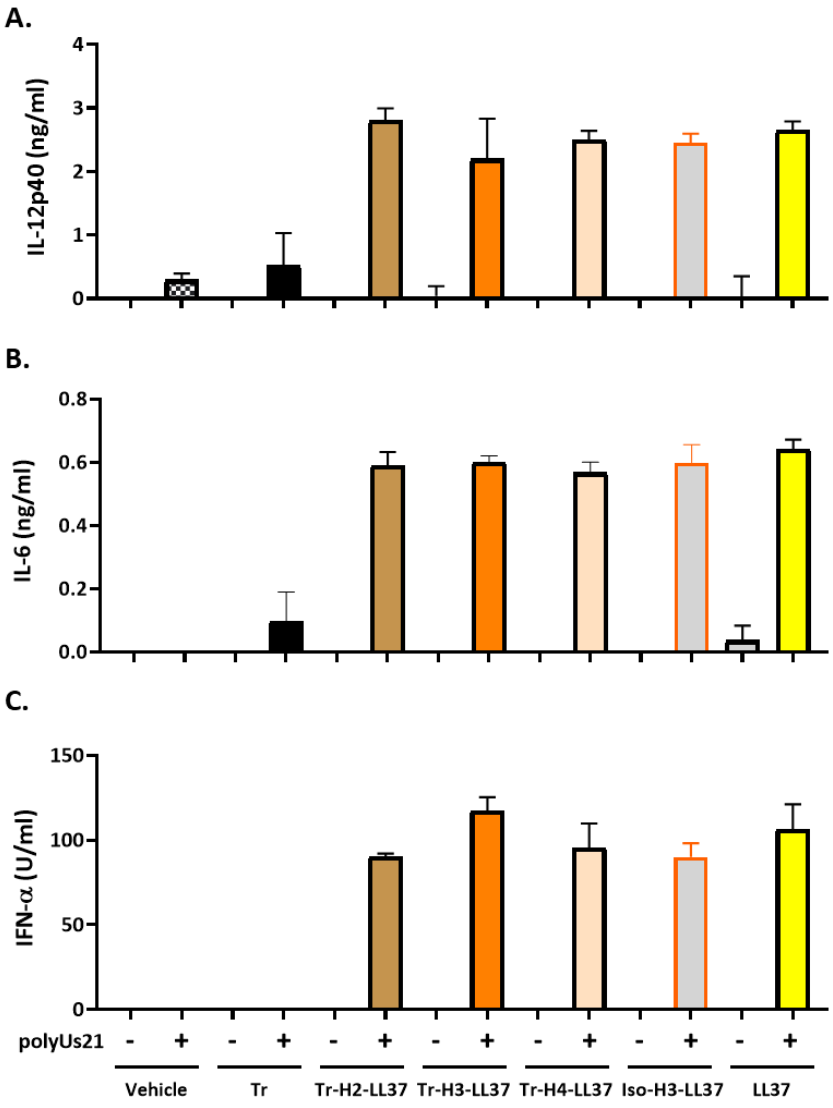


**Figure 4.13.** Impact of LL37 fusion to antibodies on mediating polyUs21 activation of Flt3L-DC. Complexes were formed at 1:1 molar ratio polyUs21 to LL37. Fused LL37 moiety of Tr-H2-LL37, Tr-H3-LL37, Tr-H4-LL37 and Iso-H3-LL37 were compared to the synthetic LL37 peptide. 1x $10^5$ Flt3L-DC were stimulated overnight with 3µg/ml polyUs21, alone or in complex with LL37 or fusion antibodies. Plates were frozen and thawed, then IL-12p40 (**A**), IL-6 (**B**) and IFN-α (**C**) was measured by respective ELISA. Data is representative of minimum 2 independent experiments, apart from Iso-H3-LL37, which was added only in one of the experiments.

Taken together, these data show that complex formation with LL37 boosted activity of polyUs21 and there was no difference between synthetic LL37 and antibody-LL37 fusion antibodies.

Since Tr-H3-LL37 showed better expression levels and was as efficient in activation assays as the LL37 peptide, we primarily used this antibody in most downstream experiments.

One of the objectives of this study is to compare, if possible, the effects of targeted delivery of CpG, a TLR9 agonist with the effects of polyUs21, a TLR7 agonist. CpG 1668 is a robust NA TLR9 agonist which does not require complex formation for immunostimulatory activity. However, to verify that complex formation with LL37 peptide or fusion antibody moiety does not influence CpG activity, we stimulated GM-CSF derived BMDCs overnight with either free CpG or complexes and detected cytokine production by ELISA as a measure of activation. Neither vehicle, Tr, Tr-H3-LL37 or Iso-H3-LL37 induce IL-12p40 (Fig. 4.14. A) or IL-6 (Fig. 4.14 B) production. CpG activated DC with comparable activity alone, with Tr or complexed with Tr-H3-LL37 or Iso-H3-LL37 (Fig. 4.14).

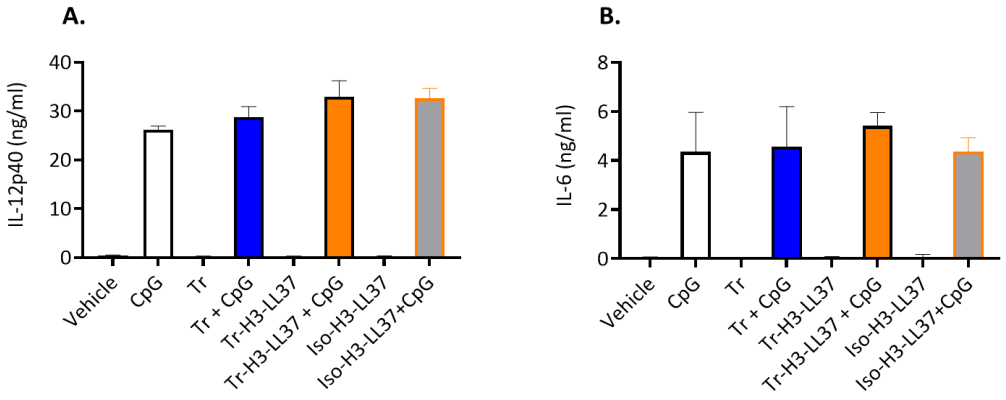


**Figure 4.14.** Tr-H3-LL37-CpG and Iso-H3-LL37-CpG complexes are as efficient in activating GM-CSF BMDCs as CpG alone. 1x $10^5$ GM-CSF BMDCs were incubated overnight with 500ng/ml of CpG, alone (white), with Tr (blue) or complexed with Tr-H3-LL37 (orange) or Iso-H3-LL37 (grey). The next day, plates were frozen and thawed and IL-12p40 (**A**) and IL-6 (**B**) were detected in supernatant as a measure of DC activation. Mean ± SD of three replicates. Data representative of 2 independent experiments.

## 4.4 Trastuzumab-linker-LL37 fusion antibodies, alone or complexed with NA TLR agonists maintain binding to human HER2

To verify that Trastuzumab-linker-LL37 (H2, H3 or H4 linkers) fusion antibodies and complexes maintain human HER2 binding properties of the parent antibody, we performed ELISA with immobilised human HER2 and an anti-human IgG detection antibody. Iso-H3-LL37, alone (Fig. 4.15 A) or complexed with CpG 1668 (Fig. 4.15 B) did not show non-specific binding. Compared to Tr, the fusion antibodies Tr-H2-LL37, Tr-H3-LL37 and Tr-H4-LL37 showed similar binding to human HER2, with only subtle differences noticeable in the linear part of the binding curve (Fig. 4.15 A). Complex formation at 1:1 CpG to LL37 molar ratio only minimally decreased binding to HER2 with mild differences noted in the linear range of the binding curve, but not upper asymptote (Fig. 4.15 B). No important differences were noticed among fusion antibodies, either alone, or complexed with CpG. Similar results were obtained when the NA TLR7 agonist polyUs21 was used for complex formation instead of CpG (data not shown).

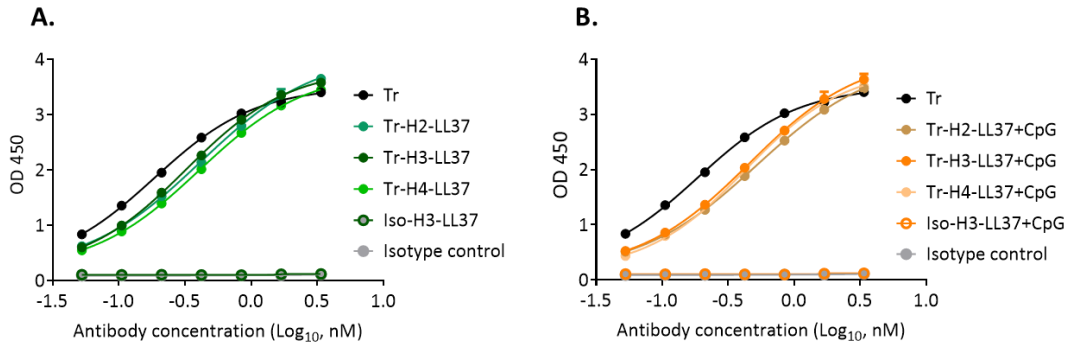


**Figure 4.15.** Human HER2 binding of fusion antibody and complexes. LL37 fusion antibodies alone (**A**) or complexed with CpG 1668 (**B**) were analysed on ELISA with immobilised human HER2. Detection was performed with anti-human IgG biotinylated antibody. Data are mean ± SD of three technical replicates and is representative of 3 experiments with Tr-linker-LL37 antibodies and complexes, 2 of them including Iso-H3-LL37 antibody and complexes.

Collectively, *in vitro* analysis of Tr-H3-LL37 showed that this fusion antibody binds human HER2 in a similar fashion with the parent antibody and forms complexes with NA TLR agonists CpG and polyUs21.

## 4.5 *In vivo* evaluation of Tr-H3-LL37 + CpG complexes

### 4.5.1 Efficiency of treatment with Tr-H3-LL37 + CpG on B14.3 Luc HER2 pulmonary tumour growth

To evaluate the impact of treatment with Tr-H3-LL37 on tumour growth, we used the pseudo-metastasis mouse model we established with B14.3 Luc HER2 cells, clone H2 (see Chapter 3). In this model, treatment with Tr does not significantly impact tumour growth, with a subtly higher tumour burden measurements in the Tr treated mice (Figure 3.13).

For the current experiment, mice were treated trice as indicated by arrows in Figure 4.16 A with vehicle (PBS), Tr or Tr-H3-LL37 + CpG in PBS and were imaged *in vivo* at 10 min after injecting luciferase substrate at the indicated time points (☼). Doses for treatment were 270 picomoles of antibody (2mg/kg body weight, 40µg per mouse), as described for figure 3.15. Previous studies showed that this dose of 2mg/kg is optimal for marked accumulation to the tumour tissue (McLarty et al. 2009). CpG was complexed at 1:1 molar ratio with LL37. For the fusion antibody dose, CpG was 3µg. The dose of CpG and sequence of repeated treatment are in range of previously published data showing immune mediated anti-tumour efficacy (Kunikata et al. 2004; Kawarada, Ganss, Garbi, Sacher, Arnold, and Hämmerling 2001; Chavez et al. 2018). To assess tumour burden, luminescence intensity (photons/s) was measured in regions of interest (ROI) of 2.647cm diameter encompassing the lung area on the mouse anterior thorax (Fig. 4.16 B). Mice bearing B16 tumours were used to establish background. Luminescence intensity increased steadily in B14.3 Luc HER2 mice with time to reach a maximum at day 18 (Fig. 4.16 C). When comparing the vehicle group with either Tr group or CpG group using the CGGC permutation test (Elso et al. 2004), global luminescence intensity profile was not significantly different (data not shown). Luminescence intensity was strikingly similar between the Tr and the Tr-H3-LL37 groups across time-points, with $p=0.756$ (Fig. 4.16 C).

At day 18 post tumour inoculation, mice were culled, lung tissue was harvested, bleached in Fekete solution and lung nodules were counted. There was no significant difference in the total number of lung tumours between either of the groups, with $p=0.7289$ determined by Kruskal-Wallis test (Fig. 4.16 D). A repeat experiment with Tr-H3-LL37 + CpG treatment is needed to boost n numbers for more robust statistical analysis and confirm our current results. These data, however, illustrate that treatment with 3 doses of Tr-H3-LL37 + CpG does not impact pulmonary B14.3 Luc HER2 (clone H2) tumour growth.

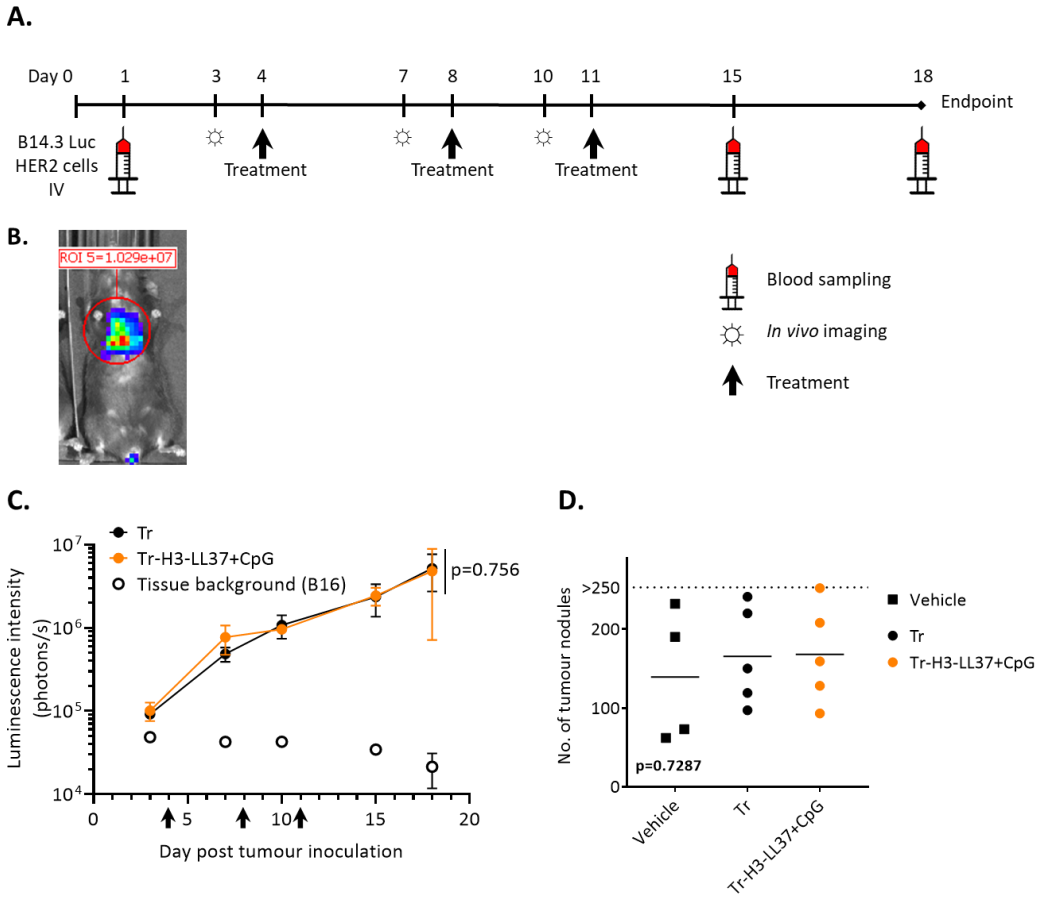


**Figure 4.16.** Treatment with Tr-H3-LL37+CpG does not influence tumour growth. **A.** Treatment regimen and timing for *in vivo* imaging. **B.** Representative image showing position of region of interest (ROI) for *in vivo* imaging of tumour burden. **C.** Luminescence intensity (photons/s) of mouse lungs with B16 tumours (background) or B14.3 Luc HER2 tumours, treated with Tr (n=5) or Tr-H3-LL37 (n=5). Data are mean ± SEM. Groups were compared using CGGC permutation test with 10 000 permutations. **D.** Number of pulmonary tumour nodules on day 18 post tumour inoculation of mice treated with vehicle (n=4), Tr (n=5), and Tr-H3-LL37 (n=5). Data from1 experiment for Tr-H3-LL37 group. Kruskal-Wallis one-way analysis of variance.

### 4.5.2 Serum concentration of Tr-H3-LL37, alone or complexed with CpG

Previously published data demonstrates that LL37 can be internalised in mammalian cells and access intracellular compartments and receptors, either alone, or complexed with nucleic acids or other anionic molecules. It was proposed that internalisation is not receptor mediated (Sandgren et al. 2004; Xhindoli et al. 2016). A previous study showed that LL37-RNA complexes uptake was higher in monocytes and reached not only the endosomal compartment, but also the cytosole (Ganguly et al. 2009). Soluble proteins are taken up by cells via pinocytosis and used as a source of energy. The long half-life of IgG antibodies is determined by interactions with neonatal Fc receptor in the endosomes, which mediate their return into circulation (Kuo and Aveson 2011). We consider that LL37, when fused with Tr, might

interfere with antibody recycling processes, changing the serum concentration of Tr-H3-LL37, relative to Tr.

To investigate this, mice were treated IV with one dose of 40µg Tr, Tr-H3-LL37 or Tr-H3-LL37 + CpG (Fig. 4.17 A). Serum samples were harvested at the indicated dates, and concentration of antibody was determined using ELISA. Tr, Tr-H3-LL37 or Tr-H3-LL37 + CpG were captured with immobilised human HER2 and detected with anti-human IgG Fc monoclonal antibody. Standard curves were prepared with Tr, Tr-H3-LL37 and Tr-H3-LL37 + CpG. Serum concentrations were obtained by interpolation from the linear range of the curve. Serum harvested before treatment was used as negative control and gave a value of 0.0067±. Among the time-points measured, serum Tr was highest at day 1 post-treatment at 23.52±3.18 µg/ml and decreased progressively to 6.78±0.45 µg/ml on day 7 post-treatment (Fig. 4.17 B). This is in line with previous publications, reporting a similar downwards trend of serum Tr upon IV administration in tumour bearing mice (Milenic et al. 2010; Borrok et al. 2015). In contrast with the profile of Tr, both Tr-H3-LL37 and Tr-H3-LL37 + CpG were rapidly depleted from circulation, with day 1 serum concentrations of only 1.82±0.56 µg/ml and 1.24±0.17 µg/ml, respectively (Fig. 4.17 B).

To confirm the rapid depletion of Tr-H3-LL37 + CpG, serum samples were harvested from tumour bearing mice which received 3 doses of treatment, as shown in Fig. 4.17 C. In mice treated with three 40µg doses of Tr, serum Tr levels reached 33.05±0.43 µg/ml on day 3 post the last treatment dose (Fig. 4.17 D), which is an approximate 1.5x fold higher than the values measured for mice treated with just one dose of Tr (Fig. 4.17 B). This is consistent with the reported half-life of Trastuzumab in (tumour-free) mice which is 12-16 days (Hurst et al. 2014). Repeated treatment with Tr-H3-LL37 + CpG however, did not improve its persistence in serum (Fig. 4.17 D).

Together, our results demonstrate that serum concentrations of Tr-H3-LL37, alone or complexed with CpG are dropping rapidly, within one day or less, which is not consistent with the parent antibody Tr or the expected behaviour of a human IgG1 in mice.

The result is especially important, as it has been shown that antibodies targeting tumour associated antigens, such as Trastuzumab, gradually concentrate into the tumour tissue over days (Mortimer et al. 2014). Since Tr-H3-LL37 (with or without CpG) is cleared rapidly from serum it cannot concentrate into the tumour tissue and activate local immune cells. Hence, IV administration of Tr-H3-LL37 complexed with CpG is not a feasible approach for targeted deposition of CpG in the tumour tissue.

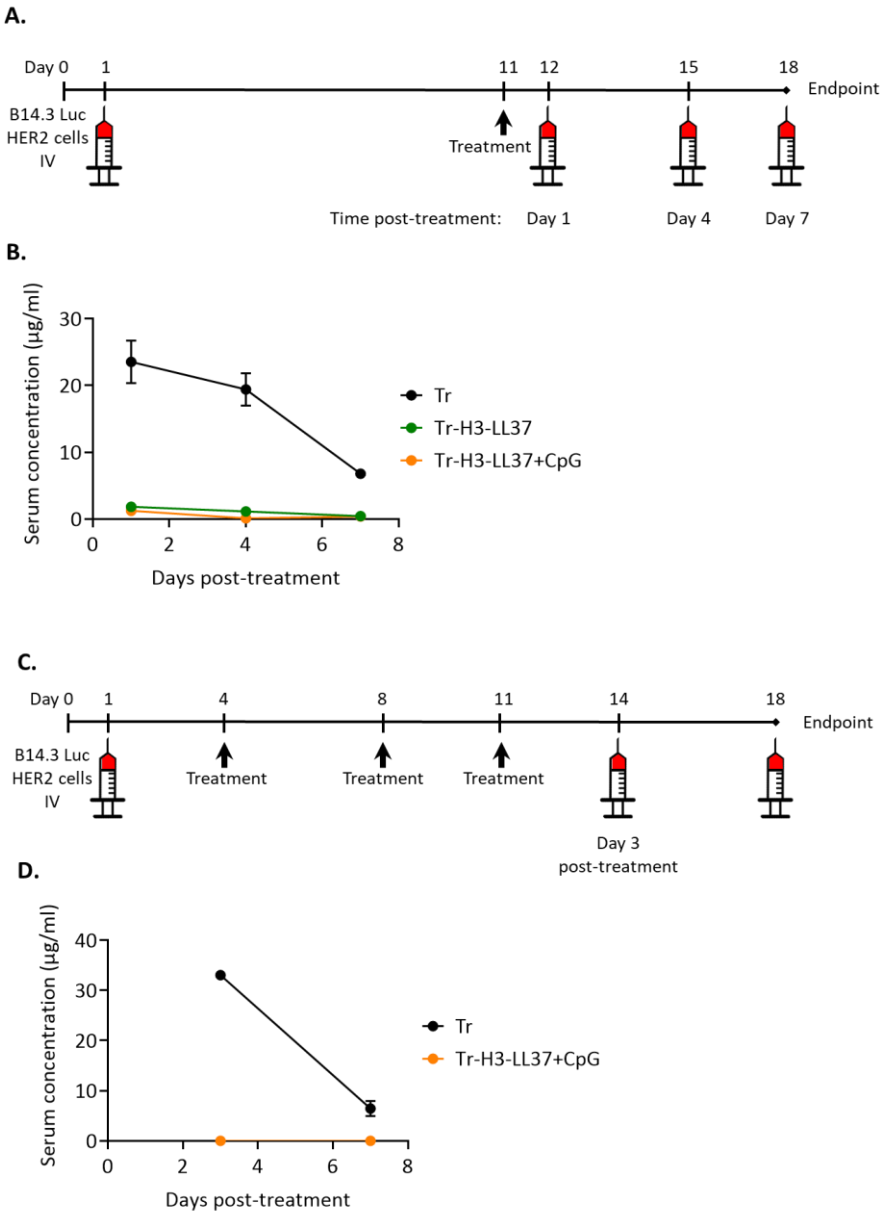


**Figure 4.17.** Serum concentration of Trastuzumab and fusion antibody in tumour bearing mice. **A-B**. Mice (n=5) were inoculated IV on day -11 with 6x105 B14.3 Luc HER2 cells. Mice were treated with 40µg of either Tr, Tr-LL37 or Tr-LL37 + CpG on day 0 (arrow). Serum was collected before treatment and at days 1, 4 and 7 post-treatment (syringe symbol). **C, D.** Mice (n=5) were inoculated IV on day -11 with 9x105 B14.3 Luc HER2 cells. Mice were treated with three doses of 40µg of either Tr, Tr-LL37 or Tr-LL37 + CpG (arrows). Serum was collected before treatment and at days 3 and 7 post-treatment (syringe symbol). **B, D.** Concentration of antibody or complexes was measured using ELISA with immobilized human HER2 and anti-human IgG1 detection antibody. Each graph shows means ± SD of data from one experiment.

## Discussion

In this chapter we fused LL37 at the heavy chain C-terminus of Trastuzumab. We showed that efficient separation of heavy chain C-terminus and LL37 via a rigid linker with at least two EAAAK repeats is required to enable expression of the fusion antibody (Fig. 4.6). We have further shown that both antigen binding (Fig. 4.15) and LL37 function are conserved (Fig. 4.13). This strategy can be used to generate and efficiently express other functional fusion antibodies with heavy chain C-terminus moieties and to enable other research projects.

*In vitro* generated LL37-nucleic acid complexes were visualised by other groups using confocal microscopy or scanning electron microscopy, as complexes are aggregated and condensed structures (Ganguly et al. 2009; Lande et al. 2007). Here we have shown that Tr-H3-LL37 + CpG complexes can be easily visualised using absorption at wavelengths higher than 320nm (Fig. 4.11), an assay which is less descriptive, but more rapid to perform and less prone to visual interpretation bias. The size and morphology of complexes has not been determined, nor do we know if and how this influences immunoactivity. Future experiments are required to correlate the conditions for complex formation to complex size and immunoactivity.

We evaluated Tr-H3-LL37 + CpG complexes *in vivo* as well. Trastuzumab is a human IgG1 antibody and therefore shows an extended half-life of days in the mouse system (Hurst et al. 2014). This is crucial for activity, as it takes time for the antibody to concentrate at the tumour site (Palm et al. 2003; Lee and Tannock 2010). In our experiments, Tr persisted in serum of tumour-bearing mice for days. In contrast, both Tr-H3-LL37 and Tr-H3-LL37+CpG complexes were rapidly cleared from serum within one day from IV administration (Fig. 4.17). This indicates that systemic delivery of Tr-H3-LL37+CpG complexes cannot achieve targeted delivery of NA TLR agonists to the tumour tissue.

Tr-H3-LL37 serum concentration was determined using an antibody against the Fc region of human IgG1. This indicates that the entire fusion antibody was removed from circulation and not just LL37. The same stands for Tr-H3-LL37 + CpG (Fig. 4.17). The mechanism for this rapid clearance remains unclear. It is possible though, that the membrane-permeating properties of LL37 and LL37 complexes lead to rapid clearing by blood cells. In the context of skin infection, as well as autoimmune diseases such as lupus or psoriasis, LL37 is produced locally and acts on neighbouring cells. It might be that the function of LL37 can be harnessed for paracrine use, but not for systemic use. The question remains about the use of LL37 fusion antibodies for other routes of administration.

To summarise this chapter, data so far indicates that Tr-H3-LL37 fusion antibodies are not appropriate means for targeted delivery of NA TLR agonists and other strategies should be explored to achieve this.

# Chapter 5 - Results

## Antibody conjugates for targeted delivery of CpG ODN to the tumour microenvironment

# Chapter 5: Antibody conjugates for targeted delivery of CpG ODN to the tumour microenvironment

## Introduction

Antibody conjugates are typically generated through biochemical conjugation of a payload to a tumour-targeting antibody, most often using heterobifunctional cross-linkers (Beck et al. 2017). In this chapter, we asked if biochemical conjugation technologies used in the field of antibody drug conjugates (ADC) can be applied to generate antibody conjugates with endosomal TLR agonists.

The model antibody we used for generation of conjugates was recombinantly expressed Trastuzumab, as described in chapter 4. In terms of cross-linkers and conjugation chemistries, we primarily used succinimidyl-4-(N-maleimidomethyl) cyclohexane-1-carboxylate (SMCC). This linker contains N-hydroxysuccinimide (NHS) esters, the most often employed group for conjugation of primary amines and maleimide, to functionalise thiol groups. This allows for two-step conjugation reactions. SMCC is non-cleavable, conferring superior conjugate stability compared with many other linkers (McCombs and Owen 2015). Therefore, we considered SMCC a valuable candidate for our conjugation reactions.

In terms of payloads for conjugate generation, these molecules should be soluble, stable and amenable to conjugation without loss of function (McCombs and Owen 2015). CpG molecules are highly potent, nuclease resistant oligonucleotides (ODN), with robust *in vitro* and *in vivo* stability and relatively low molecular weight (Krieg 2006), and can be ordered with a terminal amino or thiol group for conjugation. We considered them, therefore, suitable payloads for conjugation to antibodies.

Other endosomal TLR agonists that would be interesting for targeted deposition in the tumour tissue were, however, most likely not feasible for this biochemical conjugation approach. Resiquimod (R848) and other small molecules agonists of TLR7, contain a primary amine in their structure, indispensable for the molecule's activity, that is targetable by most commercial cross-likers (Ignacio et al. 2018). Therefore, conjugation of Resiquimod with such linkers is not appropriate, since it is expected to lead to complete loss of function. PolyUs21, a TLR7 agonistic oligonucleotide is rapidly degraded by RNases and is unstable in serum unless complexed with cationic molecules (Diebold et al. 2006). This implies that the polyUs21 molecule conjugated via one chemical group to an antibody is likely to be rapidly degraded by

RNases as well. Polyinosinic-polycytidylic acid (poly I:C), a TLR3 agonist of 1.5-8 kilobases and undefined molecular weight also requires complex formation of high-molecular weight species of poly I:C for activity (Zhou et al. 2013). Moreover, the molecular weight of poly I:C is expected to be problematic due to sterical hindrance and this agonist cannot be purchased with thiol or amine modifications, rendering it unsuitable for conjugation. Hence, in terms of harnessing antibody conjugates for targeted delivery of endosomal TLR agonist, for this project we only focused on CpG, due to its greater potential for conjugation.

## 5.1 Identifying suitable CpG ODN molecules for the project

CpG ODN molecules are typically considered species-specific, although this does not apply to all CpG ODNs (Roberts et al. 2005). To directly compare activity of different CpG ODNs on mouse and human TLR9, we performed *in vitro* activation assays (Fig. 5.1). CpG ODNs were titrated on mouse GM-CSF bone marrow-derived DCs (BMDC), which contain a mixed population of inflammatory DCs, macrophages and neutrophils (Inaba et al. 1992; Helft et al. 2015) (Fig. 5.1 A) and Flt3L BMDCs which contain a mixed population of primary DC including conventional DC (cDC) and pDC (Brawand et al. 2002; Gilliet et al. 2002) (Fig. 5.1 B). To evaluate activation of human TLR9, primary human DCs were enriched from PBMCs (Fig. 5.1 C). Each preparation of DCs was analysed by flow cytometry to confirm the expected cell populations (see Appendices K, L, M). In response to treatment with TLR9 agonists, signalling through MyD88 induces activation of DCs, which simultaneously upregulate MHC class II and costimulatory molecules and produce proinflammatory cytokines such as IL-12, IL-6 and TNF-α (Medzhitov 2001; Diebold 2008a). We used IL-6 production by ELISA as a robust and specific marker for DC activation for comparing the potency of several CpG ODNs.

We directly compared CpG 1668, a class B mouse TLR9 agonist (Kreutz et al. 2012) with CpG 2006, which was originally designed as a human TLR9 agonist (Hartmann and Krieg 2000). We also included CpG C274, a class C CpG, with reported human and mouse activity (Marshall et al. 2003). In all assays we included negative control ODN GpC 1668, which lacks the TLR9 stimulatory activity of CpG 1668. As expected, GpC-ODN induced only minute amounts of IL-6 in both mouse and human cells (Fig. 5.1). Stimulation of DCs with increasing doses of CpG ODN typically induce a bell-shaped cytokine response. Reportedly, high concentrations of CpG (or other TLR ligands) lead to increased production of the anti-inflammatory cytokine IL-10 which inhibits DC functionality via an autocrine negative feedback loop and results in lower levels of proinflammatory cytokines (Waibler et al. 2008; Chang, Kunkel, and Chang 2009; Couper, Blount, and Riley 2008). In our hands, all CpG molecules induced IL-6 in a dose-dependent manner and with different potencies in mouse versus human cells. For each CpG ODN, the maximal IL-6 level was obtained at different concentrations for mouse GM-CSF or Flt3L derived BMDCs. This is likely due to differences in cell composition and/or differences in TLR9 expression levels in the two distinct DC cultures. CpG 1668 and CpG C274 induced strong levels of IL-6 in mouse BMDCs generated with either GM-CSF (Fig. 5.1 A) or Flt3L (Fig. 5.1 B). We also measured levels of IL-12p40 in supernatant of GM-CSF derived BMDCs and found them to be in line with the IL-6 results (data not shown). As expected, human DCs enriched from PBMCs produced higher levels of

IL-6 in response to human CpG ODN 2006 (Fig. 5.1 D), which was originally designed as a human TLR9 agonist. Notably, although less potent, CpG 1668 also shows human TLR9 activity. CpG C274 showed substantial activity on both mouse and human cells (Fig. 5.1). We decided to start our conjugation experiments using CpG 1668, since it had been used for antibody-ODN conjugate generation and investigation of anti-tumour immunity induction in melanoma mouse model in our laboratory before (Kreutz et al. 2012). To test conjugates in a humanised mouse model, we would have to generate conjugates using CpG 2006 or CpG C274.

We also investigated the use of RAW 264.7, a murine macrophage cell line for *in vitro* evaluation of CpG ODN activity (Fig. 5.1 C). RAW 264.7 cells were shown to produce cytokines such as IL-6 and IL-12 when stimulated with CpG-ODNs, including CpG 1668 in similar conditions with our assay set-up (Chen et al. 2015; Yeo et al. 2003; Yi et al. 2002). However, in our experiments with RAW 264.7 cells stimulated with various doses CpG ODNs that efficiently activate mouse DC, the levels of IL-6 (Fig. 5.1 C) and IL-12p40 (data not shown) induction were comparatively low with less than 10ng/ml or less. Also, unlike for DC a clear dose dependent respond in activation was not observed. The data show that using RAW 264.7 cells results in poor resolution of the activation assay, making it difficult to distinguish small differences in CpG ODN activity. For this reason, we continued to use BMDCs, derived either with GM-CSF or Flt3L for the evaluation of the stimulatory activity of antibody-CpG conjugates in *in vitro* activation assays.

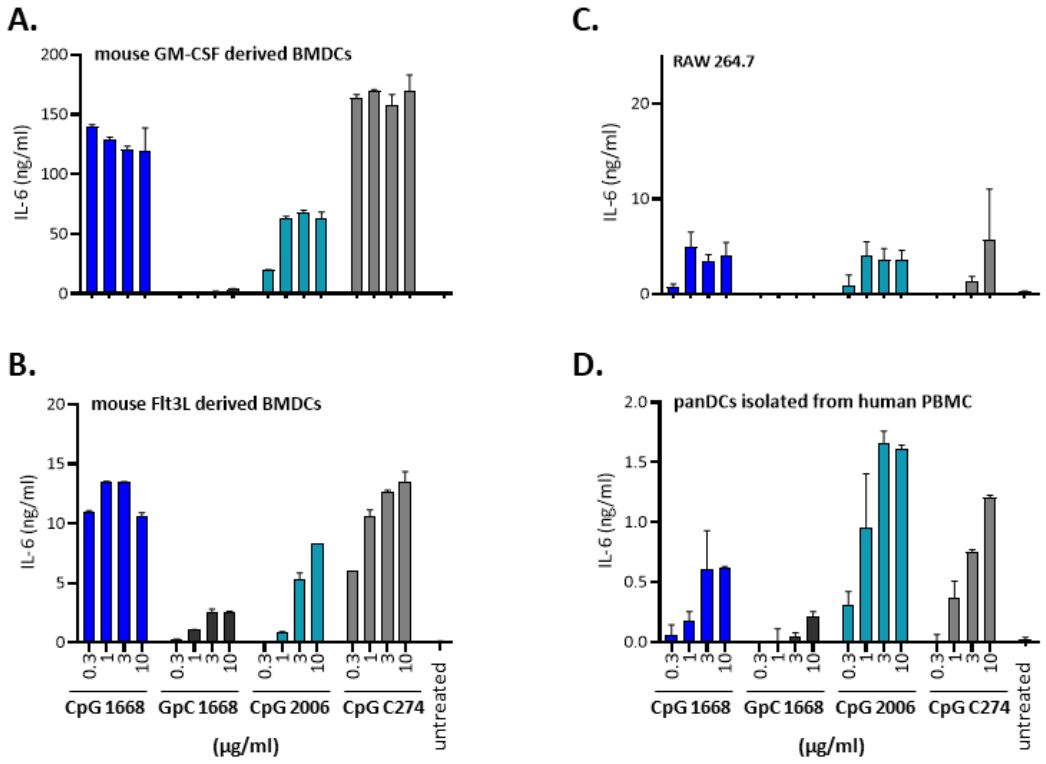


**Figure. 5.1.** *In vitro* potency of CpG ODN molecules in activating human and mouse dendritic cells. CpG-ODN molecules and control GpC were used for overnight stimulation of: $2x10^5$ mouse GM-CSF derived BMDC (**A**), mouse Flt3L derived BMDC (**B**), human DC enriched from PBMC (**D**), $0.5x\ 10^6$ RAW 264.7 cells (**C**). CpG ODN concentrations used were: 0.3µg/ml, 1µg/ml, 3µg/ml, 10µg/ml. IL-6 levels were measured in cell supernatant after overnight culture to quantify DC activation. Data are representative of two independent experiments.

## 5.2 Trastuzumab-CpG conjugates generated by conventional conjugation with SMCC

### 5.2.1 Generation of conjugates

In terms of conjugation chemistries, traditional approaches involve the use of a heterobifunctional linker. These methods are often named conventional and the resulting conjugates are often referred to as conventional or traditional conjugates in the literature (Beck et al. 2017; Sochaj, Swiderska, and Otlewski 2015; Zhou 2017).

To begin our experiments, Tr was conjugated to CpG 1668 using the heterobifunctional cross-linker SMCC, containing an NHS (N-hydroxysuccinimides) ester and a maleimide, separated by a cyclohexane ring (chemical formula included in Fig. 5.3 A). We have employed this conjugation strategy as it is a validated method, which was previously used to generate Trastuzumab-DM1 (Kadcyla®) conjugates, approved for clinical use (Chari et al. 1992; Lambert and Chari 2014). Additionally, our lab used this crosslinker to successfully generate antibody-CpG 1668 conjugates for a previous study (Kreutz et al. 2012).

An overview of the conjugation reactions is shown in Fig. 5.2. In a first step, primary amines in lysine residues on the surface of Tr were modified with SMCC to generate maleimide-activated Tr. This first reaction can be performed in PBS, at neutral pH, or in borate buffer in mild alkaline conditions (pH of about 9). After purification from unbound cross-linker, thiol-CpG 1668 or thiol-GpC 1668 were reacted in PBS + 2mM EDTA (pH=7.1-7.3) with maleimide-activated Tr, generating Tr-MCC-CpG or Tr-MCC-GpC. After CpG conjugation, 10x molar excess of cysteine was added for 10 min. In maleimide conjugation reactions, thiol-containing small molecules, including cysteine, are typically used at high molar excess after payload conjugation to cap residual maleimide groups (Kim et al. 2008; Tiwari et al. 2009; Christie et al. 2017). An additional purification step was performed to separate the conjugate from unreacted ODN and cysteine. The resulting conjugates were analysed for Tr and CpG composition. The protein concentration was determined by BCA assay with a bovine gamma globulin (BGG) standard curve. CpG 1668 concentration in the conjugate preparation was determined using spectrophotometry. We measured A260 and calculated the concentration of CpG 1668 by interpolation on a standard curve generated with a constant concentration of Tr mixed with a dilution series of CpG 1668. Following this, the payload (CpG 1668) to antibody molar ratio was determined for purified conjugates.

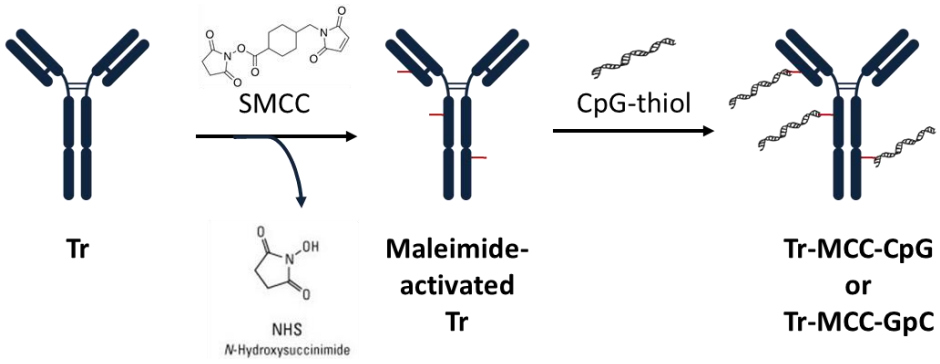


**Figure 5.2**. Schematic representation illustrating the reaction steps for conjugation of Trastuzumab with CpG using the heterobifunctional crosslinker SMCC.

### 5.2.2 Composition of resulting Tr-MCC-CpG conjugates

The IgG scaffold contains over 80 lysine residues, typically with around 20 residues at sites that are accessible for conjugation (McCombs and Owen 2015). Conjugation of SMCC to certain lysine residues on proteins depends on pH and SMCC molar excess, with different conditions resulting in distinct distribution of the payload added in the second step (Madler et al. 2009; Kalkhof and Sinz 2008; Smith 2006). To exemplify, α-amines at the N-terminus of heavy and light chains, usually deprotonated at pH=7, may be favoured for NHS modification at neutral pH, while ε-amines, which are lysine residues on the antibody surface and are usually

deprotonated at pH around 9, may be favoured for conjugation in mild alkaline conditions (Koniev and Wagner 2015). Payload molar ratio added in the second step of the reaction also impacts the final conjugate. It has been previously shown, that higher degrees of conjugation can impair antibody functionality and this depends on antibody structure and conjugation conditions (Thomas, Teicher, and Hassan 2016). To identify suitable conjugation conditions for the generation of functional Tr-MCC-CpG conjugates, we titrated both SMCC and CpG 1668 molar ratios to antibody and performed conjugations with either Tr or Herc, at neutral pH (7.1-7.3) in PBS or alkaline pH (8.9-9.1) in borate buffer (Table 5.1).

| Antibody | Buffer for conjugation of Tr with SMCC | SMCC molar excess | Payload (CpG 1668) molar excess | CpG to antibody molar ratio of resulting conjugate |
|---|---|---|---|---|
| Herc | PBS | 34 | 10 | 7.55 |
| Herc | PBS | 34 | 6 | 3.61 |
| Herc | PBS | 34 | 3 | 2.88 |
| Herc | PBS | 10 | 3 | 0.97 |
| Tr | PBS | 34 | 10 | 9.16 |
| Tr | PBS | 34 | 6 | 6.12 |
| Tr | PBS | 34 | 3 | 3.09 |
| Isotype | PBS | 34 | 6 | 2.87 |
| Herc | Borate buffer | 30 | 5 | 2.72 |
| Herc | Borate buffer | 20 | 5 | 2.13 |
| Herc | Borate buffer | 10 | 5 | 1.08 |
| Tr | Borate buffer | 30 | 4 | 2.02 |
| Tr | Borate buffer | 10 | 4 | 0.81 |
| Tr | Borate buffer | 5 | 4 | 0.40 |
| Isotype | Borate buffer | 20 | 5 | 1.82 |
| Herc | Borate buffer | 20 | 5 | 1.86 |
| Tr | Borate buffer | 20 | 5 | 2.12 |

**Table 5.1.** Antibodies and conditions used to generate conventional conjugates using SMCC. CpG to antibody molar ratio of resulting conjugate is depicted.

As mentioned before, CpG C274 is a potent human and mouse TLR9 activator and of interest for generating conjugates. However, when we attempted to generate conjugates using CpG C274 the conjugate precipitated heavily (data not shown). This is not surprising, considering that class C CpG molecules tend to spontaneously form intermolecular duplexes (Pohar et al. 2015), each duplex containing thiol groups on each strand. Upon conjugation, this most likely lead to crosslinking of antibodies by CpG C274 duplexes and precipitation. Therefore, all conjugates we describe in this chapter were generated with CpG 1668 or the negative control, GpC 1668.

To confirm conjugation and characterise the conjugates in terms of structure and molecular weight, we employed two methods, size exclusion chromatography (SEC-HPLC) and SDS-PAGE analysis.

SEC-HPLC analysis (Fig. 5.3 A) of Tr (black), monitoring absorption at 214nm, shows a symmetrical peak corresponding to monodisperse antibodies and two peaks with considerably lower area, one with shorter retention time (RT), suggestive of aggregates and one with longer RT, characteristic for antibody fragments. Relative area under the curve calculated for each of the peaks was 3.50% for aggregates, 95.43% for monodisperse antibodies and 1.07% for fragments. When Tr-MCC-GpC was analysed by HPLC (pink), the peak corresponding to monodisperse conjugates (RT=26.4 s) eluted faster than the corresponding peak for Tr (RT=27.95 s), indicating an increased MW. Elution peak of Tr-MCC-CpG was shorter and wider than elution peak of Tr and slightly asymmetric, despite injecting the same quantity of each analyte, which is suggestive of increased heterogeneity. Importantly, peaks representing higher MW species and monomeric Tr-MCC-GpC were poorly resolved and hence the measurements are imprecise. The relative area of the shoulder corresponding to higher MW species was 8.95%, while the area for the second peak, representing monodisperse conjugates was 90.09%. We propose that the column used, TSK G4000SWXL separating molecules of 20 – 7 000 kDa, was not ideal for the purpose. For future experiments and another column, TSK G3000SWXL, separating molecules of 10 – 500 kDa would be more suitable to achieve better resolution in the assay.

Tr and Tr-MCC-CpG conjugates we analysed by SDS-PAGE as well (Fig. 5.3 B). The gel was stained successively with ethidium bromide to visualise CpG / GpC content (upper Fig. 5.3 B) and Simply Blue for protein content (lower Fig. 5.3 C). This allowed us to visualise co-migration of CpG with Tr, confirming successful conjugation and show that conjugates with higher molar ratio of CpG migrate slower corresponding to their increased MW (Fig. 5.3 B).

Staining for protein illustrated that Tr preparations only contained a small amount of higher MW species migrating slower on the gel (Fig. 5.3 B lower) and a very faint band representing fragments (data not shown). This was in line with HPLC data (Fig. 5.3 A). Analysis of Tr-MCC-GpC conjugates by SDS-PAGE efficiently separated monomeric conjugates from higher MW species (Fig. 5.3 C lower). The presence of multiple bands suggested that higher MW species were heterogenous in composition.

Data from both HPLC and SDS-PAGE analyses confirm increased MW of conjugates via attached CpG or GpC and the presence of higher MW species generated via conjugation. SDS-

PAGE analysis showed overall superior resolution and we only used this method for analysis of future batches of conjugates.

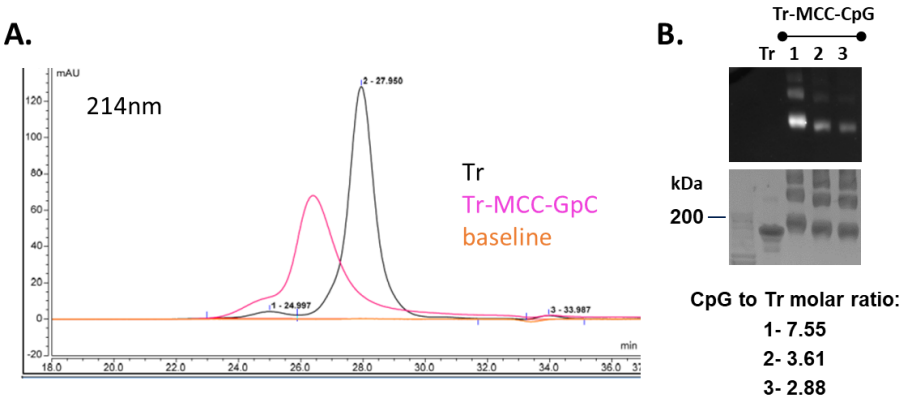


**Figure 5.3**. Characterisation of Tr-MCC-CpG conjugates by SEC-HPLC (A) and SDS-PAGE (B). **A.** HPLC analysis of Tr and Tr-MCC-GpC conjugate eluted on a TSK G4000SWXL column. Purified Tr-MCC-GpC had a GpC to Tr ratio of 6.28. Overlaid chromatograms from one experiment. **B.** SDS-PAGE analysis in non-reducing conditions of Tr and Tr-MCC-CpG conjugates and sequential staining with Ethidium Bromide (upper) for CpG and SimplyBlue (lower) for Tr. CpG to Tr molar ratio in purified conjugates is shown. Data representative of 5 independent experiments.

Importantly, higher MW species of Tr-MCC-CpG (or GpC) conjugates cannot be separated from monomeric conjugate using commercially available ultrafiltration columns and we used conjugate preparations as shown for downstream experiments. Other purification methods, such as size exclusion chromatography, may be useful to separate monomeric conjugates from higher MW species.

Next, we investigated whether the conjugation process affected the immunostimulatory activity of CpG or the functional properties of Trastuzumab.

### 5.2.3 *In vitro* immunostimulatory activity of Tr-MCC-CpG conjugates

To investigate whether conjugation of CpG to Trastuzumab affected its stimulatory activity, we performed *in vitro* activation assays. GM-CSF derived BMDCs were stimulated overnight with free or conjugated CpG. In addition, BMDCs were cocultured with B14.3 Luc HER2 cells pre-incubated with conjugates or their controls. We knew from previous experiments that maximum GM-CSF derived BMDC activation were obtained with CpG 1668 doses in the 0.3-1 µg/ml range (see Fig. 5.1 A). Therefore, we incubated cells with a dose of either 0.25 or 0.5 µg/ml ODN, normalising samples for ODN content. Free Tr was normalised to Tr content in Tr-MCC-CpG. IL-12p40 and IL-6 were measured in cell supernatant by ELISA. As expected, vehicle, Tr, free GpC nor Tr-MCC-GpC conjugates did not induce cytokine production by BMDCs. Tr-MCC-CpG induced similar, if not slightly superior levels of IL-12p40 (Fig. 5.4

A) or IL-6 (Fig. 5.4 B) compared to CpG or Tr in the presence of free CpG. This pattern was also was observed when conjugates were pre-adsorbed on HER2 positive tumour cells before incubation with BMDCs (Fig. 5.4 C, D). Interestingly, GM-CSF derived BMDCs produced approx. two times higher levels of IL-6 when stimulated alone, compared to the tumour cell co-culture (e.g. 53.11 ng/ml induced by Tr-MCC-CpG vs. 23.43 ng/ml). In contrast, the IL-12p40 response of GM-CSF BMDC to CpG ODN was unaffected by the presence of tumour cells. The same trend was observed in other experiments, where Herc-MCC-CpG conjugates were used instead (data not shown). Our data shows that Tr-MCC-CpG maintain immunostimulatory CpG activity, even when adsorbed on B14.2 Luc HER2 cells.

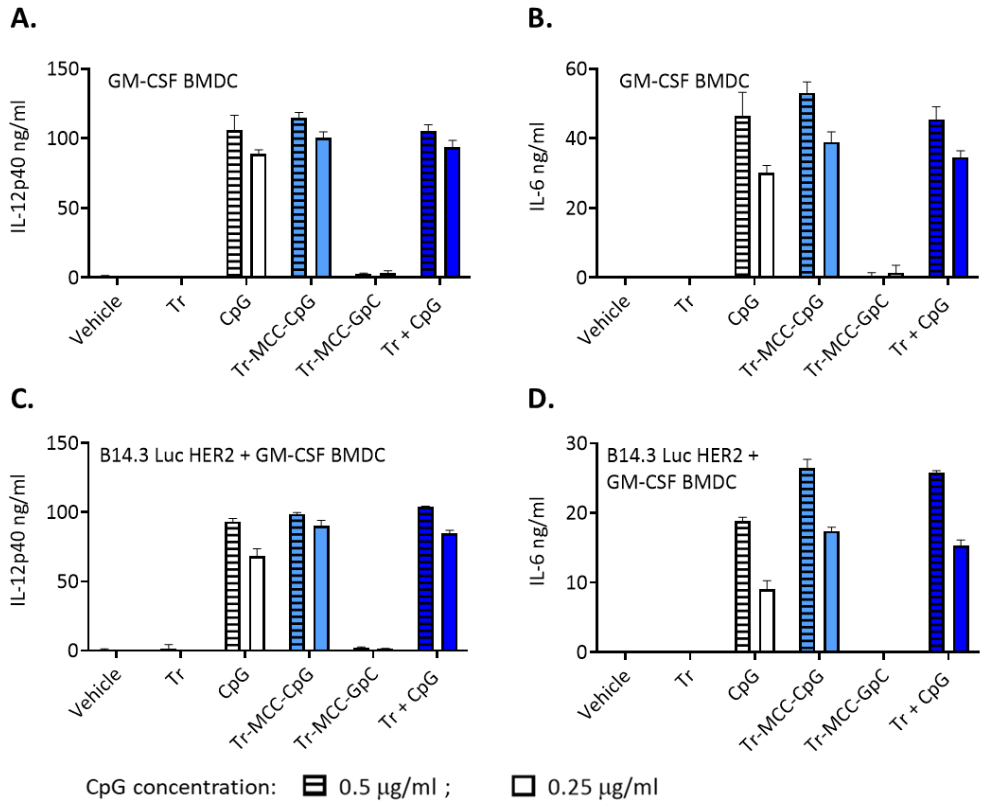


**Figure 5.4.** *In vitro* dendritic cell activation assay evaluating functionality of conjugated CpG. $0.2x10^5$ GM-CSF BMDC were stimulated overnight alone (**A** and **B**) or in the presence of $4x10^5$ tumour cells (**C** and **D**) with 0.5ug/ml (open symbols) and 0.25ug/ml (lined fill pattern) of CpG, either free (white) or conjugated with SMCC to Tr (light blue). Tr-MCC-GpC conjugates were used as negative controls. Read-out for DC activation levels of IL-12p40 (A and C) and IL-6 (B and D) measured by sandwich ELISA. Data are mean ± SD of three technical replicates and is representative of three independent experiments with different batches of conjugates.

### 5.2.4 Conventional conjugates generated with SMCC have altered HER2 binding

Since it was reported that conjugation reactions can impair antibody function, including binding to antigen and Fc function (Bakhtiar 2016; Thomas, Teicher, and Hassan 2016), we investigated the properties of conjugated Tr in comparison to the parent antibody.

First, we evaluated the binding properties of the conjugates using ELISA with immobilised human HER2. For this assay, we determined that both Tr and the commercial version Herceptin® bound HER2 in a dose dependent manner, while the isotype control did not (Fig. 4.2 B). Isotype-MCC-CpG conjugates did not bind to plate-bound HER2, indicating that CpG does not interfere with the assay (Fig. 5.5). All tested conjugates had markedly altered human HER2 binding compared with the parent antibody. Typically, there was a negative correlation between the number of CpG molecules incorporated into the conjugates and the binding affinity of the conjugates to human HER2. This was observed with both Tr and Herc-based conjugates (Fig. 5.5 A, B). Conjugates with CpG to Tr ratio of approx. 1 (green) showed strikingly improved binding over counterparts with CpG to Tr of 2 (blue) (Fig. 5.5 B). Considering that each antibody has two antigen binding sites, the data indicates that conjugation occurs preferentially in the vicinity of the antigen-binding site, with one CpG molecule hindering binding much less than 2 conjugated CpG molecules.

In our hands, conjugating in borate buffer compared to PBS only minimally improved the binding of the conjugates (Fig. 5.5 C). This minimal advantage of borate buffer is difficult to appreciate, as the antibody to CpG molar ratio of each batch of conjugates is slightly different, and in our experience, this was the factor most influencing binding to human HER2. Interestingly, conjugation in borate buffer showed higher consistency in terms of antibody to CpG molar ratio among independently conjugated batches (data not shown).

Ideally, we would want to deliver more than one CpG per molecule to the tumour tissue. Conjugates with CpG/Tr ratio of approx. 2 showed altered binding to human HER2, although this was better than for conjugates with higher CpG/Tr ratios. Therefore, in all downstream experiments, we conjugated either Tr, Herc or Isotype control in borate buffer with 20x molar excess SMCC, then 4x molar excess CpG, generating conjugates with 1.68-2.13 molecules of CpG bound to one molecule of antibody.

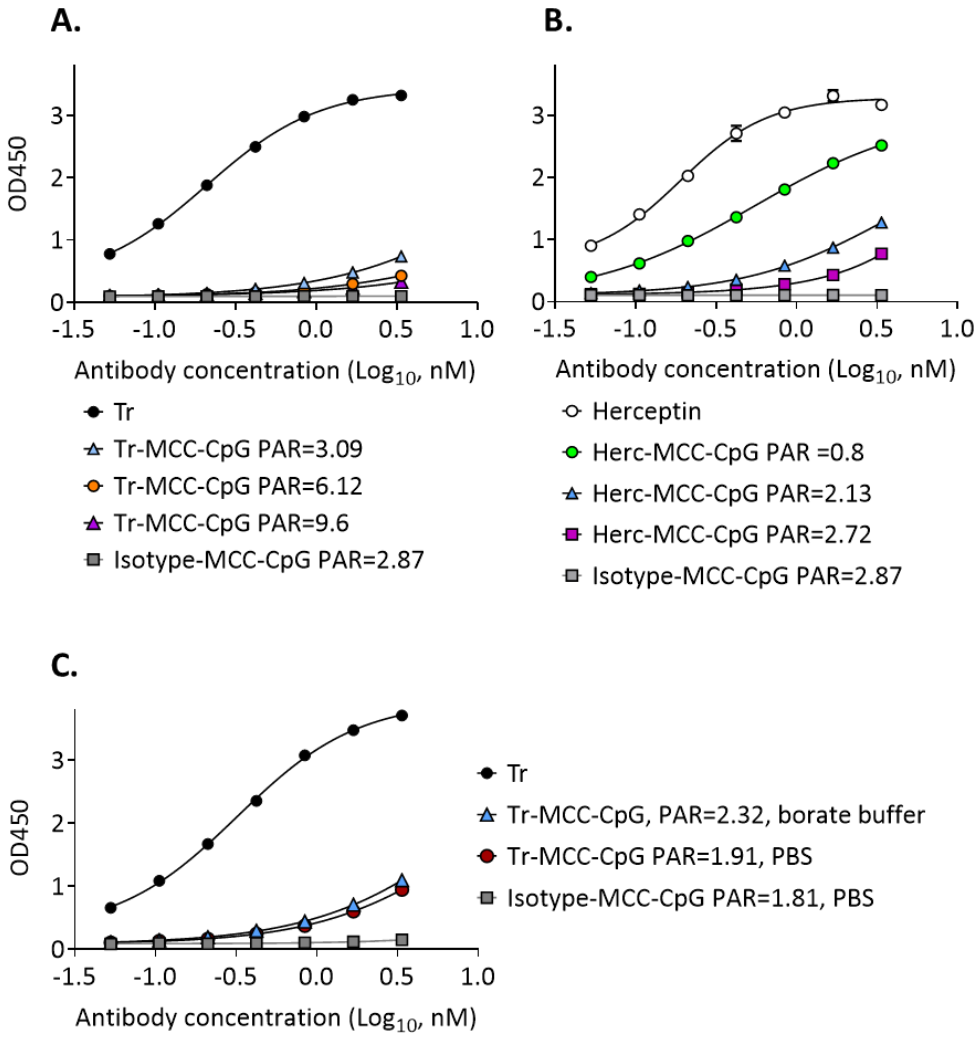


**Figure 5.5**. Impact of conjugation conditions on antigen binding properties of resulting conjugates. Tr (**A**) or Herceptin (**B**) were conjugated in either PBS (**A**) or borate buffer (**B**) at various SMCC and CpG molar excess. Either different antibody to CpG ratios resulting from SMCC and CpG titrations (**A** and **B**) or different buffers (**C**) were compared. Payload to antibody (PAR) molar ratio of the resulting conjugate depicted in the legend. ELISA plates were coated with human HER2. Antibodies and conjugates were detected using anti-human IgG Fc monoclonal antibody. Binding curves were generated using non-linear regression (variable slope) function in GraphPad Prism. Each binding curve is representative of one batch of conjugate.

Next, we asked if the impaired antigen binding of Tr-MCC-CpG conjugates was payload-specific and if other antibodies are affected as well. CpG 1668 is a large molecule of approx. 6345 Da. Other groups have conjugated small molecules, with molecular weight (MW) under 1 000 Da to Tr without marked loss in antigen binding affinity (Arlotta et al. 2018). We hypothesised that the altered HER2 binding we have observed is due to sterical hindrance mediated by the increased MW of CpG conjugated close or in the antigen binding site.

To test this, we used cysteine, an amino acid of 121.16 Da, as alternative payload instead of CpG (Fig. 5.6). Tr was conjugated with 20x molar excess of SMCC in borate buffer and then

with either 4x molar excess CpG followed in the last 10 min of reaction by 10x molar excess cysteine (to quench unreacted maleimide) or cysteine only. The resulting Tr-MCC-CpG conjugates showed CpG/Tr ratio of approx. 1.6. Tr-MCC-cysteine conjugates incorporated 3 molecules of cysteine per Tr molecule, as measured by Ellman's assay. Conversely, Tr-MCC-CpG conjugates (Fig. 5.6 B), but not Tr-MCC-cysteine conjugates (Fig. 5.6 A), showed considerably poorer binding to human HER2 compared to Tr. To confirm our observation on Tr-MCC-CpG conjugate binding, we used another antibody for detection, namely a polyclonal antibody recognising the κ light chain (Fig. 5.6 C). Independent of detection antibody, the binding curve of Tr-MCC-CpG was dramatically shifted to the right, with marked differences compared to Tr curve in lower asymptote and slope region. Higher concentrations of conjugate in the assay are needed to evaluate differences in upper asymptote. However, despite this shortcoming, the data indicates that conjugation with SMCC impairs binding of conjugates to human HER2 in a payload-dependent manner. This effect was observed when conjugates were generated with either Tr (Fig. 5.4 A-C) or Herc (data not shown).

When Cetuximab (anti-human EGFR) was used to generate conjugates as described above, ELISA binding assay showed the same trend observed for Tr, although binding of Cetuximab-MCC-CpG conjugate was affected to a lesser degree (Fig. 5.6 D).

Collectively, these data indicate that the properties of CpG ODN, most likely MW, sterically hinder binding of Tr-MCC-CpG conjugates to human HER2, while the magnitude of the effect is antibody specific. The major limitation in the depicted binding assay is that the ELISA has not been designed to calculate affinity. To quantify the diminished binding of Tr-MCC-CpG conjugates, methods such as surface plasmon resonance or isothermal titration calorimetry should be employed in the future to determine binding kinetics and constants.

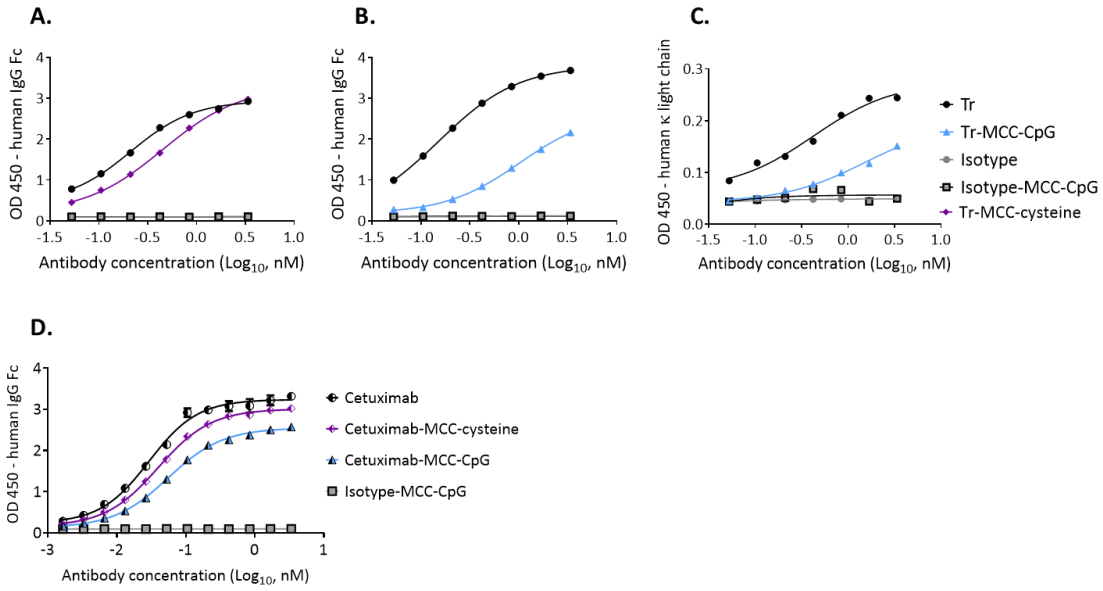


**Figure 5.6.** Conventional conjugation with SMCC hinders antigen binding properties of conjugates, which is payload dependent and antibody specific. **A-C.** Tr was conjugated using SMCC under identical conditions with either cysteine (**A**) or CpG 1668 (**B, C**). **D**. Cetuximab was conjugated with either cysteine (purple) or CpG (blue). After conjugation, payload to antibody (PAR) molar ratio was approx. 1.7 for all CpG conjugates or about 3 for all cysteine conjugates. Resulting conjugates were analysed using ELISA with immobilised human HER2. ELISA was developed using either a monoclonal antibody against human IgG Fc and the biotin-streptavidin system (**A, B, D**), or a polyclonal antibody against human kappa chain (**C**) and the HRP system. The data was fitted using a four-parameter logistic model (sigmoid curves) with log transformation of dose, performed with GraphPad Prism. Data representative of 3 independent experiments with Tr and 2 experiments with Cetuximab.

The therapeutic activity of Tr is partly determined by the ability to inhibit growth of human HER2 over-expressing tumours. This can be evaluated *in vitro*, by assessing proliferation of HER2 over-expressing and using HER2 minimal cells as control. Inhibition of proliferation is dependent on human HER2 binding, which prevents activation of downstream signalling pathways sustaining proliferation (Hudis 2007). Treatment with Tr inhibited proliferation of the human HER2 over-expressing tumour cell lines BT474 and OE-19, but not of triple-negative MDA-MB-231 cell line, frequently used for negative control in such assays (Fig. 5.7). By comparison, Tr-MCC-CpG was less efficient in inhibiting proliferation. A shift to the right of the dose-response curve was observed independent of the HER2 overexpressing cell line used (Fig. 5.7 A, B). $Log_{10}IC50$ for Tr-MCC-CpG stood at 0.2718 on BT474 cells and 0.431 on OE19 cells, much higher than $log_{10}IC50$ for Tr, 0.1820 and -0.08813, respectively. With the set-up of this assay IC50 values are difficult to determine accurately, with wide, at times incalculable confidence intervals. Half log or even narrower serial dilutions and additional repeats of the assay are required to accurately determine IC50 values and compare Tr and Tr-MCC-CpG for statistical significance.

These results, however, align with the ELISA data to confirm altered human HER2 binding of Tr-MCC-CpG conjugates, which translates into diminished direct anti-proliferative effect on human HER2 over-expressing cells.

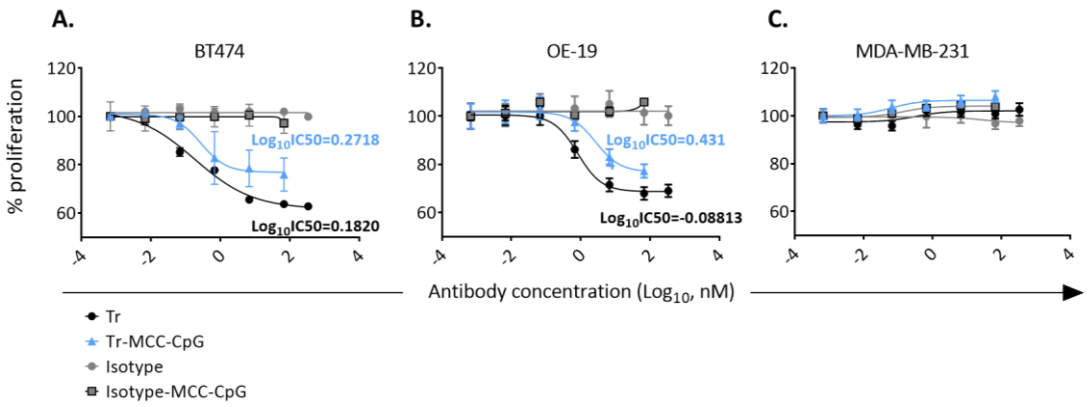


**Figure 5.7.** Tr-MCC-CpG conjugates show reduced anti-proliferative effect compared to Tr, as measured *in vitro* by MTS assay. HER2 over-expressing Trastuzumab-sensitive human cancer cell lines (**A** and **B**) and HER2 minimal cell line (**C**) were incubated with increasing concentrations of Tr (black), Tr-MCC-CpG (light blue), isotype (grey dots) or isotype-CpG (grey squares). Tr-MCC-CpG had a PAR of ~ 1.7. After 48h MTS substrate was added to the wells and signal was measured after 30 min incubation. Data was expressed as percent of untreated controls. Dose-response curves generated with non-linear fit equation with variable slope in GraphPad. Data are means ± SEM of three technical replicates and is representative of two independent experiments.

### 5.2.5 Tr-MCC-CpG conjugates maintained ADCC activity

The immune system contributes to the therapeutic effects of Tr, through mechanisms such as antibody-dependent cytotoxicity (ADCC) and antibody-dependent phagocytosis (ADCP), mediated by the antibody Fc region (Bianchini and Gianni 2014). To evaluate the impact of CpG conjugation on Fc-mediated effects, we performed antibody-dependent cytotoxicity assays (ADCC). We performed a calcein-release assay with human PBMCs as effector cells (E) and BT474 cells as targets (T), with E:T ratio of 25:1. Within the set-up of our assay, vehicle (PBS), isotype control antibody or CpG 1668, either free or conjugated to the isotype control antibody only induced minimal levels of cytotoxicity, which was expected. Surprisingly, ADCC activity of Tr-MCC-CpG conjugate was comparable to Tr-mediated ADCC, despite decreased HER2 binding, within the described set-up (Fig. 5.8).

Literature reports indicate that CpG enhances ADCC responses (Schettini et al. 2012; van Ojik et al. 2003; Hiramatsu et al. 2015), likely through an indirect mechanism that involves IFN-α and IL-12 produced by dendritic cells (Askew et al. 2000; Fernandez et al. 1999). It is unclear at this stage if CpG augmented ADCC in our *in vitro* assay. To elucidate the impact of conjugation on ADCC activity, at least two sets of future experiments are required. Altered

HER2 binding is expected to lead to decreased ADCC activity. This impact of conjugation reactions should be evaluated in the future using a homogenous, preferably TLR9 negative effector cell population. The CD16 176V NK-92.05 cell line might be suitable for this experiment (Campbell 2012). Additional antibody dilutions, as well as incubation times before read-out are also required to ensure that the system is not saturated. To investigate the impact of CpG on ADCC using human cells, future experiments with a larger dilution series are required using CpG 2006 instead, which is more efficient in triggering TLR9. Since results from *in vitro* ADCC assays do not necessarily translate *in vivo*, a humanised mouse model should be considered.

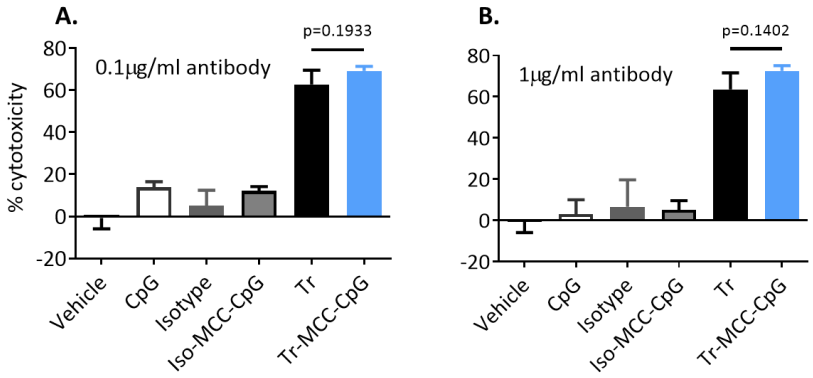


**Figure 5.8.** Evaluating ADCC function of conjugates. BT474 cells loaded with 11.2µM calcein were incubated with 0.1µg/ml (**A**) or 1µg/ml (**B**) antibodies or conjugates. Concentrations of conjugated CpG were 31.75ng/ml (**A**) and 317.5ng/ml (**B**), respectively. The same concentrations were used for the free CpG and Iso-MCC-CpG controls. PBMCs from 3 healthy donors were added at E: T=25 and the co-culture was incubated for 16 h. Afterwards, calcein released in the media was measured. Means ± SD of data generated with PBMCs from 3 healthy donors collected in 2 independent experiments. For each experiment, a different batch of Tr-MCC-CpG with CpG to Tr ratio of approx. 1.8-2 was used. Student's t test for statistical analysis.

## 5.3 Generation of conjugates using cyanuric chloride (CC)

To find an alternative for SMCC conjugates which showed altered HER2 binding, we generated conjugates using another heterobifunctional cross-linker, cyanuric chloride or 2,4,6-trichloro-1,3,5,-triazine (CC) following a previously published protocol (Abuknesha et al. 2009) with our modifications. Chemically, chlorine atoms of CC react with nucleophilic groups such as amino, thiol and hydroxyl to form covalent bonds. The first chlorine reacts at RT and neutral pH, the second chlorine requires alkaline pH and higher (37°C) temperature, while the third chlorine is almost unreactive, requiring very high temperatures and strong alkaline conditions, which are detrimental to proteins and avoided in the lab (Abuknesha et al. 2005). As such, this cross-linker can be used to first activate CpG by reacting with hydroxyl groups of deoxyribose and then conjugate CpG to primary amines on antibodies. To us, the cross-linker is interesting as it would allow us to conjugate nucleic acid TLR agonists without Thiol modifications, such as polyUs21, a TLR7 agonist.

Since Tr and Herc have identical amino acid sequence and conjugation of CpG using SMCC of either Tr or Herc generated conjugates with very similar properties, we presumed that the two antibodies are very similar in terms of availability of functional groups. To generate CpG-containing conjugates with CC, we used Herceptin (Hudis 2007), since this antibody was more readily available for these tests and unlike Tr, did not have to be produced by ourselves in Freestyle 293 cells.

The steps of the conjugation reaction are shown in Fig. 5.9 A. Firstly, CpG was conjugated with high molar excess of CC at neutral pH at room temperature. CpG was purified from unbound CC and then added to the antibody in mild alkaline pH at 37ºC. The conjugate was further purified from unbound CpG. Determined CpG/antibody molar ratio of purified Herc-CC-CpG conjugate was 1.2.

Upon SDS-PAGE analysis, the conjugate showed positive staining with ethidium bromide confirming conjugation with CpG. Also, the conjugate sample showed multiple bands migrating slower on the gel indicating the presence of higher MW species generated through conjugation (Fig. 5.9 C).

When binding to human HER2 was assessed by ELISA, Herc-CC-CpG conjugates showed reduced binding compared to Herc (Fig. 5.9 B). This effect was similar to what we have observed for other conventional conjugates, Tr-MCC-CpG, where the antibody was wither Tr expressed in our lab or the commercial Herceptin (Fig. 5.5 B).

We concluded that conjugation with CC leads to Herc-CC-CpG conjugates with altered human HER2 binding and large fraction of higher MW species in the suspension. Since these conjugates did not show superior *in vitro* profile to SMCC generated conjugates, we have not pursued the method further.

Collectively, the *in vitro* profile of conventional conjugates generated with either SMCC or CC in mild conditions and with low CpG to antibody molar ratio, indicates that linkage of the larger molecule CpG inhibits binding to human HER2 via steric hindrance, independently of the cross-linker used. Therefore, conventional conjugation methods are not suitable strategies to conjugate CpG to Tr and we considered site-specific conjugation methods as alternative approach.

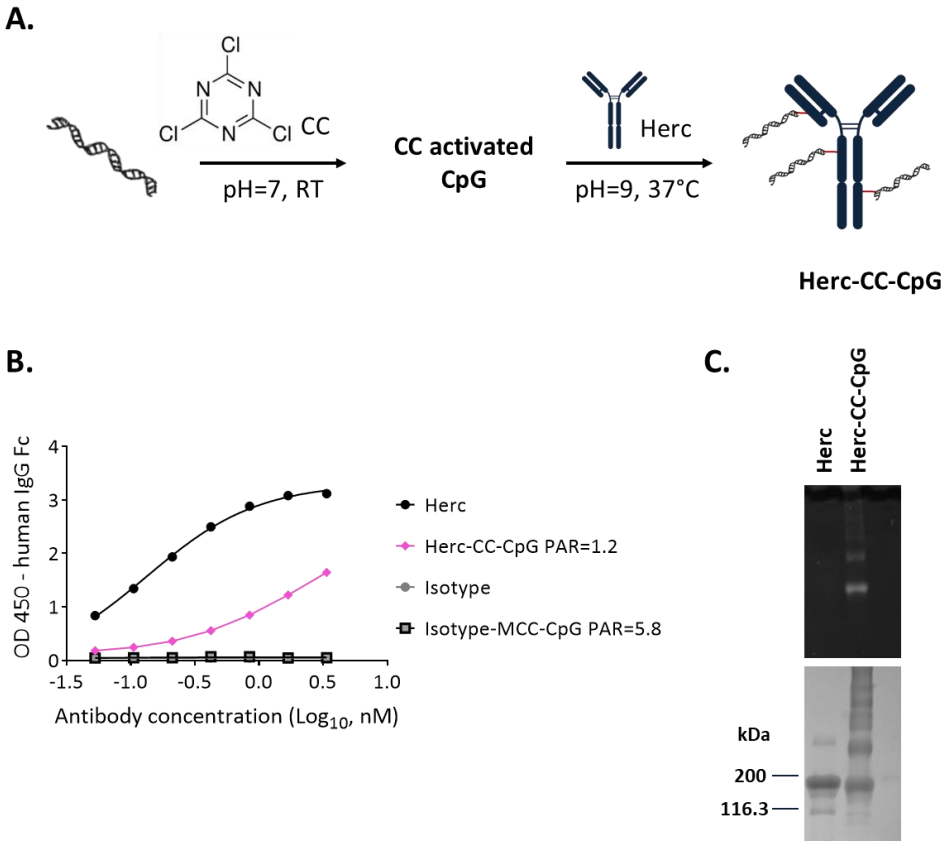


**Figure 5.9.** Generation and properties of Herc-CC-CpG conjugates. **A.** Schematic representation illustrating conjugation of CC-activated CpG 1668 to Herceptin. **B.** HER2 binding ELISA evaluating the Herc-CC-CpG as compared to the parent antibody. **C.** SDS-PAGE analysis in non-reducing conditions of Tr and Tr-CC-CpG conjugates on a 4-20% gel sequentially stained with Ethidium Bromide (top) to visualise the CpG content and SimplyBlue (bottom) for antibody content. Data was collected in one experiment. PAR = payload to antibody molar ratio in purified conjugates.

## 5.4 Trastuzumab-CpG site-specific conjugates

### 5.4.1 Generation and composition of site-specific Trastuzumab-CpG conjugates using THIOMAB technology

A large body of literature describes the many payload-independent limitations of conventional SMCC conjugation for generation of therapeutic antibody conjugates (see section 1.3.3). The resulting conjugates are heterogenous products, with various payload to antibody molar ratios. Also, unconjugated antibody in the preparation competes for antigen binding sites, while highly loaded conjugates show rapid degradation and loss of function (Hamblett et al. 2004). Conjugate heterogeneity has been shown to contribute to poor therapeutic activity (Dan et al. 2018; Beck et al. 2017). Considering these limitations, paired with our own observations of altered antigen binding of Tr-MCC-CpG conjugates, we decided to explore site-specific conjugation methods.

In addition to unaltered binding properties, site-specific conjugates promise higher payload to antibody homogeneity and *in vivo* stability, influencing both safety and therapeutic efficacy of conjugates (Zhou 2017). Among site-specific conjugation methods, we chose to use THIOMAB technology, which involves engineering cysteines at specific sites in the structure of Trastuzumab and specifically conjugating our payload of choice via a maleimide-containing linker to the thiol groups of these cysteines (Bhakta, Raab, and Junutula 2013). Cysteine residues in the structure of non-reduced IgG antibodies form disulphide bonds under native conditions, stabilising the tertiary structure of the antibody and need to be reduced to become available for conjugation (Sochaj, Swiderska, and Otlewski 2015; Behrens and Liu 2014).

It has been shown that SMCC-mediated conjugation of modified Trastuzumab in which valine has been exchanged with cysteine at position 205 in the light chain (hence labelled LC-V205C) yields conjugates with superior *in vivo* stability and enhanced therapeutic function (Shen et al. 2012). Moreover, this strategy avoids steric hindrance of the payload, which is conjugated at a distance from the antigen-binding site of the antibody.

To exploit this strategy for the generation of Trastuzumab-CpG conjugates, we have engineered cysteines at LC-V205C in Trastuzumab and generated Trastuzumab THIOMAB, henceforth referred to as Tr(TH). To achieve site-selected mutagenesis, we used PIPE cloning as described in methods section 2.2.3. Full sequences are shown in appendix F. PIPE cloning fragments were generated and purified (Fig. 5.10 A), then transformed in competent bacteria. Following the workflow described in section 4.1, we have evaluated 3 clones of pVITRO-Trastuzumab(TH) IgG1 with correct sequence for expression levels in FS 293 cells. Compared to the parent antibody Tr, expression of Tr(TH) clones #1 and #2 was similar, or even slightly

increased, respectively (Fig. 5.10 B). Purified Tr(TH) clone #2 migrates on a PAGE gel in a similar fashion with the parent antibody, corresponding to their expected molecular weights (Fig. 5.10 C). We have used this clone in all subsequent experiments.

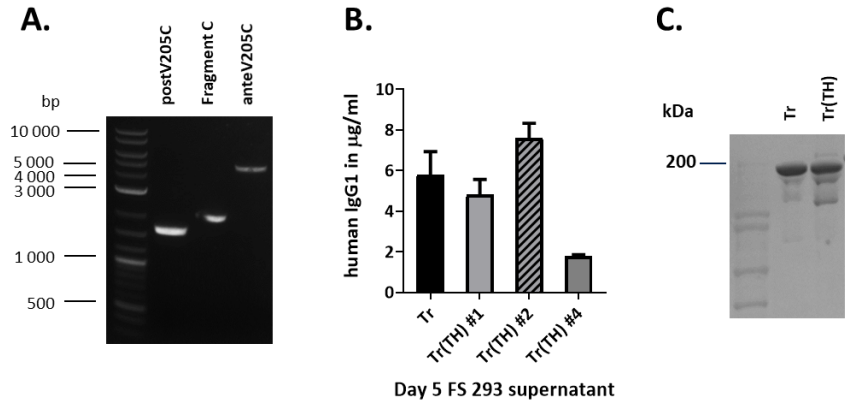


**Figure 5.10.** Generation of Tr(TH) antibody. **A.** Agarose gel analysis of PIPE cloning fragments introducing the LC-V205C mutation, showing purified bands of expected size (postV205C – 1657bp, fragment C – 2031, anteV205C - 4916). **B.** Expression levels of Tr(TH) clones. FS 293 cells were transfected with each of the plasmids and supernatant was harvested on day 5. Human IgG1 levels were assessed by ELISA. Clone Tr(TH)#2 (dark grey bar) was chosen for further experiments. **C.** SDS-PAGE analysis of Tr(TH) in non-reducing conditions.

To conjugate CpG to Tr(TH), we have optimised a previously published protocol (Nunes et al. 2017). During antibody expression, thiol groups of cysteines in the structure form disulphide bonds with other thiol-containing amino acids, named adducts, either intracellular or in the cell expression medium. To remove the adducts, we reduced the antibody in TCEP, then purified the resulting heavy and light chains by ultrafiltration. In a following step, heavy and light chain disulphide bonds were reoxidated using the accelerator dhAA for 3h RT (Fig. 5.11 A). Efficient reduction and reoxidation was verified by SDS-PAGE analysis (Fig. 5.11 B). Engineered cysteines are surrounded by positively charged amino acids and hence reoxidise at a much lower rate, remaining available for conjugation in the timeframe.

CpG 1668 synthesised with an $NH_2$ group at the 3' end was conjugated with SMCC, to obtain maleimide-activated CpG using an adaptation of a previously published protocol (Williams and Chaput 2010). After purification from excess crosslinker, maleimide-activated CpG was conjugated to reoxidated Tr(TH) (Fig. 5.11 A). CpG payload to Tr molar ratio of resulting Tr(TH)-CpG conjugates was consistently in the 1.51-1.89 range. This was determined by measuring Tr(TH) content by BCA assay and CpG content by spectrophotometry as described before (see section 2.16.2).

To visualise the CpG and Tr(TH) content, conjugates were run on a 4-12% SDS-PAGE gel, which was sequentially stained for CpG with SYBR Gold and antibody with SimplyBlue

SafeStain (Fig. 5.10 C). In contrast with conventional Tr-MCC-CpG conjugates (see Fig. 5.3 B), Tr(TH)-CpG conjugates only showed minimal multimer content (Fig. 5.11 C).

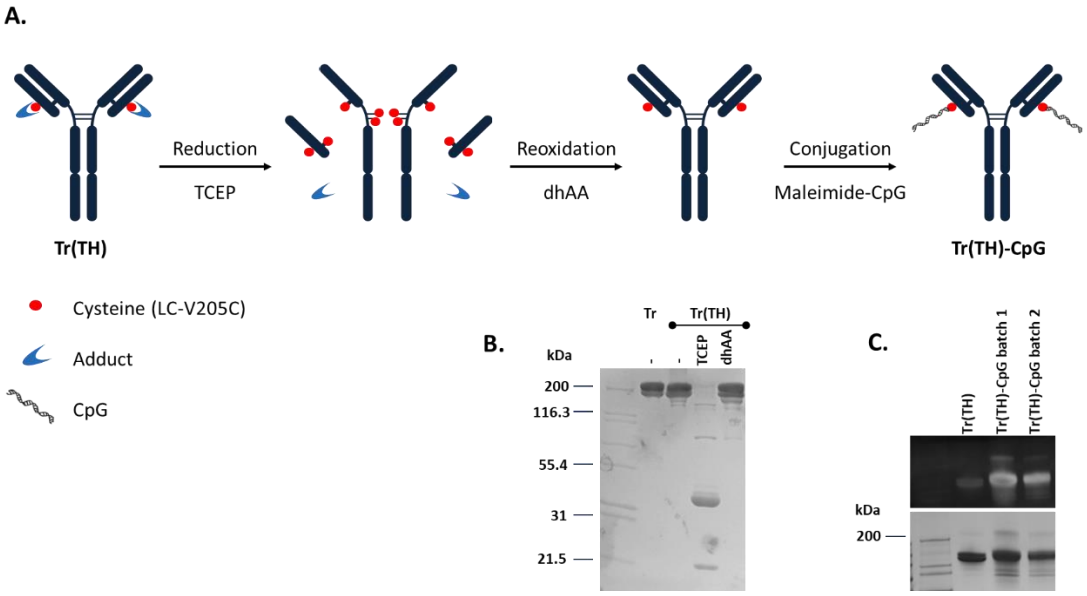


**Figure 5.11.** Generation of Tr(TH)-CpG conjugates. **A.** The process of conjugating maleimide-activated CpG 1668 to engineered cysteines (LC-V205C) of Tr(TH) is schematically represented. **B.** SDS-PAGE analysis of Tr(TH) in native, reduced and reoxidated form on 4-20% gel stained with SimplyBlue. **C.** SDS-PAGE analysis in non-reducing conditions of Tr(TH)-CpG conjugates on a 4-12% gel sequentially stained with SYBR Gold (top) to visualise the CpG content, then with SimplyBlue (bottom) for protein content. Data representative of three independent experiments.

### 5.4.2 Tr(TH)-CpG conjugates show CpG mediated immunoactivity *in vitro*

To investigates the effect of conjugation to Tr(TH) on CpG immunostimulatory activity, we performed *in vitro* dendritic cell activation assays. Briefly, GM-CSF derived BMDCs (1x $10^5$/well) were stimulated with free or conjugated thiol-modified CpG and controls (Fig. 5.12 A, B). Samples were normalised for CpG content. Tr and Tr(TH) content in samples was normalised to the Tr(TH) content of the conjugate. Additionally, conjugates and controls were pre-incubated with B14.3 Luc HER2 tumour cells for 20-30 min, then GM-CSF derived BMDCs were added (Fig. 5.12 C, D). As expected, GpC 1668 did not induce cytokine production by DCs, nor did vehicle (PBS), Tr or Tr(TH). When compared with free CpG, conjugated CpG induced production of comparable levels of IL-12p40 by dendritic cells, either alone (Fig. 5.12 B), or even slightly higher in the presence of tumour cells. Interestingly, as observed with conventional conjugates, free CpG induced slightly lower levels of IL-12p40 (Fig. 5.12 C) or IL-6 (Fig. 5.12 D) in the presence of tumour cells, compared to BMDCs only (Fig. 5.12 A and B, respectively). Notably, GM-CSF BMDCs produced higher levels of IL-6 when cultured alone, with maximum IL-6 values induced by Tr(TH)-CpG of 8.18ng/ml (Fig. 5.12 B), compared to tumour cell co-cultures, where the maximum value IL-6 values induced

by Tr(TH)-CpG of 4.05ng/ml. Taken together, these data illustrate that conjugation with Tr(TH) does not impair CpG function *in vitro*, even in the presence of human HER2-expressing cells.

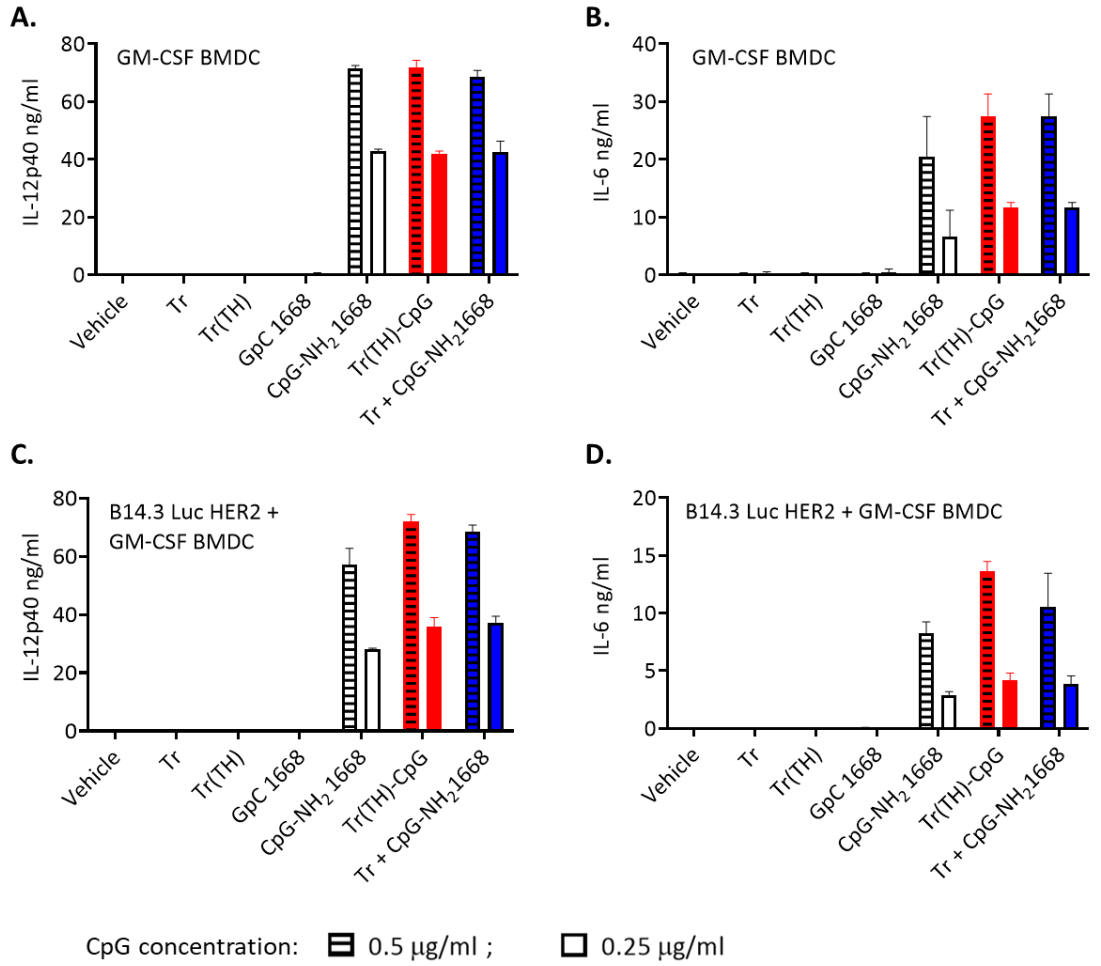


**Figure 5.12.** Assessing immunostimulatory properties of Tr(TH)-CpG *in vitro*. 1x$10^5$ GM-CSF derived BMDCs were stimulated overnight with CpG-NH2, free (white) or conjugated to Tr(TH) (red) or controls. BMDCs were stimulated alone (**A, B**) or in the presence of 3x $10^5$ B14.3 Luc HER2 H2 tumour cells (**C, D**). For markers of DC maturation, IL-12p40 (**A, C**) and IL-6 (**B, D**) were measured in cell supernatant. Samples were normalised for concentration of CpG of 0.5µg/ml (line fill pattern) or 0.5µg/ml (open fill). Data are mean ± SD of three technical replicates and is representative of two independent experiments.

### 5.4.3. Human HER2 binding is comparable for Tr and Tr(TH)-CpG conjugates

To investigate the binding properties of Tr(TH)-CpG to human HER2, we performed ELISA with recombinant human HER2 immobilised to the plate. Antibody and conjugates binding to the immobilised HER2 was detected using an anti-human IgG Fc biotinylated antibody. Neither isotype control antibody nor isotype-CpG conjugate bind human HER2 in this assay, suggesting that CpG does not mediate unspecific binding of conjugate. As expected, Tr(TH) binding is comparable with Tr. The conjugate only showed minimal differences in binding, noticeable in the linear part of the curve, but not the upper asymptote (Fig. 5.13).

Furthermore, direct inhibition of proliferation was assessed using an MTS assay. Proliferation of human HER2-overexpressing, Tr sensitive cells was decreased *in vitro* in the presence of Tr (Fig. 5.14 A, B), while proliferation of the negative control cell line MDA-MB-231 was not impacted (Fig. 5.14 C). Proliferation was not influenced by CpG. Treatment with Tr(TH)-CpG inhibited proliferation of HER2 overexpressing tumour cell lines to the same degree as Tr, with only very small differences noticeable between the two curves. $Log_{10}IC50$ for Tr and Tr(TH)-CpG were also comparable, 0.06446 vs -0.1311 respectively for BT474 cells and -1.250 vs -0.8609 respectively on OE19 cell (Fig. 5.14 A, B). The confidence intervals for these values however are wide.

Collectively, the two assays showed that HER2 binding was only slightly lower for Tr(TH)-CpG compared to Tr. Differences were evident in ELISA data, since the assay had superior resolution to the cell-based proliferation assay. In this second assay the variability between replicates was much higher.

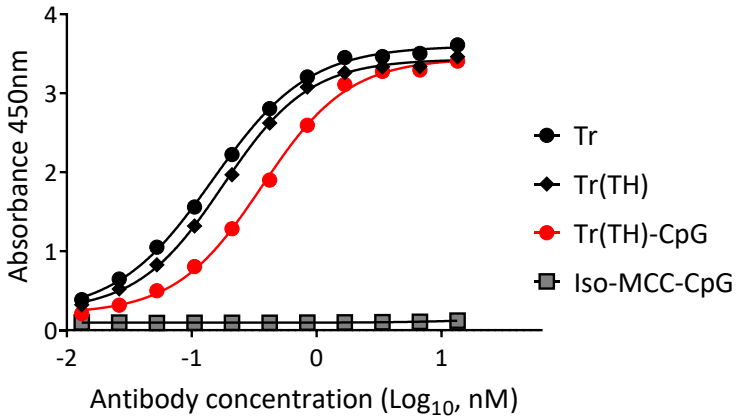


**Figure 5.13.** Tr(TH)-CpG binds human HER2 comparably with Tr *in vitro.* ELISA with immobilised recombinant human HER2 was performed. CpG/Tr(TH) molar ratio of conjugates was approx. 1.7. Curves generated using nonlinear regression function with variable slopes of GraphPad prism of. Data representative of 4 independent experiments with individual batches of conjugates.

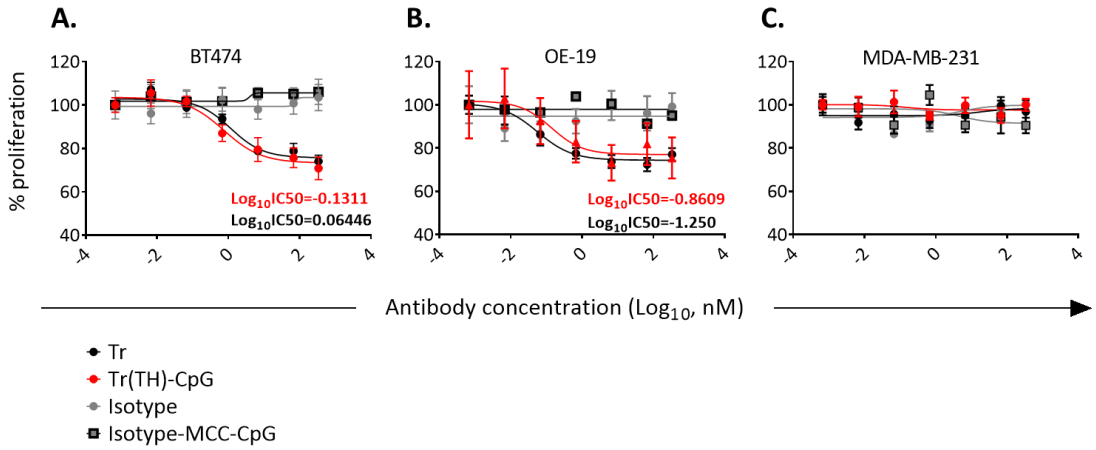


**Figure 5.14**. Tr(TH)-CpG maintains the anti-proliferative effect of Tr measured *in vitro* by MTS assay. Human HER2 overexpressing, Tr sensitive human tumour cell lines BT474 (**A**), OE19 (**B**) and the negative control MDA-MB-231 (**C**) were cultured for 48 h with 1/2 log dilutions of Tr, Tr(TH)-CpG, isotype or isotype-CpG. CpG/Tr(TH) molar ration for all conjugates was approx. 1.6. The MTS substrate was added to asses proliferation. Data was normalised to vehicle (PBS) treated cells and expressed as percent proliferation. Data are representative of two independent experiments with individual batches of conjugates.

## 5.5 Evaluating endotoxin contamination of conjugates

To ensure that the immune responses triggered by conjugates are mediated by CpG, and not by an endotoxin contamination, we tested the antibodies used for conjugation as well as the resulting conjugates for endotoxin. As discussed in section 4.2.3, although it has been shown that mice tolerate much higher doses of endotoxin without inflammatory responses (Copeland et al. 2005), we wanted keep the endotoxin levels as low as possible. For a 20g mouse receiving single dose per day of 0.1ml, the calculated limit based on recommendations from the European Pharmacopoeia is 1 IU/ml. Keeping to this limit would allow us to assess conjugate effects on human cells, either *in vitro* or *in vivo* using a humanised mouse model in the future without having to change our current protocols.

To ensure the antibodies we used for conjugations are endotoxin-free, we tested individual preparations using the limulus amoebocyte lysate (LAL) gel-clot assay. Tr(TH) was diluted to 0.4mg/ml for the test, as this was the concentration of mouse IV inoculum. All preparations tested had undetectable endotoxin levels, under 0.3 IU/ml. Similar results were observed for Tr as well (Table 4.2). As discussed in section 4.2.2, we took ample precautions to avoid endotoxin contamination in our purification workflow and no endotoxin contamination was expected.

Next, we tested finished conjugates as well. The LAL gel clot assay is semiquantitative and the results are expressed as intervals and not discrete values. The results for our assay set-up fall under the following intervals: <0.3 IU, 0.3-3 IU, 3-30 IU, 30-300 IU etc. Surprisingly, the gel-clot assay showed levels of endotoxin in the interval of 30-300 IU/ml in all six tested conjugate samples, including conventional and site-specific conjugates. A similar conjugation protocol and plastic-ware were used in our lab for another project, where conjugates showed only low endotoxin levels, as measured by the chromogenic LAL assay instead of the gel-clotting method (Kreutz et al. 2012). Literature reports that multiple factors can interfere with the LAL gel-clot assay and it is likely that not all have been identified yet (European Pharmacopeia 2019). Among them, the synthetic nucleic acid poly I:C was shown to induce clotting, as a consequence of intrinsic polarity of nucleic acids, leading to false-positive results (Elin and Utter 1980). We consider that CpG may have a similar effect and the gel-clot LAL assay may be inappropriate to measure endotoxin levels in CpG containing samples.

To assess if our CpG conjugates contain endotoxin or just interfere with the LAL gel-clot assay, we decided to perform an additional assay using the same samples and using the same NIBSC endotoxin standard. The monocyte activation assay is accepted as sensitive and accurate for pyrogen detection including endotoxin (European Pharmacopeia 2017). This

assay can be performed using a variety of cell populations, including whole blood, PBMCs or monocytic cell lines (Franco et al. 2018). In our lab we have experience in working with monocyte-derived DCs and have confirmed that the cells respond to TLR4 activation by LPS (Brencicova et al. 2017), but not to TLR9 stimulation in response to CpG ODN (data not published). Therefore, we decided to evaluate endotoxin contamination of Tr-CpG conjugates in a monocyte-derived DC activation assay (Fig. 5.15). Monocyte-derived DCs were incubated overnight with endotoxin or conjugates or controls. Final concentration was 0.4mg/ml for Tr and 30µg/ml for CpG, either free or conjugated. These are the concentrations we intend to use in mouse experiments. 3-7 different batches of conjugate were pooled and tested as one sample. As expected, endotoxin induced IL-6 production in a dose-dependent manner, while CpG did not. Neither of the conjugate samples induced IL-6 production, indicating that endotoxin levels in these preparations were lower than 1 IU/ml.

To summarise the *in vitro* data, we were able to generate conjugates using a traditional conjugation method and SMCC and a novel, site-specific method, the Thiomab technology. Traditional conjugation methods resulted in CpG conjugates with altered human HER2 binding, while site-specific conjugates did not. Conjugated CpG maintained immunostimulatory activity comparable to unconjugated CpG. The conjugate preparations were low in endotoxin if not entirely endotoxin-free and importantly, these pooled samples provided sufficient material to move into *in vivo* investigations.

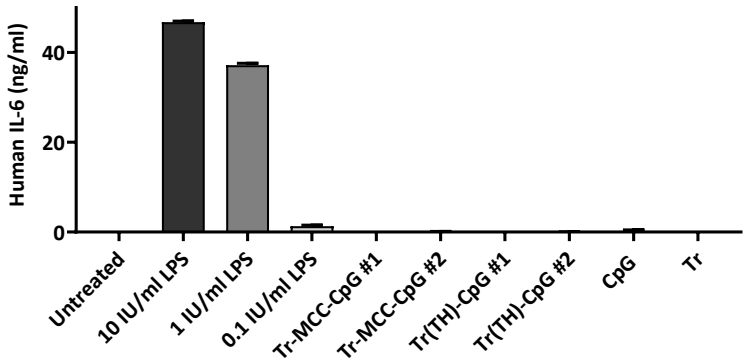


**Figure 5.15.** Monocyte-derived dendritic cell activation assay to detect endotoxin (LPS) contamination in conjugate preparations. Monocytes were enriched from health donor PBMCs and differentiated into DCs using 20ng/ml human GM-CSF and 20ng/ml IL-4. 1x $10^5$ monocyte derived DCs were cultured overnight with the indicated conjugates and controls. Tr, either free or conjugated was 0.4 mg/ml, while CpG, either free or conjugated was approx. 30µg/ml. Read-out was human IL-6 production measured by ELISA. Data are mean ± SD of technical duplicates from one experiment and are representative of 2 independent experiments with cells from 2 individual donors.

## 5.6 *In vivo* evaluation of Trastuzumab-CpG conjugates

### 5.6.1 Impact of treatment with Trastuzumab-CpG conjugates on tumour growth

To evaluate the *in vivo* profile of Trastuzumab-CpG conjugates, we used the B14.3 Luc HER2 clone H2 pseudo-metastasis model described in Chapter 3. Importantly, the tumour cells themselves do no express TLR9 (Appendix I) and do not respond to treatment with Tr (Fig. 3.14). Upon inoculation in mice, tumour cells maintain a moderate degree of human HER2 expression (Fig. 3.13).

In this model, tumour cells were injected IV to generate pulmonary tumours (Fig. 5.16 A). Mice were treated with 2mg/kg body weight (40µg for a 20g mouse) of Trastuzumab and this was normalised across samples. We chose this dose as it is in the range of clinical used doses (Nemeth et al. 2017) and preclinical mouse *in vivo* imaging studies showed successful accumulation of Tr dosed in this range in HER2-expressing tumours (Dennis et al. 2007; McLarty et al. 2009). 40µg of Tr(TH)-CpG carried approx. 2.5µg of conjugated CpG at a CpG/Tr molar ratio of ~1.8. This CpG dose was also kept constant across treated groups. Tr-MCC-CpG conjugates were generated for *in vivo* experiments to achieve CpG/Tr molar ratio of 1.8-2 and showed altered HER2 binding (Fig. 5.3 A, B). Therapeutic treatment was initiated on day 4 post tumour-inoculation and repeated twice, on day 8 and day 11 (Fig. 5.16 A). We chose this schedule because many studies showing CpG efficacy in tumour immunotherapy, administered CpG repeatedly, usually biweekly, with at least 3 doses administered for effect (Kunikata et al. 2004; Kawarada, Ganss, Garbi, Sacher, Arnold, and Hammerling 2001; Chavez et al. 2018; Rakhmilevich et al. 2017; Sagiv-Barfi et al. 2018; Wang et al. 2016; Westwood et al. 2014; Yin et al. 2016; Gallotta et al. 2018). The timing of dosing is in line with transcriptional data of splenocytes from CpG treated mice, showing that CpG-mediated gene regulation drops 3 days after treatment (Bode et al. 2011). Importantly, all our *in vivo* experiments include a direct comparison of targeted CpG in the form of conjugates with untargeted CpG, alone or in combination with unconjugated Tr. *In vivo* imaging was employed for non-invasive monitoring of tumour burden at days 3, 7, 10, 15 (☼). Endpoint was at day 18, when lungs were harvested and fixed in Fekete solution to enable counting of tumour nodules. (Fig. 5.16 A).

Importantly, tumour-bearing mice do not respond to treatment with Tr, making this a Tr-resistant mouse model (Fig. 5.16 B and D). Within this schedule of treatment, CpG alone did not inhibit tumour growth compared to vehicle (PBS) treated mice, as illustrated by the tumour nodules count (Fig. 5.16 B) and by *in vivo* imaging and (Fig. 5.16 D). To the contrary, tumour

burden was slightly higher for Tr and for CpG treated mice. Compared to these 2 controls, treatment with unconjugated Tr + CpG synergised to delay tumour growth, with differences that were significant in terms of lung nodule count (Fig. 5.16 B), but not in terms of luminescence intensity (Fig. 5.16 F).

In terms of conjugates, mice treated with Tr-MCC-CpG conventional conjugates only showed minimally decreased tumour burden, compared to mice treated with equimolar doses of either Tr or CpG, which did not achieve significant differences in terms of lung nodules nor luminescence profile across time (Fig. 5.16 B, E, respectively). No differences were observed for the isotype control (Fig. 5.16 B and E). In contrast, mice treated with Tr(TH)-CpG conjugates had significantly lower numbers of lung tumours at day 18 (Fig. 5.16 B). The delay in tumour growth was more pronounced from day 10 after tumour inoculation onwards, when luminescence intensity plateaued at around $10^6$ photons/s of mice treated with Tr(TH)-CpG, but increased steadily close to $10^7$ photons/s for CpG treated mice (Fig. 5.16 G). Representative images of luminescence signal (Fig. 5.16 H) and mouse lungs after bleaching in Fekete solution to highlight melanoma tumour nodules (Fig. 5.16 C) are shown. This indicates that site-specific conjugation of anti-HER2 antibody with CpG improves efficacy of Tr therapy in the mouse model. Interestingly, when Tr(TH)-CpG treatment group was compared with vehicle treated mice, the differences were not statistically significant in terms of lung nodules, nor luminescence intensity of tumours. The same was observed for the Tr + CpG treated group as well. The reasons for this are unclear and larger treatment groups may be required to obtain a robust data set and to establish statistical significance over all experimental groups.

Collectively, the data indicate that treatment with site-specific conjugates (Tr(TH)-CpG), but not conventional conjugates (Tr-MCC-CpG) delays tumour growth in mice with B14.3 Luc HER2 pulmonary tumours. Tr(TH)-CpG conjugates showed a therapeutic benefit compared to Tr alone, as well as compared to untargeted CpG. However, efficacy of Tr(TH)-CpG was not superior to a unconjugated combination of Tr and CpG. This was rather surprising and indicates that in this mouse model, combination of Tr with CpG is of therapeutic benefit, but that targeted delivery of CpG via Tr(TH)-CpG conjugates was either suboptimal, or does not bring an additional benefit. As described in chapter 1, in this model, tumour cells only show mild to moderate human HER2 expression *in vivo.* Further work evaluating the efficacy of Tr(TH)-CpG is required, including the use of an additional tumour mouse model to overcome the limitations of the used tumour model.

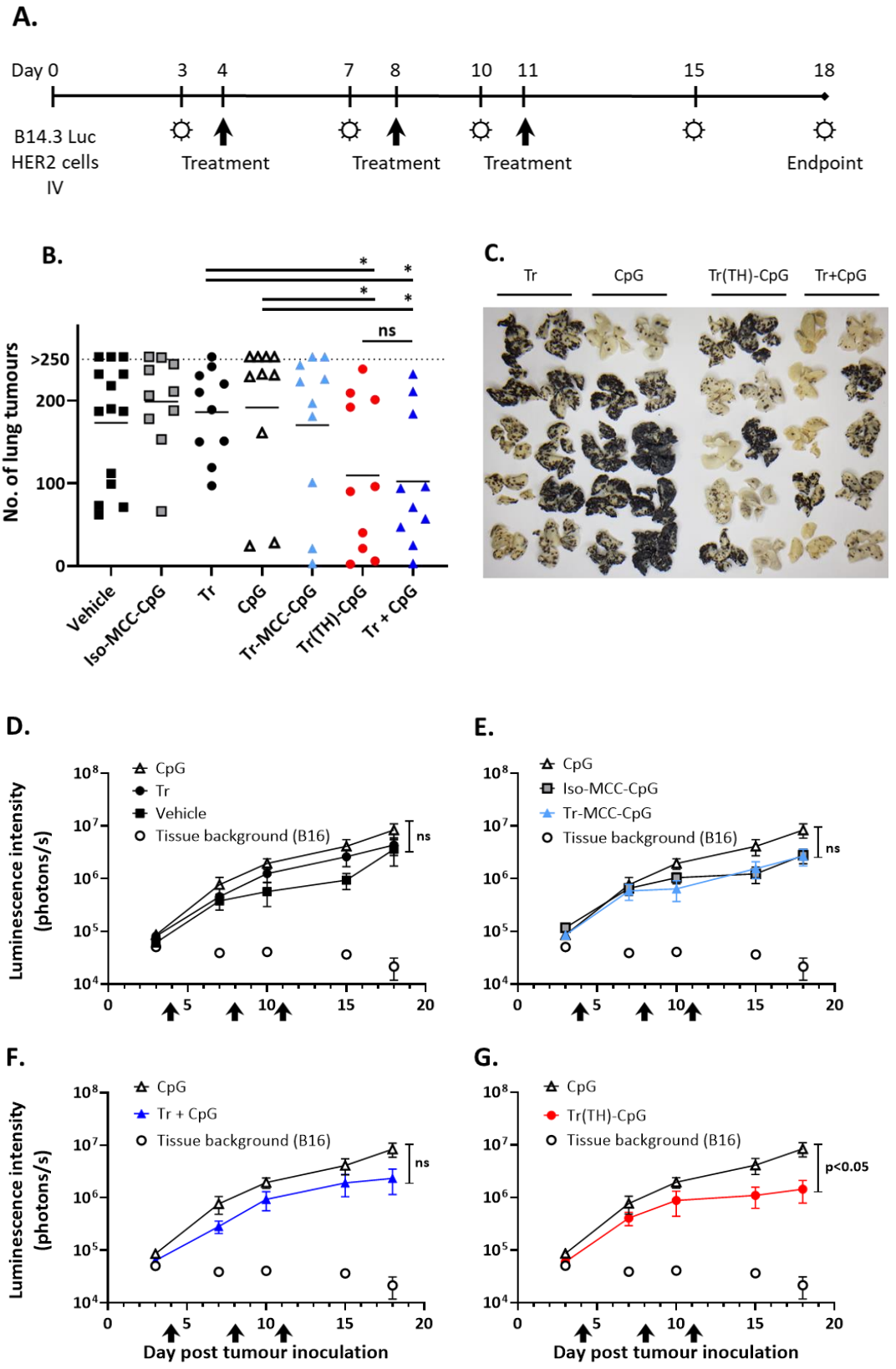


**Figure 5.16.** Continued on next page.

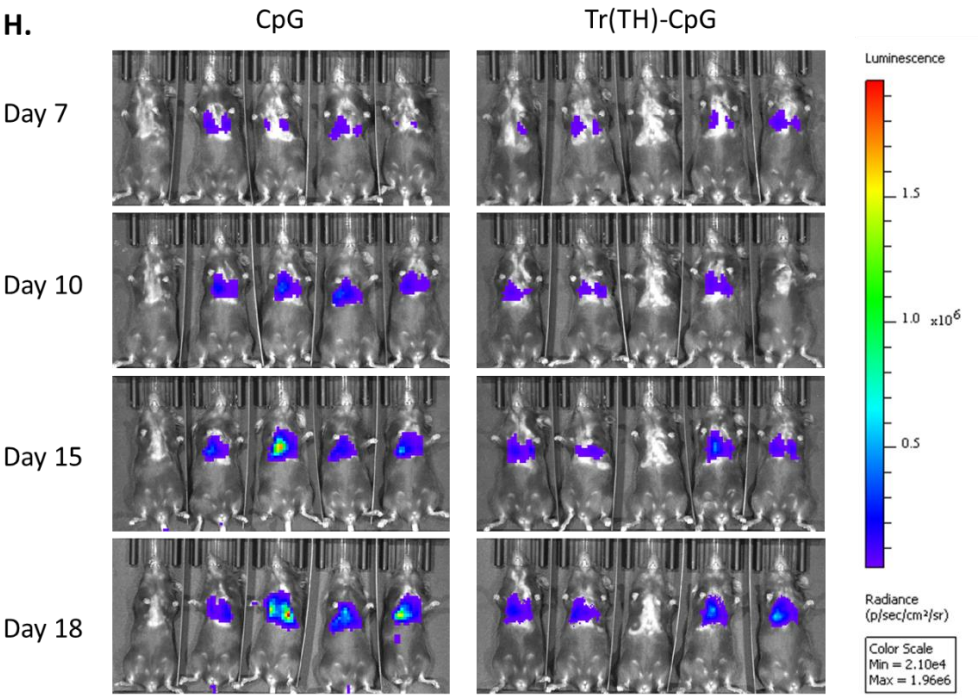


**Figure 5.16.** Repeated treatment with Tr(TH)-CpG only minimally decreases tumour burden in mice with pulmonary B14.3 Luc HER2 mice, but is not superior to unconjugated Tr + CpG. **A.** Mice (n=10 for all groups, except vehicle where n=9) were inoculated with 9x $10^5$ B14.3 Luc HER2 clone H2 cells on day 0 and treated at days 4, 8 and 11 (arrows) with 40µg Tr or isotype control, with or without 3µg CpG 1668 either unconjugated or conjugated to antibody via the stochastic or site-specific (Thiomab) method. Tumour burden was monitored using in vivo imaging on days 3, 7, 10, 15 and 18 post-tumour inoculation (☼). **B**. Number of pulmonary nodules counted on the lung surface at day 18 post-tumour inoculation (end point). Each data point and mean are shown. Mann-Whitney T test; * $p<0.05$; ns – not significant. **C.** Representative images of mouse lungs bearing B14.3 Luc HER2 clone H2 tumours at day 18 post tumour inoculation (endpoint). **D-G.** Tumour growth profiles represented as luminescence signal of mice imaged at the indicated time-points. Data are shown as mean ± SEM. Groups were compared using CGGC permutation test with 10 000 permutations. **H.** Representative images of tumour burden monitored by measuring luminescence signal in vivo. Data are pooled from 3 independent experiments.

### 5.6.2 Serum concentration of conjugates over time

CpG containing conjugates show additional binding to dendritic cells via the CpG moiety (Kreutz et al. 2012). This is likely accounted for by specificity of CpG ODN for scavenger receptors, expressed by dendritic cells and macrophages (Jozefowski et al. 2006; Kissick et al. 2014). Since these and possibly other mechanisms could impact on serum persistence of Tr and Tr-derived CpG-containing conjugates, we investigated this parameter by ELISA.

In this assay, human HER2-specific antibodies or conjugates were captured on human HER2-coated plates and subsequently detected with an anti-human IgG1 Fc antibody. A standard ladder of Tr or conjugate was used to calculate the respective serum concentration. In our ELISA set-up, serum form mice treated with CpG or isotype-MCC-CpG treatment did not increase assay background, suggesting that neither free nor conjugated CpG interfered with the assay (data not shown). Since we observed that Tr(TH)-CpG conjugates were more efficient than Tr-MCC-CpG conjugates in delaying tumour growth, we primarily focused our efforts toward understanding the profile of Tr(TH)-CpG conjugates.

First, we determined serum concentration after one dose of treatment. Mice were inoculated with B14.3 Luc HER2 tumour cells at day 0. At day 10 the presence of tumour burden was confirmed using *in vivo* imaging. Mice were treated with one dose of either Tr(TH) or Tr(TH)-CpG on day 11. Serum was collected at day 1, 4 and 7 after IV treatment, which represents day 12, 15 and 16 after tumour inoculation, respectively (Fig. 5.17 A). Among tested time-points, serum concentration of Tr(TH) was greatest on day 1 at 21.16±5.97 µg/ml, then decreased progressively and dropped to 6.78±0.458 µg/ml on day 7 post-treatment. These results were comparable to Tr results (Figure 4.17 B). Serum concentration of Tr(TH)-CpG was comparable to Tr(TH) on day 1 and day 7, at 23.14±1.76 µg/ml and 6.28±1.27 µg/ml, respectively. Serum concentration on day 4 however, was decreased for Tr(TH)-CpG (12.18±4.69 µg/ml) compared to Tr (18.11±3.61 µg/ml). Notably, standard deviations are high (Fig. 5.17 B). Considering that we observed high variability in tumour burden within groups and that tumour cells are involved in antibody metabolism, high variability in serum concentrations of antibody are not surprising for our set of samples.

Secondly, we investigated whether there is a difference in serum concentration of Tr and conjugates at day 14 and 18 in mice treated repeatedly with a total of 3 doses on days 4, 8 and 11 (Fig. 5.18 A). In this experiment, we observed a mild delay in tumour growth in mice treated either with Tr + CpG or Tr(TH)-CpG compared to controls (Fig. 5.16). Tumour burden was markedly variable within groups (Fig. 5.18). Serum concentration of Tr or conjugates was also highly variable within groups (Fig. 5.18 B-D). Serum concentration of Tr stood at

29.46±11.25 µg/ml on day 3 and decreased to 17.08±11.78 µg/ml on day 7 post treatment (days 14 and 18 of the experiment, respectively). Addition of CpG to the Tr treatment did not influence the serum concentration of Tr (Fig. 5.18 B). The conventional conjugate Tr-MCC-CpG showed statistically significant lower serum concentration on both day 3 and day 7 post-treatment (Fig. 5.18 C). This could be due to more rapid up-take of the conjugate by myeloid cells via the CpG moiety or rapid up-take of the higher MW species in the heterogenous mixture of conjugates. Surprisingly, serum concentration of Tr(TH)-CpG however, was only slightly lower than for Tr at both time-points, and differences did not reach statistical significance (Fig. 5.18 D).

Taken together, our data indicates that metabolism of Tr(TH)-CpG conjugates is similar to Tr after three doses of treatment, as demonstrated by comparable serum concentration across time. In contrast, serum concentration of Tr-MCC-CpG was significantly decreased and may have contributed to the lack of impact on tumour burden observed for these mice (Fig. 5.16). The experimental set-up was limited in terms of time-points and therefore we cannot establish the maximum serum concentration or calculate pharmacokinetic parameters such as terminal half-life.

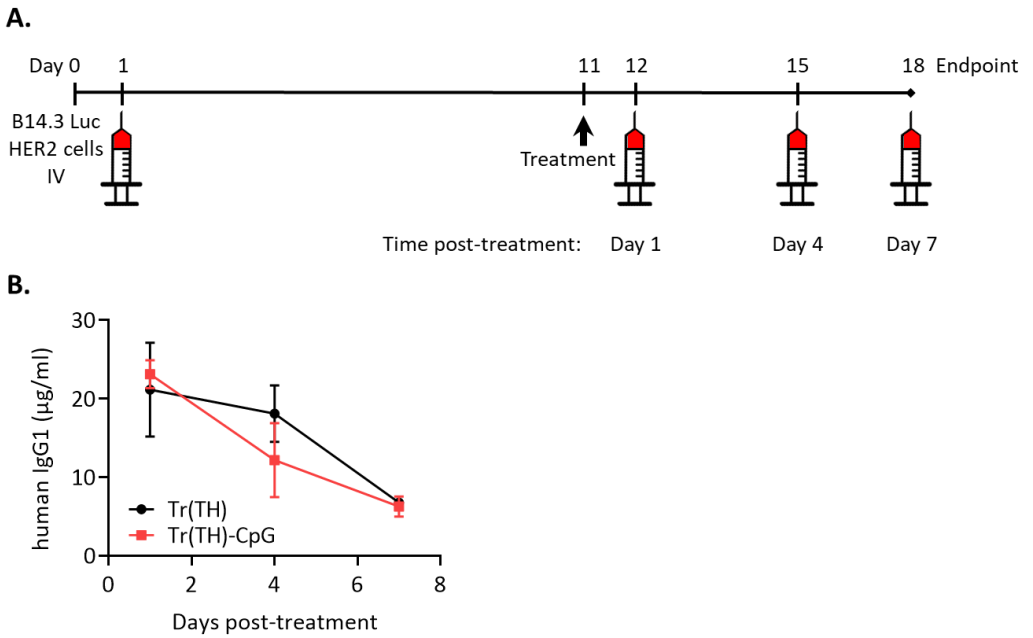


**Figure 5.17.** Serum concentration over time of Tr(TH) and Tr(TH)-CpG after single IV administration. **A.** Mice (n=5) bearing B14.3 Luc HER2 tumours were treated once at day 0 with 40µg Tr(TH) or Tr(TH)-CpG. Blood sampling was performed at day 1, 4 and 7 post-treatment. **B.** Tr(TH) (black) and Tr(TH)-CpG (red) were detected on ELISA with immobilised human HER2 and anti-human IgG Fc detection antibody, then serum concentration was calculated using the respective standard ladder in the linear range. Data are mean ± SD and were generated in one experiment.

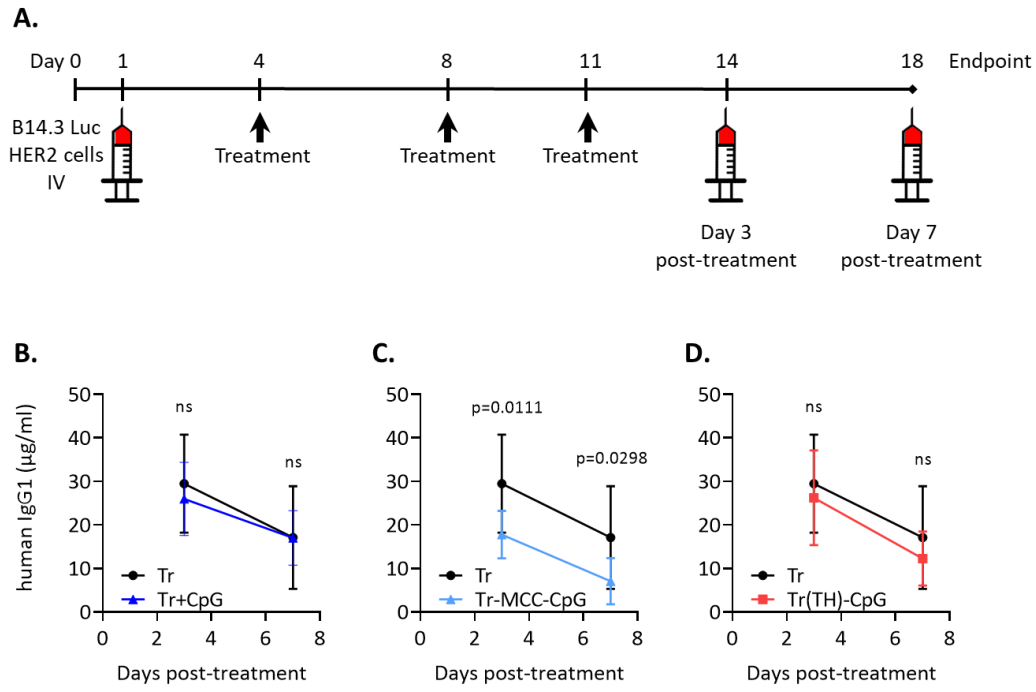


**Figure 5.18.** Serum concentration over time of Tr or conjugates after administration of 3 doses. **A.** Mice bearing B14.3 Luc HER2 tumours (n=10) were treated 3 times with 40µg Tr, Tr-MCC-CpG, or Tr(TH)-CpG. Serum samples were harvested at day 3 and day 7 after the last round of treatment. **B-D.** Antibody or conjugate serum concentration was determined by ELISA using an antibody or respective conjugate standard curve. Data are shown as mean ± SD and are pooled from 3 independent experiments.

### 5.6.3 Treatment with Tr(TH)-CpG promotes anti-tumour T cell responses

One of the major effects of CpG-mediated TLR9 signalling is instructing adaptive immune responses towards a Th1 phenotype with strong cytotoxic T cell effector functions (Iwasaki and Medzhitov 2015). Therefore, we investigated T cell responses induced by treatment with CpG alone, with Tr or in the form of conjugates.

Mice were treated with three doses as previously described in Fig. 5.18. In these experiments, treatment with Tr(TH)-CpG and Tr + CpG showed a minor benefit in terms of tumour burden (Fig. 5.16). At endpoint, spleens were harvested, and single cell suspensions were generated. Splenocytes were stained with the following T cell markers: CD3, CD4, CD8, CD44 and CD62L and analysed by flow cytometry (Fig. 5.19 A). CD44 is a marker for activated T cells. Double staining with CD44 and CD62L allows for separation of activated T cells in the spleen into central memory T cells ($CD44^+CD62L^+$) and effector memory T cells ($CD44^+CD62L^-$) (Sallusto, Geginat, and Lanzavecchia 2004). Mice showed comparable numbers of $CD4^+$ and $CD8^+$ T cells across treatment groups (data not shown). Most $CD44^+$ activated T cells were also $CD62L^+$, indicating a central memory phenotype (representative plots in Fig. 19 B and C). This was expected, as these T cell responses were investigated at the experiment endpoint, which was 14 days from treatment initiation and 7 days since the last dose. Percentages of $CD44^+CD62L^+$ cells in the $CD8^+$ T population were significantly higher in mice treated with CpG compared to mice treated with vehicle or Tr, and this was independent of the therapeutic format of CpG, either alone, with Tr or conjugated (Fig. 5.19 D). The same trend was observed for counts of $CD44^+CD62L^+$ $CD8^+$ T cells and differences were statistically significant, except for counts of $CD44^+CD62L^+$ $CD8^+$ T cells in spleens of mice treated with Tr-MCC-CpG or Tr + CpG (Fig. 5.19 E). In these groups, standard deviations were much higher. A statistically significant increase in $CD44^+CD62L^+$ population was observed for $CD4^+$ T cells as well, in all groups receiving treatment with CpG, either conjugated or not (Fig. 5.19 F, G).

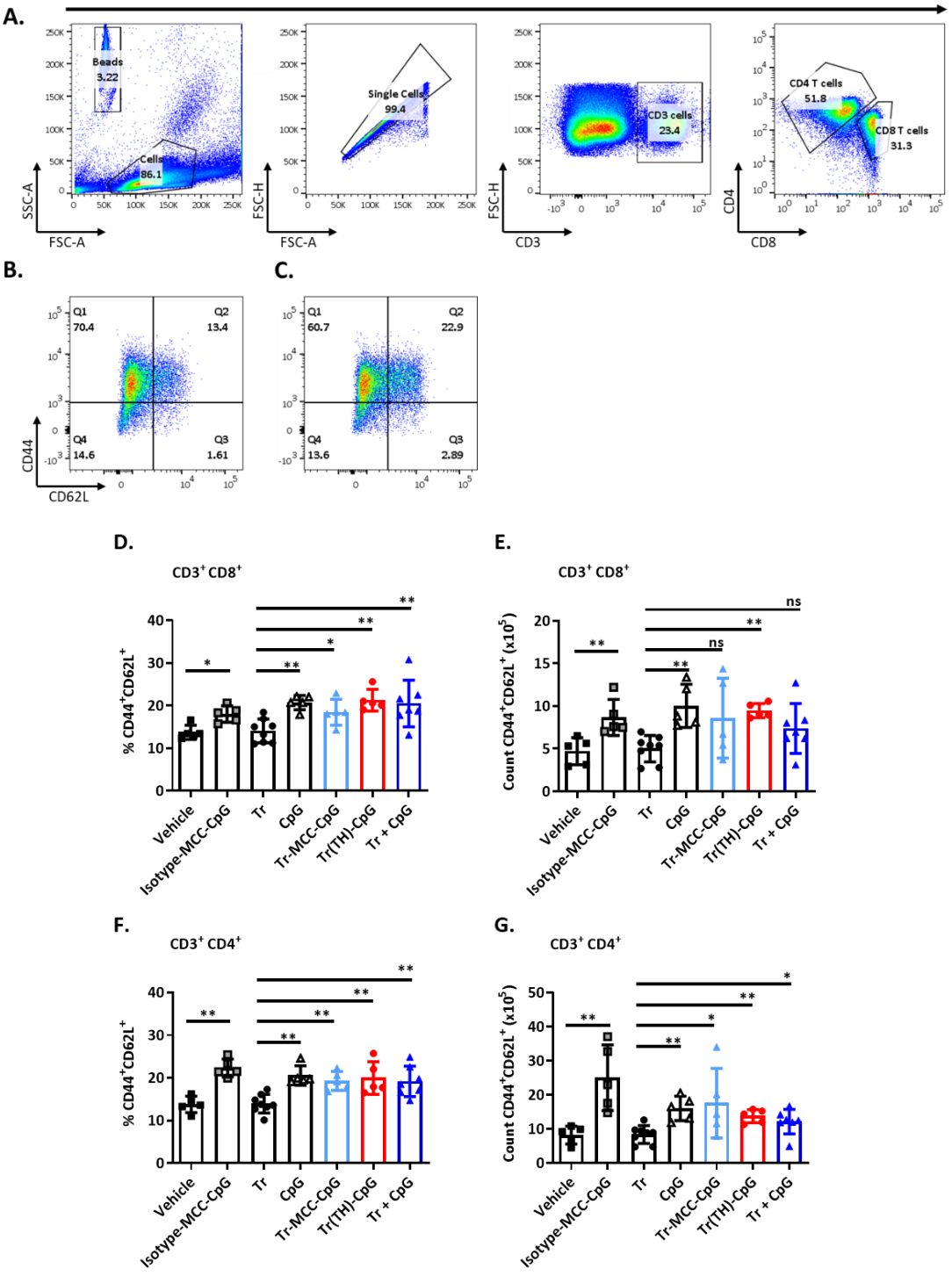


**Figure 5.19.** Treatment with 3 doses of CpG increases number of activated, central memory (CD44+, CD62L+) T cells. Splenocytes from mice treated 3 times with the indicated drugs, were harvested at day 18, stained and analysed by flow cytometry. **A.** Gating strategy used to analyse $CD4^+$ and $CD8^+$ T cells separately. **B-C.** Representative plots of $CD8^+$ T cells from mice treated with Tr (**B**) or Tr(TH)-CpG (**C**) with gating for CD44 and CD62L. Percentages (**D, F**) and counts (**E, G**) of $CD44^+CD62L^+$ cells in the $CD8^+$ T cell population (**D, E**) and $CD4^+$ T cell population. Each symbol represents a mouse with n=5 for vehicle, Iso-MCC-CpG, Tr-MCC-CpG and Tr(TH)-CpG; n=8 for Tr and n=7 for Tr + CpG. Means (represented by bars) ± SD of samples from 2 independent experiments. Mann-Whitney two tailed test; *p<0.05; **p<0.01; ns – not significant.

Next, we asked if the observed T cell responses are tumour specific. To evaluate this, splenocytes were labelled with CFSE, which is typically diluted with each cell division, and then cocultured for three days with dendritic cells presenting a variety of tumour-specific antigens. The percentage of proliferating T cells was determined by flow cytometry. Tumour specific proteins and peptides included the extracellular domain of human HER2, the class I peptide SIINFEKL of OVA antigen and multiple predicted class I and class II peptides of TRP-1 and TRP-2, which are melanocyte-specific proteins present in B14.3 tumours.

Proliferation of activated ($CD44^+$) T cells upon tumour antigen re-encounter was measured in splenocyte populations from mice treated at day 11 with one dose of Tr, CpG or Tr(TH)-CpG (Fig. 5.20 A). Gating strategy is shown in Fig. 5.20 B. Representative histograms for $CD44^+CD8^+$ gated T cells from mice treated with Tr(TH) or Tr(TH)-CpG are shown in Fig. 5.20 C. In this assay, our negative control consisting of cells from untreated mice that had not received tumour cells showed a degree of proliferation as well, with values of 20.3 ± 7.42 for activated $CD8^+$ T cells (Fig. 5.20 D) and 14.3 ± 3.3% for activated $CD4^+$ T cells (Fig. 5.20 E). After one dose of treatment, mice treated with either Tr, CpG or Tr(TH)-CpG showed increased percentages of proliferating activated $CD8^+$ T cells (Fig. 5.20 D) and activated $CD4^+$ T cells (Fig. 5.20 E). Treatment with Tr(TH)-CpG only minimally increased the percentage of tumour specific T cells in comparison to the other treatment groups and this was observed for both $CD8^+$ and $CD4^+$ T cell subtypes (Fig. 5.20 D and E).

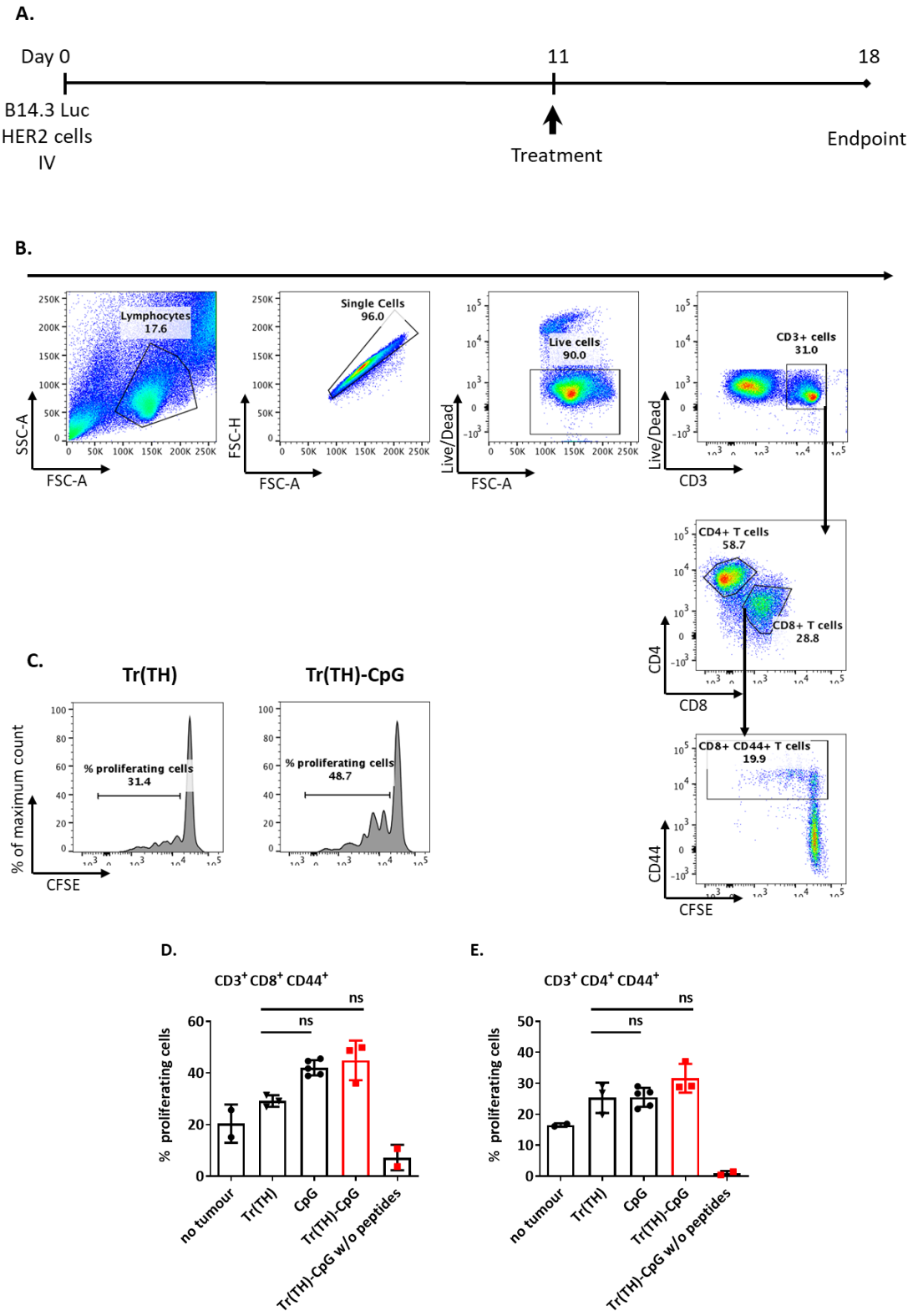


**Figure 5.20.** Effect of treatment with one dose of Tr(TH)-CpG in promoting anti-tumour T cell responses. **A.** Mice were treated once at day 11 with Tr(TH)-CpG (n=4) comprising 40µg Tr and 2.5µg CpG or normalised controls: Tr(TH) (n=3), CpG (n=5). Spleens were harvested at day 18. **B**. Splenocytes were labelled with CFSE and cultured for 3 days with GM-CSF derived BMDCs loaded with tumour specific proteins and peptides: extracellular domain of human HER2, SIINFEKL (class I OVA-peptide), and multiple class I and class II TRP-1 and TRP-2 peptides. Incubated splenocytes were stained for CD3,

CD4, CD8, CD44 and analysed by flow cytometry. FMO controls were used for gating. **C.** The percentage of CFSE diluting cells was calculated and served as a marker of proliferation. Representative histograms of activated $CD8^+$ T cells from Tr(TH) and Tr(TH)-CpG treated mice. **D.** Percent proliferating activated $CD8^+$ T cells. **E.** Percent proliferating activated $CD4^+$ T cells. Each data point represents cells from an individual mouse. Mean ± SD are shown. Mann-Whitney two tailed test; ns – not significant. Data from one experiment.

T cell antigen specific recall responses were also measured in splenocyte samples from mice treated repeatedly, with three doses of conjugates or controls. Spleens were also harvested at day 18 (Fig. 5.21 A). The experiment and analysis were performed as described above. Proliferation of activated T cells was observed for vehicle treated mice as well and stood at 17.5 ± 3.1% for activated $CD8^+$ T cells (Fig. 5.21 B) and 31.3 ± 5.9% for activated $CD4^+$ T cells (Fig. 5.20 H). In the absence of tumour antigens, only low levels of proliferation were observed. Treatment with either Tr or CpG significantly increased the percentage of proliferating $CD8^+$ T cells (Fig. 5.21 B), but only a subtle effect was observed for $CD4^+$ T cells (Fig. 5.21 C). The increase in tumour specific T cells by treatment with Tr has been described in the literature before and has been attributed to Fc mediated facilitated uptake of tumour cells by DCs (Bianchini and Gianni 2014). Compared to the Tr or CpG controls, treatment with Tr(TH)-CpG, but not Tr-MCC-CpG, Iso-MCC-CpG or Tr + CpG was superior in promoting tumour antigen specific T cells even further, for both the $CD8^+$ and $CD4^+$ T cell populations (Fig. 5.21 B, C). Differences between Tr(TH)-CpG treatment and Tr treatment did not reach statistical significance for $CD8^+$ T cells (Fig. 5.21 B), but were significant for $CD4^+$ T cells (Fig. 5.21 C). When percentages for Tr(TH)-CpG group were compared to unconjugated CpG controls, differences were statistically significant for both $CD8^+$ (Fig. 5.21 B) and $CD4^+$ T cell (Fig. 5.21 C) populations. In this assay proliferation of vehicle treated mice was not compared to tumour-free mice and it is currently unclear if there is a difference in the background levels of these two controls.

Together, these two experiments indicate that treatment with Tr or CpG moderately increase the percentage of tumour specific T cells. Treatment with Tr(TH)-CpG is substantially superior in this respect, even when compared to unconjugated Tr + CpG. This suggests that distinct mechanisms are responsible for the partial tumour growth control we observed in mice treated with Tr(TH)-CpG or Tr + CpG. Repeated treatment is required to increase the levels of tumour specific T cells by conjugate. This was observed for both $CD8^+$ T cell and $CD4^+$ T cell responses.

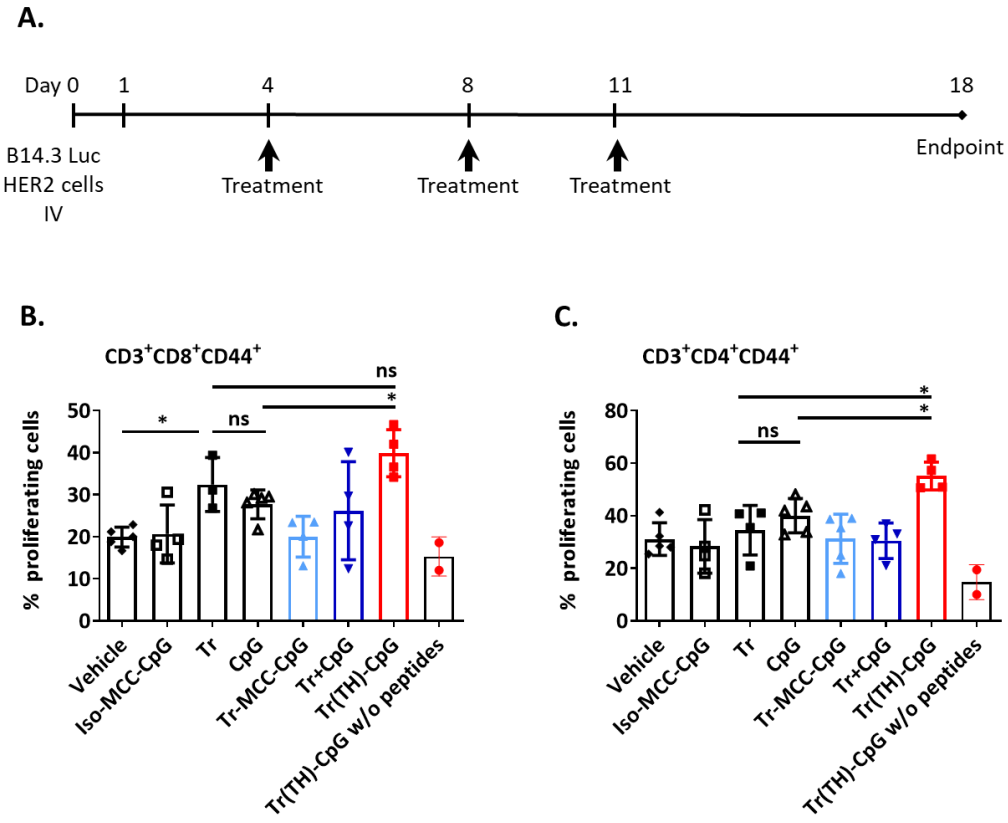


**Figure 5.21.** Repeated treatment with Tr(TH)-CpG promotes anti-tumour T cell responses. **A.** Mice were treated 3 times with Tr(TH)-CpG comprising 40µg Tr and 2.5µg CpG and normalised controls, or with Tr-MCC-CpG. Splenocytes were incubated with peptides and analysed as described above. B. Proliferation of activated $CD8^+$ T cells in percentage. C. Proliferation of activated $CD4^+$ T cells in percentage. Each data point represents an individual mouse (n=4 or 5). Bars show mean, lines show SD. Mann-Whitney two tailed tests; *p<0.05; ns – not significant. Data from one experiment.

Additional experiments are needed in the future to confirm these observations. Measuring other markers of proliferation such as Ki67 and IL-2 levels in cell supernatant would be useful to increase the power in future experiments.

It is unclear at this stage if these T cell responses are directed mostly against the foreign antigen HER2, against OVA or the melanoma-associated antigens TRP-1 and TRP-2. The resolution of the proliferation assays is far from ideal and it does not seem to permit such investigations. Experiments using multimeric MHC / peptide complexes for detection of specific T cell receptors (TCR), however, might be better suited. Pentamers or dextramers detecting anti-human HER2 specific mouse TCRs are not yet commercially available, but pentamers staining for SIINFEKL specific T cell receptors are and we employed them to detect anti-OVA specific T cells (Fig. 5.22).

Splenocytes were collected at day 18 from tumour inoculation of mice treated with three doses of conjugates or controls as described above (Fig. 5.21 A). Splenocytes were cultured for 3

days with SIINFEKL peptide loaded onto GM-CSF derived DCs, then stained for CD8 expression and with H-2Kb-SIINFEKL pentamer. Representative plots of Tr or Tr(TH)-CpG treated mice are shown (Fig. 5.22 A). Negatively selected lymph node OT-1 $CD8^+$ T cells, which are specific for the OVA-peptide SIINFEKL (Hogquist et al. 1994) were used for positive control, to confirm assay performance (Fig. 5.22 B). No changes in the percentage of SIINFEKL binding $CD8^+$ T cells were detected for any of the treatment groups, with all means standing between 0.15 and 0.20% (Fig. 5.22 C). This indicates that the tumour-specific T cells detected at higher levels in tumour-bearing mice treated with Tr(TH)-CpG (Fig. 5.21) are unlikely to be specific for the OVA model antigen (Fig. 5.22).

Further investigations of the specificity of anti-tumour T cell responses promoted by treatment with Tr(TH)-CpG are required to better understand the effects of treatment.

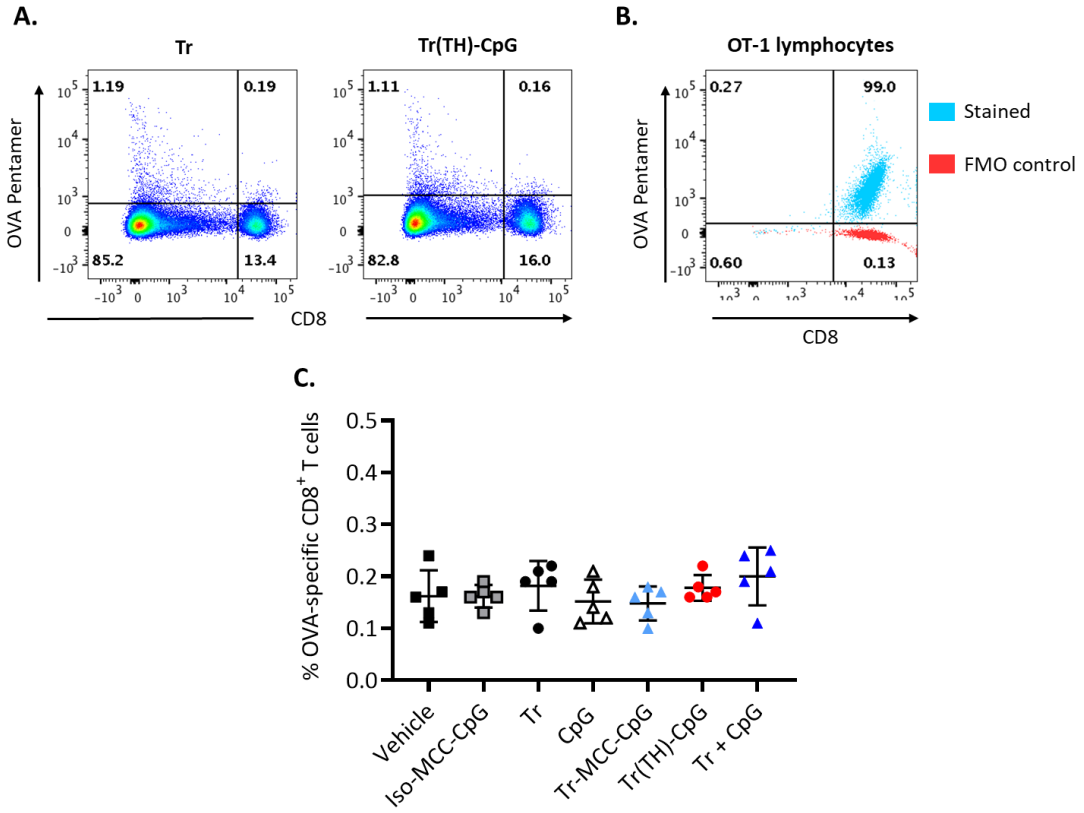


**Figure 5.22.** Anti-tumour CD8+ T cell responses are not specific for OVA-peptide SIINFEKL. **A.** Representative plots of splenocytes incubated for 3 days with 1µM of the OVA-peptide SINNFEKL presented by DCs and stained for CD8 and SIINFEKL specific TCR with pentamer. **B.** Percent OVA-specific CD8+ T cells. Each data point represents an individual mouse (n=5 per group). Mean ± SD are shown. Multiple Mann-Whitney two tailed tests showed no statistically significant differences. Data collected from one experiment.

### 5.6.4 *In vivo* antibody responses to treatment with conjugates

Humoral anti-tumour responses were evaluated as well. We focused on groups of mice treated with Tr(TH)-CpG or Tr + CpG as we observed a small delay in tumour burden in these mice, and included their controls, mice treated with either vehicle, Tr or CpG. We assessed total serum antibody titres pre- and post-treatment (Fig. 5.23) and subsequently investigated if antibodies present in day 18 were raised against tumour-specific antigens (Figure 5.24).

To assess total antibody titres, serum was harvested from tumour-bearing mice on day 1 after tumour inoculation (pre-treatment) and on days 14 and 18 after tumour inoculation, which are 3- and 7-days post-treatment (Fig. 5.23 A). The treatment schedule and doses were previously described in section 5.6, while the tumour-burden response to treatment of these mice is shown in Fig. 5.16. The Mouse Immunoglobulin Isotyping Panel from BioLegend was used to measure total serum levels. Serum from tumour-free mice was measured as well (green symbols). Tr or derived conjugate (human IgG1 isotype) did not cross-react with mouse immunoglobulin isotyping panel (data not shown). Variability within mouse treatment groups as well as among treatment groups at pre-treatment baseline (day 1) was observed in this assay. Across antibody isotypes, day 1 serum from all treatment groups contained lower levels of antibodies, at comparable, or slightly higher levels than tumour-free mice. Apart from IgA (Fig. 5.23 F), serum levels of all other measured isotypes were increased at day 14 and 18 post-tumour inoculation compared to day 1. This trend was observed for vehicle (PBS) treated mice as well, suggesting that the tumour cells, which were human HER2-transgenic, OVA-GFP transgenic and luciferase-transgenic, induced a humoral immune response on their own.

Levels of mouse IgG1 (Fig. 5.20 B) were comparable among all treatment groups. Mouse IgM (Fig. 5.23 G) levels were highest for CpG treated mice. Mouse IgG2c (Fig. 5.23 C), IgG2b (Fig. 5.23 E), IgG3 (Fig. 5.23 D) levels were higher in mice treated with either Tr, CpG, Tr + CpG or Tr(TH)-CpG compared to vehicle treated group. Treatment with Tr(TH)-CpG (red symbols) did not substantially influence serum levels of any of the determined antibody isotypes when compared to Tr, CpG or Tr + CpG treated mice. These data show increased serum antibody levels in tumour-bearing mice, which are moderately elevated by treatment with either Tr(TH)-CpG, unconjugated Tr + CpG, Tr or CpG alone.

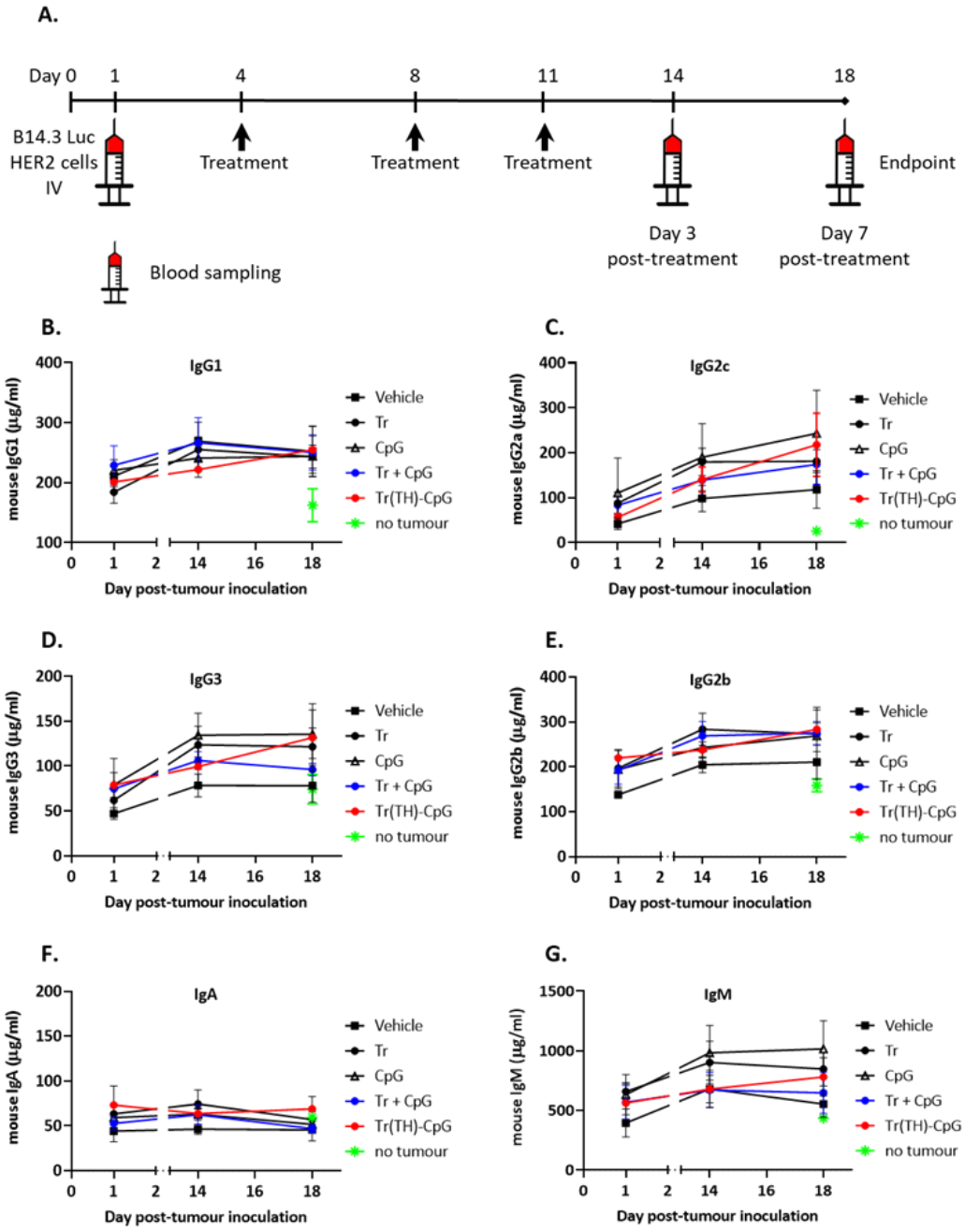


**Figure 5.23.** Serum mouse immunoglobulin titres. Total antibody levels were measured in serum harvested from tumour-free mice (green symbols) or tumour-bearing mice treated with conjugates or controls at different time-points (**A**) after tumour inoculation using the LEGENDplex Mouse Immunoglobulin Isotyping Panel (BioLegend). Serum levels of mouse antibody isotypes IgG1 (**B**), IgG2c (**C**), IgG3 (**D**), IgG2b (**E**), IgA (**F**), IgM (**G**) were detected. At time-point day 1 (pre-treatment), mouse serum within treatment groups was pooled and analysed together, as one sample per group per experiment. For time-points day 14 and day 18, serum from individual mice was analysed separately, with n=10 for each treatment group. Data pooled from two independent experiments is shown as mean ± SEM.

Additionally, we asked whether the observed antibody responses were directed at B14.3 Luc HER2 tumour-specific antigens (Fig. 5.24), such as human HER2 and ovalbumin (OVA). For

this, day 18 serum was analysed by ELISA with immobilised human HER2 (Fig. 5.24 A, C, E) or immobilised OVA (Fig. 5.24 B, D, F). Anti-mouse IgG1 (Fig. 5.24 A, B), IgG2c (Fig. 5.24 C, D) or IgM (Fig. 5.24 E, F) biotinylated antibodies were used to detect mouse antibody isotypes. We verified that neither of the detection antibodies used in this assay cross-reacted with human IgG1 isotype (data not shown). Serum from tumour-free mice (green) did not increase OD 450 readings over background in the mouse IgG1 (Fig. 5.24 A, B) or IgG2c (Fig. 5.24 C, D) ELISA. In terms of T cell dependent antibody responses, B14.2 HER2 Luc tumour-bearing mice developed anti-human HER2 mouse IgG1 (Fig. 5.24 A) and mouse IgG2c antibodies (Fig. 5.24 C) and treatment with Tr(TH)-CpG or controls did not influence levels of these antibodies. No mouse IgG1 (Fig. 5.24 B) or mouse IgG2c (Fig. 5.24 D) responses were detected for OVA antigen. To confirm the performance of the OVA-specific mouse antibody ELISA, a purified anti-OVA mouse IgG1 antibody (Sigma) was used as positive control.

IgM responses, which do not require T cell help, were detected against both human HER2 (Fig. 5.24 E) and OVA antigen (Fig. 5.24 F) and interestingly, albeit at lower levels, in the serum from tumour-free mice as well. This observation might be explained by the presence of natural antibodies in these healthy, antigen-free mice (Maddur et al. 2019), or might just be background. Anti-HER2 and anti-OVA IgM levels were indistinguishable between tumour-free and B16-bearing mice (data not shown). Surprisingly, Tr(TH)-CpG treated mice had lower levels of anti-HER2 or anti-OVA IgM antibodies than vehicle or CpG treated mice at day 18 post-tumour inoculation. Ideally, tumour antigen-specific antibody responses would have been investigated in dynamic, at different time-points. In terms of localisation of humoral responses, further experiments evaluating germinal centre B cells and plasma cells in tumour tissue, tumour draining lymph nodes and spleen of these mice are required.

Together, these data indicate that there is a humoral immune response to B14.3 Luc HER2 tumour cells, which includes anti-human HER2, but not anti-OVA antibodies. Treatment with either Tr(TH)-CpG, Tr + CpG, Tr or CpG alone moderately increases total serum levels of mouse IgG2c, IgG2b and IgG3. When compared to vehicle, the increased serum IgG2c did not contain higher levels of anti-HER2 or anti-OVA IgG2c. At this stage, it is unclear whether the increased pool of antibodies of multiple isotypes are specific to other tumour antigens we did not test for or mouse self-antigens.

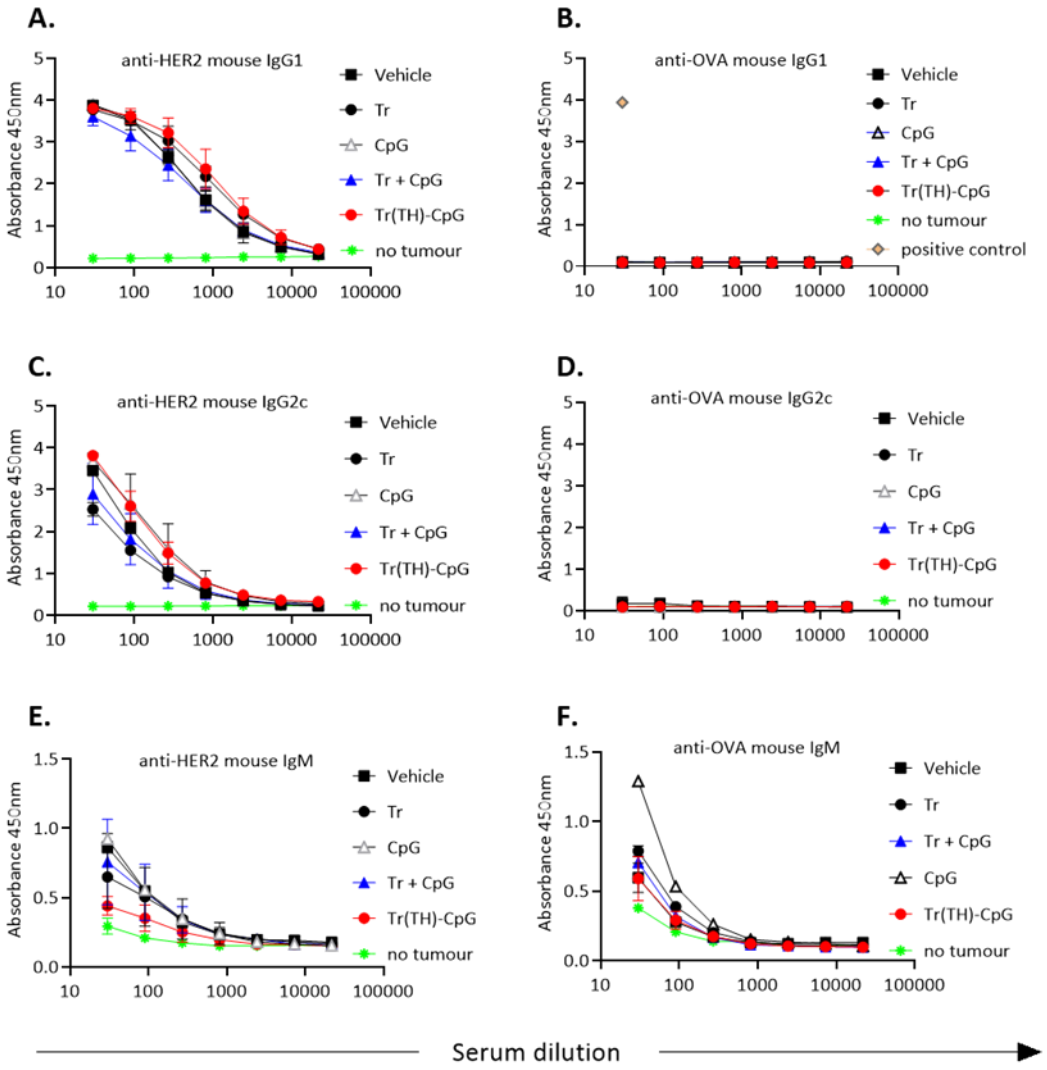


**Figure 5.24.** Detecting anti-human HER2 and anti-OVA specific antibody responses in mouse serum. Serum was collected from tumour-free mice and from tumour-bearing mice at day 18 post-tumour inoculation, which is 7 days after the last dose of treatment with either vehicle, Tr, CpG, Tr + CpG or Tr(TH)-CpG. Serum was pooled from n=5 mice per treatment group or n=2 for tumour-free mice and was analysed on ELISA with immobilised human HER2 (**A, C, E**) or OVA (**B, D, F**). Mouse IgG1 (**A, B**), IgG2c (**C, D**) and IgM (**E, F**) were detected with specific antibodies. Purified anti-OVA mouse IgG1 diluted at 15ng/ml was used as positive control (**B**). Mean ± SEM of data from two independent experiments.

### 5.6.5 *In vivo* cytokine response to treatment with conjugates

TLR9-mediated response to CpG ODN include the production of proinflammatory cytokines by innate immune cells, such as TNF-α and IL-6 (Krieg 2000). Overstimulation with CpG can induce IL-10 production (Waibler et al. 2008). Treatment with CpG induces maturation of dendritic cells and polarisation of $CD4^+$ T cells towards a Th1 phenotype promoting CTL responses (Iwasaki and Medzhitov 2015). Activated T cells in turn produce IL-2 and IFN-ɣ and CTLs can produce TNF-α as well (Mehta, Gracias, and Croft 2018). We investigated

serum cytokine levels in mice treated with free or conjugated CpG or controls using the LEGENDplex mouse Th1 panel from BioLegend (Fig. 5.25). The panel included IFN-ɣ, TNF-α, IL-2, IL-6 and IL-10. Serum was harvested from mice treated three times with 40µg Tr or Iso, free or conjugated with approx. 2.5-3µg CpG as shown in Fig. 5.25 A. Blood sampling were performed either 3 or 7 days after the last round of treatment.

Serum levels of TNF-α and IL-2 were below the assay detection limit at both time-points (data not shown). Only minute amounts of IL-6 were detected at day 3 post-treatment (Fig. 5.25 D), which seemed slightly higher at day 7 (Fig. 5.25 E). IL-6 levels were not influenced by treatment.

Mice treated with CpG, either free or conjugated to Tr or Iso showed increased IFN-ɣ levels at day 3 post-treatment, which achieved statistical significance, with the exception of the Tr(TH)-CpG group (red) (Fig. 5.25 B). IFN-ɣ levels dropped massively by day 7 (Fig. 5.25 C). This indicates that the systemic inflammatory response induced by CpG was lowest in mice treated with Tr(TH)-CpG conjugates.

At day 3 post-treatment, serum of vehicle (PBS) treated mice showed a mean of 71.99±27.53pg/ml of the immunosuppressive cytokine IL-10 (Fig. 5.25 F). This is in line with other studies using B16 or B16F10 melanoma tumours (Sato et al. 2011; Liu et al. 2013) and is a marker of the immunosuppressive tumour microenvironment. Treatment with CpG only minimally if at all decreased serum IL-10. Serum from mice treated with Tr(TH)-CpG showed the lowest IL-10 values, but no statistical significance was achieved (Fig. 5.25 F). Notably, the variability within treatment groups was high. At day 7 post-treatment, we could not detect IL-10 in serum (Fig. 5.25 G). Importantly, the detection limit for this assay stood at 82.35 pg/ml and IL-10 levels could have been just slightly under the threshold, resembling day 3 levels.

Together, these data indicate that treatment with CpG induces moderate serum IFN-ɣ levels, but not TNF-α or IL-2 or IL-6 at day 3 post-treatment. Since CpG-induced gene transcription has been shown to decrease in mice after 3 days from treatment (Bode et al. 2011), for future experiments, an earlier time-point would be beneficial, especially for evaluating TNF-α, IL-6 and IL-10 levels. Notably, serum IFN-ɣ was lower in mice treated with Tr(TH)-CpG. Decreased levels of IFN-ɣ in systemic circulation may point to an improved safety profile of Tr(TH)-CpG compared to unconjugated CpG.

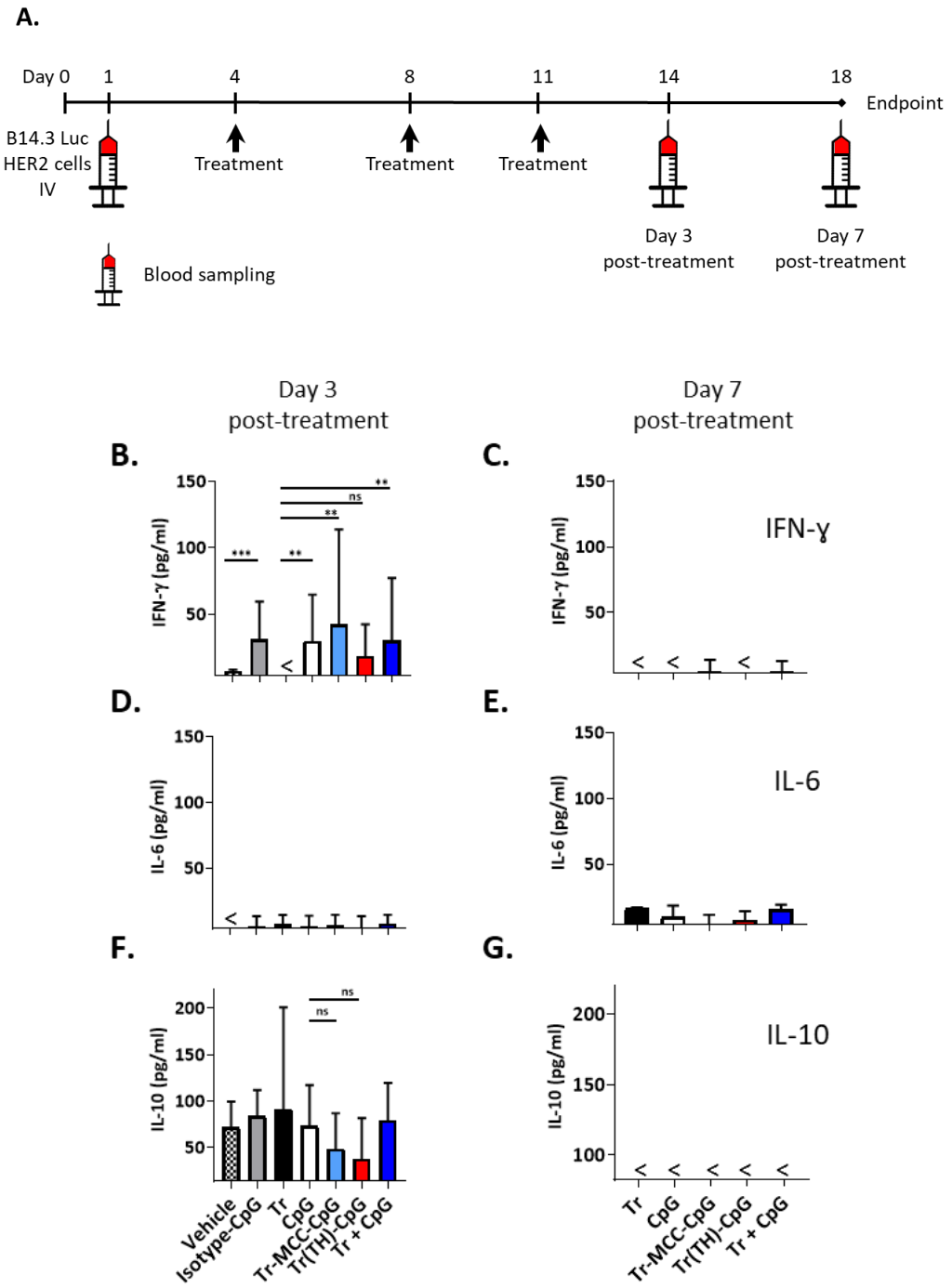


**Figure 5.25.** Serum cytokine levels induced by treatment with conjugates. **A.** Mice were inoculated with 9x 105 B14.3 Luc HER2 clone H2 cells on day 0 and treated at days 4, 8 and 11 (arrows) with 40µg Tr or isotype control, with or without 3µg CpG 1668 either unconjugated or conjugated to antibody via the stochastic or site-specific (Thiomab) method. Blood samples were collected before treatment, 3 (day 7) and 7 (day 18) days after the last dose of treatment (syringe symbol). **B-G.** Cytokines were detected in serum collected 3 days after treatment (day 14) or 7 days after treatment (day 18) using the LEGENDplex cytokine kit. Data are mean ± SD of n=10 mice for all day3 post-treatment groups, except for vehicle group where n=5 and Tr group where n=7. For day 7 post-treatment, n=3 in all groups, except Tr-MCC-CpG, where n=2. Mann-Whitney test; *p<0.05; **p<0.01; ***p<0.001; ns – not significant; < - below detection limit.

## Discussion

In this chapter, we explored antibody drug conjugation techniques to generate Trastuzumab-CpG conjugates. We showed that conjugates generated using site-specific conjugation chemistry were superior to non-specific, conventional conjugates in both *in vitro* and *in vivo* assays, and warrant further investigation.

Non-specific, stochastic conjugation of CpG with SMCC to lysine residues on Trastuzumab (Tr) impaired binding affinity of Trastuzumab to human HER2 (Fig. 5.5). This impairment was payload specific, with CpG, an oligo of approx. 6.5kDa, inducing a much more pronounced effect than the amino acid cysteine of 0.1 kDa (Fig. 5.6). The results for Trastuzumab-cysteine conjugates are in line with results from other groups reporting that SMCC conjugation of Trastuzumab with other small molecules did not impair HER2 binding (Arlotta et al. 2018; Abedi et al. 2019). Antigen binding was affected after conjugation with CpG for both Trastuzumab and another human IgG1 antibody, Cetuximab, although the impairment was more substantial for Trastuzumab (Fig. 5.6). Another study employing a rat antibody (anti-DEC205) conjugated via SMCC to CpG 1668 showed only a mild decrease in antigen binding of the resulting conjugate (Kreutz et al. 2012), supporting our findings that the magnitude of the effect is antibody-specific.

SMCC non-specific conjugation of Trastuzumab was reported by other groups, with various payloads. Since the method was employed to generate the approved conjugate Trastuzumab-emtansine (Kadcyla®), the stability and efficacy of the conjugation method was extensively studied. The consensus is that non-specific, conventional conjugations methods yield conjugate preparations that are structurally heterogenous, with antibodies that bear no payload and antibodies that are conjugated to a degree that abolishes their activity (Behrens and Liu 2014; Bakhtiar 2016; Chau, Steeg, and Figg 2019). Moreover, serum stability is poor, due to linker maleimide exchanges from the conjugate to thiol groups in serum proteins such as albumin (Alley et al. 2008). One of the reported elegant solution to these shortcomings is site-specific conjugation using Thiomab technology (Junutula et al. 2008; Shen et al. 2012). Here, we showed that this conjugation chemistry results in Tr(TH)-CpG conjugates with HER2 binding properties comparable to Tr (Fig. 5.13).

In terms of CpG activity, this did not seem to be affected by either method of conjugation (Fig.5.4 and Fig. 5.12). For *in vivo* evaluation of Trastuzumab-CpG conjugates, we used a human HER2 expressing mouse model generated with HER2-transgenic B14.3 luciferase cells

transplanted into immunocompetent mice. This model allows for the evaluation of adaptive anti-tumour immune responses.

Overall, we used only two in vivo experimental set-ups. In one set-up, mice received only one dose of treatment at day 11 post-tumour inoculation. Since mice were treated at a stage of substantial tumour burden and only once, we cannot expect much in terms of tumour growth control. The set-up allowed for direct comparison of serum concentration of Tr(TH)-CpG with the unconjugated antibody Tr(TH). Just one dose of Tr(TH)-CpG, which persisted in the serum comparably to Tr(Th) (Fig. 5.17), mildly increased the number of tumour antigen specific T cells over the unconjugated antibody in mouse spleens 7 days after treatment (Fig. 5.20).

In further experiments, mice received three doses of treatment, starting with day 4 post-tumour inoculation, at 3-4 days interval. With this set-up, when compared with the parent antibody Tr or even unconjugated CpG, in mice treated with Tr(TH)-CpG but not with Tr-MCC-CpG conjugates we observed a mild delay in tumour growth (Fig. 5.16) and tumour antigen specific T cell responses in the spleens of (Fig. 5.21). These results were expected, since there is ample literature reporting the efficacy of CpG in promoting anti-tumour T cell responses, which controlled tumour growth (Kawarada, Ganss, Garbi, Sacher, Arnold, and Hammerling 2001; Kunikata et al. 2004; Wang et al. 2016; Lonsdorf et al. 2003). The mentioned studies were performed using CpG injected directly into the tumour and the T cell responses were much more robust. Further studies are needed to establish if the anti-tumour T cell responses we observed can be enhanced using increased doses of conjugated CpG while avoiding increased levels of immunotoxicity observed for high doses of unconjugated CpG. The mouse model we used only expressed moderate levels of human HER2 *in vivo* (Fig. 3.13). It would be interesting to evaluate the effects of treatment with Tr(TH)-CpG in a HER2-overexpressing mouse model. Direct comparison between intratumoral injection and targeted delivery using Tr(TH)-CpG would help establish the efficiency of the conjugate. To achieve this, we would require either a human HER2 transgenic mouse or a humanised mouse model bearing a HER2 overexpressing xenograft.

Notably, tumour growth was delayed in mice treated with unconjugated Tr + CpG comparably with mice treated with Tr(TH)-CpG. Considering that Tr was shown to promote anti-tumour T cell responses on its own (Bianchini and Gianni 2014), and this effect is well documented for CpG (Krieg 2007), it is not surprising for treatment with Tr + CpG to synergise. Interestingly, Tr(TH)-CpG conjugates induced increased levels of anti-tumour T cell responses compared to unconjugated Tr + CpG. This indicates that distinct immune activation profile may be responsible for the observed delay in tumour growth and importantly, it is likely

that multiple cell populations contribute to the effect. For instance, treatment with CpG has been shown to boost Tr mediated antibody-dependent cytotoxicity that delayed tumour growth of a Tr resistant tumour (Damiano et al. 2009). In this study, we have only analysed splenic T cells in different treatment groups. For the future, it would be important to analyse immune responses in the tumour microenvironment, to further unravel the effects of different treatments.

Importantly, when drugs are administered IV the first capillary bed reached is in the lung (Chao et al. 2010). It is therefore possible, that the anatomic location of the tumours in our mouse model favours activity of Tr + CpG. Another study using subcutaneous B16F10-OVA tumours showed that when combined with cryosurgery IV CpG has anti-tumour effects as well, although intratumoral CpG is much more potent. The B14.3 Luc HER2 cells we used to generate pulmonary nodules generate variable tumour burden when transplanted subcutaneously, with some mice rejecting the tumours completely (Fig. 3.16). Another mouse model for subcutaneous tumour implantation would be required for accurate comparison of IV delivery of Tr + CpG and conjugated Tr(TH)-CpG versus intratumoural application of Tr +CpG.

In addition to investigating tumour growth and T cell responses in mice treated thrice with Tr(TH)-CpG or controls, we also investigated antibody responses. Importantly, titres of serum IgG isotypes increased with time (Fig. 5.23) and implicitly, with tumour growth. This confirms our suspicions that the B14.3 Luc HER2 cells are recognised by the immune system of C57/BL6 mice. Interestingly, anti-human HER2 mouse antibodies, but not anti-OVA mouse antibodies were detected in B14.3 Luc HER2-bearing mice and no treatment substantially influenced levels (Fig. 5.24). These results indicate that human HER2 is more immunogenic in the mouse system than OVA model antigen and explain the spontaneous tumour growth control we have observed for B14.3 Luc HER2 tumours (Fig. 3.10) which was not encountered for B14.3 tumours expressing OVA but not human HER2 (Kreutz et al. 2012; Rajagopal et al. 2010). The role of the Firefly luciferase in this was not investigated by us. Literature reports, however, that Firefly luciferase is immunogenic in mice of the C57/BL6 background (Liao et al. 2015).

Notably, most studies combined CpG with other therapies (Krieg 2007). This suggests that the effects of CpG are not regarded sufficient for effective tumour treatment. One of the emerging regimens is combining treatment with CpG with immune checkpoint inhibitors. While the role of CpG is to promote anti-tumour immune responses, immune checkpoint inhibitors are used to alleviate T cell dysfunction mediated by the tumour microenvironment. This strategy is

currently explored both *in vivo* (Sato-Kaneko et al. 2017; Wang et al. 2016) and in the clinic (Ribas et al. 2018). In terms of our experimental setting, it remains to be determined if synergic effects of Tr and CpG, at higher doses then what we used, administered under various routes are sufficient to treat HER2 expressing, tumour-bearing, immunocompetent mice and induce long term protection.

To summarise the findings in this chapter, conventional conjugation of CpG to Trastuzumab results in conjugates with poor binding specificity, accelerated clearance from serum and no anti-tumour effect. Site-specific conjugates generated using the THIOMAB technology were highly specific for human HER2 and promoted tumour specific T cell responses *in vivo*. These T cell response were more pronounced in mice treated with Tr(TH)-CpG, than in mice treated with unconjugated Tr and CpG. Both treatments, however, delayed tumour growth in mice bearing tumours with moderate HER2 expression in a comparable way.

# Chapter 6

# Discussion

In this study we explore antibody-based targeted delivery of endosomal TLR agonists to the tumour tissue for the promotion of anti-tumour immunotherapy. Presently, the interest of the scientific community in using endosomal TLR agonists to boost anti-tumour immunity is increasing (Tang et al. 2018; Tang, Shalabi, and Hubbard-Lucey 2018). For activity, endosomal TLR agonists need to concentrate to the tumour microenvironment. Additionally, concentration at the tumour site has the potential to minimise activation of immune cells in the healthy tissue, thus preventing immune-mediated side-effects (Murthy, Minehart, and Sterman 2017; Marabelle et al. 2018). In light of the current landscape, exploring targeted delivery approaches for endosomal TLR agonists becomes a relevant research avenue. Successful targeted delivery of endosomal TLR agonists would enable their investigation in patients with metastatic disease that is not safely accessible to direct injection.

In this project, one strategy for targeted delivery of nucleic acid endosomal TLR agonists employs complex formation of these nucleic acids with LL37 cationic peptides, fused with the anti-human HER2 antibody Trastuzumab. In terms of the fusion antibody, we show that efficient recombinant expression requires a suitable linker to separate the cationic LL37 from the CH3 domain of the antibody, which requires homodimerization mediated by ionic interactions to ensure appropriate antibody folding. Among tested linkers, H3 linker was found to facilitate highest levels of antibody expression. In the current scientific context, where fusion proteins and especially fusion antibodies are being extensively explored as therapies, these findings are significant, identifying a linker that allows recombinant expression of full-length fusion antibodies with a LL37, a peptide with strong cationic charge. In addition to allowing for efficient recombinant expression, the linker H3 enabled maintained function of each moiety. Trastuzumab-H3-LL37 showed comparable HER2 binding affinity to the parent Trastuzumab, and similar nucleic acid binding affinity with the LL37 synthetic peptide.

Typically, significant concentration of anti-tumour monoclonal antibodies at the tumour site can be observed after hours to days from intravenous administration (Massicano, Marquez-Nostra, and Lapi 2018). In stark contrast with Trastuzumab, the fusion antibody Trastuzumab-H3-LL37 is undetectable in serum after one day since injection and we believe this is an effect of the LL37 moiety. The same is true for Trastuzumab-H3-LL37 complexed with CpG. These results are important, as they highlight that Trastuzumab-H3-LL37 antibodies or CpG

complexes are highly unlikely to concentrate to the tumour tissue. This implies that the properties of Trastuzumab-H3-LL37 + CpG make this approach unsuitable for systemic administration. Local administration to the tumour site, on the other hand, may be efficient in inducing anti-tumour immune responses and is worth investigating. Considering that LL37 facilitates access of nucleic acid TLR agonists to the endosomal compartment, and nucleic acid TLR agonists are powerful adjuvants, LL37, either alone or fused with other proteins, may be a useful tool in developing vaccines.

A previous study demonstrates that LL37 can deliver nucleic acids intracellularly using lipid rafts, in a process that depends on glycans on the cell surface (Sandgren et al. 2004). Other studies showed that LL37 interacts with various cell receptors (Kahlenberg and Kaplan 2013), and even changes the physico- chemical state of the cell membrane (Di Nardo et al. 2007; Perregaux et al. 2002; Zughaier, Shafer, and Stephens 2005). It is therefore possible, that cells in the blood consume LL37 rapidly through mechanisms that are not yet well understood, leading to low serum availability. We believe that further exploring the behaviour of LL37 in serum is valuable, as it may inform on how to potentially harness LL37 efficiently for therapy.

In addition to generating fusion antibodies, this study also explored biochemical conjugation technologies to generate Trastuzumab conjugates with the TLR9 agonist CpG. To generate conjugates, both conventional and site-specific conjugation methods were used. CpG can be synthesised either with a 3' terminal thiol group, and used to generate conventional conjugates, or with a terminal 3' amino group to be used in generating THIOMABs. In both cases, functionality of CpG is maintained post-conjugation, supporting other reports of maintained CpG activity upon conjugation at the 3' end (Kramer, Young, and Walker 2017; Kandimalla et al. 2002). Furthermore, we show that for CpG conjugates, the conjugation chemistry heavily impacts the functionality of resulting purified conjugates in vitro. In contrast with site-specific conjugates generated using THIOMAB technology, conventional conjugation using the SMCC linker results in Trastuzumab-MCC-CpG conjugates with markedly reduced binding affinity compared to Trastuzumab. This study highlights that linking nucleic acid molecules such as CpG to monoclonal anti-tumour antibodies such as Trastuzumab is technically challenging and requires advanced technologies such as THIOMAB generation. In our experience, the process is labour intensive as well.

To investigate the effects of conjugates in vivo, we have developed a mouse model with human HER2 transgenic B16 cells in immunocompetent mice. In our mouse model, tumour growth can be tracked over time by measuring luminescence activity and experimental turn-around is rapid for a tumour mouse model, of 18 days. Using this mouse model, we demonstrate that

biochemical conjugates have longer persistence in serum than complexes. Interestingly, Tr(TH)-CpG site-specific conjugates, generated using THIOMAB technology, persist in circulation at higher concentrations than conventional conjugates. Moreover, these site-specific conjugates delay tumour growth in immunocompetent mice bearing pulmonary human HER2-transgenic B16 tumours, even when HER2 expression is at moderate levels. The conjugates, however, are not superior in this respect to soluble Trastuzumab + CpG. Importantly, we show that treatment with Tr(TH)-CpG promotes tumour-specific T cell responses, which are more pronounced than for treatment with Trastuzumab + CpG or either of the components. In light of these results, it remains to be confirmed if treatment with Tr(TH)-CpG is in any way superior to treatment with unconjugated Trastuzumab + CpG in mice with pulmonary tumours. Another important question that remains to be answered in the future is how the two treatments compare in mice with tumours localised at other sites, which unlike the lung, are not the first reached capillary bed. Importantly, it remains to be determined if higher doses are more efficient, and if other routes of administration are more suitable. These experiments would help establish if the conjugates are more efficient than co-injection of the components.

It is now accepted that CpG directly activates B cells and results in increased antibody responses of IgM and IgG isotypes (Alugupalli et al. 2007; Browne 2012; Hua and Hou 2013). In our experimental set-up, there is little evidence that B cells are specifically activated by treatment with CpG, in either therapeutic format, as evidenced by similar levels of antibodies against tumour antigens compared to vehicle treated mice.

Importantly, our study did not address changes in immune responses at the tumour site. Since it is well known that the tumour microenvironment is immunosuppressive and leads to T cell dysfunction (Anderson, Stromnes, and Greenberg 2017), it would be good to investigate the tumour T cell infiltrate and activation levels. There are other studies showing that treatment with CpG expands anti-tumour T cells, but the immune suppression of the tumour microenvironment precludes optimal function, and this can be alleviated by concomitant treatment with an immune checkpoint inhibitor (Wang et al. 2016; Sato-Kaneko et al. 2017). It would be interesting to investigate if a similar pattern is observed after treatment with Tr(TH)-CpG or controls. In addition to evaluating T cell responses, it would be interesting to investigate if other immune cells in the tumour microenvironment are activated by treatment and contribute to tumour growth control. To exemplify, it has been shown that NK cells induce ADCC contributing to tumour growth control (Lo Nigro et al. 2019), and that these responses may be enhanced by cytokines induced by CpG stimulation of dendritic cells (Asselin-Paturel

and Trinchieri 2005; Marshall et al. 2006). Flow cytometry could be used to define tumour infiltrating cell populations and their activation status. Another interesting experiment would be to evaluate local cytokine production as a function of treatment, for instance using RT PCR.

While this study focuses largely on the generation and initial characterisation of conjugates, their adverse effects are an important question to be addressed. It is now accepted that systemic administration of endosomal TLR agonists can be dangerous, with several clinical trials being stopped due to immune mediated adverse effects. It remains to be determined if conjugation to antibodies such as Trastuzumab achieves sufficient concentration to the tumour site while sparing other tissue from unintended inflammation. We know from previous publications as well as experience in our lab that CpG can bind to membrane receptors on myeloid cells (Kreutz et al. 2012), likely scavenger receptors (Jozefowski et al. 2006; Kissick et al. 2014). It is currently unclear to what extent site-specific conjugates are taken up in myeloid cell rich tissues such as the spleen and if this leads to adverse effects. Future experiments are required to establish tissue distribution of conjugates as well as immune activation in those tissues. From our limited set of in vivo experiments, we can point out that treatment with CpG, alone, with Tr or conjugated to a THIOMAB increases the numbers of activated T cells in the spleen. Only a fraction of these cells, however, proliferate in the presence of tumour-specific peptides, raising the question about the specificity of the rest of the population and the potential for adverse effects.

In terms of evaluating adverse effects, a good future step would be to investigate immune responses at multiple time-points during treatment. This would allow us to investigate T cell responses at their peak and better delineate their specificity. Additionally, serum cytokines should be measured as well. The experiments we have already performed for cytokine responses are suboptimal in terms of set-up, with serum harvested at only one time-point, late, at day 3 after the last dose of treatment. This time-point is not appropriate to measure levels of cytokines produced by innate immune cells in response to CpG activation such as IL-12, IL-6 and TNF-α. Future experiments measuring levels of a variety of cytokine would be helpful in investigating safety of treatment with free and conjugated CpG, since it is accepted that high serum levels of cytokines such as TNF-α and interferons are indicative of systemic immune activation leading to adverse effects (Tisoncik et al. 2012; Clark 2007).

For this study, we used Trastuzumab, which is a human IgG1 isotype antibody in a mouse system. There is a good degree of cross-talk between human IgG1 and mouse innate immune cells, and decent levels of antibody-mediated effects are observed (Overdijk et al. 2012). However, Fc interactions could be further improved by using another isotype and by using

mouse antibodies in mouse systems or human antibodies in humanised mouse systems. Recent reports show that antibodies targeting tumour antigens of the IgE isotype are superior in mediating antibody-dependent effects, as well as recruiting other immune cell populations against tumours, and are more efficient in controlling tumour growth in rat tumour models (Josephs et al. 2015; Josephs et al. 2017) and humanised mouse models bearing patient derived xenografts (Cheung et al. 2018). It would be very interesting for our project compare the IgG with an IgE antibody in the composition of conjugates.

In terms of the mouse model, we identified a few important limitations in the course of the study. For one, human HER2 expression is significantly diminished in vivo in immunocompetent mice compared to levels of in vitro cultured cells. This is relevant, since it impacts accumulation of conjugates at the tumour site. It would be interesting to study the effect of Tr(TH)-CpG conjugates compared with the unconjugated components in mice bearing HER2 overexpressing tumours. This may be achieved by using human HER2 transgenic mice as host for the B14.3 Luc HER2 cells to enable HER2 tolerance (Piechocki et al. 2003). Another option would be to use humanised mouse models engrafted with human immune cells and bearing HER2 xenografts. These humanised mouse models, however, have their own limitations, which include lymph nodes that are not fully developed and incomplete reconstitution of certain cell populations (Morton et al. 2016; De La Rochere et al. 2018).

Another significant limitation is that some mice spontaneously control tumour growth. We demonstrated that mice bearing B14.3 Luc HER2 tumours have increased levels of serum antibodies compared to tumour-free mice. Anti-HER2 IgG antibodies, but not anti-ovalbumin antibodies can be detected in the serum of these tumour-bearing mice. We know from previous work in our lab that B14.3 tumours, which are ovalbumin transgenic, are not spontaneously controlled by mice, we can assume that human HER2 is a more powerful antigen in the mouse system, either because it is a human protein, or due to the extracellular domain, or both. It would be of interest to us to explore the use of human HER2 transgenic mice as hosts for the B14.3 Luc HER2 cells (Piechocki et al. 2003) and evaluate immune responses in the presence and absence of treatment.

Effective evaluation of Tr(TH)-CpG in vivo is further complicated by distinct TLR9 expression patterns in the mouse and human immune system. Rodent macrophages and myeloid dendritic cells express TLR9, while human macrophages do not (Anwar et al. 2019). This is especially relevant in the context of tumours, which contain high numbers of tumour associated macrophages which modulate the tumour microenvironment (Pollard 2004). An ideal tumour animal model, therefore, would be reconstituted with both human antigen-

presenting cells and T cells. This may be difficult to achieve using humanised mouse models, since tissue-resident dendritic cell populations are not easy to reconstitute efficiently. Currently, literature reports that for efficient DC reconstitution, treatment of NSG mice with specific growth factors such as Flt3L is required (Ding et al. 2014). Additionally, engraftment with human CD34 stem cells, but not PBMCs is required for generation of DCs, significantly increasing the cost of the model and the reconstitution time from 2 to 12-16 weeks (Skelton, Ortega-Prieto, and Dorner 2018).

Importantly, TLR9, as well as other endosomal TLRs can be expressed by tumour cells as well and may be functional, leading to tumour growth (Gao et al. 2018; Shahriari et al. 2017; Ren et al. 2007; Cen, Liu, and Cheng 2018). These finding are important, and the effects of CpG in growth of TLR9 expressing tumour cells should be tested in the experimental setting. In terms of The B16 cells we used to develop our mouse model, we know that they are TLR9 negative, and we expect CpG to only trigger TLR9-expressing immune cells.

To conclude, we demonstrate that generation of Trastuzumab-CpG conjugates with retained antibody specificity and CpG immunoactivity is feasible using site-specific conjugation and the THIOMAB technology. Current in vivo data highlights the difficulty and complexity in evaluating the effects of the conjugate. However, the approach has merit and it is worth exploring further in the aforementioned mouse models. This would further inform on the potential and limitations of Tr(TH)-CpG conjugates, as well as enable defining the requirements of a more effective targeted delivery method of endosomal TLR agonists to the tumour tissue for the promotion of anti-tumour immunity.

**References**

Abedi, M., R. A. Cohan, F. Mahboudi, M. A. Faramarzi, R. Fazel, N. Damavandi, M. S. Ardestani, and F. Davami. 2019. 'Novel trastuzumab-DM1 conjugate: Synthesis and bio-evaluation', *J Cell Physiol*, 234: 18206-13.

Abuknesha, R. A., F. Jeganathan, J. Wu, and Z. Baalawy. 2009. 'Labeling of biotin antibodies with horseradish peroxidase using cyanuric chloride', *Nat Protoc*, 4: 452-60.

Abuknesha, R. A., C. Y. Luk, H. H. Griffith, A. Maragkou, and D. Iakovaki. 2005. 'Efficient labelling of antibodies with horseradish peroxidase using cyanuric chloride', *J Immunol Methods*, 306: 211-7.

Adams, S., D. W. O'Neill, D. Nonaka, E. Hardin, L. Chiriboga, K. Siu, C. M. Cruz, A. Angiulli, F. Angiulli, E. Ritter, R. M. Holman, R. L. Shapiro, R. S. Berman, N. Berner, Y. Shao, O. Manches, L. Pan, R. R. Venhaus, E. W. Hoffman, A. Jungbluth, S. Gnjatic, L. Old, A. C. Pavlick, and N. Bhardwaj. 2008. 'Immunization of malignant melanoma patients with full-length NY-ESO-1 protein using TLR7 agonist imiquimod as vaccine adjuvant', *J Immunol*, 181: 776-84.

Agrawal, S., and S. Gupta. 2011. 'TLR1/2, TLR7, and TLR9 signals directly activate human peripheral blood naive and memory B cell subsets to produce cytokines, chemokines, and hematopoietic growth factors', *J Clin Immunol*, 31: 89-98.

Akira, S., S. Uematsu, and O. Takeuchi. 2006. 'Pathogen recognition and innate immunity', *Cell*, 124: 783-801.

Alexopoulou, L., B. Desnues, and O. Demaria. 2012. '[Toll-like receptor 8: the awkward TLR]', *Med Sci (Paris)*, 28: 96-102.

Alexopoulou, L., A. C. Holt, R. Medzhitov, and R. A. Flavell. 2001. 'Recognition of double-stranded RNA and activation of NF-kappaB by Toll-like receptor 3', *Nature*, 413: 732-8.

Alley, S. C., D. R. Benjamin, S. C. Jeffrey, N. M. Okeley, D. L. Meyer, R. J. Sanderson, and P. D. Senter. 2008. 'Contribution of linker stability to the activities of anticancer immunoconjugates', *Bioconjug Chem*, 19: 759-65.

Alugupalli, K. R., S. Akira, E. Lien, and J. M. Leong. 2007. 'MyD88- and Bruton's tyrosine kinase-mediated signals are essential for T cell-independent pathogen-specific IgM responses', *J Immunol*, 178: 3740-9.

Amet, N., H. F. Lee, and W. C. Shen. 2009. 'Insertion of the designed helical linker led to increased expression of tf-based fusion proteins', *Pharm Res*, 26: 523-8.

Anderson, K. G., I. M. Stromnes, and P. D. Greenberg. 2017. 'Obstacles Posed by the Tumor Microenvironment to T cell Activity: A Case for Synergistic Therapies', *Cancer Cell*, 31: 311-25.

Anwar, M. A., M. Shah, J. Kim, and S. Choi. 2019. 'Recent clinical trends in Toll-like receptor targeting therapeutics', *Med Res Rev*, 39: 1053-90.

Appay, V., C. Jandus, V. Voelter, S. Reynard, S. E. Coupland, D. Rimoldi, D. Lienard, P. Guillaume, A. M. Krieg, J. C. Cerottini, P. Romero, S. Leyvraz, N. Rufer, and D. E. Speiser. 2006. 'New generation vaccine induces effective melanoma-specific CD8+ T cells in the circulation but not in the tumor site', *J Immunol*, 177: 1670-8.

Arai, R., H. Ueda, A. Kitayama, N. Kamiya, and T. Nagamune. 2001. 'Design of the linkers which effectively separate domains of a bifunctional fusion protein', *Protein Eng*, 14: 529-32.

Aranda, F., E. Vacchelli, F. Obrist, A. Eggermont, J. Galon, C. Sautes-Fridman, I. Cremer, J. Henrik Ter Meulen, L. Zitvogel, G. Kroemer, and L. Galluzzi. 2014. 'Trial Watch: Toll-like receptor agonists in oncological indications', *Oncoimmunology*, 3: e29179.

Arlotta, K. J., A. V. Gandhi, H. N. Chen, C. S. Nervig, J. F. Carpenter, and S. C. Owen. 2018. 'In-Depth Comparison of Lysine-Based Antibody-Drug Conjugates Prepared on Solid Support Versus in Solution', *Antibodies (Basel)*, 7.

Askew, D., R. S. Chu, A. M. Krieg, and C. V. Harding. 2000. 'CpG DNA induces maturation of dendritic cells with distinct effects on nascent and recycling MHC-II antigen-processing mechanisms', *J Immunol*, 165: 6889-95.

Asselin-Paturel, C., and G. Trinchieri. 2005. 'Production of type I interferons: plasmacytoid dendritic cells and beyond', *J Exp Med*, 202: 461-5.

Aznar, M. A., L. Planelles, M. Perez-Olivares, C. Molina, S. Garasa, I. Etxeberria, G. Perez, I. Rodriguez, E. Bolanos, P. Lopez-Casas, M. E. Rodriguez-Ruiz, J. L. Perez-Gracia, I. Marquez-Rodas, A. Teijeira, M. Quintero, and I. Melero. 2019. 'Immunotherapeutic effects of intratumoral nanoplexed poly I:C', *J Immunother Cancer*, 7: 116.

Bai, Y., and W. C. Shen. 2006. 'Improving the oral efficacy of recombinant granulocyte colony-stimulating factor and transferrin fusion protein by spacer optimization', *Pharm Res*, 23: 2116-21.

Bakhtiar, R. 2016. 'Antibody drug conjugates', *Biotechnol Lett*, 38: 1655-64.

Barbalat, R., S. E. Ewald, M. L. Mouchess, and G. M. Barton. 2011. 'Nucleic acid recognition by the innate immune system', *Annu Rev Immunol*, 29: 185-214.

Barok, M., M. Tanner, K. Koninki, and J. Isola. 2011. 'Trastuzumab-DM1 causes tumour growth inhibition by mitotic catastrophe in trastuzumab-resistant breast cancer cells in vivo', *Breast Cancer Res*, 13: R46.

Barr, T. A., S. Brown, G. Ryan, J. Zhao, and D. Gray. 2007. 'TLR-mediated stimulation of APC: Distinct cytokine responses of B cells and dendritic cells', *Eur J Immunol*, 37: 3040-53.

Beck, A., L. Goetsch, C. Dumontet, and N. Corvaia. 2017. 'Strategies and challenges for the next generation of antibody-drug conjugates', *Nat Rev Drug Discov*, 16: 315-37.

Behrens, C. R., and B. Liu. 2014. 'Methods for site-specific drug conjugation to antibodies', *MAbs*, 6: 46-53.

Bekeredjian-Ding, I., and G. Jego. 2009. 'Toll-like receptors--sentries in the B-cell response', *Immunology*, 128: 311-23.

Bernasconi, N. L., N. Onai, and A. Lanzavecchia. 2003. 'A role for Toll-like receptors in acquired immunity: up-regulation of TLR9 by BCR triggering in naive B cells and constitutive expression in memory B cells', *Blood*, 101: 4500-4.

Bhakta, S., H. Raab, and J. R. Junutula. 2013. 'Engineering THIOMABs for site-specific conjugation of thiol-reactive linkers', *Methods Mol Biol*, 1045: 189-203.

Bianchini, G., and L. Gianni. 2014. 'The immune system and response to HER2-targeted treatment in breast cancer', *Lancet Oncol*, 15: e58-68.

Blasius, A. L., and B. Beutler. 2010. 'Intracellular toll-like receptors', *Immunity*, 32: 305-15.

Bode, C., G. Zhao, F. Steinhagen, T. Kinjo, and D. M. Klinman. 2011. 'CpG DNA as a vaccine adjuvant', *Expert Rev Vaccines*, 10: 499-511.

Botos, I., L. Liu, Y. Wang, D. M. Segal, and D. R. Davies. 2009. 'The toll-like receptor 3:dsRNA signaling complex', *Biochim Biophys Acta*, 1789: 667-74.

Boule, M. W., C. Broughton, F. Mackay, S. Akira, A. Marshak-Rothstein, and I. R. Rifkin. 2004. 'Toll-like receptor 9-dependent and -independent dendritic cell activation by chromatin-immunoglobulin G complexes', *J Exp Med*, 199: 1631-40.

Bourke, E., D. Bosisio, J. Golay, N. Polentarutti, and A. Mantovani. 2003. 'The toll-like receptor repertoire of human B lymphocytes: inducible and selective expression of TLR9 and TLR10 in normal and transformed cells', *Blood*, 102: 956-63.

Bournazos, S., and J. V. Ravetch. 2015. 'Fcgamma receptor pathways during active and passive immunization', *Immunol Rev*, 268: 88-103.

———. 2017. 'Fcgamma Receptor Function and the Design of Vaccination Strategies', *Immunity*, 47: 224-33.

Brawand, P., D. R. Fitzpatrick, B. W. Greenfield, K. Brasel, C. R. Maliszewski, and T. De Smedt. 2002. 'Murine plasmacytoid pre-dendritic cells generated from Flt3 ligand-supplemented bone marrow cultures are immature APCs', *J Immunol*, 169: 6711-9.

Brencicova, E., and S. S. Diebold. 2013. 'Nucleic acids and endosomal pattern recognition: how to tell friend from foe?', *Front Cell Infect Microbiol*, 3: 37.

Brencicova, E., A. L. Jagger, H. G. Evans, M. Georgouli, A. Laios, S. Attard Montalto, G. Mehra, J. Spencer, A. A. Ahmed, S. Raju-Kankipati, L. S. Taams, and S. S. Diebold. 2017. 'Interleukin-10 and prostaglandin E2 have complementary but distinct suppressive effects on Toll-like receptor-mediated dendritic cell activation in ovarian carcinoma', *PLoS One*, 12: e0175712.

Browne, E. P. 2012. 'Regulation of B-cell responses by Toll-like receptors', *Immunology*, 136: 370-9.

Campbell, J. D. 2017. 'Development of the CpG Adjuvant 1018: A Case Study', *Methods Mol Biol*, 1494: 15-27.

Campbell, K.S. 2012. Genetically modified human natural killer cell lines. US patent 8,313,943 B2, filed, July 8, 2005, and granted November 17, 2009.

Cen, X., S. Liu, and K. Cheng. 2018. 'The Role of Toll-Like Receptor in Inflammation and Tumor Immunity', *Front Pharmacol*, 9: 878.

Chang, J., S. L. Kunkel, and C. H. Chang. 2009. 'Negative regulation of MyD88-dependent signaling by IL-10 in dendritic cells', *Proc Natl Acad Sci U S A*, 106: 18327-32.

Chao, P., M. Deshmukh, H. L. Kutscher, D. Gao, S. S. Rajan, P. Hu, D. L. Laskin, S. Stein, and P. J. Sinko. 2010. 'Pulmonary targeting microparticulate camptothecin delivery system: anticancer evaluation in a rat orthotopic lung cancer model', *Anticancer Drugs*, 21: 65-76.

Chari, R. V., B. A. Martell, J. L. Gross, S. B. Cook, S. A. Shah, W. A. Blattler, S. J. McKenzie, and V. S. Goldmacher. 1992. 'Immunoconjugates containing novel maytansinoids: promising anticancer drugs', *Cancer Res*, 52: 127-31.

Chau, C. H., P. S. Steeg, and W. D. Figg. 2019. 'Antibody-drug conjugates for cancer', *Lancet*, 394: 793-804.

Chavez, M., M. T. Silvestrini, E. S. Ingham, B. Z. Fite, L. M. Mahakian, S. M. Tam, A. Ilovitsh, A. M. Monjazeb, W. J. Murphy, N. E. Hubbard, R. R. Davis, C. G.

Tepper, A. D. Borowsky, and K. W. Ferrara. 2018. 'Distinct immune signatures in directly treated and distant tumors result from TLR adjuvants and focal ablation', *Theranostics*, 8: 3611-28.

Chen, D. S., and I. Mellman. 2013. 'Oncology meets immunology: the cancer-immunity cycle', *Immunity*, 39: 1-10.

Chen, T. A., C. C. Liao, Y. C. Cheng, Y. P. Chen, Y. F. Hsu, C. M. Liang, and S. M. Liang. 2015. 'Stimulation of Proliferation and Migration of Mouse Macrophages by Type B CpG-ODNs Is F-Spondin and IL-1Ra Dependent', *PLoS One*, 10: e0128926.

Cheung, A., J. Opzoomer, K. M. Ilieva, P. Gazinska, R. M. Hoffmann, H. Mirza, R. Marlow, E. Francesch-Domenech, M. Fittall, D. Dominguez Rodriguez, A. Clifford, L. Badder, N. Patel, S. Mele, G. Pellizzari, H. J. Bax, S. Crescioli, G. Petranyi, D. Larcombe-Young, D. H. Josephs, S. Canevari, M. Figini, S. Pinder, F. O. Nestle, C. Gillett, J. F. Spicer, A. Grigoriadis, A. N. J. Tutt, and S. N. Karagiannis. 2018. 'Anti-Folate Receptor Alpha-Directed Antibody Therapies Restrict the Growth of Triple-negative Breast Cancer', *Clin Cancer Res*, 24: 5098-111.

Christie, R. J., A. C. Tiberghien, Q. Du, B. Bezabeh, R. Fleming, A. Shannon, S. Mao, S. Breen, J. Zhang, H. Zhong, J. Harper, H. Wu, P. W. Howard, and C. Gao. 2017. 'Pyrrolobenzodiazepine Antibody-Drug Conjugates Designed for Stable Thiol Conjugation', *Antibodies (Basel)*, 6.

Clark, I. A. 2007. 'How TNF was recognized as a key mechanism of disease', *Cytokine Growth Factor Rev*, 18: 335-43.

Codony-Servat, J., J. Albanell, J. C. Lopez-Talavera, J. Arribas, and J. Baselga. 1999. 'Cleavage of the HER2 ectodomain is a pervanadate-activable process that is inhibited by the tissue inhibitor of metalloproteases-1 in breast cancer cells', *Cancer Res*, 59: 1196-201.

Cooper, C. L., H. L. Davis, M. L. Morris, S. M. Efler, M. A. Adhami, A. M. Krieg, D. W. Cameron, and J. Heathcote. 2004. 'CPG 7909, an immunostimulatory TLR9 agonist oligodeoxynucleotide, as adjuvant to Engerix-B HBV vaccine in healthy adults: a double-blind phase I/II study', *J Clin Immunol*, 24: 693-701.

Copeland, S., H. S. Warren, S. F. Lowry, S. E. Calvano, D. Remick, Inflammation, and Investigators the Host Response to Injury. 2005. 'Acute inflammatory response to endotoxin in mice and humans', *Clin Diagn Lab Immunol*, 12: 60-7.

Council of Europe: Strasbourg, France. 2017. 2.6.30. Monocyte Activation Test. In European Pharmacopeia 9.0., 9th ed.; pp. 193–194; ISNB 978-9-2871-8133-6.

Council of Europe 2019. European Pharmacopoeia -10th edition: 2.6.14 Bacterial endotoxins. Page 209-213. This is how to perform the test (LAL gel-clot is method A).5.1.10 Guidelines for using the test for bacterial endotoxins. Page 639-642.

Couper, K. N., D. G. Blount, and E. M. Riley. 2008. 'IL-10: the master regulator of immunity to infection', *J Immunol*, 180: 5771-7.

Currie, A. J., R. G. van der Most, S. A. Broomfield, A. C. Prosser, M. G. Tovey, and B. W. Robinson. 2008. 'Targeting the effector site with IFN-alphabeta-inducing TLR ligands reactivates tumor-resident CD8 T cell responses to eradicate established solid tumors', *J Immunol*, 180: 1535-44.

Damelin, M., W. Zhong, J. Myers, and P. Sapra. 2015. 'Evolving Strategies for Target Selection for Antibody-Drug Conjugates', *Pharm Res*, 32: 3494-507.

Damiano, V., S. Garofalo, R. Rosa, R. Bianco, R. Caputo, T. Gelardi, G. Merola, L. Racioppi, C. Garbi, E. R. Kandimalla, S. Agrawal, and G. Tortora. 2009. 'A novel toll-like receptor 9 agonist cooperates with trastuzumab in trastuzumab-resistant breast tumors through multiple mechanisms of action', *Clin Cancer Res*, 15: 6921-30.

Dan, N., S. Setua, V. K. Kashyap, S. Khan, M. Jaggi, M. M. Yallapu, and S. C. Chauhan. 2018. 'Antibody-Drug Conjugates for Cancer Therapy: Chemistry to Clinical Implications', *Pharmaceuticals (Basel)*, 11.

De La Rochere, P., S. Guil-Luna, D. Decaudin, G. Azar, S. S. Sidhu, and E. Piaggio. 2018. 'Humanized Mice for the Study of Immuno-Oncology', *Trends Immunol*, 39: 748-63.

Dennis, M. S., H. Jin, D. Dugger, R. Yang, L. McFarland, A. Ogasawara, S. Williams, M. J. Cole, S. Ross, and R. Schwall. 2007. 'Imaging tumors with an albumin-binding Fab, a novel tumor-targeting agent', *Cancer Res*, 67: 254-61.

Deonarain, M. P., G. Yahioglu, I. Stamati, and J. Marklew. 2015. 'Emerging formats for next-generation antibody drug conjugates', *Expert Opin Drug Discov*, 10: 463-81.

Dere, R., J. H. Yi, C. Lei, O. M. Saad, C. Huang, Y. Li, J. Baudys, and S. Kaur. 2013. 'PK assays for antibody-drug conjugates: case study with ado-trastuzumab emtansine', *Bioanalysis*, 5: 1025-40.

Dhodapkar, K. M., and M. V. Dhodapkar. 2005. 'Recruiting dendritic cells to improve antibody therapy of cancer', *Proc Natl Acad Sci U S A*, 102: 6243-4.

Dhodapkar, M. V., K. M. Dhodapkar, and A. K. Palucka. 2008. 'Interactions of tumor cells with dendritic cells: balancing immunity and tolerance', *Cell Death Differ*, 15: 39-50.

Di Nardo, A., M. H. Braff, K. R. Taylor, C. Na, R. D. Granstein, J. E. McInturff, S. Krutzik, R. L. Modlin, and R. L. Gallo. 2007. 'Cathelicidin antimicrobial peptides block dendritic cell TLR4 activation and allergic contact sensitization', *J Immunol*, 178: 1829-34.

Diamantis, N., and U. Banerji. 2016. 'Antibody-drug conjugates--an emerging class of cancer treatment', *Br J Cancer*, 114: 362-7.

Diao, Y., X. Wang, Y. Wan, J. Zhong, D. Gao, Y. Liu, N. Gao, W. Li, B. Liu, X. Huang, Z. Jin, B. Peng, Z. Wang, L. Fu, S. Chen, and G. Jin. 2016. 'Antitumor activity of a novel small molecule TLR7 agonist via immune response induction and tumor microenvironment modulation', *Oncol Rep*, 35: 793-800.

Diebold, S. S. 2008a. 'Determination of T-cell fate by dendritic cells', *Immunol Cell Biol*, 86: 389-97.

———. 2008b. 'Recognition of viral single-stranded RNA by Toll-like receptors', *Adv Drug Deliv Rev*, 60: 813-23.

———. 2009. 'Activation of dendritic cells by toll-like receptors and C-type lectins', *Handb Exp Pharmacol*: 3-30.

Diebold, S. S., T. Kaisho, H. Hemmi, S. Akira, and C. Reis e Sousa. 2004. 'Innate antiviral responses by means of TLR7-mediated recognition of single-stranded RNA', *Science*, 303: 1529-31.

Diebold, S. S., C. Massacrier, S. Akira, C. Paturel, Y. Morel, and C. Reis e Sousa. 2006. 'Nucleic acid agonists for Toll-like receptor 7 are defined by the presence of uridine ribonucleotides', *Eur J Immunol*, 36: 3256-67.

Ding, Y., A. Wilkinson, A. Idris, B. Fancke, M. O'Keeffe, D. Khalil, X. Ju, M. H. Lahoud, I. Caminschi, K. Shortman, R. Rodwell, S. Vuckovic, and K. J.

Radford. 2014. 'FLT3-ligand treatment of humanized mice results in the generation of large numbers of CD141+ and CD1c+ dendritic cells in vivo', *J Immunol*, 192: 1982-9.

Dodev, T. S., P. Karagiannis, A. E. Gilbert, D. H. Josephs, H. Bowen, L. K. James, H. J. Bax, R. Beavil, M. O. Pang, H. J. Gould, S. N. Karagiannis, and A. J. Beavil. 2014. 'A tool kit for rapid cloning and expression of recombinant antibodies', *Sci Rep*, 4: 5885.

Dranoff, G. 2011. 'Experimental mouse tumour models: what can be learnt about human cancer immunology?', *Nat Rev Immunol*, 12: 61-6.

du Plessis, W. J., L. Kleynhans, N. du Plessis, K. Stanley, S. T. Malherbe, E. Maasdorp, K. Ronacher, N. N. Chegou, G. Walzl, and A. G. Loxton. 2016. 'The Functional Response of B Cells to Antigenic Stimulation: A Preliminary Report of Latent Tuberculosis', *PLoS One*, 11: e0152710.

Duthie, M. S., H. P. Windish, C. B. Fox, and S. G. Reed. 2011. 'Use of defined TLR ligands as adjuvants within human vaccines', *Immunol Rev*, 239: 178-96.

Edwards, A. D., S. S. Diebold, E. M. Slack, H. Tomizawa, H. Hemmi, T. Kaisho, S. Akira, and C. Reis e Sousa. 2003. 'Toll-like receptor expression in murine DC subsets: lack of TLR7 expression by CD8 alpha+ DC correlates with unresponsiveness to imidazoquinolines', *Eur J Immunol*, 33: 827-33.

Elgueta, R., M. J. Benson, V. C. de Vries, A. Wasiuk, Y. Guo, and R. J. Noelle. 2009. 'Molecular mechanism and function of CD40/CD40L engagement in the immune system', *Immunol Rev*, 229: 152-72.

Elin, R. J., and A. E. Utter. 1980. 'Positive Limulus amoebocyte lysate reactions with polyriboinosinic acid x polyribocytidylic acid', *J Clin Microbiol*, 12: 502-5.

Elso, C. M., L. J. Roberts, G. K. Smyth, R. J. Thomson, T. M. Baldwin, S. J. Foote, and E. Handman. 2004. 'Leishmaniasis host response loci (lmr1-3) modify disease severity through a Th1/Th2-independent pathway', *Genes Immun*, 5: 93-100.

Engel, A. L., G. E. Holt, and H. Lu. 2011. 'The pharmacokinetics of Toll-like receptor agonists and the impact on the immune system', *Expert Rev Clin Pharmacol*, 4: 275-89.

Erdbrugger, U., C. K. Rudy, M. E. Etter, K. A. Dryden, M. Yeager, A. L. Klibanov, and J. Lannigan. 2014. 'Imaging flow cytometry elucidates limitations of microparticle analysis by conventional flow cytometry', *Cytometry A*, 85: 756-70.

Feige, M. J., L. M. Hendershot, and J. Buchner. 2010. 'How antibodies fold', *Trends Biochem Sci*, 35: 189-98.

Fernandez, N. C., A. Lozier, C. Flament, P. Ricciardi-Castagnoli, D. Bellet, M. Suter, M. Perricaudet, T. Tursz, E. Maraskovsky, and L. Zitvogel. 1999. 'Dendritic cells directly trigger NK cell functions: cross-talk relevant in innate anti-tumor immune responses in vivo', *Nat Med*, 5: 405-11.

Fourcade, J., P. Kudela, P. A. Andrade Filho, B. Janjic, S. R. Land, C. Sander, A. Krieg, A. Donnenberg, H. Shen, J. M. Kirkwood, and H. M. Zarour. 2008. 'Immunization with analog peptide in combination with CpG and montanide expands tumor antigen-specific CD8+ T cells in melanoma patients', *J Immunother*, 31: 781-91.

Franco, E., V. Garcia-Recio, P. Jimenez, M. Garrosa, T. Girbes, M. Cordoba-Diaz, and D. Cordoba-Diaz. 2018. 'Endotoxins from a Pharmacopoeial Point of View', *Toxins (Basel)*, 10.

Gabriel, R., M. Schmidt, and C. von Kalle. 2012. 'Integration of retroviral vectors', *Curr Opin Immunol*, 24: 592-7.

Gallotta, M., H. Assi, E. Degagne, S. K. Kannan, R. L. Coffman, and C. Guiducci. 2018. 'Inhaled TLR9 Agonist Renders Lung Tumors Permissive to PD-1 Blockade by Promoting Optimal CD4(+) and CD8(+) T-cell Interplay', *Cancer Res*, 78: 4943-56.

Ganguly, D., G. Chamilos, R. Lande, J. Gregorio, S. Meller, V. Facchinetti, B. Homey, F. J. Barrat, T. Zal, and M. Gilliet. 2009. 'Self-RNA-antimicrobial peptide complexes activate human dendritic cells through TLR7 and TLR8', *J Exp Med*, 206: 1983-94.

Gao, C., T. Qiao, B. Zhang, S. Yuan, X. Zhuang, and Y. Luo. 2018. 'TLR9 signaling activation at different stages in colorectal cancer and NF-kappaB expression', *Onco Targets Ther*, 11: 5963-71.

Garcia-Martinez, E., M. Smith, A. Buque, F. Aranda, F. A. de la Pena, A. Ivars, M. S. Canovas, M. A. V. Conesa, J. Fucikova, R. Spisek, L. Zitvogel, G. Kroemer, and L. Galluzzi. 2018. 'Trial Watch: Immunostimulation with recombinant cytokines for cancer therapy', *Oncoimmunology*, 7: e1433982.

Gilliet, M., A. Boonstra, C. Paturel, S. Antonenko, X. L. Xu, G. Trinchieri, A. O'Garra, and Y. J. Liu. 2002. 'The development of murine plasmacytoid dendritic cell precursors is differentially regulated by FLT3-ligand and granulocyte/macrophage colony-stimulating factor', *J Exp Med*, 195: 953-8.

Gilliet, M., Lande, R., Liu, Y.J. 2012. Inhibitors of LL37-mediated immune reactivity to self nucleic acids. United States Patent Application Publication. US 2010/0315290 A1.

Gunturu, K. S., Y. Woo, N. Beaubier, H. E. Remotti, and M. W. Saif. 2013. 'Gastric cancer and trastuzumab: first biologic therapy in gastric cancer', *Ther Adv Med Oncol*, 5: 143-51.

Guo, C., M. H. Manjili, J. R. Subjeck, D. Sarkar, P. B. Fisher, and X. Y. Wang. 2013. 'Therapeutic cancer vaccines: past, present, and future', *Adv Cancer Res*, 119: 421-75.

Gururajan, M., J. Jacob, and B. Pulendran. 2007. 'Toll-like receptor expression and responsiveness of distinct murine splenic and mucosal B-cell subsets', *PLoS One*, 2: e863.

Haas, T., J. Metzger, F. Schmitz, A. Heit, T. Muller, E. Latz, and H. Wagner. 2008. 'The DNA sugar backbone 2' deoxyribose determines toll-like receptor 9 activation', *Immunity*, 28: 315-23.

Hamblett, K. J., P. D. Senter, D. F. Chace, M. M. Sun, J. Lenox, C. G. Cerveny, K. M. Kissler, S. X. Bernhardt, A. K. Kopcha, R. F. Zabinski, D. L. Meyer, and J. A. Francisco. 2004. 'Effects of drug loading on the antitumor activity of a monoclonal antibody drug conjugate', *Clin Cancer Res*, 10: 7063-70.

Hamid, O., R. Ismail, and I. Puzanov. 2019. 'Intratumoral Immunotherapy-Update 2019', *Oncologist*.

Hartmann, G., J. Battiany, H. Poeck, M. Wagner, M. Kerkmann, N. Lubenow, S. Rothenfusser, and S. Endres. 2003. 'Rational design of new CpG oligonucleotides that combine B cell activation with high IFN-alpha induction in plasmacytoid dendritic cells', *Eur J Immunol*, 33: 1633-41.

Hartmann, G., and A. M. Krieg. 2000. 'Mechanism and function of a newly identified CpG DNA motif in human primary B cells', *J Immunol*, 164: 944-53.

Heil, F., H. Hemmi, H. Hochrein, F. Ampenberger, C. Kirschning, S. Akira, G. Lipford, H. Wagner, and S. Bauer. 2004. 'Species-specific recognition of single-stranded RNA via toll-like receptor 7 and 8', *Science*, 303: 1526-9.

Helft, J., J. Bottcher, P. Chakravarty, S. Zelenay, J. Huotari, B. U. Schraml, D. Goubau, and C. Reis e Sousa. 2015. 'GM-CSF Mouse Bone Marrow Cultures Comprise a Heterogeneous Population of CD11c(+)MHCII(+) Macrophages and Dendritic Cells', *Immunity*, 42: 1197-211.

Hemmi, H., T. Kaisho, O. Takeuchi, S. Sato, H. Sanjo, K. Hoshino, T. Horiuchi, H. Tomizawa, K. Takeda, and S. Akira. 2002. 'Small anti-viral compounds activate immune cells via the TLR7 MyD88-dependent signaling pathway', *Nat Immunol*, 3: 196-200.

Hiramatsu, K., S. Serada, K. Kobiyama, S. Nakagawa, A. Morimoto, S. Matsuzaki, Y. Ueda, M. Fujimoto, K. Yoshino, K. J. Ishii, T. Enomoto, T. Kimura, and T. Naka. 2015. 'CpG oligodeoxynucleotides potentiate the antitumor activity of anti-BST2 antibody', *Cancer Sci*, 106: 1474-8.

Hirsh, V., L. Paz-Ares, M. Boyer, R. Rosell, G. Middleton, W. E. Eberhardt, A. Szczesna, P. Reiterer, M. Saleh, O. Arrieta, E. Bajetta, R. T. Webb, J. Raats, R. J. Benner, C. Fowst, S. J. Meech, D. Readett, and J. H. Schiller. 2011. 'Randomized phase III trial of paclitaxel/carboplatin with or without PF-3512676 (Toll-like receptor 9 agonist) as first-line treatment for advanced non-small-cell lung cancer', *J Clin Oncol*, 29: 2667-74.

Hoffmann, R. M., B. G. T. Coumbe, D. H. Josephs, S. Mele, K. M. Ilieva, A. Cheung, A. N. Tutt, J. F. Spicer, D. E. Thurston, S. Crescioli, and S. N. Karagiannis. 2018. 'Antibody structure and engineering considerations for the design and function of Antibody Drug Conjugates (ADCs)', *Oncoimmunology*, 7: e1395127.

Hogquist, K. A., S. C. Jameson, W. R. Heath, J. L. Howard, M. J. Bevan, and F. R. Carbone. 1994. 'T cell receptor antagonist peptides induce positive selection', *Cell*, 76: 17-27.

Hollingsworth, R. E., and K. Jansen. 2019. 'Turning the corner on therapeutic cancer vaccines', *NPJ Vaccines*, 4: 7.

Hommelgaard, A. M., M. Lerdrup, and B. van Deurs. 2004. 'Association with membrane protrusions makes ErbB2 an internalization-resistant receptor', *Mol Biol Cell*, 15: 1557-67.

Hosonaga, M., Y. Arima, O. Sampetrean, D. Komura, I. Koya, T. Sasaki, E. Sato, H. Okano, J. Kudoh, S. Ishikawa, H. Saya, and T. Ishikawa. 2018. 'HER2 Heterogeneity Is Associated with Poor Survival in HER2-Positive Breast Cancer', *Int J Mol Sci*, 19.

Hou, W., Q. Zhang, Z. Yan, R. Chen, H. J. Zeh Iii, R. Kang, M. T. Lotze, and D. Tang. 2013. 'Strange attractors: DAMPs and autophagy link tumor cell death and immunity', *Cell Death Dis*, 4: e966.

Hua, Z., and B. Hou. 2013. 'TLR signaling in B-cell development and activation', *Cell Mol Immunol*, 10: 103-6.

Hudis, C. A. 2007. 'Trastuzumab--mechanism of action and use in clinical practice', *N Engl J Med*, 357: 39-51.

Hurst, J., and P. von Landenberg. 2008. 'Toll-like receptors and autoimmunity', *Autoimmun Rev*, 7: 204-8.

Hurst, S., A. M. Ryan, C. K. Ng, J. M. McNally, L. G. Lorello, G. L. Finch, M. W. Leach, S. A. Ploch, J. A. Fohey, and T. A. Smolarek. 2014. 'Comparative

nonclinical assessments of the proposed biosimilar PF-05280014 and trastuzumab (Herceptin((R)))', *BioDrugs*, 28: 451-9.

Hutmacher, C., and D. Neri. 2019. 'Antibody-cytokine fusion proteins: Biopharmaceuticals with immunomodulatory properties for cancer therapy', *Adv Drug Deliv Rev*, 141: 67-91.

Ignacio, B. J., T. J. Albin, A. P. Esser-Kahn, and M. Verdoes. 2018. 'Toll-like Receptor Agonist Conjugation: A Chemical Perspective', *Bioconjug Chem*, 29: 587-603.

Inaba, K., M. Inaba, N. Romani, H. Aya, M. Deguchi, S. Ikehara, S. Muramatsu, and R. M. Steinman. 1992. 'Generation of large numbers of dendritic cells from mouse bone marrow cultures supplemented with granulocyte/macrophage colony-stimulating factor', *J Exp Med*, 176: 1693-702.

Iribarren, K., N. Bloy, A. Buque, I. Cremer, A. Eggermont, W. H. Fridman, J. Fucikova, J. Galon, R. Spisek, L. Zitvogel, G. Kroemer, and L. Galluzzi. 2016. 'Trial Watch: Immunostimulation with Toll-like receptor agonists in cancer therapy', *Oncoimmunology*, 5: e1088631.

Iwasaki, A., and R. Medzhitov. 2004. 'Toll-like receptor control of the adaptive immune responses', *Nat Immunol*, 5: 987-95.

———. 2015. 'Control of adaptive immunity by the innate immune system', *Nat Immunol*, 16: 343-53.

Jain, N., S. W. Smith, S. Ghone, and B. Tomczuk. 2015. 'Current ADC Linker Chemistry', *Pharm Res*, 32: 3526-40.

Johnson, D. B., S. Chandra, and J. A. Sosman. 2018. 'Immune Checkpoint Inhibitor Toxicity in 2018', *JAMA*, 320: 1702-03.

Josephs, D. H., H. J. Bax, T. Dodev, M. Georgouli, M. Nakamura, G. Pellizzari, L. Saul, P. Karagiannis, A. Cheung, C. Herraiz, K. M. Ilieva, I. Correa, M. Fittall, S. Crescioli, P. Gazinska, N. Woodman, S. Mele, G. Chiaruttini, A. E. Gilbert, A. Koers, M. Bracher, C. Selkirk, H. Lentfer, C. Barton, E. Lever, G. Muirhead, S. Tsoka, S. Canevari, M. Figini, A. Montes, N. Downes, D. Dombrowicz, C. J. Corrigan, A. J. Beavil, F. O. Nestle, P. S. Jones, H. J. Gould, V. Sanz-Moreno, P. J. Blower, J. F. Spicer, and S. N. Karagiannis. 2017. 'Anti-Folate Receptor-alpha IgE but not IgG Recruits Macrophages to Attack Tumors via TNFalpha/MCP-1 Signaling', *Cancer Res*, 77: 1127-41.

Josephs, D. H., H. J. Bax, H. Lentfer, C. Selkirk, J. F. Spicer, and S. N. Karagiannis. 2015. 'Potential for monocyte recruitment by IgE immunotherapy for cancer in a rat model of tumour metastasis', *Lancet*, 385 Suppl 1: S53.

Jozefowski, S., T. H. Sulahian, M. Arredouani, and L. Kobzik. 2006. 'Role of scavenger receptor MARCO in macrophage responses to CpG oligodeoxynucleotides', *J Leukoc Biol*, 80: 870-9.

Junutula, Jagath R., Helga Raab, Suzanna Clark, Sunil Bhakta, Douglas D. Leipold, Sylvia Weir, Yvonne Chen, Michelle Simpson, Siao Ping Tsai, Mark S. Dennis, Yanmei Lu, Y. Gloria Meng, Carl Ng, Jihong Yang, Chien C. Lee, Eileen Duenas, Jeffrey Gorrell, Viswanatham Katta, Amy Kim, Kevin McDorman, Kelly Flagella, Rayna Venook, Sarajane Ross, Susan D. Spencer, Wai Lee Wong, Henry B. Lowman, Richard Vandlen, Mark X. Sliwkowski, Richard H. Scheller, Paul Polakis, and William Mallet. 2008. 'Site-specific conjugation of a cytotoxic drug to an antibody improves the therapeutic index', *Nature Biotechnology*, 26: 925.

Kahlenberg, J. M., and M. J. Kaplan. 2013. 'Little peptide, big effects: the role of LL-37 in inflammation and autoimmune disease', *J Immunol*, 191: 4895-901.

Kaito, A., T. Kuwata, M. Tokunaga, K. Shitara, R. Sato, T. Akimoto, and T. Kinoshita. 2019. 'HER2 heterogeneity is a poor prognosticator for HER2-positive gastric cancer', *World J Clin Cases*, 7: 1964-77.

Kalkhof, S., and A. Sinz. 2008. 'Chances and pitfalls of chemical cross-linking with amine-reactive N-hydroxysuccinimide esters', *Anal Bioanal Chem*, 392: 305-12.

Kandimalla, E. R., L. Bhagat, D. Yu, Y. Cong, J. Tang, and S. Agrawal. 2002. 'Conjugation of ligands at the 5'-end of CpG DNA affects immunostimulatory activity', *Bioconjug Chem*, 13: 966-74.

Kato, H., O. Takeuchi, E. Mikamo-Satoh, R. Hirai, T. Kawai, K. Matsushita, A. Hiiragi, T. S. Dermody, T. Fujita, and S. Akira. 2008. 'Length-dependent recognition of double-stranded ribonucleic acids by retinoic acid-inducible gene-I and melanoma differentiation-associated gene 5', *J Exp Med*, 205: 1601-10.

Kawarada, Y., R. Ganss, N. Garbi, T. Sacher, B. Arnold, and G. J. Hammerling. 2001. 'NK- and CD8(+) T cell-mediated eradication of established tumors by peritumoral injection of CpG-containing oligodeoxynucleotides', *J Immunol*, 167: 5247-53.

Kawarada, You, Ruth Ganss, Natalio Garbi, Torsten Sacher, Bernd Arnold, and Günter J. Hämmerling. 2001. 'NK- and CD8<sup>+</sup> T Cell-Mediated Eradication of Established Tumors by Peritumoral Injection of CpG-Containing Oligodeoxynucleotides', *The Journal of Immunology*, 167: 5247-53.

Keizer, R. J., A. D. Huitema, J. H. Schellens, and J. H. Beijnen. 2010. 'Clinical pharmacokinetics of therapeutic monoclonal antibodies', *Clin Pharmacokinet*, 49: 493-507.

Kennedy, L. B., and A. K. S. Salama. 2020. 'A review of cancer immunotherapy toxicity', *CA Cancer J Clin*.

Khalil, D. N., E. L. Smith, R. J. Brentjens, and J. D. Wolchok. 2016. 'The future of cancer treatment: immunomodulation, CARs and combination immunotherapy', *Nat Rev Clin Oncol*, 13: 273-90.

Kim, Y., S. O. Ho, N. R. Gassman, Y. Korlann, E. V. Landorf, F. R. Collart, and S. Weiss. 2008. 'Efficient site-specific labeling of proteins via cysteines', *Bioconjug Chem*, 19: 786-91.

Kissick, H. T., L. K. Dunn, S. Ghosh, M. Nechama, L. Kobzik, and M. S. Arredouani. 2014. 'The scavenger receptor MARCO modulates TLR-induced responses in dendritic cells', *PLoS One*, 9: e104148.

Knutson, K. L., R. Clynes, B. Shreeder, P. Yeramian, K. P. Kemp, K. Ballman, K. S. Tenner, C. L. Erskine, N. Norton, D. Northfelt, W. Tan, C. Calfa, M. Pegram, E. A. Mittendorf, and E. A. Perez. 2016. 'Improved Survival of HER2+ Breast Cancer Patients Treated with Trastuzumab and Chemotherapy Is Associated with Host Antibody Immunity against the HER2 Intracellular Domain', *Cancer Res*, 76: 3702-10.

Koniev, O., and A. Wagner. 2015. 'Developments and recent advancements in the field of endogenous amino acid selective bond forming reactions for bioconjugation', *Chem Soc Rev*, 44: 5495-551.

Kontermann, R. E. 2012. 'Antibody-cytokine fusion proteins', *Arch Biochem Biophys*, 526: 194-205.

Koster, B. D., Mfcm van den Hout, B. J. R. Sluijter, B. G. Molenkamp, Rjclm Vuylsteke, A. Baars, P. A. M. van Leeuwen, R. J. Scheper, M. Petrousjka van den Tol, A. J. M. van den Eertwegh, and T. D. de Gruijl. 2017. 'Local Adjuvant Treatment with Low-Dose CpG-B Offers Durable Protection against Disease Recurrence in Clinical Stage I-II Melanoma: Data from Two Randomized Phase II Trials', *Clin Cancer Res*, 23: 5679-86.

Kramer, K., S. L. Young, and G. F. Walker. 2017. 'Comparative Study of 5'- and 3'-Linked CpG-Antigen Conjugates for the Induction of Cellular Immune Responses', *ACS Omega*, 2: 227-35.

Kreutz, M., B. Giquel, Q. Hu, R. Abuknesha, S. Uematsu, S. Akira, F. O. Nestle, and S. S. Diebold. 2012. 'Antibody-antigen-adjuvant conjugates enable co-delivery of antigen and adjuvant to dendritic cells in cis but only have partial targeting specificity', *PLoS One*, 7: e40208.

Krieg, A. M. 2000. 'Immune effects and mechanisms of action of CpG motifs', *Vaccine*, 19: 618-22.

———. 2002. 'CpG motifs in bacterial DNA and their immune effects', *Annu Rev Immunol*, 20: 709-60.

———. 2006. 'Therapeutic potential of Toll-like receptor 9 activation', *Nat Rev Drug Discov*, 5: 471-84.

———. 2007. 'Development of TLR9 agonists for cancer therapy', *J Clin Invest*, 117: 1184-94.

Krysko, D. V., A. D. Garg, A. Kaczmarek, O. Krysko, P. Agostinis, and P. Vandenabeele. 2012. 'Immunogenic cell death and DAMPs in cancer therapy', *Nat Rev Cancer*, 12: 860-75.

Kunikata, N., K. Sano, M. Honda, K. Ishii, J. Matsunaga, R. Okuyama, K. Takahashi, H. Watanabe, G. Tamura, H. Tagami, and T. Terui. 2004. 'Peritumoral CpG oligodeoxynucleotide treatment inhibits tumor growth and metastasis of B16F10 melanoma cells', *J Invest Dermatol*, 123: 395-402.

Kuo, T. T., and V. G. Aveson. 2011. 'Neonatal Fc receptor and IgG-based therapeutics', *MAbs*, 3: 422-30.

Kutscher, H. L., P. Chao, M. Deshmukh, Y. Singh, P. Hu, L. B. Joseph, D. C. Reimer, S. Stein, D. L. Laskin, and P. J. Sinko. 2010. 'Threshold size for optimal passive pulmonary targeting and retention of rigid microparticles in rats', *J Control Release*, 143: 31-7.

Lambert, J. M., and R. V. Chari. 2014. 'Ado-trastuzumab Emtansine (T-DM1): an antibody-drug conjugate (ADC) for HER2-positive breast cancer', *J Med Chem*, 57: 6949-64.

Lande, R., J. Gregorio, V. Facchinetti, B. Chatterjee, Y. H. Wang, B. Homey, W. Cao, Y. H. Wang, B. Su, F. O. Nestle, T. Zal, I. Mellman, J. M. Schroder, Y. J. Liu, and M. Gilliet. 2007. 'Plasmacytoid dendritic cells sense self-DNA coupled with antimicrobial peptide', *Nature*, 449: 564-9.

Lazar, G. A., W. Dang, S. Karki, O. Vafa, J. S. Peng, L. Hyun, C. Chan, H. S. Chung, A. Eivazi, S. C. Yoder, J. Vielmetter, D. F. Carmichael, R. J. Hayes, and B. I. Dahiyat. 2006. 'Engineered antibody Fc variants with enhanced effector function', *Proc Natl Acad Sci U S A*, 103: 4005-10.

Lechner, M. G., S. S. Karimi, K. Barry-Holson, T. E. Angell, K. A. Murphy, C. H. Church, J. R. Ohlfest, P. Hu, and A. L. Epstein. 2013. 'Immunogenicity of murine solid tumor models as a defining feature of in vivo behavior and response to immunotherapy', *J Immunother*, 36: 477-89.

Lee, C. M., and I. F. Tannock. 2010. 'The distribution of the therapeutic monoclonal antibodies cetuximab and trastuzumab within solid tumors', *BMC Cancer*, 10: 255.

Levene, A. P., G. Singh, and C. Palmieri. 2005. 'Therapeutic monoclonal antibodies in oncology', *J R Soc Med*, 98: 146-52.

Lewis Phillips, G. D., G. Li, D. L. Dugger, L. M. Crocker, K. L. Parsons, E. Mai, W. A. Blattler, J. M. Lambert, R. V. Chari, R. J. Lutz, W. L. Wong, F. S. Jacobson, H. Koeppen, R. H. Schwall, S. R. Kenkare-Mitra, S. D. Spencer, and M. X. Sliwkowski. 2008. 'Targeting HER2-positive breast cancer with trastuzumab-DM1, an antibody-cytotoxic drug conjugate', *Cancer Res*, 68: 9280-90.

Liao, J. B., K. J. Ovenell, E. E. Curtis, D. L. Cecil, M. R. Koehnlein, L. R. Rastetter, E. A. Gad, and M. L. Disis. 2015. 'Preservation of tumor-host immune interactions with luciferase-tagged imaging in a murine model of ovarian cancer', *J Immunother Cancer*, 3: 16.

Lin, L., A. J. Gerth, and S. L. Peng. 2004. 'CpG DNA redirects class-switching towards "Th1-like" Ig isotype production via TLR9 and MyD88', *Eur J Immunol*, 34: 1483-7.

Liu, B., X. Wang, T. Z. Chen, G. L. Li, C. C. Tan, Y. Chen, and S. Q. Duan. 2016. 'Polarization of M1 tumor associated macrophage promoted by the activation of TLR3 signal pathway', *Asian Pac J Trop Med*, 9: 484-8.

Liu, L., G. Li, Q. Li, Z. Jin, L. Zhang, J. Zhou, X. Hu, T. Zhou, J. Chen, and N. Gao. 2013. 'Triptolide induces apoptosis in human leukemia cells through caspase-3-mediated ROCK1 activation and MLC phosphorylation', *Cell Death Dis*, 4: e941.

Liu, T., T. Matsuguchi, N. Tsuboi, T. Yajima, and Y. Yoshikai. 2002. 'Differences in expression of toll-like receptors and their reactivities in dendritic cells in BALB/c and C57BL/6 mice', *Infect Immun*, 70: 6638-45.

Liu, Y. J. 2001. 'Dendritic cell subsets and lineages, and their functions in innate and adaptive immunity', *Cell*, 106: 259-62.

Lo Nigro, C., M. Macagno, D. Sangiolo, L. Bertolaccini, M. Aglietta, and M. C. Merlano. 2019. 'NK-mediated antibody-dependent cell-mediated cytotoxicity in solid tumors: biological evidence and clinical perspectives', *Ann Transl Med*, 7: 105.

Lonsdorf, A. S., H. Kuekrek, B. V. Stern, B. O. Boehm, P. V. Lehmann, and M. Tary-Lehmann. 2003. 'Intratumor CpG-oligodeoxynucleotide injection induces protective antitumor T cell immunity', *J Immunol*, 171: 3941-6.

Lund, J. M., L. Alexopoulou, A. Sato, M. Karow, N. C. Adams, N. W. Gale, A. Iwasaki, and R. A. Flavell. 2004. 'Recognition of single-stranded RNA viruses by Toll-like receptor 7', *Proc Natl Acad Sci U S A*, 101: 5598-603.

Maddur, M. S., S. Lacroix-Desmazes, J. D. Dimitrov, M. D. Kazatchkine, J. Bayry, and S. V. Kaveri. 2019. 'Natural Antibodies: from First-Line Defense Against Pathogens to Perpetual Immune Homeostasis', *Clin Rev Allergy Immunol*.

Madler, S., C. Bich, D. Touboul, and R. Zenobi. 2009. 'Chemical cross-linking with NHS esters: a systematic study on amino acid reactivities', *J Mass Spectrom*, 44: 694-706.

Majer, O., B. Liu, and G. M. Barton. 2017. 'Nucleic acid-sensing TLRs: trafficking and regulation', *Curr Opin Immunol*, 44: 26-33.

Manicassamy, S., and B. Pulendran. 2009. 'Modulation of adaptive immunity with Toll-like receptors', *Semin Immunol*, 21: 185-93.

Marabelle, A., R. Andtbacka, K. Harrington, I. Melero, R. Leidner, T. de Baere, C. Robert, P. A. Ascierto, J. F. Baurain, M. Imperiale, S. Rahimian, D. Tersago, E. Klumper, M. Hendriks, R. Kumar, M. Stern, K. Ohrling, C. Massacesi, I. Tchakov, A. Tse, J. Y. Douillard, J. Tabernero, J. Haanen, and J. Brody. 2018. 'Starting the fight in the tumor: expert recommendations for the development of human intratumoral immunotherapy (HIT-IT)', *Ann Oncol*, 29: 2163-74.

Marabelle, A., H. Kohrt, C. Caux, and R. Levy. 2014. 'Intratumoral immunization: a new paradigm for cancer therapy', *Clin Cancer Res*, 20: 1747-56.

Marabelle, A., L. Tselikas, T. de Baere, and R. Houot. 2017. 'Intratumoral immunotherapy: using the tumor as the remedy', *Ann Oncol*, 28: xii33-xii43.

Marcucci, F., M. Bellone, C. Rumio, and A. Corti. 2013. 'Approaches to improve tumor accumulation and interactions between monoclonal antibodies and immune cells', *MAbs*, 5: 34-46.

Marshall, J. D., K. Fearon, C. Abbate, S. Subramanian, P. Yee, J. Gregorio, R. L. Coffman, and G. Van Nest. 2003. 'Identification of a novel CpG DNA class and motif that optimally stimulate B cell and plasmacytoid dendritic cell functions', *J Leukoc Biol*, 73: 781-92.

Marshall, J. D., D. S. Heeke, C. Abbate, P. Yee, and G. Van Nest. 2006. 'Induction of interferon-gamma from natural killer cells by immunostimulatory CpG DNA is mediated through plasmacytoid-dendritic-cell-produced interferon-alpha and tumour necrosis factor-alpha', *Immunology*, 117: 38-46.

Massicano, A. V. F., B. V. Marquez-Nostra, and S. E. Lapi. 2018. 'Targeting HER2 in Nuclear Medicine for Imaging and Therapy', *Mol Imaging*, 17: 1536012117745386.

Mattson, G., E. Conklin, S. Desai, G. Nielander, M. D. Savage, and S. Morgensen. 1993. 'A practical approach to crosslinking', *Mol Biol Rep*, 17: 167-83.

Maurer, T., A. Heit, H. Hochrein, F. Ampenberger, M. O'Keeffe, S. Bauer, G. B. Lipford, R. M. Vabulas, and H. Wagner. 2002. 'CpG-DNA aided cross-presentation of soluble antigens by dendritic cells', *Eur J Immunol*, 32: 2356-64.

McCombs, J. R., and S. C. Owen. 2015. 'Antibody drug conjugates: design and selection of linker, payload and conjugation chemistry', *AAPS J*, 17: 339-51.

McLarty, K., A. Fasih, D. A. Scollard, S. J. Done, D. C. Vines, D. E. Green, D. L. Costantini, and R. M. Reilly. 2009. '18F-FDG small-animal PET/CT differentiates trastuzumab-responsive from unresponsive human breast cancer xenografts in athymic mice', *J Nucl Med*, 50: 1848-56.

Medzhitov, R. 2001. 'Toll-like receptors and innate immunity', *Nat Rev Immunol*, 1: 135-45.

———. 2007. 'Recognition of microorganisms and activation of the immune response', *Nature*, 449: 819-26.

Mehta, A. K., D. T. Gracias, and M. Croft. 2018. 'TNF activity and T cells', *Cytokine*, 101: 14-18.

Menke-van der Houven van Oordt, C. W., E. C. Gootjes, M. C. Huisman, D. J. Vugts, C. Roth, A. M. Luik, E. R. Mulder, R. C. Schuit, R. Boellaard, O. S. Hoekstra, G. A. van Dongen, and H. M. Verheul. 2015. '89Zr-cetuximab PET imaging in patients with advanced colorectal cancer', *Oncotarget*, 6: 30384-93.

Michaelis, K. A., M. A. Norgard, X. Zhu, P. R. Levasseur, S. Sivagnanam, S. M. Liudahl, K. G. Burfeind, B. Olson, K. R. Pelz, D. M. Angeles Ramos, H. C. Maurer, K. P. Olive, L. M. Coussens, T. K. Morgan, and D. L. Marks. 2019.

'The TLR7/8 agonist R848 remodels tumor and host responses to promote survival in pancreatic cancer', *Nat Commun*, 10: 4682.

Milano, F., M. Guarriera, A. M. Rygiel, and K. K. Krishnadath. 2010. 'Trastuzumab mediated T-cell response against HER-2/neu overexpressing esophageal adenocarcinoma depends on intact antigen processing machinery', *PLoS One*, 5: e12424.

Mittendorf, E. A., Y. Liu, S. L. Tucker, T. McKenzie, N. Qiao, S. Akli, A. Biernacka, Y. Liu, L. Meijer, K. Keyomarsi, and K. K. Hunt. 2010. 'A novel interaction between HER2/neu and cyclin E in breast cancer', *Oncogene*, 29: 3896-907.

Molenkamp, B. G., P. A. van Leeuwen, S. Meijer, B. J. Sluijter, P. G. Wijnands, A. Baars, A. J. van den Eertwegh, R. J. Scheper, and T. D. de Gruijl. 2007. 'Intradermal CpG-B activates both plasmacytoid and myeloid dendritic cells in the sentinel lymph node of melanoma patients', *Clin Cancer Res*, 13: 2961-9.

Mortimer, J. E., J. R. Bading, D. M. Colcher, P. S. Conti, P. H. Frankel, M. I. Carroll, S. Tong, E. Poku, J. K. Miles, J. E. Shively, and A. A. Raubitschek. 2014. 'Functional imaging of human epidermal growth factor receptor 2-positive metastatic breast cancer using (64)Cu-DOTA-trastuzumab PET', *J Nucl Med*, 55: 23-9.

Mortimer, J. E., J. R. Bading, J. M. Park, P. H. Frankel, M. I. Carroll, T. T. Tran, E. K. Poku, R. C. Rockne, A. A. Raubitschek, J. E. Shively, and D. M. Colcher. 2018. 'Tumor Uptake of (64)Cu-DOTA-Trastuzumab in Patients with Metastatic Breast Cancer', *J Nucl Med*, 59: 38-43.

Morton, J. J., G. Bird, Y. Refaeli, and A. Jimeno. 2016. 'Humanized Mouse Xenograft Models: Narrowing the Tumor-Microenvironment Gap', *Cancer Res*, 76: 6153-58.

Motoshima, S., K. Yonemoto, H. Kamei, M. Morita, and R. Yamaguchi. 2018. 'Prognostic implications of HER2 heterogeneity in gastric cancer', *Oncotarget*, 9: 9262-72.

Muller, K. E., J. D. Marotti, and L. J. Tafe. 2019. 'Pathologic Features and Clinical Implications of Breast Cancer With HER2 Intratumoral Genetic Heterogeneity', *Am J Clin Pathol*, 152: 7-16.

Mullins, S. R., J. P. Vasilakos, K. Deschler, I. Grigsby, P. Gillis, J. John, M. J. Elder, J. Swales, E. Timosenko, Z. Cooper, S. J. Dovedi, A. J. Leishman, N. Luheshi, J. Elvecrog, A. Tilahun, R. Goodwin, R. Herbst, M. A. Tomai, and R. W. Wilkinson. 2019. 'Intratumoral immunotherapy with TLR7/8 agonist MEDI9197 modulates the tumor microenvironment leading to enhanced activity when combined with other immunotherapies', *J Immunother Cancer*, 7: 244.

Murer, P., and D. Neri. 2019. 'Antibody-cytokine fusion proteins: A novel class of biopharmaceuticals for the therapy of cancer and of chronic inflammation', *N Biotechnol*, 52: 42-53.

Murray, P. J. 2017. 'Macrophage Polarization', *Annu Rev Physiol*, 79: 541-66.

Murthy, V., J. Minehart, and D. H. Sterman. 2017. 'Local Immunotherapy of Cancer: Innovative Approaches to Harnessing Tumor-Specific Immune Responses', *J Natl Cancer Inst*, 109.

Nagato, T., Y. R. Lee, Y. Harabuchi, and E. Celis. 2014. 'Combinatorial immunotherapy of polyinosinic-polycytidylic acid and blockade of programmed death-ligand 1 induce effective CD8 T-cell responses against established tumors', *Clin Cancer Res*, 20: 1223-34.

Neelapu, S. S., S. Tummala, P. Kebriaei, W. Wierda, C. Gutierrez, F. L. Locke, K. V. Komanduri, Y. Lin, N. Jain, N. Daver, J. Westin, A. M. Gulbis, M. E. Loghin, J. F. de Groot, S. Adkins, S. E. Davis, K. Rezvani, P. Hwu, and E. J. Shpall. 2018. 'Chimeric antigen receptor T-cell therapy - assessment and management of toxicities', *Nat Rev Clin Oncol*, 15: 47-62.

Nemeth, B. T., Z. V. Varga, W. J. Wu, and P. Pacher. 2017. 'Trastuzumab cardiotoxicity: from clinical trials to experimental studies', *Br J Pharmacol*, 174: 3727-48.

Nierkens, S., M. H. den Brok, Z. Garcia, S. Togher, J. Wagenaars, M. Wassink, L. Boon, T. J. Ruers, C. G. Figdor, S. P. Schoenberger, G. J. Adema, and E. M. Janssen. 2011. 'Immune adjuvant efficacy of CpG oligonucleotide in cancer treatment is founded specifically upon TLR9 function in plasmacytoid dendritic cells', *Cancer Res*, 71: 6428-37.

Nierkens, S., M. H. den Brok, T. Roelofsen, J. A. Wagenaars, C. G. Figdor, T. J. Ruers, and G. J. Adema. 2009. 'Route of administration of the TLR9 agonist CpG critically determines the efficacy of cancer immunotherapy in mice', *PLoS One*, 4: e8368.

Nierkens, S., M. H. den Brok, R. P. Sutmuller, O. M. Grauer, E. Bennink, M. E. Morgan, C. G. Figdor, T. J. Ruers, and G. J. Adema. 2008. 'In vivo colocalization of antigen and CpG [corrected] within dendritic cells is associated with the efficacy of cancer immunotherapy', *Cancer Res*, 68: 5390-6.

Nunes, J. P. M., V. Vassileva, E. Robinson, M. Morais, M. E. B. Smith, R. B. Pedley, S. Caddick, J. R. Baker, and V. Chudasama. 2017. 'Use of a next generation maleimide in combination with THIOMAB (TM) antibody technology delivers a highly stable, potent and near homogeneous THIOMAB (TM) antibody-drug conjugate (TDC)', *Rsc Advances*, 7: 24828-32.

O'Neill, L. A., and A. G. Bowie. 2007. 'The family of five: TIR-domain-containing adaptors in Toll-like receptor signalling', *Nat Rev Immunol*, 7: 353-64.

O'Neill, L. A., C. E. Bryant, and S. L. Doyle. 2009. 'Therapeutic targeting of Toll-like receptors for infectious and inflammatory diseases and cancer', *Pharmacol Rev*, 61: 177-97.

O'Neill, L. A., D. Golenbock, and A. G. Bowie. 2013. 'The history of Toll-like receptors - redefining innate immunity', *Nat Rev Immunol*, 13: 453-60.

Overdijk, M. B., S. Verploegen, A. Ortiz Buijsse, T. Vink, J. H. Leusen, W. K. Bleeker, and P. W. Parren. 2012. 'Crosstalk between human IgG isotypes and murine effector cells', *J Immunol*, 189: 3430-8.

Palle, J., A. Rochand, S. Pernot, C. Gallois, J. Taieb, and A. Zaanan. 2020. 'Human Epidermal Growth Factor Receptor 2 (HER2) in Advanced Gastric Cancer: Current Knowledge and Future Perspectives', *Drugs*.

Palm, S., R. M. Enmon, Jr., C. Matei, K. S. Kolbert, S. Xu, P. B. Zanzonico, R. L. Finn, J. A. Koutcher, S. M. Larson, and G. Sgouros. 2003. 'Pharmacokinetics and Biodistribution of (86)Y-Trastuzumab for (90)Y dosimetry in an ovarian carcinoma model: correlative MicroPET and MRI', *J Nucl Med*, 44: 1148-55.

Park, S., J. R. Nedrow, A. Josefsson, and G. Sgouros. 2017. 'Human HER2 overexpressing mouse breast cancer cell lines derived from MMTV.f.HuHER2 mice: characterization and use in a model of metastatic breast cancer', *Oncotarget*, 8: 68071-82.

Parslow, A. C., S. Parakh, F. T. Lee, H. K. Gan, and A. M. Scott. 2016. 'Antibody-Drug Conjugates for Cancer Therapy', *Biomedicines*, 4.

Perregaux, D. G., K. Bhavsar, L. Contillo, J. Shi, and C. A. Gabel. 2002. 'Antimicrobial peptides initiate IL-1 beta posttranslational processing: a novel role beyond innate immunity', *J Immunol*, 168: 3024-32.

Petricevic, B., J. Laengle, J. Singer, M. Sachet, J. Fazekas, G. Steger, R. Bartsch, E. Jensen-Jarolim, and M. Bergmann. 2013. 'Trastuzumab mediates antibody-dependent cell-mediated cytotoxicity and phagocytosis to the same extent in both adjuvant and metastatic HER2/neu breast cancer patients', *J Transl Med*, 11: 307.

Pettengill, M. A., S. D. van Haren, N. Li, D. J. Dowling, I. Bergelson, J. Jans, G. Ferwerda, and O. Levy. 2016. 'Distinct TLR-mediated cytokine production and immunoglobulin secretion in human newborn naive B cells', *Innate Immun*, 22: 433-43.

Phillips, G. D., C. T. Fields, G. Li, D. Dowbenko, G. Schaefer, K. Miller, F. Andre, H. A. Burris, 3rd, K. S. Albain, N. Harbeck, V. Dieras, D. Crivellari, L. Fang, E. Guardino, S. R. Olsen, L. M. Crocker, and M. X. Sliwkowski. 2014. 'Dual targeting of HER2-positive cancer with trastuzumab emtansine and pertuzumab: critical role for neuregulin blockade in antitumor response to combination therapy', *Clin Cancer Res*, 20: 456-68.

Piechocki, M. P., Y. S. Ho, S. Pilon, and W. Z. Wei. 2003. 'Human ErbB-2 (Her-2) transgenic mice: a model system for testing Her-2 based vaccines', *J Immunol*, 171: 5787-94.

Pollard, J. W. 2004. 'Tumour-educated macrophages promote tumour progression and metastasis', *Nat Rev Cancer*, 4: 71-8.

Rajagopal, D., C. Paturel, Y. Morel, S. Uematsu, S. Akira, and S. S. Diebold. 2010. 'Plasmacytoid dendritic cell-derived type I interferon is crucial for the adjuvant activity of Toll-like receptor 7 agonists', *Blood*, 115: 1949-57.

Rakhmilevich, A. L., M. Felder, L. Lever, J. Slowinski, K. Rasmussen, A. Hoefges, T. J. Van De Voort, H. Loibner, A. J. Korman, S. D. Gillies, and P. M. Sondel. 2017. 'Effective Combination of Innate and Adaptive Immunotherapeutic Approaches in a Mouse Melanoma Model', *J Immunol*, 198: 1575-84.

Rawlings, D. J., M. A. Schwartz, S. W. Jackson, and A. Meyer-Bahlburg. 2012. 'Integration of B cell responses through Toll-like receptors and antigen receptors', *Nat Rev Immunol*, 12: 282-94.

Raynal, B., P. Lenormand, B. Baron, S. Hoos, and P. England. 2014. 'Quality assessment and optimization of purified protein samples: why and how?', *Microb Cell Fact*, 13: 180.

Ren, T., Z. K. Wen, Z. M. Liu, Y. J. Liang, Z. L. Guo, and L. Xu. 2007. 'Functional expression of TLR9 is associated to the metastatic potential of human lung cancer cell: functional active role of TLR9 on tumor metastasis', *Cancer Biol Ther*, 6: 1704-9.

Ribas, A., T. Medina, S. Kummar, A. Amin, A. Kalbasi, J. J. Drabick, M. Barve, G. A. Daniels, D. J. Wong, E. V. Schmidt, A. F. Candia, R. L. Coffman, A. C. F. Leung, and R. S. Janssen. 2018. 'SD-101 in Combination with Pembrolizumab in Advanced Melanoma: Results of a Phase Ib, Multicenter Study', *Cancer Discov*, 8: 1250-57.

Richards, D. A. 2018. 'Exploring alternative antibody scaffolds: Antibody fragments and antibody mimics for targeted drug delivery', *Drug Discov Today Technol*, 30: 35-46.

Roberts, T. L., M. J. Sweet, D. A. Hume, and K. J. Stacey. 2005. 'Cutting edge: species-specific TLR9-mediated recognition of CpG and non-CpG phosphorothioate-modified oligonucleotides', *J Immunol*, 174: 605-8.

Rodabe, A. 2015. Intratumoral injections of LL37 for melanoma. https://clinicaltrials.gov/ct2/show/record/NCT02225366.Accessed November 26, 2017.

Rodell, C. B., S. P. Arlauckas, M. F. Cuccarese, C. S. Garris, R. Li, M. S. Ahmed, R. H. Kohler, M. J. Pittet, and R. Weissleder. 2018. 'TLR7/8-agonist-loaded nanoparticles promote the polarization of tumour-associated macrophages to enhance cancer immunotherapy', *Nat Biomed Eng*, 2: 578-88.

Rookhuizen, D. C., and A. L. DeFranco. 2014. 'Toll-like receptor 9 signaling acts on multiple elements of the germinal center to enhance antibody responses', *Proc Natl Acad Sci U S A*, 111: E3224-33.

Rosenberg, S. A. 1997. 'Cancer vaccines based on the identification of genes encoding cancer regression antigens', *Immunol Today*, 18: 175-82.

Sagiv-Barfi, I., D. K. Czerwinski, S. Levy, I. S. Alam, A. T. Mayer, S. S. Gambhir, and R. Levy. 2018. 'Eradication of spontaneous malignancy by local immunotherapy', *Sci Transl Med*, 10.

Sallusto, F., J. Geginat, and A. Lanzavecchia. 2004. 'Central memory and effector memory T cell subsets: function, generation, and maintenance', *Annu Rev Immunol*, 22: 745-63.

Samulowitz, U., M. Weber, R. Weeratna, E. Uhlmann, B. Noll, A. M. Krieg, and J. Vollmer. 2010. 'A novel class of immune-stimulatory CpG oligodeoxynucleotides unifies high potency in type I interferon induction with preferred structural properties', *Oligonucleotides*, 20: 93-101.

Sandgren, S., A. Wittrup, F. Cheng, M. Jonsson, E. Eklund, S. Busch, and M. Belting. 2004. 'The human antimicrobial peptide LL-37 transfers extracellular DNA plasmid to the nuclear compartment of mammalian cells via lipid rafts and proteoglycan-dependent endocytosis', *J Biol Chem*, 279: 17951-6.

Sato-Kaneko, F., S. Yao, A. Ahmadi, S. S. Zhang, T. Hosoya, M. M. Kaneda, J. A. Varner, M. Pu, K. S. Messer, C. Guiducci, R. L. Coffman, K. Kitaura, T. Matsutani, R. Suzuki, D. A. Carson, T. Hayashi, and E. E. Cohen. 2017. 'Combination immunotherapy with TLR agonists and checkpoint inhibitors suppresses head and neck cancer', *JCI Insight*, 2.

Sato, T., M. Terai, Y. Tamura, V. Alexeev, M. J. Mastrangelo, and S. R. Selvan. 2011. 'Interleukin 10 in the tumor microenvironment: a target for anticancer immunotherapy', *Immunol Res*, 51: 170-82.

Schettini, J., A. Kidiyoor, D. M. Besmer, T. L. Tinder, L. D. Roy, J. Lustgarten, S. J. Gendler, and P. Mukherjee. 2012. 'Intratumoral delivery of CpG-conjugated anti-MUC1 antibody enhances NK cell anti-tumor activity', *Cancer Immunol Immunother*, 61: 2055-65.

Schillie, S., A. Harris, R. Link-Gelles, J. Romero, J. Ward, and N. Nelson. 2018. 'Recommendations of the Advisory Committee on Immunization Practices for Use of a Hepatitis B Vaccine with a Novel Adjuvant', *MMWR Morb Mortal Wkly Rep*, 67: 455-58.

Schmidt, C. 2007. 'Clinical setbacks for toll-like receptor 9 agonists in cancer', *Nat Biotechnol*, 25: 825-6.

Schrama, D., R. A. Reisfeld, and J. C. Becker. 2006. 'Antibody targeted drugs as cancer therapeutics', *Nat Rev Drug Discov*, 5: 147-59.

Schreibelt, G., J. Tel, K. H. Sliepen, D. Benitez-Ribas, C. G. Figdor, G. J. Adema, and I. J. de Vries. 2010. 'Toll-like receptor expression and function in human dendritic cell subsets: implications for dendritic cell-based anti-cancer immunotherapy', *Cancer Immunol Immunother*, 59: 1573-82.

Sester, D. P., S. Naik, S. J. Beasley, D. A. Hume, and K. J. Stacey. 2000. 'Phosphorothioate backbone modification modulates macrophage activation by CpG DNA', *J Immunol*, 165: 4165-73.

Shahriari, S., S. Rezaeifard, H. R. Moghimi, M. R. Khorramizadeh, and Z. Faghih. 2017. 'Cell membrane and intracellular expression of toll-like receptor 9 (TLR9) in colorectal cancer and breast cancer cell-lines', *Cancer Biomark*, 18: 375-80.

Sharma, S. K., and K. D. Bagshawe. 2017. 'Antibody Directed Enzyme Prodrug Therapy (ADEPT): Trials and tribulations', *Adv Drug Deliv Rev*, 118: 2-7.

Shen, Ben-Quan, Keyang Xu, Luna Liu, Helga Raab, Sunil Bhakta, Margaret Kenrick, Kathryn L. Parsons-Reponte, Janet Tien, Shang-Fan Yu, Elaine Mai, Dongwei Li, Jay Tibbitts, Jakub Baudys, Ola M. Saad, Suzie J. Scales, Paul J. McDonald, Philip E. Hass, Charles Eigenbrot, Trung Nguyen, Willy A. Solis, Reina N. Fuji, Kelly M. Flagella, Darshana Patel, Susan D. Spencer, Leslie A. Khawli, Allen Ebens, Wai Lee Wong, Richard Vandlen, Surinder Kaur, Mark X. Sliwkowski, Richard H. Scheller, Paul Polakis, and Jagath R. Junutula. 2012. 'Conjugation site modulates the in vivo stability and therapeutic activity of antibody-drug conjugates', *Nature Biotechnology*, 30: 184.

Shi, Y., X. Fan, H. Deng, R. J. Brezski, M. Rycyzyn, R. E. Jordan, W. R. Strohl, Q. Zou, N. Zhang, and Z. An. 2015. 'Trastuzumab triggers phagocytic killing of high HER2 cancer cells in vitro and in vivo by interaction with Fcgamma receptors on macrophages', *J Immunol*, 194: 4379-86.

Shields, R. L., A. K. Namenuk, K. Hong, Y. G. Meng, J. Rae, J. Briggs, D. Xie, J. Lai, A. Stadlen, B. Li, J. A. Fox, and L. G. Presta. 2001. 'High resolution mapping of the binding site on human IgG1 for Fc gamma RI, Fc gamma RII, Fc gamma RIII, and FcRn and design of IgG1 variants with improved binding to the Fc gamma R', *J Biol Chem*, 276: 6591-604.

Singh, D., R. Vaughan, and C. C. Kao. 2014. 'LL-37 peptide enhancement of signal transduction by Toll-like receptor 3 is regulated by pH: identification of a peptide antagonist of LL-37', *J Biol Chem*, 289: 27614-24.

Singh, M., H. Khong, Z. Dai, X. F. Huang, J. A. Wargo, Z. A. Cooper, J. P. Vasilakos, P. Hwu, and W. W. Overwijk. 2014. 'Effective innate and adaptive antimelanoma immunity through localized TLR7/8 activation', *J Immunol*, 193: 4722-31.

Skelton, J. K., A. M. Ortega-Prieto, and M. Dorner. 2018. 'A Hitchhiker's guide to humanized mice: new pathways to studying viral infections', *Immunology*, 154: 50-61.

Smaglo, B. G., D. Aldeghaither, and L. M. Weiner. 2014. 'The development of immunoconjugates for targeted cancer therapy', *Nat Rev Clin Oncol*, 11: 637-48.

Smith, G. P. 2006. 'Kinetics of amine modification of proteins', *Bioconjug Chem*, 17: 501-6.
Smith, M., E. Garcia-Martinez, M. R. Pitter, J. Fucikova, R. Spisek, L. Zitvogel, G. Kroemer, and L. Galluzzi. 2018. 'Trial Watch: Toll-like receptor agonists in cancer immunotherapy', *Oncoimmunology*, 7: e1526250.
Sochaj, A. M., K. W. Swiderska, and J. Otlewski. 2015. 'Current methods for the synthesis of homogeneous antibody-drug conjugates', *Biotechnol Adv*, 33: 775-84.
Swiecki, M., and M. Colonna. 2015. 'The multifaceted biology of plasmacytoid dendritic cells', *Nat Rev Immunol*, 15: 471-85.
Takeda, K., and S. Akira. 2005. 'Toll-like receptors in innate immunity', *Int Immunol*, 17: 1-14.
Takeda, K., T. Kaisho, and S. Akira. 2003. 'Toll-like receptors', *Annu Rev Immunol*, 21: 335-76.
Tang, J., L. Pearce, J. O'Donnell-Tormey, and V. M. Hubbard-Lucey. 2018. 'Trends in the global immuno-oncology landscape', *Nat Rev Drug Discov*, 17: 783-84.
Tang, J., A. Shalabi, and V. M. Hubbard-Lucey. 2018. 'Comprehensive analysis of the clinical immuno-oncology landscape', *Ann Oncol*, 29: 84-91.
Tanner, M., A. I. Kapanen, T. Junttila, O. Raheem, S. Grenman, J. Elo, K. Elenius, and J. Isola. 2004. 'Characterization of a novel cell line established from a patient with Herceptin-resistant breast cancer', *Mol Cancer Ther*, 3: 1585-92.
Taylor, C., D. Hershman, N. Shah, N. Suciu-Foca, D. P. Petrylak, R. Taub, L. Vahdat, B. Cheng, M. Pegram, K. L. Knutson, and R. Clynes. 2007. 'Augmented HER-2 specific immunity during treatment with trastuzumab and chemotherapy', *Clin Cancer Res*, 13: 5133-43.
Teicher, B. A., and R. V. Chari. 2011. 'Antibody conjugate therapeutics: challenges and potential', *Clin Cancer Res*, 17: 6389-97.
Thomas, A., B. A. Teicher, and R. Hassan. 2016. 'Antibody-drug conjugates for cancer therapy', *Lancet Oncol*, 17: e254-e62.
Tisoncik, J. R., M. J. Korth, C. P. Simmons, J. Farrar, T. R. Martin, and M. G. Katze. 2012. 'Into the eye of the cytokine storm', *Microbiol Mol Biol Rev*, 76: 16-32.
Tiwari, D. K., S. Tanaka, Y. Inouye, K. Yoshizawa, T. M. Watanabe, and T. Jin. 2009. 'Synthesis and Characterization of Anti-HER2 Antibody Conjugated CdSe/CdZnS Quantum Dots for Fluorescence Imaging of Breast Cancer Cells', *Sensors (Basel)*, 9: 9332-64.
Trinchieri, G. 2003. 'Interleukin-12 and the regulation of innate resistance and adaptive immunity', *Nat Rev Immunol*, 3: 133-46.
Ueno, Y., H. Sakurai, S. Tsunoda, M. K. Choo, M. Matsuo, K. Koizumi, and I. Saiki. 2008. 'Heregulin-induced activation of ErbB3 by EGFR tyrosine kinase activity promotes tumor growth and metastasis in melanoma cells', *Int J Cancer*, 123: 340-47.
Uppal, H., E. Doudement, K. Mahapatra, W. C. Darbonne, D. Bumbaca, B. Q. Shen, X. Du, O. Saad, K. Bowles, S. Olsen, G. D. Lewis Phillips, D. Hartley, M. X. Sliwkowski, S. Girish, D. Dambach, and V. Ramakrishnan. 2015. 'Potential mechanisms for thrombocytopenia development with trastuzumab emtansine (T-DM1)', *Clin Cancer Res*, 21: 123-33.
Valmori, D., N. E. Souleimanian, V. Tosello, N. Bhardwaj, S. Adams, D. O'Neill, A. Pavlick, J. B. Escalon, C. M. Cruz, A. Angiulli, F. Angiulli, G. Mears, S. M. Vogel, L. Pan, A. A. Jungbluth, E. W. Hoffmann, R. Venhaus, G. Ritter, L. J.

Old, and M. Ayyoub. 2007. 'Vaccination with NY-ESO-1 protein and CpG in Montanide induces integrated antibody/Th1 responses and CD8 T cells through cross-priming', *Proc Natl Acad Sci U S A*, 104: 8947-52.

van Ojik, H. H., L. Bevaart, C. E. Dahle, A. Bakker, M. J. Jansen, M. J. van Vugt, J. G. van de Winkel, and G. J. Weiner. 2003. 'CpG-A and B oligodeoxynucleotides enhance the efficacy of antibody therapy by activating different effector cell populations', *Cancer Res*, 63: 5595-600.

Vanpouille-Box, C., J. A. Hoffmann, and L. Galluzzi. 2019. 'Pharmacological modulation of nucleic acid sensors - therapeutic potential and persisting obstacles', *Nat Rev Drug Discov*, 18: 845-67.

Vidyarthi, A., N. Khan, T. Agnihotri, S. Negi, D. K. Das, M. Aqdas, D. Chatterjee, O. R. Colegio, M. K. Tewari, and J. N. Agrewala. 2018. 'TLR-3 Stimulation Skews M2 Macrophages to M1 Through IFN-alphabeta Signaling and Restricts Tumor Progression', *Front Immunol*, 9: 1650.

Vollmer, J., R. Weeratna, P. Payette, M. Jurk, C. Schetter, M. Laucht, T. Wader, S. Tluk, M. Liu, H. L. Davis, and A. M. Krieg. 2004. 'Characterization of three CpG oligodeoxynucleotide classes with distinct immunostimulatory activities', *Eur J Immunol*, 34: 251-62.

Waibler, Z., M. Anzaghe, A. Konur, S. Akira, W. Muller, and U. Kalinke. 2008. 'Excessive CpG 1668 stimulation triggers IL-10 production by cDC that inhibits IFN-alpha responses by pDC', *Eur J Immunol*, 38: 3127-37.

Wainberg, Z. A., A. Anghel, A. J. Desai, R. Ayala, T. Luo, B. Safran, M. S. Fejzo, J. R. Hecht, D. J. Slamon, and R. S. Finn. 2010. 'Lapatinib, a dual EGFR and HER2 kinase inhibitor, selectively inhibits HER2-amplified human gastric cancer cells and is synergistic with trastuzumab in vitro and in vivo', *Clin Cancer Res*, 16: 1509-19.

Wallberg, H., and A. Orlova. 2008. 'Slow internalization of anti-HER2 synthetic affibody monomer 111In-DOTA-ZHER2:342-pep2: implications for development of labeled tracers', *Cancer Biother Radiopharm*, 23: 435-42.

Wang, S., I. A. Astsaturov, C. A. Bingham, K. M. McCarthy, M. von Mehren, W. Xu, R. K. Alpaugh, Y. Tang, B. A. Littlefield, L. D. Hawkins, S. T. Ishizaka, and L. M. Weiner. 2012. 'Effective antibody therapy induces host-protective antitumor immunity that is augmented by TLR4 agonist treatment', *Cancer Immunol Immunother*, 61: 49-61.

Wang, S., J. Campos, M. Gallotta, M. Gong, C. Crain, E. Naik, R. L. Coffman, and C. Guiducci. 2016. 'Intratumoral injection of a CpG oligonucleotide reverts resistance to PD-1 blockade by expanding multifunctional CD8+ T cells', *Proc Natl Acad Sci U S A*, 113: E7240-E49.

Weber, J. S., H. Zarour, B. Redman, U. Trefzer, S. O'Day, A. J. van den Eertwegh, E. Marshall, and S. Wagner. 2009. 'Randomized phase 2/3 trial of CpG oligodeoxynucleotide PF-3512676 alone or with dacarbazine for patients with unresectable stage III and IV melanoma', *Cancer*, 115: 3944-54.

Weiner, L. M., M. V. Dhodapkar, and S. Ferrone. 2009. 'Monoclonal antibodies for cancer immunotherapy', *Lancet*, 373: 1033-40.

Westwood, J. A., T. C. Potdevin Hunnam, H. J. Pegram, R. J. Hicks, P. K. Darcy, and M. H. Kershaw. 2014. 'Routes of delivery for CpG and anti-CD137 for the treatment of orthotopic kidney tumors in mice', *PLoS One*, 9: e95847.

Williams, B. A., and J. C. Chaput. 2010. 'Synthesis of peptide-oligonucleotide conjugates using a heterobifunctional crosslinker', *Curr Protoc Nucleic Acid Chem*, Chapter 4: Unit4 41.

Yan, Y., Z. Cao, M. Yang, H. Li, H. Wei, Y. Fu, D. Song, L. Wang, and Y. Yu. 2012. 'A CpG oligodeoxynucleotide potentiates the anti-tumor effect of HSP65-Her2 fusion protein against Her2 positive B16 melanoma in mice', *Int Immunopharmacol*, 12: 402-7.

Yang, N. J., and M. J. Hinner. 2015. 'Getting across the cell membrane: an overview for small molecules, peptides, and proteins', *Methods Mol Biol*, 1266: 29-53.

Yeo, S. J., J. G. Yoon, S. C. Hong, and A. K. Yi. 2003. 'CpG DNA induces self and cross-hyporesponsiveness of RAW264.7 cells in response to CpG DNA and lipopolysaccharide: alterations in IL-1 receptor-associated kinase expression', *J Immunol*, 170: 1052-61.

Yi, A. K., J. G. Yoon, S. J. Yeo, S. C. Hong, B. K. English, and A. M. Krieg. 2002. 'Role of mitogen-activated protein kinases in CpG DNA-mediated IL-10 and IL-12 production: central role of extracellular signal-regulated kinase in the negative feedback loop of the CpG DNA-mediated Th1 response', *J Immunol*, 168: 4711-20.

Yin, P., X. Liu, A. S. Mansfield, S. M. Harrington, Y. Li, Y. Yan, and H. Dong. 2016. 'CpG-induced antitumor immunity requires IL-12 in expansion of effector cells and down-regulation of PD-1', *Oncotarget*, 7: 70223-31.

Yoo, B., K. Ma, L. Zhang, A. Burns, S. Sequeira, I. Mellinghoff, C. Brennan, U. Wiesner, and M. S. Bradbury. 2015. 'Ultrasmall dual-modality silica nanoparticle drug conjugates: Design, synthesis, and characterization', *Bioorg Med Chem*, 23: 7119-30.

Young, P. A., S. L. Morrison, and J. M. Timmerman. 2014. 'Antibody-cytokine fusion proteins for treatment of cancer: engineering cytokines for improved efficacy and safety', *Semin Oncol*, 41: 623-36.

Yu, D., and M. C. Hung. 2000. 'Overexpression of ErbB2 in cancer and ErbB2-targeting strategies', *Oncogene*, 19: 6115-21.

Zhang, S., W. C. Huang, P. Li, H. Guo, S. B. Poh, S. W. Brady, Y. Xiong, L. M. Tseng, S. H. Li, Z. Ding, A. A. Sahin, F. J. Esteva, G. N. Hortobagyi, and D. Yu. 2011. 'Combating trastuzumab resistance by targeting SRC, a common node downstream of multiple resistance pathways', *Nat Med*, 17: 461-9.

Zhao, H., S. Gulesserian, S. K. Ganesan, J. Ou, K. Morrison, Z. Zeng, V. Robles, J. Snyder, L. Do, H. Avina, S. Karki, D. R. Stover, and F. Donate. 2017. 'Inhibition of Megakaryocyte Differentiation by Antibody-Drug Conjugates (ADCs) is Mediated by Macropinocytosis: Implications for ADC-induced Thrombocytopenia', *Mol Cancer Ther*, 16: 1877-86.

Zhou, Q. 2017. 'Site-Specific Antibody Conjugation for ADC and Beyond', *Biomedicines*, 5.

Zhou, Y., M. Guo, X. Wang, J. Li, Y. Wang, L. Ye, M. Dai, L. Zhou, Y. Persidsky, and W. Ho. 2013. 'TLR3 activation efficiency by high or low molecular mass poly I:C', *Innate Immun*, 19: 184-92.

Zolot, R. S., S. Basu, and R. P. Million. 2013. 'Antibody-drug conjugates', *Nat Rev Drug Discov*, 12: 259-60.

Zughaier, S. M., W. M. Shafer, and D. S. Stephens. 2005. 'Antimicrobial peptides and endotoxin inhibit cytokine and nitric oxide release but amplify respiratory burst response in human and murine macrophages', *Cell Microbiol*, 7: 1251-62.

Appendix A

**Vector map of pcDNA3-HER2WT**

(Addgene # 16257; http://n2t.net/addgene:16257; RRID:Addgene_16257)

Sequence downloaded from:

https://www.addgene.org/browse/sequence/43248/

and annotated with Geneious 10.2.3

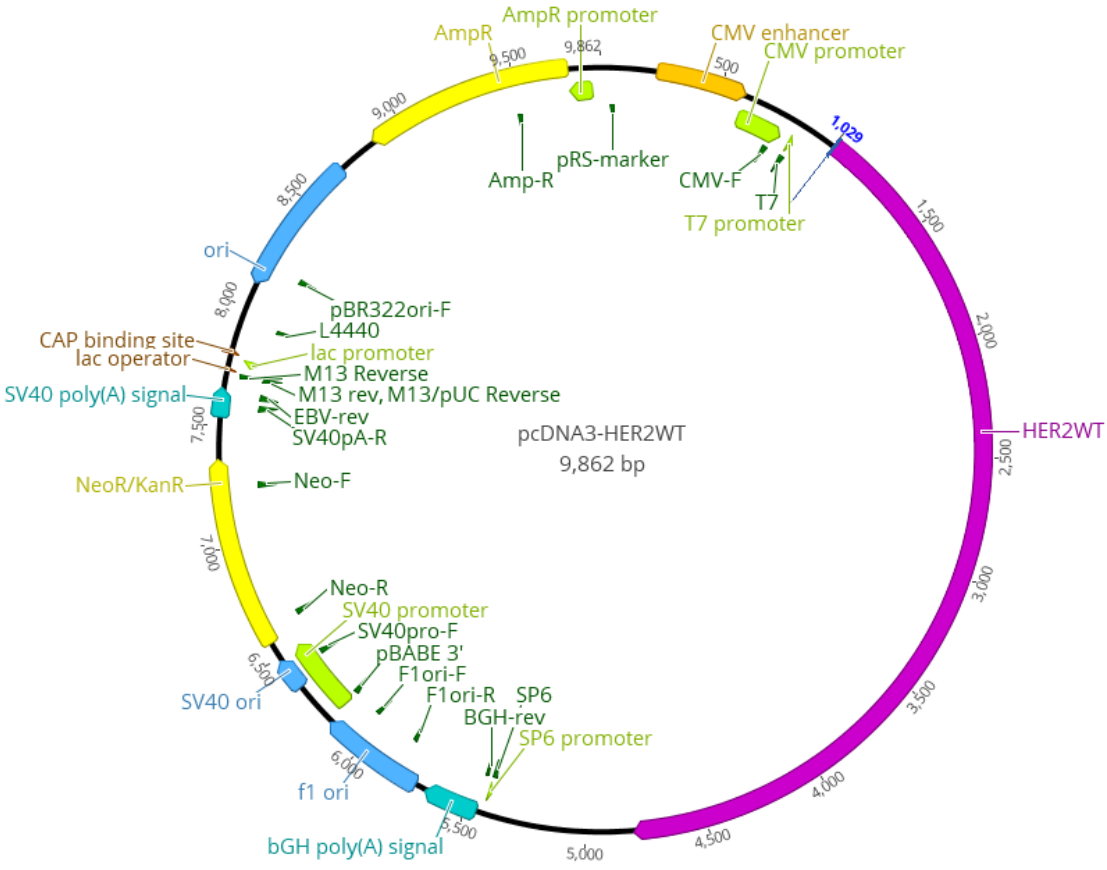

Appendix B

**Sequence of pcDNA3-HER2WT as downloaded from Addgene**

https://www.addgene.org/browse/sequence/43248/

GACGGATCGGGAGATCTCCCGATCCCCTATGGTGCACTCTCAGTACAATCTG
CTCTGATGCCGCATAGTTAAGCCAGTATCTGCTCCCTGCTTGTGTGTTGGAG
GTCGCTGAGTAGTGCGCGAGCAAAATTTAAGCTACAACAAGGCAAGGCTTG
ACCGACAATTGCATGAAGAATCTGCTTAGGGTTAGGCGTTTTGCGCTGCTTC
GCGATGTACGGGCCAGATATACGCGTTGACATTGATTATTGACTAGTTATTA
ATAGTAATCAATTACGGGGTCATTAGTTCATAGCCCATATATGGAGTTCCGC
GTTACATAACTTACGGTAAATGGCCCGCCTGGCTGACCGCCCAACGACCCC
CGCCCATTGACGTCAATAATGACGTATGTTCCCATAGTAACGCCAATAGGG
ACTTTCCATTGACGTCAATGGGTGGAGTATTTACGGTAAACTGCCCACTTGG
CAGTACATCAAGTGTATCATATGCCAAGTACGCCCCCTATTGACGTCAATGA
CGGTAAATGGCCCGCCTGGCATTATGCCCAGTACATGACCTTATGGGACTTT
CCTACTTGGCAGTACATCTACGTATTAGTCATCGCTATTACCATGGTGATGC
GGTTTTGGCAGTACATCAATGGGCGTGGATAGCGGTTTGACTCACGGGGAT
TTCCAAGTCTCCACCCCATTGACGTCAATGGGAGTTTGTTTTGGCACCAAAA
TCAACGGGACTTTCCAAAATGTCGTAACAACTCCGCCCCATTGACGCAAAT
GGGCGGTAGGCGTGTACGGTGGGAGGTCTATATAAGCAGAGCTCTCTGGCT
AACTAGAGAACCCACTGCTTACTGGCTTATCGAAATTAATACGACTCACTAT
AGGGAGACCCAAGCTTGGGGCAGCCGCGCGCCCCTTCCCACGGGGCCCTTT
ACTGCGCCGCGCGCCCGGCCCCCACCCCTCGCAGCACCCCGCGCCCCGCGC
CCTCCCAGCCGGGTCCAGCCGGAGCCATGGGGCCGGAGCCGCAGTGAGCAC
CATGGAGCTGGCGGCCTTGTGCCGCTGGGGGCTCCTCCTCGCCCTCTTGCCC
CCCGGAGCCGCGAGCACCCAAGTGTGCACCGGCACAGACATGAAGCTGCGG
CTCCCTGCCAGTCCCGAGACCCACCTGGACATGCTCCGCCACCTCTACCAGG
GCTGCCAGGTGGTGCAGGGAAACCTGGAACTCACCTACCTGCCCACCAATG
CCAGCCTGTCCTTCCTGCAGGATATCCAGGAGGTGCAGGGCTACGTGCTCAT
CGCTCACAACCAAGTGAGGCAGGTCCCACTGCAGAGGCTGCGGATTGTGCG
AGGCACCCAGCTCTTTGAGGACAACTATGCCCTGGCCGTGCTAGACAATGG
AGACCCGCTGAACAATACCACCCCTGTCACAGGGGCCTCCCCAGGAGGCCT
GCGGGAGCTGCAGCTTCGAAGCCTCACAGAGATCTTGAAAGGAGGGGTCTT
GATCCAGCGGAACCCCCAGCTCTGCTACCAGGACACGATTTTGTGGAAGGA
CATCTTCCACAAGAACAACCAGCTGGCTCTCACACTGATAGACACCAACCG
CTCTCGGGCCTGCCACCCCTGTTCTCCGATGTGTAAGGGCTCCCGCTGCTGG
GGAGAGAGTTCTGAGGATTGTCAGAGCCTGACGCGCACTGTCTGTGCCGGT
GGCTGTGCCCGCTGCAAGGGGCCACTGCCCACTGACTGCTGCCATGAGCAG
TGTGCTGCCGGCTGCACGGGCCCCAAGCACTCTGACTGCCTGGCCTGCCTCC
ACTTCAACCACAGTGGCATCTGTGAGCTGCACTGCCCAGCCCTGGTCACCTA
CAACACAGACACGTTTGAGTCCATGCCCAATCCCGAGGGCCGGTATACATT
CGGCGCCAGCTGTGTGACTGCCTGTCCCTACAACTACCTTTCTACGGACGTG
GGATCCTGCACCCTCGTCTGCCCCCTGCACAACCAAGAGGTGACAGCAGAG
GATGGAACACAGCGGTGTGAGAAGTGCAGCAAGCCCTGTGCCCGAGTGTGC
TATGGTCTGGGCATGGAGCACTTGCGAGAGGTGAGGGCAGTTACCAGTGCC

AATATCCAGGAGTTTGCTGGCTGCAAGAAGATCTTTGGGAGCCTGGCATTTC
TGCCGGAGAGCTTTGATGGGGACCCAGCCTCCAACACTGCCCCGCTCCAGC
CAGAGCAGCTCCAAGTGTTTGAGACTCTGGAAGAGATCACAGGTTACCTAT
ACATCTCAGCATGGCCGGACAGCCTGCCTGACCTCAGCGTCTTCCAGAACCT
GCAAGTAATCCGGGGACGAATTCTGCACAATGGCGCCTACTCGCTGACCCT
GCAAGGGCTGGGCATCAGCTGGCTGGGGCTGCGCTCACTGAGGGAACTGGG
CAGTGGACTGGCCCTCATCCACCATAACACCCACCTCTGCTTCGTGCACACG
GTGCCCTGGGACCAGCTCTTTCGGAACCCGCACCAAGCTCTGCTCCACACTG
CCAACCGGCCAGAGGACGAGTGTGTGGGCGAGGGCCTGGCCTGCCACCAGC
TGTGCGCCCGAGGGCACTGCTGGGGTCCAGGGCCCACCCAGTGTGTCAACT
GCAGCCAGTTCCTTCGGGGCCAGGAGTGCGTGGAGGAATGCCGAGTACTGC
AGGGGCTCCCCAGGGAGTATGTGAATGCCAGGCACTGTTTGCCGTGCCACC
CTGAGTGTCAGCCCCAGAATGGCTCAGTGACCTGTTTTGGACCGGAGGCTG
ACCAGTGTGTGGCCTGTGCCCACTATAAGGACCCTCCCTTCTGCGTGGCCCG
CTGCCCCAGCGGTGTGAAACCTGACCTCTCCTACATGCCCATCTGGAAGTTT
CCAGATGAGGAGGGCGCATGCCAGCCTTGCCCCATCAACTGCACCCACTCC
TGTGTGGACCTGGATGACAAGGGCTGCCCCGCCGAGCAGAGAGCCAGCCCT
CTGACGTCCATCATCTCTGCGGTGGTTGGCATTCTGCTGGTCGTGGTCTTGG
GGGTGGTCTTTGGGATCCTCATCAAGCGACGGCAGCAGAAGATCCGGAAGT
ACACGATGCGGAGACTGCTGCAGGAAACGGAGCTGGTGGAGCCGCTGACA
CCTAGCGGAGCGATGCCCAACCAGGCGCAGATGCGGATCCTGAAAGAGAC
GGAGCTGAGGAAGGTGAAGGTGCTTGGATCTGGCGCTTTTGGCACAGTCTA
CAAGGGCATCTGGATCCCTGATGGGGAGAATGTGAAAATTCCAGTGGCCAT
CAAAGTGTTGAGGGAAAACACATCCCCCAAAGCCAACAAAGAAATCTTAGA
CGAAGCATACGTGATGGCTGGTGTGGGCTCCCCATATGTCTCCCGCCTTCTG
GGCATCTGCCTGACATCCACGGTGCAGCTGGTGACACAGCTTATGCCCTATG
GCTGCCTCTTAGACCATGTCCGGGAAAACCGCGGACGCCTGGGCTCCCAGG
ACCTGCTGAACTGGTGTATGCAGATTGCCAAGGGGATGAGCTACCTGGAGG
ATGTGCGGCTCGTACACAGGGACTTGGCCGCTCGGAACGTGCTGGTCAAGA
GTCCCAACCATGTCAAAATTACAGACTTCGGGCTGGCTCGGCTGCTGGACAT
TGACGAGACAGAGTACCATGCAGATGGGGGCAAGGTGCCCATCAAGTGGAT
GGCGCTGGAGTCCATTCTCCGCCGGCGGTTCACCCACCAGAGTGATGTGTG
GAGTTATGGTGTGACTGTGTGGGAGCTGATGACTTTTGGGGCCAAACCTTAC
GATGGGATCCCAGCCCGGGAGATCCCTGACCTGCTGGAAAAGGGGGAGCG
GCTGCCCCAGCCCCCCATCTGCACCATTGATGTCTACATGATCATGGTCAAA
TGTTGGATGATTGACTCTGAATGTCGGCCAAGATTCCGGGAGTTGGTGTCTG
AATTCTCCCGCATGGCCAGGGACCCCCAGCGCTTTGTGGTCATCCAGAATGA
GGACTTGGGCCCAGCCAGTCCCTTGGACAGCACCTTCTACCGCTCACTGCTG
GAGGACGATGACATGGGGGACCTGGTGGATGCTGAGGAGTATCTGGTACCC
CAGCAGGGCTTCTTCTGTCCAGACCCTGCCCCGGGCGCTGGGGGCATGGTCC
ACCACAGGCACCGCAGCTCATCTACCAGGAGTGGCGGTGGGGACCTGACAC
TAGGGCTGGAGCCCTCTGAAGAGGAGGCCCCCAGGTCTCCACTGGCACCCT
CCGAAGGGGCTGGCTCCGATGTATTTGATGGTGACCTGGGAATGGGGGCAG
CCAAGGGGCTGCAAAGCCTCCCCACACATGACCCCAGCCCTCTACAGCGGT
ACAGTGAGGACCCCACAGTACCCCTGCCCTCTGAGACTGATGGCTACGTTG
CCCCCCTGACCTGCAGCCCCCAGCCTGAATATGTGAACCAGCCAGATGTTCG
GCCCCAGCCCCCTTCGCCCCGAGAGGGCCCTCTGCCTGCTGCCCGACCTGCT
GGTGCCACTCTGGAAAGGCCCAAGACTCTCTCCCCAGGGAAGAATGGGGTC

GTCAAAGACGTTTTTGCCTTTGGGGGTGCCGTGGAGAACCCCGAGTACTTGA
CACCCCAGGGAGGAGCTGCCCCTCAGCCCCACCCTCCTCCTGCCTTCAGCCC
AGCCTTCGACAACCTCTATTACTGGGACCAGGACCCACCAGAGCGGGGGGC
TCCACCCAGCACCTTCAAAGGGACACCTACGGCAGAGAACCCAGAGTACCT
GGGTCTGGACGTGCCAGTGTGAACCAGAAGGCCAAGTCCGCAGAAGCCCTG
ATGTGTCCTCAGGGAGCAGGGAAGGCCTGACTTCTGCTGGCATCAAGAGGT
GGGAGGGCCCTCCGACCACTTCCAGGGGAACCTGCCATGCCAGGAACCTGT
CCTAAGGAACCTTCCTTCCTGCTTGAGTTCCCAGATGGCTGGAAGGGGTCCA
GCCTCGTTGGAAGAGGAACAGCACTGGGGAGTCTTTGTGGATTCTGAGGCC
CTGCCCAATGAGACTCTAGGGTCCAGTGGATGCCACAGCCCAGCTTGGCCC
TTTCCTTCCAGATCCTGGGTACTGAAAGCCTTAGGGAAGCTGGCCTGAGAG
GGGAAGCGGCCCTAAGGGAGTGTCTAAGAACAAAAGCGACCCATTCAGAG
ACTGTCCCTGAAACCTAGTACTGCCCCCCATGAGGAAGGAACAGCAATGGT
GTCAGTATCCAGGCTTTGTACAGAGTGCTTTTCTGTTTAGTTTTTACTTTTTT
TGTTTTGTTTTTTTCAAGCTTGGTACCGAGCTCGGATCCACTAGTAACGGCC
GCCAGTGTGCTGGAATTCTGCAGATATCCATCACACTGGCGGCCGCTCGAG
CATGCATCTAGAGGGCCCTATTCTATAGTGTCACCTAAATGCTAGAGCTCGC
TGATCAGCCTCGACTGTGCCTTCTAGTTGCCAGCCATCTGTTGTTTGCCCCTC
CCCCGTGCCTTCCTTGACCCTGGAAGGTGCCACTCCCACTGTCCTTTCCTAAT
AAAATGAGGAAATTGCATCGCATTGTCTGAGTAGGTGTCATTCTATTCTGGG
GGGTGGGGTGGGGCAGGACAGCAAGGGGGAGGATTGGGAAGACAATAGCA
GGCATGCTGGGGATGCGGTGGGCTCTATGGCTTCTGAGGCGGAAAGAACCA
GCTGGGGCTCTAGGGGGTATCCCCACGCGCCCTGTAGCGGCGCATTAAGCG
CGGCGGGTGTGGTGGTTACGCGCAGCGTGACCGCTACACTTGCCAGCGCCC
TAGCGCCCGCTCCTTTCGCTTTCTTCCCTTCCTTTCTCGCCACGTTCGCCGGC
TTTCCCCGTCAAGCTCTAAATCGGGGGCTCCCTTTAGGGTTCCGATTTAGTG
CTTTACGGCACCTCGACCCCAAAAAACTTGATTAGGGTGATGGTTCACGTAG
TGGGCCATCGCCCTGATAGACGGTTTTTCGCCCTTTGACGTTGGAGTCCACG
TTCTTTAATAGTGGACTCTTGTTCCAAACTGGAACAACACTCAACCCTATCT
CGGTCTATTCTTTTGATTTATAAGGGATTTTGCCGATTTCGGCCTATTGGTTA
AAAAATGAGCTGATTTAACAAAAATTTAACGCGAATTAATTCTGTGGAATG
TGTGTCAGTTAGGGTGTGGAAAGTCCCCAGGCTCCCCAGCAGGCAGAAGTA
TGCAAAGCATGCATCTCAATTAGTCAGCAACCAGGTGTGGAAAGTCCCCAG
GCTCCCCAGCAGGCAGAAGTATGCAAAGCATGCATCTCAATTAGTCAGCAA
CCATAGTCCCGCCCCTAACTCCGCCCATCCCGCCCCTAACTCCGCCCAGTTC
CGCCCATTCTCCGCCCCATGGCTGACTAATTTTTTTTATTTATGCAGAGGCCG
AGGCCGCCTCTGCCTCTGAGCTATTCCAGAAGTAGTGAGGAGGCTTTTTTGG
AGGCCTAGGCTTTTGCAAAAAGCTCCCGGGAGCTTGTATATCCATTTTCGGA
TCTGATCAAGAGACAGGATGAGGATCGTTTCGCATGATTGAACAAGATGGA
TTGCACGCAGGTTCTCCGGCCGCTTGGGTGGAGAGGCTATTCGGCTATGACT
GGGCACAACAGACAATCGGCTGCTCTGATGCCGCCGTGTTCCGGCTGTCAG
CGCAGGGGCGCCCGGTTCTTTTTGTCAAGACCGACCTGTCCGGTGCCCTGAA
TGAACTGCAGGACGAGGCAGCGCGGCTATCGTGGCTGGCCACGACGGGCGT
TCCTTGCGCAGCTGTGCTCGACGTTGTCACTGAAGCGGGAAGGGACTGGCT
GCTATTGGGCGAAGTGCCGGGGCAGGATCTCCTGTCATCTCACCTTGCTCCT
GCCGAGAAAGTATCCATCATGGCTGATGCAATGCGGCGGCTGCATACGCTT
GATCCGGCTACCTGCCCATTCGACCACCAAGCGAAACATCGCATCGAGCGA
GCACGTACTCGGATGGAAGCCGGTCTTGTCGATCAGGATGATCTGGACGAA

GAGCATCAGGGGCTCGCGCCAGCCGAACTGTTCGCCAGGCTCAAGGCGCGC
ATGCCCGACGGCGAGGATCTCGTCGTGACCCATGGCGATGCCTGCTTGCCG
AATATCATGGTGGAAAATGGCCGCTTTTCTGGATTCATCGACTGTGGCCGGC
TGGGTGTGGCGGACCGCTATCAGGACATAGCGTTGGCTACCCGTGATATTG
CTGAAGAGCTTGGCGGCGAATGGGCTGACCGCTTCCTCGTGCTTTACGGTAT
CGCCGCTCCCGATTCGCAGCGCATCGCCTTCTATCGCCTTCTTGACGAGTTC
TTCTGAGCGGGACTCTGGGGTTCGAAATGACCGACCAAGCGACGCCCAACC
TGCCATCACGAGATTTCGATTCCACCGCCGCCTTCTATGAAAGGTTGGGCTT
CGGAATCGTTTTCCGGGACGCCGGCTGGATGATCCTCCAGCGCGGGGATCT
CATGCTGGAGTTCTTCGCCCACCCCAACTTGTTTATTGCAGCTTATAATGGTT
ACAAATAAAGCAATAGCATCACAAATTTCACAAATAAAGCATTTTTTTCACT
GCATTCTAGTTGTGGTTTGTCCAAACTCATCAATGTATCTTATCATGTCTGTA
TACCGTCGACCTCTAGCTAGAGCTTGGCGTAATCATGGTCATAGCTGTTTCC
TGTGTGAAATTGTTATCCGCTCACAATTCCACACAACATACGAGCCGGAAG
CATAAAGTGTAAAGCCTGGGGTGCCTAATGAGTGAGCTAACTCACATTAAT
TGCGTTGCGCTCACTGCCCGCTTTCCAGTCGGGAAACCTGTCGTGCCAGCTG
CATTAATGAATCGGCCAACGCGCGGGGAGAGGCGGTTTGCGTATTGGGCGC
TCTTCCGCTTCCTCGCTCACTGACTCGCTGCGCTCGGTCGTTCGGCTGCGGC
GAGCGGTATCAGCTCACTCAAAGGCGGTAATACGGTTATCCACAGAATCAG
GGGATAACGCAGGAAAGAACATGTGAGCAAAAGGCCAGCAAAAGGCCAGG
AACCGTAAAAAGGCCGCGTTGCTGGCGTTTTTCCATAGGCTCCGCCCCCCTG
ACGAGCATCACAAAAATCGACGCTCAAGTCAGAGGTGGCGAAACCCGACA
GGACTATAAAGATACCAGGCGTTTCCCCCTGGAAGCTCCCTCGTGCGCTCTC
CTGTTCCGACCCTGCCGCTTACCGGATACCTGTCCGCCTTTCTCCCTTCGGGA
AGCGTGGCGCTTTCTCATAGCTCACGCTGTAGGTATCTCAGTTCGGTGTAGG
TCGTTCGCTCCAAGCTGGGCTGTGTGCACGAACCCCCCGTTCAGCCCGACCG
CTGCGCCTTATCCGGTAACTATCGTCTTGAGTCCAACCCGGTAAGACACGAC
TTATCGCCACTGGCAGCAGCCACTGGTAACAGGATTAGCAGAGCGAGGTAT
GTAGGCGGTGCTACAGAGTTCTTGAAGTGGTGGCCTAACTACGGCTACACT
AGAAGAACAGTATTTGGTATCTGCGCTCTGCTGAAGCCAGTTACCTTCGGAA
AAAGAGTTGGTAGCTCTTGATCCGGCAAACAAACCACCGCTGGTAGCGGTG
GTTTTTTTGTTTGCAAGCAGCAGATTACGCGCAGAAAAAAAGGATCTCAAG
AAGATCCTTTGATCTTTTCTACGGGGTCTGACGCTCAGTGGAACGAAAACTC
ACGTTAAGGGATTTTGGTCATGAGATTATCAAAAAGGATCTTCACCTAGATC
CTTTTAAATTAAAAATGAAGTTTTAAATCAATCTAAAGTATATATGAGTAAA
CTTGGTCTGACAGTTACCAATGCTTAATCAGTGAGGCACCTATCTCAGCGAT
CTGTCTATTTCGTTCATCCATAGTTGCCTGACTCCCCGTCGTGTAGATAACTA
CGATACGGGAGGGCTTACCATCTGGCCCCAGTGCTGCAATGATACCGCGAG
ACCCACGCTCACCGGCTCCAGATTTATCAGCAATAAACCAGCCAGCCGGAA
GGGCCGAGCGCAGAAGTGGTCCTGCAACTTTATCCGCCTCCATCCAGTCTAT
TAATTGTTGCCGGGAAGCTAGAGTAAGTAGTTCGCCAGTTAATAGTTTGCGC
AACGTTGTTGCCATTGCTACAGGCATCGTGGTGTCACGCTCGTCGTTTGGTA
TGGCTTCATTCAGCTCCGGTTCCCAACGATCAAGGCGAGTTACATGATCCCC
CATGTTGTGCAAAAAAGCGGTTAGCTCCTTCGGTCCTCCGATCGTTGTCAGA
AGTAAGTTGGCCGCAGTGTTATCACTCATGGTTATGGCAGCACTGCATAATT
CTCTTACTGTCATGCCATCCGTAAGATGCTTTTCTGTGACTGGTGAGTACTC
AACCAAGTCATTCTGAGAATAGTGTATGCGGCGACCGAGTTGCTCTTGCCCG
GCGTCAATACGGGATAATACCGCGCCACATAGCAGAACTTTAAAAGTGCTC

ATCATTGGAAAACGTTCTTCGGGGCGAAAACTCTCAAGGATCTTACCGCTGT
TGAGATCCAGTTCGATGTAACCCACTCGTGCACCCAACTGATCTTCAGCATC
TTTTACTTTCACCAGCGTTTCTGGGTGAGCAAAAACAGGAAGGCAAAATGC
CGCAAAAAAGGGAATAAGGGCGACACGGAAATGTTGAATACTCATACTCTT
CCTTTTTCAATATTATTGAAGCATTTATCAGGGTTATTGTCTCATGAGCGGAT
ACATATTTGAATGTATTTAGAAAAATAAACAAATAGGGGTTCCGCGCACAT
TTCCCCGAAAAGTGCCACCTGAG

Sequence of human HER2

Appendix C

**Vector map of pSIN-SFFV-luc2.1** (from Kam Zaki)

annotated with Geneious

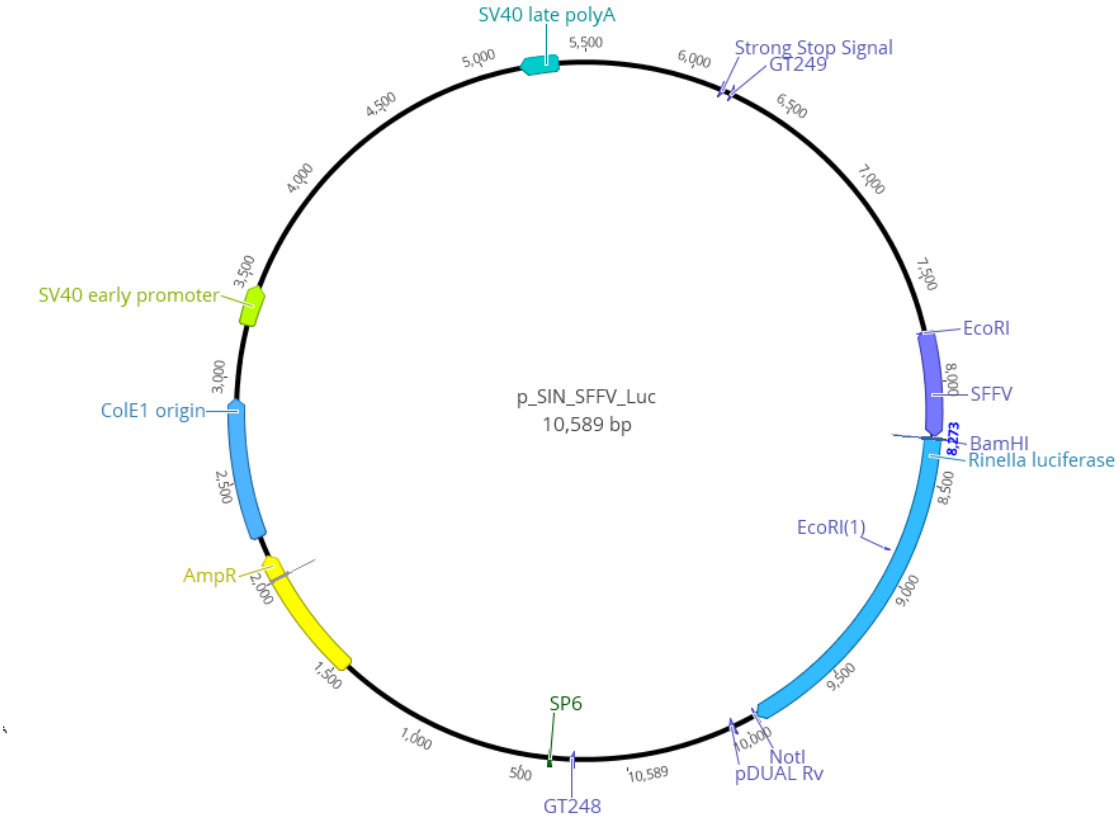

Appendix D

**Sequence of pSIN-SFFV-luc2.1** as received from Kam Zaki

TCGAGGGAATTAATTCGAGCTCGGTACCTTTAAGACCAATGACTTACAAGN
TGCAGCTGTAGATCTTAGCCACTTTTTAAAAGAAAAGGGGGGACTGGAAGG
GCTAATTCACTCCCAACGAAGACAAGATCTGCTTTTTGCTTGTACTGGGTCT
CTCTGGTTAGACCAGATCTGAGCCTGGGAGCTCTCTGGCTAACTAGGGAAC
CCACTGCTTAAGCCTCAATAAAGCTTGCCTTGAGTGCTTCAAGTAGTGTGTG
CCCGTCTGTTGTGTGACTCTGGTAACTAGAGATCCCTCAGACCCTTTTAGTC
AGTGTGGAAAATCTCTAGCAGCATCTAGAATTAATTCCGTGTATTCTATAGT
GTCACCTAAATCGTATGTGTATGATACATAAGGTTATGTATTAATTGTAGCC
GCGTTCTAACGACAATATGTACAAGCCTAATTGTGTAGCATCTGGCTTACTG
AAGCAGACCCTATCATCTCTCTCGTAAACTGCCGTCAGAGTCGGTTTGGTTG
GACGAACCTTCTGAGTTTCTGGTAACGCCGTCCCGCACCCGGAAATGGTCA
GCGAACCAATCAGCAGGGTCATCGCTAGCCAGATCCTCTACGCCGGACGCA
TCGTGGCCGGCATCACCGGCGCCACAGGTGCGGTTGCTGGCGCCTATATCG
CCGACATCACCGATGGGGAAGATCGGGCTCGCCACTTCGGGCTCATGAGCG
CTTGTTTCGGCGTGGGTATGGTGGCAGGCCCCGTGGCCGGGGGACTGTTGG
GCGCCATCTCCTTGCATGCACCATTCCTTGCGGCGGCGGTGCTCAACGGCCT
CAACCTACTACTGGGCTGCTTCCTAATGCAGGAGTCGCATAAGGGAGAGCG
TCGAATGGTGCACTCTCAGTACAATCTAGCTCTGATGCCGCATAGTTAAGCC
AGCCCCGACACCCGCCAACACCCGCTGACGCGCCCTGACGGGCTTGTCTGC
TCCCGGCATCCGCTTACAGACAAGCTGTGACCGTCTCCGGGAGCTGCATGTG
TCAGAGGTTTTCACCGTCATCACCGAAACGCGCGAGACGAAAGGGCCTCGT
GATACGCCTATTTTTATAGGTTAATGTCATGATAATAATGGTTTCTTAGACG
TCAGGTGGCACTTTTCGGGGAAATGTGCGCGGAACCCCTATTTGTTTATTTT
TCTAAATACATTCAAATATGTATCCGCTCATGAGACAATAACCCTGATAAAT
GCTTCAATAATATTGAAAAAGGAAGAGTATGAGTATTCAACATTTCCGTGTC
GCCCTTATTCCCTTTTTTGCGGCATTTTGCCTTCCTGTTTTTGCTCACCCAGA
AACGCTGGTGAAAGTAAAAGATGCTGAAGATCAGTTGGGTGCACGAGTGGG
TTACATCGAACTGGATCTCAACAGCGGTAAGATCCTTGAGAGTTTTCGCCCC

GAAGAACGTTTTCCAATGATGAGCACTTTTAAAGTTCTGCTATGTGGCGCGG
TATTATCCCGTATTGACGCCGGGCAAGAGCAACTCGGTCGCCGCATACACT
ATTCTCAGAATGACTTGGTTGAGTACTCACCAGTCACAGAAAAGCATCTTAC
GGATGGCATGACAGTAAGAGAATTATGCAGTGCTGCCATAACCATGAGTGA
TAACACTGCGGCCAACTTACTTCTGACAACGATCGGAGGACCGAAGGAGCT
AACCGCTTTTTTGCACAACATGGGGGATCATGTAACTCGCCTTGATCGTTGG
GAACCGGAGCTGAATGAAGCCATACCAAACGACGAGCGTGACACCACGAT
GCCTGTAGCAATGGCAACAACGTTGCGCAAACTATTAACTGGCGAACTACT
TACTCTAGCTTCCCGGCAACAATTAATAGACTGGATGGAGGCGGATAAAGT
TGCAGGACCACTTCTGCGCTCGGCCCTTCCGGCTGGCTGGTTTATTGCTGAT
AAATCTGGAGCCGGTGAGCGTGGGTCTCGCGGTATCATTGCAGCACTGGGG
CCAGATGGTAAGCCCTCCCGTATCGTAGTTATCTACACGACGGGGAGTCAG
GCAACTATGGATGAACGAAATAGACAGATCGCTGAGATAGGTGCCTCACTG
ATTAAGCATTGGTAACTGTCAGACCAAGTTTACTCATATATACTTTAGATTG
ATTTAAAACTTCATTTTTAATTTAAAAGGATCTAGGTGAAGATCCTTTTTGA
TAATCTCATGACCAAAATCCCTTAACGTGAGTTTTCGTTCCACTGAGCGTCA
GACCCCGTAGAAAAGATCAAAGGATCTTCTTGAGATCCTTTTTTTCTGCGCG
TAATCTGCTGCTTGCAAACAAAAAAACCACCGCTACCAGCGGTGGTTTGTTT
GCCGGATCAAGAGCTACCAACTCTTTTTCCGAAGGTAACTGGCTTCAGCAG
AGCGCAGATACCAAATACTGTCCTTCTAGTGTAGCCGTAGTTAGGCCACCAC
TTCAAGAACTCTGTAGCACCGCCTACATACCTCGCTCTGCTAATCCTGTTAC
CAGTGGCTGCTGCCAGTGGCGATAAGTCGTGTCTTACCGGGTTGGACTCAA
GACGATAGTTACCGGATAAGGCGCAGCGGTCGGGCTGAACGGGGGGTTCGT
GCACACAGCCCAGCTTGGAGCGAACGACCTACACCGAACTGAGATACCTAC
AGCGTGAGCTATGAGAAAGCGCCACGCTTCCCGAAGGGAGAAAGGCGGAC
AGGTATCCGGTAAGCGGCAGGGTCGGAACAGGAGAGCGCACGAGGGAGCT
TCCAGGGGGAAACGCCTGGTATCTTTATAGTCCTGTCGGGTTTCGCCACCTC
TGACTTGAGCGTCGATTTTTGTGATGCTCGTCAGGGGGGCGGAGCCTATGGA
AAAACGCCAGCAACGCGGCCTTTTTACGGTTCCTGGCCTTTTGCTGGCCTTT
TGCTCACATGTTCTTTCCTGCGTTATCCCCTGATTCTGTGGATAACCGTATTA
CCGCCTTTGAGTGAGCTGATACCGCTCGCCGCAGCCGAACGACCGAGCGCA
GCGAGTCAGTGAGCGAGGAAGCGGAAGAGCGCCCAATACGCAAACCGCCT

CTCCCCGCGCGTTGGCCGATTCATTAATGCAGCTGTGGAATGTGTGTCAGTT
AGGGTGTGGAAAGTCCCCAGGCTCCCCAGCAGGCAGAAGTATGCAAAGCAT
GCATCTCAATTAGTCAGCAACCAGGTGTGGAAAGTCCCCAGGCTCCCCAGC
AGGCAGAAGTATGCAAAGCATGCATCTCAATTAGTCAGCAACCATAGTCCC
GCCCCTAACTCCGCCCATCCCGCCCCTAACTCCGCCCAGTTCCGCCCATTCT
CCGCCCCATGGCTGACTAATTTTTTTTATTTATGCAGAGGCCGAGGCCGCCT
CGGCCTCTGAGCTATTCCAGAAGTAGTGAGGAGGCTTTTTTGGAGGCCTAG
GCTTTTGCAAAAAGCTTGGACACAAGACAGGCTTGCGAGATATGTTTGAGA
ATACCACTTTATCCCGCGTCAGGGAGAGGCAGTGCGTAAAAAGACGCGGAC
TCATGTGAAATACTGGTTTTTAGTGCGCCAGATCTCTATAATCTCGCGCAAC
CTATTTTCCCCTCGAACACTTTTTAAGCCGTAGATAAACAGGCTGGGACACT
TCACATGAGCGAAAAATACATCGTCACCTGGGACATGTTGCAGATCCATGC
ACGTAAACTCGCAAGCCGACTGATGCCTTCTGAACAATGGAAAGGCATTAT
TGCCGTAAGCCGTGGCGGTCTGTACCGGGTGCGTTACTGGCGCGTGAACTG
GGTATTCGTCATGTCGATACCGTTTGTATTTCCAGCTACGATCACGACAACC
AGCGCGAGCTTAAAGTGCTGAAACGCGCAGAAGGCGATGGCGAAGGCTTC
ATCGTTATTGATGACCTGGTGGATACCGGTGGTACTGCGGTTGCGATTCGTG
AAATGTATCCAAAAGCGCACTTTGTCACCATCTTCGCAAAACCGGCTGGTCG
TCCGCTGGTTGATGACTATGTTGTTGATATCCCGCAAGATACCTGGATTGAA
CAGCCGTGGGATATGGGCGTCGTATTCGTCCCGCCAATCTCCGGTCGCTAAT
CTTTTCAACGCCTGGCACTGCCGGGCGTTGTTCTTTTTAACTTCAGGCGGGTT
ACAATAGTTTCCAGTAAGTATTCTGGAGGCTGCATCCATGACACAGGCAAA
CCTGAGCGAAACCCTGTTCAAACCCCGCTTTAAACATCCTGAAACCTCGACG
CTAGTCCGCCGCTTTAATCACGGCGCACAACCGCCTGTGCAGTCGGCCCTTG
ATGGTAAAACCATCCCTCACTGGTATCGCATGATTAACCGTCTGATGTGGAT
CTGGCGCGGCATTGACCCACGCGAAATCCTCGACGTCCAGGCACGTATTGT
GATGAGCGATGCCGAACGTACCGACGATGATTTATACGATACGGTGATTGG
CTACCGTGGCGGCAACTGGATTTATGAGTGGGCCCCGGATCTTTGTGAAGG
AACCTTACTTCTGTGGTGTGACATAATTGGACAAACTACCTACAGAGATTTA
AAGCTCTAAGGTAAATATAAAATTTTTAAGTGTATAATGTGTTAAACTACTG
ATTCTAATTGTTTGTGTATTTTAGATTCCAACCTATGGAACTGATGAATGGG
AGCAGTGGTGGAATGCCTTTAATGAGGAAAACCTGTTTTGCTCAGAAGAAA

TGCCATCTAGTGATGATGAGGCTACTGCTGACTCTCAACATTCTACTCCTCC
AAAAAAGAAGAGAAAGGTAGAAGACCCCAAGGACTTTCCTTCAGAATTGCT
AAGTTTTTTGAGTCATGCTGTGTTTAGTAATAGAACTCTTGCTTGCTTTGCTA
TTTACACCACAAAGGAAAAAGCTGCACTGCTATACAAGAAAATTATGGAAA
AATATTCTGTAACCTTTATAAGTAGGCATAACAGTTATAATCATAACATACT
GTTTTTTCTTACTCCACACAGGCATAGAGTGTCTGCTATTAATAACTATGCTC
AAAAATTGTGTACCTTTAGCTTTTTAATTTGTAAAGGGGTTAATAAGGAATA
TTTGATGTATAGTGCCTTGACTAGAGATCATAATCAGCCATACCACATTTGT
AGAGGTTTTACTTGCTTTAAAAAACCTCCCACACCTCCCCCTGAACCTGAAA
CATAAAATGAATGCAATTGTTGTTGTTAACTTGTTTATTGCAGCTTATAATG
GTTACAAATAAAGCAATAGCATCACAAATTTCACAAATAAAGCATTTTTTTC
ACTGCATTCTAGTTGTGGTTTGTCCAAACTCATCAATGTATCTTATCATGTCT
GGATCAACTGGATAACTCAAGCTAACCAAAATCATCCCAAACTTCCCACCC
CATACCCTATTACCACTGCCAATTACCTAGTGGTTTCATTTACTCTAAACCTG
TGATTCCTCTGAATTATTTTCATTTTAAAGAAATTGTATTTGTTAAATATGTA
CTACAAACTTAGTAGTTGGAAGGGCTAATTCACTCCCAAAGAAGACAAGAT
ATCCTTGATCTGTGGATCTACCACACACAAGGCTACTTCCCTGATTAGCAGA
ACTACACACCAGGGCCAGGGGTCAGATATCCACTGACCTTTGGATGGTGCT
ACAAGCTAGTACCAGTTGAGCCAGATAAGGTAGAAGAGGCCAATAAAGGA
GAGAACACCAGCTTGTTACACCCTGTGAGCCTGCATGGGATGGATGACCCG
GAGAGAGAAGTGTTAGAGTGGAGGTTTGACAGCCGCCTAGCATTTCATCAC
GTGGCCCGAGAGCTGCATCCGGAGTACTTCAAGAACTGCTGATATCGAGCT
TGCTACAAGGGACTTTCCGCTGGGGACTTTCCAGGGAGGCGTGGCCTGGGC
GGGACTGGGGAGTGGCGAGCCCTCAGATCCTGCATATAAGCAGCTGCTTTT
TGCCTGTACTGGGTCTCTCTGGTTAGACCAGATCTGAGCCTGGGAGCTCTCT
GGCTAACTAGGGAACCCACTGCTTAAGCCTCAATAAAGCTTGCCTTGAGTG
CTTCAAGTAGTGTGTGCCCGTCTGTTGTGTGACTCTGGTAACTAGAGATCCC
TCAGACCCTTTTAGTCAGTGTGGAAAATCTCTAGCAGTGGCGCCCGAACAG
GGACTTGAAAGCGAAAGGGAAACCAGAGGAGCTCTCTCGACGCAGGACTC
GGCTTGCTGAAGCGCGCACGGCAAGAGGCGAGGGGCGGCGACTGGTGAGT
ACGCCAAAAATTTTGACTAGCGGAGGCTAGAAGGAGAGAGATGGGTGCGA
GAGCGTCAGTATTAAGCGGGGGAGAATTAGATCGCGATGGGAAAAAATTCG

GTTAAGGCCAGGGGGAAAGAAAAAATATAAATTAAAACATATAGTATGGG
CAAGCAGGGAGCTAGAACGATTCGCAGTTAATCCTGGCCTGTTAGAAACAT
CAGAAGGCTGTAGACAAATACTGGGACAGCTACAACCATCCCTTCAGACAG
GATCAGAAGAACTTAGATCATTATATAATACAGTAGCAACCCTCTATTGTGT
GCATCAAAGGATAGAGATAAAAGACACCAAGGAAGCTTTAGACAAGATAG
AGGAAGAGCAAAACAAAAGTAAGACCACCGCACAGCAAGCGGCCGGCCGC
TGATCTTCAGACCTGGACGATATATATGAGGGACAATTGGAGAAGTGAATT
ATATAAATATAAAGTAGTAAAAATTGAACCATTAGGAGTAGCACCCACCAA
GGCAAAGAGAAGAGTGGTGCAGAGAGAAAAAAGAGCAGTGGGAATAGGA
GCTTTGTTCCTTGGGTTCTTGGGAGCAGCAGGAAGCACTATGGGCGCAGCGT
CAATGACGCTGACGGTACAGGCCAGACAATTATTGTCTGGTATAGTGCAGC
AGCAGAACAATTTGCTGAGGGCTATTGAGGCGCAACAGCATCTGTTGCAAC
TCACAGTCTGGGGCATCAAGCAGCTCCAGGCAAGAATCCTGGCTGTGGAAA
GATACCTAAAGGATCAACAGCTCCTGGGGATTTGGGGTTGCTCTGGAAAAC
TCATTTGCACCACTGCTGTGCCTTGGAATGCTAGTTGGAGTAATAAATCTCT
GGAACAGATTTGGAATCACACGACCTGGATGGAGTGGGACAGAGAAATTA
ACAATTACACAAGCTTAATACACTCCTTAATTGAAGAATCGCAAAACCAGC
AAGAAAAGAATGAACAAGAATTATTGGAATTAGATAAATGGGCAAGTTTGT
GGAATTGGTTTAACATAACAAATTGGCTGTGGTATATAAAATTATTCATAAT
GATAGTAGGAGGCTTGGTAGGTTTAAGAATAGTTTTTGCTGTACTTTCTATA
GTGAATAGAGTTAGGCAGGGATATTCACCATTATCGTTTCAGACCCACCTCC
CAACCCCGAGGGGACCCGACAGGCCCGAAGGAATAGAAGAAGAAGGTGGA
GAGAGAGACAGAGACAGATCCATTCGATTAGTGAACGGATCTCGACGGTCG
CCAAATGGCAGTATTCATCCACAATTTTAAAAGAAAAGGGGGGATTGGCTG
GGGTACAGTGCAGGGGAAAGAATAGTAGACATAATAGCAACAGACATACA
AACTAAAGAATTACAAAAACAAATTACAAAAATTCAAAATTTTCGGGTTTA
TTACAGGGACAGCAGAGATCCAGTTTGGATCGATAAGCTTGATATCGAATT
CCTGCAGCCCCGATAAAATAAAAGATTTTATTTAGTCTCCAGAAAAAGGGG
GGAATGAAAGACCCCACCTGTAGGTTATGGCAAGCTAGCTGCAGTAACGCC
ATTATTGCAAGGCATGGAAAAATACCAAACCAAGAATAGAGAAGTTCAGAT
CAAGGGCGGGTACATGAAAATAGCTAACGTAGGGCCAAACAGGATATCTGC
GGTGAGCAGTTTCGGCCCCGGCCCGGGGCCAAGAACAGATGGTCACCGCAG

TTTCGGCCCCGGCCCGAGGCCAAGAGCAGATGGTCCCCAGATATGGCCCAA
CCCTCAGCAGTTTCTTAAGACCCATCAGATGTTTCCAGGCTCCCCCAAGGAC
CTGAAATGACCCTGCGCCTTATTTGAATTAACCAATCAGCCTGCTTCTCGCT
TCTGTTCGCGCGCTTCTGCTTCCCGAGCTCTATAAAAGAGCTCACAACCCCT
CACTCGGCGCGCCAGTCCTCCGACAGACTGAGTCGCCCGGGGGGGATCCAT
GGAAGACGCCAAAAACATAAAGAAAGGCCCGGCGCCATTCTATCCTCTAGA
GGATGGAACCGCTGGAGAGCAACTGCATAAGGCTATGAAGAGATACGCCCT
GGTTCCTGGAACAATTGCTTTTACAGATGCACATATCGAGGTGAACATCACG
TACGCGGAATACTTCGAAATGTCCGTTCGGTTGGCAGAAGCTATGAAACGA
TATGGGCTGAATACAAATCACAGAATCGTCGTATGCAGTGAAAACTCTCTTC
AATTCTTTATGCCGGTGTTGGGCGCGTTATTTATCGGAGTTGCAGTTGCGCC
CGCGAACGACATTTATAATGAACGTGAATTGCTCAACAGTATGAACATTTC
GCAGCCTACCGTAGTGTTTGTTTCCAAAAAGGGGTTGCAAAAAATTTTGAAC
GTGCAAAAAAAATTACCAATAATCCAGAAAATTATTATCATGGATTCTAAA
ACGGATTACCAGGGATTTCAGTCGATGTACACGTTCGTCACATCTCATCTAC
CTCCCGGTTTTAATGAATACGATTTTGTACCAGAGTCCTTTGATCGTGACAA
AACAATTGCACTGATAATGAATTCCTCTGGATCTACTGGGTTACCTAAGGGT
GTGGCCCTTCCGCATAGAACTGCCTGCGTCAGATTCTCGCATGCCAGAGATC
CTATTTTTGGCAATCAAATCATTCCGGATACTGCGATTTTAAGTGTTGTTCCA
TTCCATCACGGTTTTGGAATGTTTACTACACTCGGATATTTGATATGTGGATT
TCGAGTCGTCTTAATGTATAGATTTGAAGAAGAGCTGTTTTTACGATCCCTT
CAGGATTACAAAATTCAAAGTGCGTTGCTAGTACCAACCCTATTTTCATTCT
TCGCCAAAAGCACTCTGATTGACAAATACGATTTATCTAATTTACACGAAAT
TGCTTCTGGGGGCGCACCTCTTTCGAAAGAAGTCGGGGAAGCGGTTGCAAA
ACGCTTCCATCTTCCAGGGATACGACAAGGATATGGGCTCACTGAGACTAC
ATCAGCTATTCTGATTACACCCGAGGGGGATGATAAACCGGGCGCGGTCGG
TAAAGTTGTTCCATTTTTTGAAGCGAAGGTTGTGGATCTGGATACCGGGAAA
ACGCTGGGCGTTAATCAGAGAGGCGAATTATGTGTCAGAGGACCTATGATT
ATGTCCGGTTATGTAAACAATCCGGAAGCGACCAACGCCTTGATTGACAAG
GATGGATGGCTACATTCTGGAGACATAGCTTACTGGGACGAAGACGAACAC
TTCTTCATAGTTGACCGCTTGAAGTCTTTAATTAAATACAAAGGATATCAGG
TGGCCCCCGCTGAATTGGAATCGATATTGTTACAACACCCCAACATCTTCGA

CGCGGGCGTGGCAGGTCTTCCCGACGATGACGCCGGTGAACTTCCCGCCGC
CGTTGTTGTTTTGGAGCACGGAAAGACGATGACGGAAAAAGAGATCGTGGA
TTACGTCGCCAGTCAAGTAACAACCGCGAAAAAGTTGCGCGGAGGAGTTGT
GTTTGTGGACGAAGTACCGAAAGGTCTTACCGGAAAACTCGACGCAAGAAA
AATCAGAGAGATCCTCATAAAGGCCAAGAAGGGCGGAAAGTCCAAATTGT
AAGCGGCCGCGACTCTAGAGTCGACCTGCAGGCATGCAAGCTTGATATCAA
GCTTATCGATAATCAACCTCTGGATTACAAAATTTGTGAAAGATTGACTGGT
ATTCTTAACTATGTTGCTCCTTTTACGCTATGTGGATACGCTGCTTTAATGCC
TTTGTATCATGCTATTGCTTCCCGTATGGCTTTCATTTTCTCCTCCTTGTATAA
ATCCTGGTTGCTGTCTCTTTATGAGGAGTTGTGGCCCGTTGTCAGGCAACGT
GGCGTGGTGTGCACTGTGTTTGCTGACGCAACCCCCACTGGTTGGGGCATTG
CCACCACCTGTCAGCTCCTTTCCGGGACTTTCGCTTTCCCCCTCCCTATTGCC
ACGGCGGAACTCATCGCCGCCTGCCTTGCCCGCTGCTGGACAGGGGCTCGG
CTGTTGGGCACTGACAATTCCGTGGTGTTGTCGGGGAAATCATCGTCCTTTC
CTTGGCTGCTCGCCTGTGTTGCCACCTGGATTCTGCGCGGGACGTCCTTCTG
CTACGTCCCTTCGGCCCTCAATCCAGCGGACCTTCCTTCCCGCGGCCTGCTG
CCGGCTCTGCGGCCTCTTCCGCGTCTTCGCCTTCGCCCTCAGACGAGTCGGA
TCTCCCTTTGGGCCGCCTCCCCGCATCGATACCGTCGACC

SFFV promoter

Rinella luciferase insert

Appendix E

**Vector map of pVITRO1-Trastuzumab-IgG1/κ**

(Addgene plasmid # 61883; http://n2t.net/addgene:61883; RRID: Addgene_61883)

Sequence downloaded from

https://www.addgene.org/browse/sequence/212721/

and annotated with Geneious 10.2.3

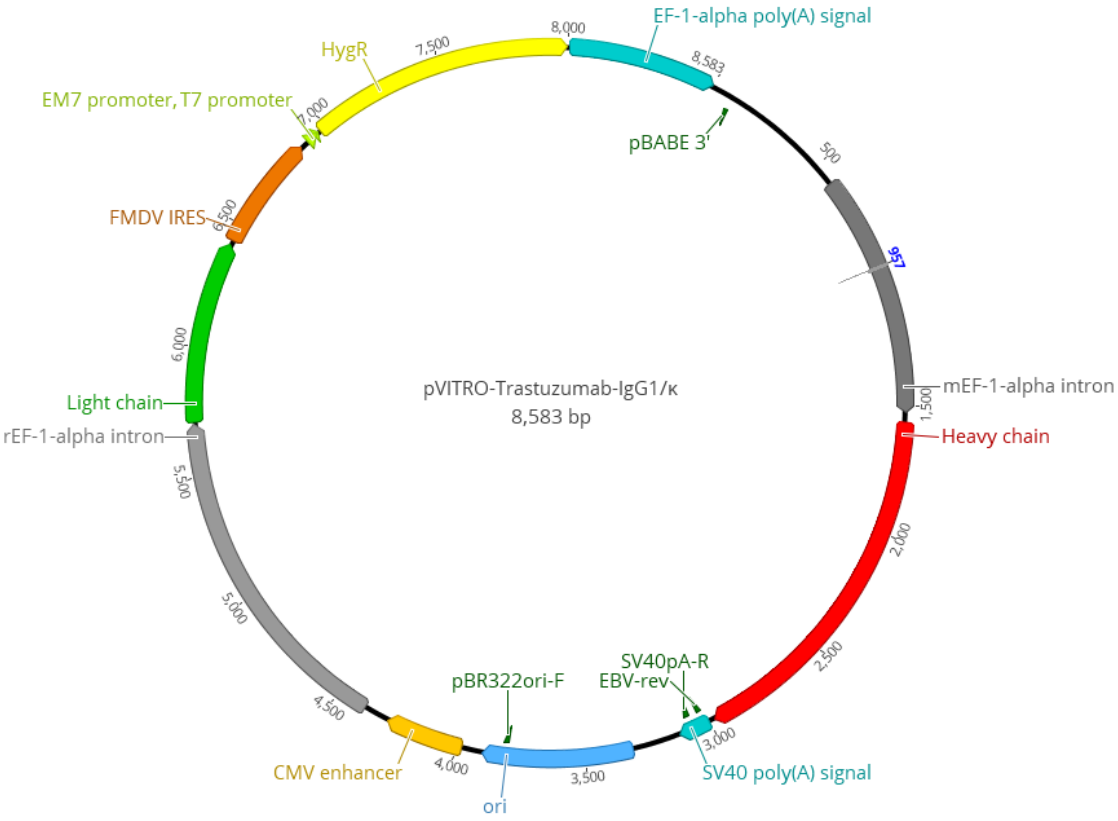

Appendix F

**Sequence of pVITRO plasmid encoding Trastuzumab IgG1/κ** as recovered from Addgene. Annotations illustrate changes we performed in the sequence

CCTGCAGGGCCTGAAATAACCTCTGAAAGAGGAACTTGGTTAGGTACCTTC
TGAGGCGGAAAGAACCAGCTGTGGAATGTGTGTCAGTTAGGGTGTGGAAAG
TCCCCAGGCTCCCCAGCAGGCAGAAGTATGCAAAGCATGCATCTCAATTAG
TCAGCAACCAGGTGTGGAAAGTCCCCAGGCTCCCCAGCAGGCAGAAGTATG
CAAAGCATGCATCTCAATTAGTCAGCAACCATAGTCCCACTAGTGGAGCCG
AGAGTAATTCATACAAAAGGAGGGATCGCCTTCGCAAGGGGAGAGCCCAG
GGACCGTCCCTAAATTCTCACAGACCCAAATCCCTGTAGCCGCCCCACGAC
AGCGCGAGGAGCATGCGCTCAGGGCTGAGCGCGGGGAGAGCAGAGCACAC
AAGCTCATAGACCCTGGTCGTGGGGGGGAGGACCGGGGAGCTGGCGCGGG
GCAAACTGGGAAAGCGGTGTCGTGTGCTGGCTCCGCCCTCTTCCCGAGGGT
GGGGGAGAACGGTATATAAGTGCGGCAGTCGCCTTGGACGTTCTTTTTCGC
AACGGGTTTGCCGTCAGAACGCAGGTGAGGGGCGGGTGTGGCTTCCGCGGG
CCGCCGAGCTGGAGGTCCTGCTCCGAGCGGGCCGGGCCCCGCTGTCGTCGG
CGGGGATTAGCTGCGAGCATTCCCGCTTCGAGTTGCGGGCGGCGCGGGAGG
CAGAGTGCGAGGCCTAGCGGCAACCCCGTAGCCTCGCCTCGTGTCCGGCTT
GAGGCCTAGCGTGGTGTCCGCGCCGCCGCCGCGTGCTACTCCGGCCGCACT
CTGGTCTTTTTTTTTTTTGTTGTTGTTGCCCTGCTGCCTTCGATTGCCGTTCAG
CAATAGGGGCTAACAAAGGGAGGGTGCGGGGCTTGCTCGCCCGGAGCCCG
GAGAGGTCATGGTTGGGGAGGAATGGAGGGACAGGAGTGGCGGCTGGGGC
CCGCCCGCCTTCGGAGCACATGTCCGACGCCACCTGGATGGGGCGAGGCCT
GGGGTTTTTCCCGAAGCAACCAGGCTGGGGTTAGCGTGCCGAGGCCATGTG
GCCCCAGCACCCGGCACGATCTGGCTTGGCGGCGCCGCGTTGCCCTGCCTCC
CTAACTAGGGTGAGGCCATCCCGTCCGGCACCAGTTGCGTGCGTGGAAAGA
TGGCCGCTCCCGGGCCCTGTTGCAAGGAGCTCAAAATGGAGGACGCGGCAG
CCCGGTGGAGCGGGCGGGTGAGTCACCCACACAAAGGAAGAGGGCCTGGT
CCCTCACCGGCTGCTGCTTCCTGTGACCCCGTGGTCCTATCGGCCGCAATAG

TCACCTCGGGCTTTTGAGCACGGCTAGTCGCGGCGGGGGGAGGGGATGTAA
TGGCGTTGGAGTTTGTTCACATTTGGTGGGTGGAGACTAGTCAGGCCAGCCT
GGCGCTGGAAGTCATTTTTGGAATTTGTCCCCTTGAGTTTTGAGCGGAGCTA
ATTCTCGGGCTTCTTAGCGGTTCAAAGGTATCTTTTAAACCCTTTTTTAGGTG
TTGTGAAAACCACCGCTAATTCAAAGCAACCGGTATGGACTGGACCTGGAG
GATCCTCTTCTTGGTGGCGGCCGCCACAGGCGCGCACTCCGAGGTGCAGCT
GGTGGAGTCTGGTGGTGGTCTTGTTCAACCTGGTGGTTCTCTTCGTCTTTCTT
GTGCTGCTTCTGGTTTTAATATTAAAGATACTTATATTCATTGGGTTCGTCAA
GCTCCTGGTAAAGGTCTTGAATGGGTTGCTCGTATTTATCCTACTAATGGTT
ATACTCGTTATGCTGATTCTGTTAAAGGTCGTTTTACTATTTCTGCTGATACT
TCTAAAAATACTGCTTATCTTCAAATGAACTCTCTTCGTGCTGAAGATACTG
CTGTTTATTATTGTTCTCGTTGGGGTGGTGATGGTTTTTATGCTATGGATTAT
TGGGGTCAAGGTACTCTTGTCACCGTCTCCTCAGCTAGCACCAAGGGCCCAT
CGGTCTTCCCCCTGGCACCCTCCTCCAAGAGCACCTCTGGGGGCACAGCGGC
CCTGGGCTGCCTGGTCAAGGACTACTTCCCCGAACCGGTGACGGTGTCGTG
GAACTCAGGCGCCCTGACCAGCGGCGTGCACACCTTCCCGGCTGTCCTACA
GTCCTCAGGACTCTACTCCCTCAGCAGCGTGGTGACCGTGCCCTCCAGCAGC
TTGGGCACCCAGACCTACATCTGCAACGTGAATCACAAGCCCAGCAACACC
AAGGTGGACAAGAAAGTTGAGCCCAAATCTTGTGACAAAACTCACACATGC
CCACCGTGCCCAGCACCTGAACTCCTGGGGGGACCGTCAGTCTTCCTCTTCC
CCCCAAAACCCAAGGACACCCTCATGATCTCCCGGACCCCTGAGGTCACAT
GCGTGGTGGTGGACGTGAGCCACGAAGACCCTGAGGTCAAGTTCAACTGGT
ACGTGGACGGCGTGGAGGTGCATAATGCCAAGACAAAGCCGCGGGAGGAG
CAGTACAACAGCACGTACCGGGTGGTCAGCGTCCTCACCGTCCTGCACCAG
GACTGGCTGAATGGCAAGGAGTACAAGTGCAAGGTCTCCAACAAAGCCCTC
CCAGCCCCCATCGAGAAAACCATCTCCAAAGCCAAAGGGCAGCCCCGAGAA
CCACAGGTGTACACCCTGCCCCCATCCCGGGATGAGCTGACCAAGAACCAG
GTCAGCCTGACCTGCCTGGTCAAAGGCTTCTATCCCAGCGACATCGCCGTGG
AGTGGGAGAGCAATGGGCAGCCGGAGAACAACTACAAGACCACGCCTCCC
GTGCTGGACTCCGACGGCTCCTTCTTCCTCTACAGCAAGCTCACCGTGGACA
AGAGCAGGTGGCAGCAGGGGAACGTCTTCTCATGCTCCGTGATGCATGAGG
CTCTGCACAACCACTACACGCAGAAGAGCCTCTCCCTGTCTCCGGGTAAA

- linker sequence - LL37 sequence TGA

AGATCTTGTACAGCTAGCTGGCCAGACATGATAAGATACATTGATGAGTTT
GGACAAACCACAACTAGAATGCAGTGAAAAAAATGCTTTATTTGTGAAATT
TGTGATGCTATTGCTTTATTTGTAACCATTATAAGCTGCAATAAACAAGTTA
ACAACAACAATTGCATTCATTTTATGTTTCAGGTTCAGGGGGAGGTGTGGGA
GGTTTTTTAAAGCAAGTAAAACCTCTACAAATGTGGTATGGAAATGTTAATT
AACTAGCCATGACCAAAATCCCTTAACGTGAGTTTTCGTTCCACTGAGCGTC
AGACCCCGTAGAAAAGATCAAAGGATCTTCTTGAGATCCTTTTTTTCTGCGC
GTAATCTGCTGCTTGCAAACAAAAAAACCACCGCTACCAGCGGTGGTTTGTT
TGCCGGATCAAGAGCTACCAACTCTTTTTCCGAAGGTAACTGGCTTCAGCAG
AGCGCAGATACCAAATACTGTTCTTCTAGTGTAGCCGTAGTTAGGCCACCAC
TTCAAGAACTCTGTAGCACCGCCTACATACCTCGCTCTGCTAATCCTGTTAC
CAGTGGCTGCTGCCAGTGGCGATAAGTCGTGTCTTACCGGGTTGGACTCAA
GACGATAGTTACCGGATAAGGCGCAGCGGTCGGGCTGAACGGGGGGTTCGT
GCACACAGCCCAGCTTGGAGCGAACGACCTACACCGAACTGAGATACCTAC
AGCGTGAGCTATGAGAAAGCGCCACGCTTCCCGAAGGGAGAAAGGCGGAC
AGGTATCCGGTAAGCGGCAGGGTCGGAACAGGAGAGCGCACGAGGGAGCT
TCCAGGGGGAAACGCCTGGTATCTTTATAGTCCTGTCGGGTTTCGCCACCTC
TGACTTGAGCGTCGATTTTTGTGATGCTCGTCAGGGGGGCGGAGCCTATGGA
AAAACGCCAGCAACGCGGCCTTTTTACGGTTCCTGGCCTTTTGCTGGCCTTT
TGCTCACATGTTCTTAATTAACCTGCAGGCGTTACATAACTTACGGTAAATG
GCCCGCCTGGCTGACCGCCCAACGACCCCCGCCCATTGACGTCAATAATGA
CGTATGTTCCCATAGTAACGCCAATAGGGACTTTCCATTGACGTCAATGGGT
GGAGTATTTACGGTAAACTGCCCACTTGGCAGTACATCAAGTGTATCATATG
CCAAGTACGCCCCCTATTGACGTCAATGACGGTAAATGGCCCGCCTGGCATT
ATGCCCAGTACATGACCTTATGGGACTTTCCTACTTGGCAGTACATCTACGT
ATTAGTCATCGCTATTACCATGATGATGCGGTTTTGGCAGTACATCAATGGG
CGTGGATAGCGGTTTGACTCACGGGGATTTCCAAGTCTCCACCCCATTGACG
TCAATGGGAGTTTGTTTTGACTAGTGGAGCCGAGAGTAATTCATACAAAAG
GAGGGATCGCCTTCGCAAGGGGAGAGCCCAGGGACCGTCCCTAAATTCTCA
CAGACCCAAATCCCTGTAGCCGCCCCACGACAGCGCGAGGAGCATGCGCCC
AGGGCTGAGCGCGGGTAGATCAGAGCACACAAGCTCACAGTCCCCGGCGGT

GGGGGGAGGGGCGCGCTGAGCGGGGGCCAGGGAGCTGGCGCGGGGCAAAC
TGGGAAAGTGGTGTCGTGTGCTGGCTCCGCCCTCTTCCCGAGGGTGGGGGA
GAACGGTATATAAGTGCGGTAGTCGCCTTGGACGTTCTTTTTCGCAACGGGT
TTGCCGTCAGAACGCAGGTGAGTGGCGGGTGTGGCTTCCGCGGGCCCCGGA
GCTGGAGCCCTGCTCTGAGCGGGCCGGGCTGATATGCGAGTGTCGTCCGCA
GGGTTTAGCTGTGAGCATTCCCACTTCGAGTGGCGGGCGGTGCGGGGGTGA
GAGTGCGAGGCCTAGCGGCAACCCCGTAGCCTCGCCTCGTGTCCGGCTTGA
GGCCTAGCGTGGTGTCCGCCGCCGCGTGCCACTCCGGCCGCACTATGCGTTT
TTTGTCCTTGCTGCCCTCGATTGCCTTCCAGCAGCATGGGCTAACAAAGGGA
GGGTGTGGGGCTCACTCTTAAGGAGCCCATGAAGCTTACGTTGGATAGGAA
TGGAAGGGCAGGAGGGGCGACTGGGGCCCGCCCGCCTTCGGAGCACATGTC
CGACGCCACCTGGATGGGGCGAGGCCTGTGGCTTTCCGAAGCAATCGGGCG
TGAGTTTAGCCTACCTGGGCCATGTGGCCCTAGCACTGGGCACGGTCTGGCC
TGGCGGTGCCGCGTTCCCTTGCCTCCCAACAAGGGTGAGGCCGTCCCGCCCG
GCACCAGTTGCTTGCGCGGAAAGATGGCCGCTCCCGGGGCCCTGTTGCAAG
GAGCTCAAAATGGAGGACGCGGCAGCCCGGTGGAGCGGGCGGGTGAGTCA
CCCACACAAAGGAAGAGGGCCTTGCCCCTCGCCGGCCGCTGCTTCCTGTGA
CCCCGTGGTCTATCGGCCGCATAGTCACCTCGGGCTTCTCTTGAGCACCGCT
CGTCGCGGCGGGGGGAGGGGATCTAATGGCGTTGGAGTTTGTTCACATTTG
GTGGGTGGAGACTAGTCAGGCCAGCCTGGCGCTGGAAGTCATTCTTGGAAT
TTGCCCCTTTGAGTTTGGAGCGAGGCTAATTCTCAAGCCTCTTAGCGGTTCA
AAGGTATTTTCTAAACCCGTTTCCAGGTGTTGTGAAAGCCACCGCTAATTCA
AAGCAATCCGGAATGTTGCCATCACAACTCATTGGGTTTCTGCTGCTCTGGG
TTCCAGCTAGCCGCGGTGACATCCAGATGACCCAGTCTCCTTCTTCTCTTTCT
GCTTCTGTTGGTGATCGTGTTACTATTACTTGTCGTGCTTCTCAAGATGTTAA
TACTGCTGTTGCTTGGTATCAACAAAAACCTGGTAAAGCTCCTAAACTTCTT
ATTTATTCTGCTTCTTTTCTTTATTCTGGTGTTCCTTCTCGTTTTTCTGGTTCTC
GTTCTGGTACTGATTTTACTCTTACTATTTCTTCTCTTCAACCTGAAGATTTT
GCTACTTATTATTGTCAACAACATTATACTACTCCTCCTACTTTTGGTCAAGG
TACCAAGCTGGAGATCAAACGTACGGTGGCGGCGCCATCTGTCTTCATCTTC
CCGCCATCTGATGAGCAGTTGAAATCTGGAACTGCCTCTGTTGTGTGCCTGC
TGAATAACTTCTATCCCAGAGAGGCCAAAGTACAGTGGAAGGTGGATAACG

CCCTCCAATCGGGTAACTCCCAGGAGAGTGTCACAGAGCAGGACAGCAAGG
ACAGCACCTACAGCCTCAGCAGCACCCTGACGCTGAGCAAAGCAGACTACG
AGAAACACAAAGTCTACGCCTGCGAAGTCACCCATCAGGGCCTGAGCTCGC
CC**GTC**ACAAAGAGCTTCAACAGGGGAGAGTGT**TAG**GGATCCCGTACGCCTA
GGAGCAGGTTTCCCCAATGACACAAAACGTGCAACTTGAAACTCCGCCTGG
TCTTTCCAGGTCTAGAGGGGTAACACTTTGTACTGCGTTTGGCTCCACGCTC
GATCCACTGGCGAGTGTTAGTAACAGCACTGTTGCTTCGTAGCGGAGCATG
ACGGCCGTGGGAACTCCTCCTTGGTAACAAGGACCCACGGGGCCAAAAGCC
ACGCCCACACGGGCCCGTCATGTGTGCAACCCCAGCACGGCGACTTTACTG
CGAAACCCACTTTAAAGTGACATTGAAACTGGTACCCACACACTGGTGACA
GGCTAAGGATGCCCTTCAGGTACCCCGAGGTAACACGCGACACTCGGGATC
TGAGAAGGGGACTGGGGCTTCTATAAAAGCGCTCGGTTTAAAAAGCTTCTA
TGCCTGAATAGGTGACCGGAGGTCGGCACCTTTCCTTTGCAATTACTGACCC
TATGAATACACTGACTGTTTGACAATTAATCATCGGCATAGTATATCGGCAT
AGTATAATACGACTCACTATAGGAGGGCCACCATGAAGAAACCTGAACTGA
CAGCAACTTCTGTTGAGAAGTTTCTCATTGAAAAATTTGATTCTGTTTCTGAT
CTCATGCAGCTGTCTGAAGGTGAAGAAAGCAGAGCCTTTTCTTTTGATGTTG
GAGGAAGAGGTTATGTTCTGAGGGTCAATTCTTGTGCTGATGGTTTTTACAA
AGACAGATATGTTTACAGACACTTTGCCTCTGCTGCTCTGCCAATTCCAGAA
GTTCTGGACATTGGAGAATTTTCTGAATCTCTCACCTACTGCATCAGCAGAA
GAGCACAAGGAGTCACTCTCCAGGATCTCCCTGAAACTGAGCTGCCAGCTG
TTCTGCAACCTGTTGCTGAAGCAATGGATGCCATTGCAGCAGCTGATCTGAG
CCAAACCTCTGGATTTGGTCCTTTTGGTCCCCAAGGCATTGGTCAGTACACC
ACTTGGAGGGATTTCATTTGTGCCATTGCTGATCCTCATGTCTATCACTGGC
AGACTGTGATGGATGACACAGTTTCTGCTTCTGTTGCTCAGGCACTGGATGA
ACTCATGCTGTGGGCAGAAGATTGTCCTGAAGTCAGACACCTGGTCCATGCT
GATTTTGGAAGCAACAATGTTCTGACAGACAATGGCAGAATCACTGCAGTC
ATTGACTGGTCTGAAGCCATGTTTGGAGATTCTCAATATGAGGTTGCCAACA
TTTTTTTTTGGAGACCTTGGCTGGCTTGCATGGAACAACAAACAAGATATTT
TGAAAGAAGACACCCAGAACTGGCTGGTTCCCCCAGACTGAGAGCCTACAT
GCTCAGAATTGGCCTGGACCAACTGTATCAATCTCTGGTTGATGGAAACTTT
GATGATGCTGCTTGGGCACAAGGAAGATGTGATGCCATTGTGAGGTCTGGT

GCTGGAACTGTTGGAAGAACTCAAATTGCAAGAAGGTCTGCTGCTGTTTGG
ACTGATGGATGTGTTGAAGTTCTGGCTGACTCTGGAAACAGGAGACCCTCC
ACAAGACCCAGAGCCAAGGAATGAATATTAGCTAGATTATCCCTAATACCT
GCCACCCCACTCTTAATCAGTGGTGGAAGAACGGTCTCAGAACTGTTTGTTT
CAATTGGCCATTTAAGTTTAGTAGTAAAAGACTGGTTAATGATAACAATGC
ATCGTAAAACCTTCAGAAGGAAAGGAGAATGTTTTGTGGACCACTTTGGTTT
TCTTTTTTGCGTGTGGCAGTTTTAAGTTATTAGTTTTTAAAATCAGTACTTTT
TAATGGAAACAACTTGACCAAAAATTTGTCACAGAATTTTGAGACCCATTA
AAAAAGTTAAATGAGAAACCTGTGTGTTCCTTTGGTCAACACCGAGACATTT
AGGTGAAAGACATCTAATTCTGGTTTTACGAATCTGGAAACTTCTTGAAAAT
GTAATTCTTGAGTTAACACTTCTGGGTGGAGAATAGGGTTGTTTTCCCCCCA
CATAATTGGAAGGGGAAGGAATATCATTTAAAGCTATGGGAGGGTTGCTTT
GATTACAACACTGGAGAGAAATGCAGCATGTTGCTGATTGCCTGTCACTAA
AACAGGCCAAAAACTGAGTCCTTGGGTTGCATAGAAAGCTG

**Legend**

Heavy chain sequence

Variable region exchanged to generate isotype controls

Linker sequence

LL37 sequence

Stop codon

Light chain sequence

Variable region exchanged to generate isotype controls

**Valine at position 205** (Kabat numbering) exchanged with Cysteine (codon TGT) to generate THIOMAB LC-V205C

Appendix G

**Sequences introduced in the pVITRO1-Trastuzumab-IgG1/κ to generate Trastuzumab-linker-LL37**

**LL37:**

Nucleotide sequence – 111bp:

CTGCTGGGTGATTTCTTCCGGAAATCTAAAGAGAAGATTGGCAAAGAGTTT AAAAGAATTGTCCAGAGAATCAAGGATTTTTTGCGGAATCTTGTACCCAGG ACAGAGTCC

Amino acid sequence (single letter amino acid code) – 37aa:

LLGDFFRKSKEKIGKEFKRIVQRIKDFLRNLVPRTES

**Linker sequences:**

1. Hinge region of human IgG2

Nucleotide sequence – 57bp:

GAGCGCAAATGTTGTGTCGAGTGCCCACCGTGCCCAGCACCACCTGTGGCA GGACCG

Amino acid sequence - 19aa: ERKCCVECPPCPAPPVAGP

2. G4S

Nucleotide sequence - 15bp: GGAGGTGGAGGTTGT

Amino acid sequence – 5aa: GGGGS

3. (G4S)x2

Nucleotide sequence – 30bp: GGTGGAGGCGGTTCAGGCGGAGGTGGCTCT

Amino acid sequence – 10aa: GGGGSGGGGS

4. (G4S)x3

Nucleotide sequence – 45bp:

GGTGGAGGCGGTTCAGGCGGAGGTGGCTCTGGCGGTGGCGGATCG

Amino acid sequence – 15aa: GGGGSGGGGSGGGGS

5. H1– LEAEAAAKALE

Nucleotide sequence – 33bp: CTGGAAGCTGAGGCAGCGGCCAAGGCCCTTGAG
Amino acid sequence – 11aa: LEAEAAAKALE

6. H2 – LEA$(EAAAK)_2$ALE

Nucleotide sequence - 48bp:
CTGGAAGCTGAGGCAGCGGCCAAGGAAGCTGCAGCCAAGGCCCTTGAG
Amino acid sequence - 16aa: LEAEAAAKEAAAKALE

7. H3 – LEA$(EAAAK)_3$ALE

Nucleotide sequence - 60bp:
CTGGAGGCCGAGGCCGCCGCCAAGGAGGCCGCCGCCAAGGAGGCCGCCGC
CAAGCTGGAG
Amino acid sequence - 20aa: LEAEAAAKEAAAKEAAAKLE

8. H4 – LEA$(EAAAK)_4$ALE

Nucleotide sequence - 78bp:
CTGGAAGCAGAGGCGGCTGCAAAGGAGGCTGCAGCCAAAGAGGCCGCTGC
TAAAGAAGCCGCCGCCAAGGCCCTCGAA
Amino acid sequence - 26aa: LEAEAAAKEAAAKEAAAKEAAAKALE

Appendix H

**Sequences of variable regions exchanged in pVITRO1-Trastuzumab-IgG1/κ plasmid to generate isotype controls for Trastuzumab, Trastuzumab-LL37 or THIOMAB**

1F6 heavy chain insert:

GAGGTCCAGCTGCAGCAGTCTGGACCTGAACTAGTGAAGACTGGGGCTTCA
GTGAAGATATCCTGCAAGGCTTCTGGTTACTCATTCACTGATTACTACATAC
ACTGGGTCAAGCAGAGCCATGGAAAGAGCCTTGAGTGGATTGGATATATTA
GTTGTTCCAGTGGTGCTACTATCTACAACCAGAAGTTCAAGGCCAAGGCCA
CATTTACTGTAGACACATCCTCCAGCACAGCCTACATGCAGTTCAACAGCCT
GACATCTGAAGACTCTGCGGTCTACTACTGTGCAAGGTCTACTATGATTACG
CCAGACTACTGGGGCCAAGGCACCACTCTCACAGTCTCCTCA

Mac49 light chain insert:

GATGTTGTGCTGACCCAGACTCCACCCACTTTATCGGCTACCATTGGACAAT
CGGTCTCCATCTCTTGCAGGTCAAGTCAGAGTCTCTTAGATAGTGATGGAGA
TACCTATTTAAATTGGTTGATACAGAGGCCAGGCCAATCTCCACAGCTTCTA
ATTTATTCGGTATCCAACCTGGAATCTGGGGTCCCCAACAGGTTCAGTGGCA
GTGGGTCAGAAACAGATTTCACACTCAAAATCAGTGGAGTGGAGGCTGAAG
ATTTGGGAATTTATTACTGCATGCAAGCTACCCATGTTCCTCTGACGTTCGG
TGGAGGCACCAAGCTGGAATTGAAA

# Appendix I

## Expression of endosomal Toll-like Receptors (TLR) in steady-state mouse tumour cell lines

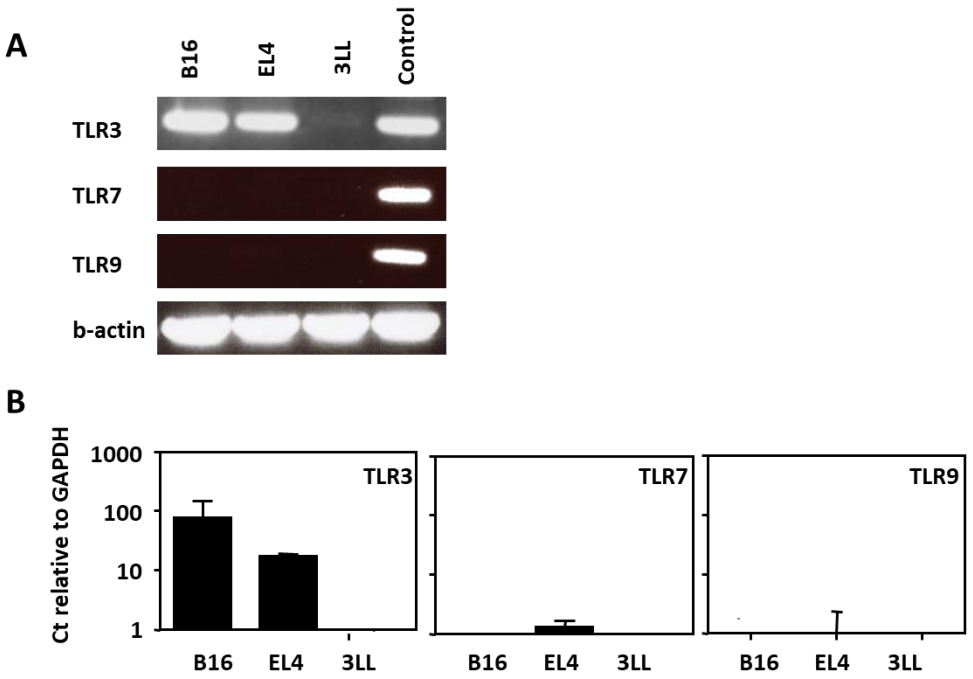


**Figure I.** Expression of endosomal TLR in steady-state mouse tumour cell lines. **A.** Semi-quantitative RT-PCR where control cells are enriched CD11c splenocytes. **B.** Real time PCR levels (Ct) are shown relative to the house keeping gene GADPH. Data are representative of 2 independent experiments. Data were generated by Dr. Sandra S. Diebold.

# Appendix J

## Validation of human IgG1 isotype controls expressed from pVITRO-1F6/Mac IgG1 plasmids

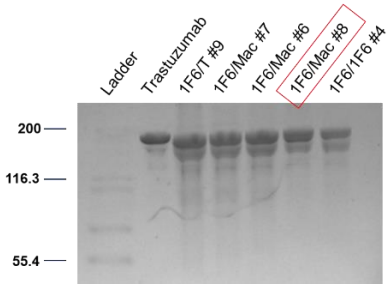


**Figure J1**. Human IgG1 isotype controls generated in our lab analysed by SDS-PAGE in non-reducing conditions. Compared to the human IgG1 antibody Trastuzumab, all isotype control antibodies, including clone 1F6/Mac #8 (red), migrated similarly. The gel was stained with SimplyBlue.

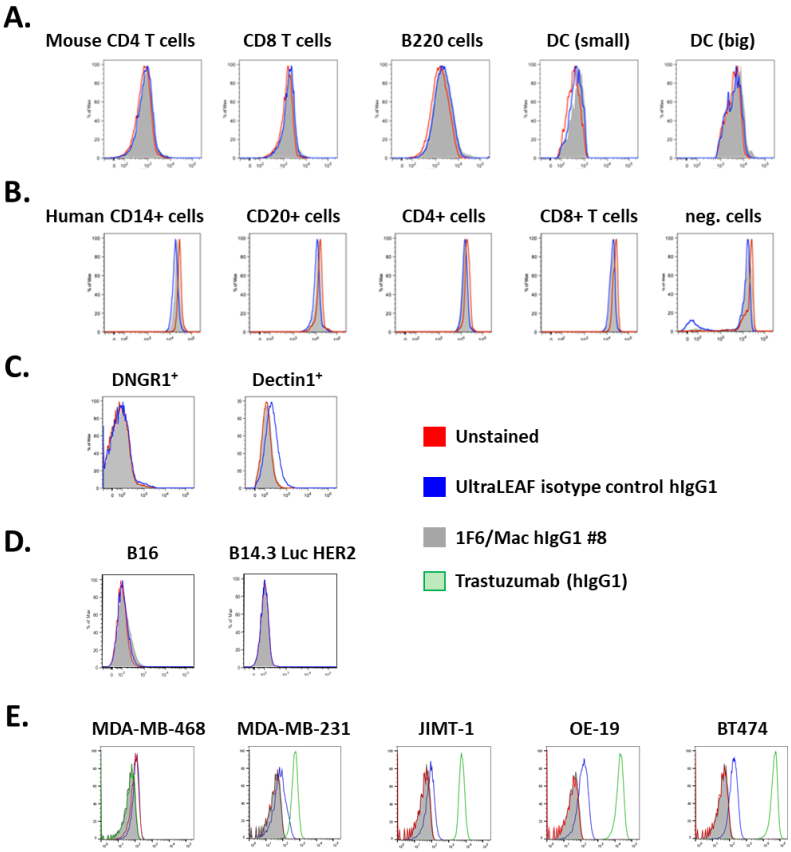


**Figure J2.** Isotype control 1F6/Mac hIgG1 shows similar, if not lower background staining than the commercial antibody UltraLEAF hIgG1. Mouse splenocytes (**A**), human PBMCs (**B**), DNGR1$^+$ B3Z cells (**C**), mouse melanoma cell lines (**D**) and human cancer cell lines (**E**) were stained with either the commercial UltraLEAF isotype control (open blue histogram), 1F6/Mac hIgG1 (filled grey) or Trastuzumab hIgG1 (green) for positive control, then an anti-human IgG secondary. Mouse splenocytes (**A**) and human PBMCs (**B**) were also stained with the indicated surface markers. Cells were analysed by flow cytometry. Representative histograms from one experiment (**E**). Data in A-D was generated by Dr. Sandra S. Diebold.

# Appendix K

## Immunophenotyping of mouse GM-CSF-derived BMDCs

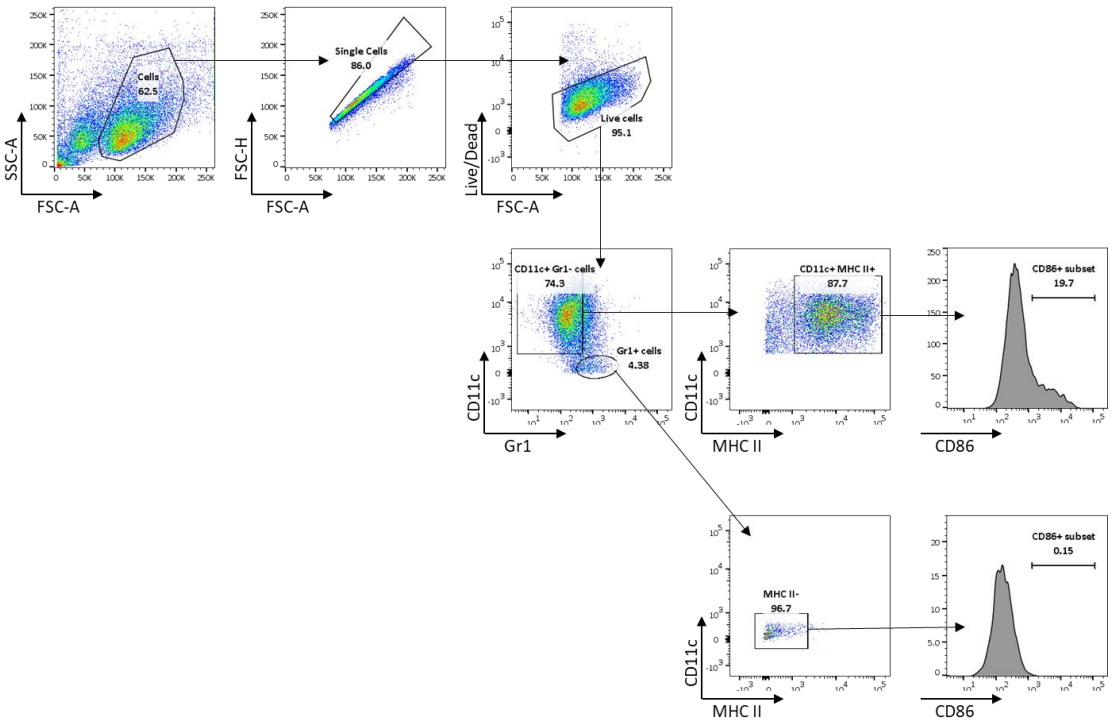


**Figure K.** Analysis of mouse GM-CSF derived BMDCs by flow cytometry. Cells were harvested, stained and analysed at day 6 of culture. All gating was performed according to full minus one + isotype (FMO) controls. $CD11c^{+}$ MHC $II^{+}$ $Gr\text{-}1^{-}$ cells comprising macrophages and dendritic cells contain a $CD86^{+}$ subset. Granulocytes are defined as $Gr\text{-}1^{+}$ $CD11c^{-}$ cells and were confirmed MHC $II^{-}$ and $CD86^{-}$. Data representative of two independent experiments.

# Appendix L

## Cell populations in mouse Flt3L-derived BMDCs

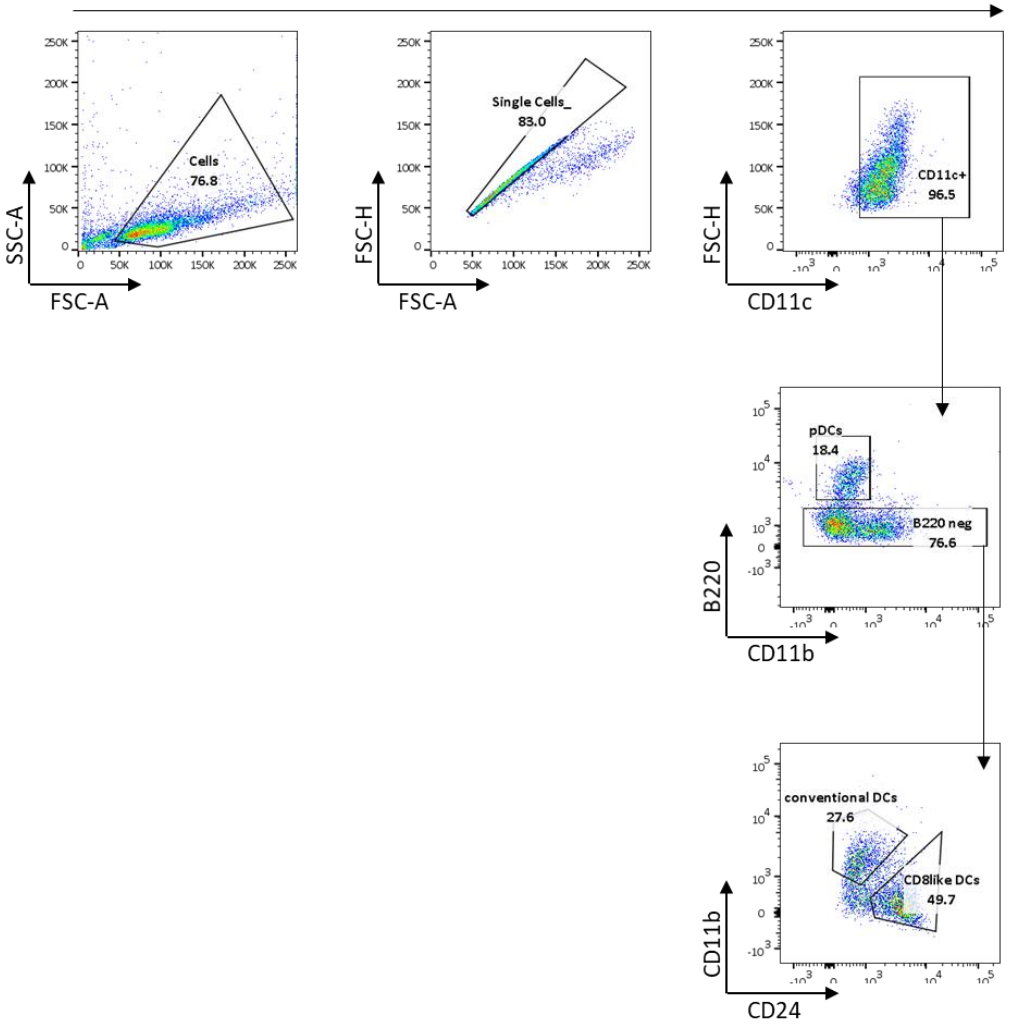


**Figure L.** Analysis of mouse Flt3L-derived BMDCs by flow cytometry. Unstimulated cells were harvested, stained and analysed at day 10 of culture. All gating was performed according to full minus one + isotype (FMO) controls. Plasmacytoid DC (pDCs) were defined as $CD11c^{+}$ $B220^{+}$ $CD11b^{-}$ cells. Conventional DCs were defined as $CD11c^{+}$ $CD11b^{high}$ $B220^{-}$ $CD24^{-}$ cells. CD8α-like DCs were defined as $CD11c^{+}$ $CD24^{+}$ $CD11b^{low}$ $B220^{-}$ cells. Data representative of two independent experiments.

# Appendix M

## Cell populations in panDCs isolated from human PBMCs

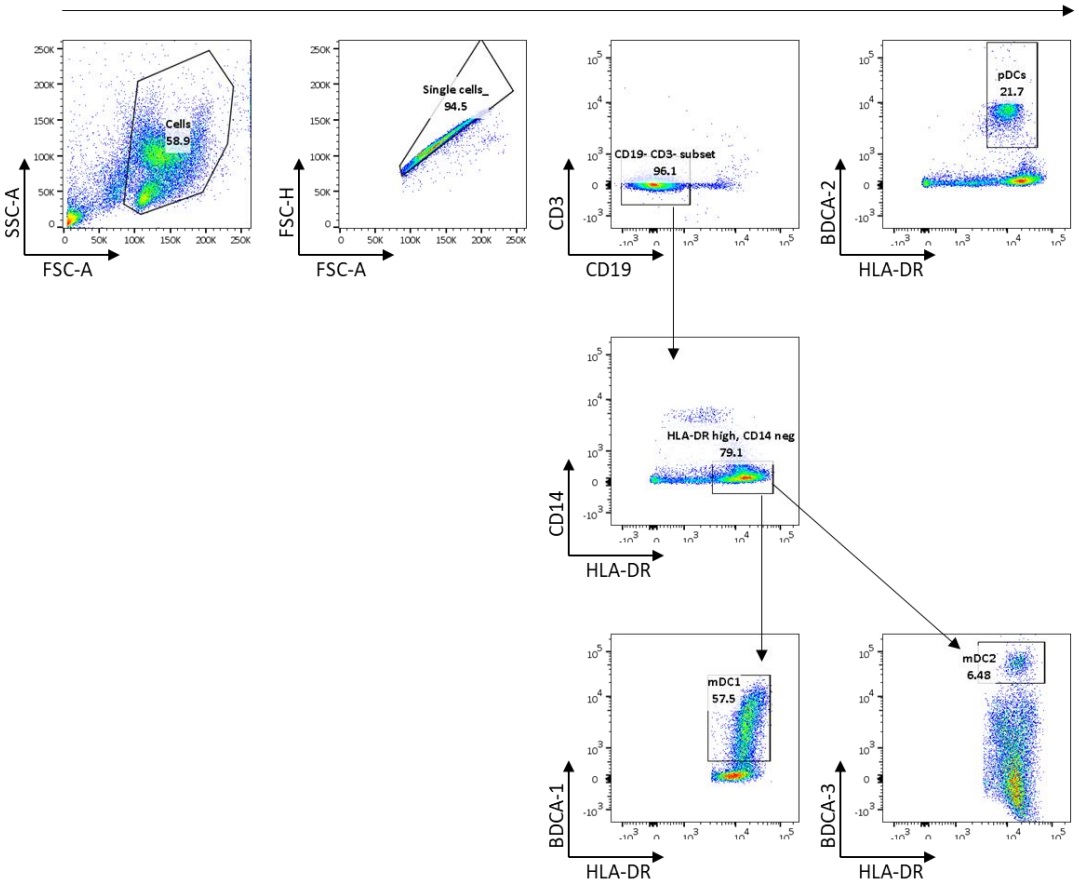


**Figure M.** Flow cytometry analysis of panDCs isolated from human PBMCs. panDCs were isolated using the EasySep® Human panDC Enrichment Kit and Silver Magnet (Stem Cell Technologies). Cells were stained for surface markers and analysed on BD Canto II. Full minus one (FMO) controls were employed for gating. Plasmacytoid DC (pDCs) were defined as BDCA-2$^{+}$ HLA-DR$^{high}$, CD19$^{-}$ cells. Myeloid DCs type 1 (mDC1) were defined as BDCA-1+ HLA-DRbright CD14- CD19- cells. Myeloid DCs type 2 (mDC2) were defined as BDCA-3$^{+}$ HLA-DR$^{high}$ CD14$^{-}$ CD19$^{-}$ cells. Data representative of two independent experiments with cells from individual donors.

# Supplementary file

# Additional information

# Supplementary file

## Additional information

### S1. Toll-like receptors (TLR) - general structure

Toll-like receptors (TLRs) are membrane bound proteins that recognise pathogen-associated molecular patterns (PAMPs), triggering immune responses (Medzhitov 2007). TLRs are type I transmembrane glycoproteins, each containing extracellular, transmembrane and intracellular signaling domains (Gay and Gangloff 2007). As described in section 1.2 of this thesis, TLRs localise either to the cell surface, recognising molecular motifs present on the surface of microbes (lipids, lipoproteins, glycans), or in the endosomal compartment, recognising nucleic acid molecules (Iwasaki and Medzhitov 2015).

Despite the broad spectrum of motifs recognised by TLRs, the ligand-binding domains of these receptors are surprisingly similar. The extracellular domain (ECD) of all TLRs consists of tandem repeats of leucine-rich repeats (LRR) motifs. Each LRR motif is typically 22-29 residues long. The extracellular domain of all TLRs adopt a horseshoe shape with glycans distributed throughout the structure, except for the N-terminal ascending loop (Fig. S1 A), which is most often non-glycosylated, leaving it free to bind ligands and be involved in dimerization (Fig. S1 B). While the general structure of TLR ECDs follows the same principles, these structures cannot be superimposed due to differences in curvature (Botos, Segal, and Davies 2011).

Importantly, ligand binding induces dimerization of TLRs, forming an m-shape with the C-termini in immediate proximity, and this induces dimerization of the intracellular domains triggering receptor signaling. In terms of endosomal TLR agonists, crystallography experiments determined the structures of multiple TLR-ligand complexes. For TLR9 activation, it was shown that a single CpG molecule interacts with both the N-terminus (LRR1–10) of one TLR9 ECD, as well as a C-terminal ECD region (LRR20–22) of an adjacent TLR9 molecule, inducing formation of an m-shaped dimer (Ohto et al. 2015). Similarly, each TLR3 contains two binding sites for dsRNA, and ligand binding induces TLR3 dimerization (Liu et al. 2008). Both TLR7 and TLR8 ECDs contain a binding site for nucleosides, labelled site 1 and a binding site for oligoribonucleotides, labelled site 2. Site 1 interfaces contribute most to receptor dimerization. For site 1, TLR7 prefers guanosine, while TLR8 prefers uridine. The similarities in structure of guanosine and uridine, as well as potent small antiviral molecules such as imidazoquinolines

imiquimod and resiquimod, explain to a degree how these ligands can activate both TLR7 and TLR8 (Tanji et al. 2015; Zhang et al. 2016; Zhang, Ohto, and Shimizu 2017).

In terms of the transmembrane domains of TLR receptors, these mostly consist of hydrophobic residues and differ in sequence for cell membrane TLRs and endosomal TLRs. The transmembrane domain of endosomal TLRs interact with the multispan transmembrane protein UNC93B, and traffic to the endosomal compartment (Brinkmann et al. 2007), while other TLRs do not, trafficking directly to the cell membrane.

The signaling domain of TLRs share homology with signaling domains of IL-1 receptor family and are hence called Toll IL-1 receptor (TIR) domains (O'Neill and Bowie 2007). Importantly, dimerization of the ECDs induces dimerization of the signaling TIR domains, which in turn recruit adaptor proteins, of which MyD88 is most often employed (Jin and Lee 2008). For details on the signaling cascade of endosomal TLRs and differences between TLR3 and TLR7/8/9 signaling, please see section 1.2.1.

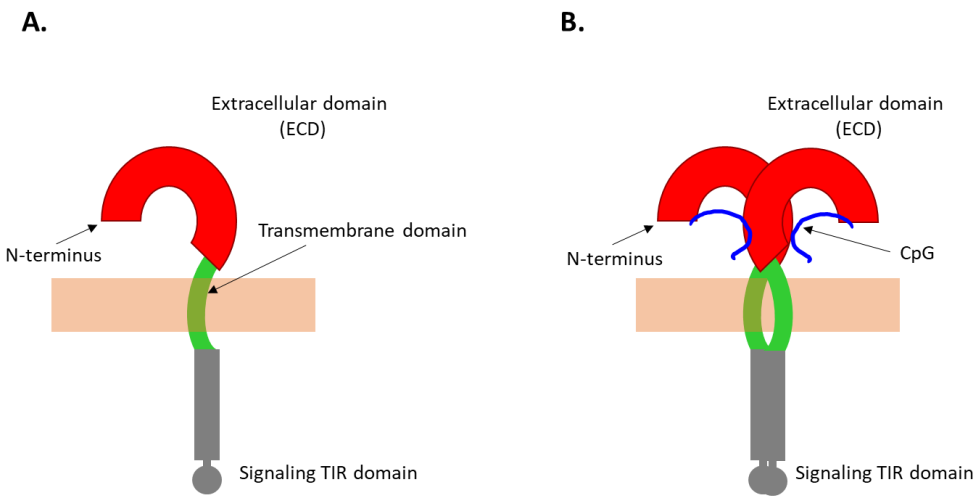


**Fig. S1.** Schematic structure of TLRs. **A.** Structure of TLR monomers. N-terminus, extracellular domain (red), transmembrane (green) and signalling domains (grey) are labelled. **B.** Schematic representation of ligand induced dimerization of TLR receptors, exemplified for TLR9 and CpG molecules (blue).

### S2. Approved immunotherapies containing endosomal TLR agonists

Presently, only two TLR agonist preparations are approved as immunotherapies for cancer: bacillus Calmette–Guérin (BCG) and imiquimod.

Bacillus Calmette–Guérin (BCG) is an immunotherapy approved for the treatment of superficial bladder cancer. The delivery method is by intravesical instillation (Guallar-Garrido and Julian 2020). Essentially, BCG is a live attenuated preparation of *Mycobacterium bovis*, containing high

levels of unmethylated CpG motifs and peptidoglycans, which simulate primarily TLR9, TLR2 and TLR4 (Kaczanowska, Joseph et al. 2013). While the mechanisms leading to tumour growth control and protection from recurrence have not been completely elucidated, it has been shown that the inflammation resulting from TLR triggering is responsible for efficacy, with CD4 and CD8 T cells playing an important role (Biot, Rentsch et al. 2012). Despite being first reported as an efficient therapy for superficial bladder cancer in 1976 (Morales 1976) and approved for clinical use by the Food and Drug Administration (FDA) in 1990 (Morales 2017), intravesical BCG remains one of the most often used and efficient therapies for treating high-risk superficial bladder cancer. Importantly, treatment with BCG offers protection from recurrence and progression of disease (Guallar-Garrido and Julian 2020).

There are, however, numerous limitations to BCG immunotherapy. These include poor efficiency for invasive bladder cancers, a possibility of infection due to BCG, and adverse effects (Guallar-Garrido and Julian 2020). The EORTC trial showed that 70% of patients experienced adverse effects, milder ones including flu-like symptoms and bladder discomfort, while 8% of patients discontinued treatment due to the severity of adverse effects (Brausi, Oddens et al. 2014).

The only other approved TLR agonist for cancer immunotherapy is Imiquimod. This lipophilic small molecule from the class of imidazoquinolines (Fig. S2) is an agonist of human TLR7 and TLR8 (Schon and Schon 2008). Imiquimod is approved for topical treatment, in the form of a cream, of a range of cutaneous lesions, including superficial basal cell carcinoma (Scarfi et al. 2020) and melanoma *in situ* (stage zero melanoma) (NICE Pathways 2020). The mechanism of action involves TLR 7/8 activation at the tumour site, inducing an inflammatory response characterised by cytokine production (IL-1, IFN-α, IFN-γ, and TNF-α), CD4 and CD8 T cell responses (Urosevic et al. 2003). Additionally, research also showed that accumulation of activated plasmacytoid dendritic cells (pDCs) into the tumour tissue contributes to the therapeutic effect in patients (Dummer et al. 2003).

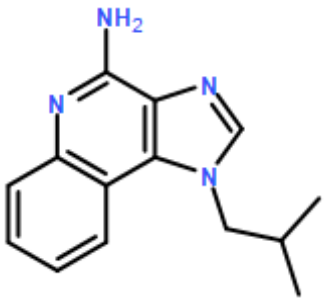


**Fig. S2**. Chemical structure of the imidazoquinoline derivative Imiquimod.

A 5% imiquimod cream was shown to induce clinical and histological clearance of superficial basal cell carcinoma with a 3 year of success rate of 83.6% (Williams et al. 2017). Treatment with imiquimod is an approved alternative for patients with skin tumours at sites where surgical excision is not feasible or for patients that would no undergo surgical treatment. Notably, treatment with imiquimod has only been shown to be effective for superficial, low-risk skin tumours (Love, Bernhard, and Bordeaux 2009; Scarfi et al. 2020). In terms of side effects, the most common ones are local and include pruritus, pain and burning at the site of application. Rarely, back pain, sinusitis or even upper respiratory tract infections were noted in patients. Typically, adverse effects are quite mild, and only rarely result in stopping the treatment (Geisse et al. 2004; Love, Bernhard, and Bordeaux 2009).

To summarise, both TLR-based immunotherapies currently approved for treatment of cancers are delivered locally to the tumour tissue to induce anti-tumour immune responses. Their broader use is currently limited by both side effects, and the requirement for the drug to spatially co-localise with the tumour tissue.

### S3. Potential for utilising cross-linking reagents beyond SMCC

In this thesis we explored two types of conjugation strategies to generate Trastuzumab-CpG conjugates. Both strategies, namely conventional biochemical conjugation to amines on Trastuzumab and site-specific conjugation using THIOMAB technology made use of the SMCC cross-linker (Fig. S3 A). The justification for using this reagent was presented at length in Chapter 5 - Introduction. In short, SMCC is a non-cleavable linker, allowing for conjugation of primary amines via the NHS ester and conjugation to thiol groups via the maleimide. The two functional groups are separated by a cyclohexane ring spacer, which is 8.3 angstrom long. This cyclohexane ring confers added stability to the maleimide group by decreasing its rate of hydrolysis (Brinkley 1992; Mattson et al. 1993). When used to generate Trastuzumab-DM1 conjugates, SMCC provided higher serum stability to conjugates compared to other cross-linkers (Lewis Phillips et al. 2008). This linker is also well described in literature, and commercially available.

One of the limitations of this study is that only one cross-linker was used to generate conjugates. Other cross-linkers containing an NHS ester and a maleimide group are available, with different spacers, that confer different properties to the cross-linker, and may in turn influence the properties of the conjugate. For instance, the cross-linker LC-SMCC (Fig. S3 B) is a variation of SMCC containing a long cyclohexane-stabilised spacer arm of 16.2 angstroms (Masuko 2003; Mattson et al. 1993). The presence of the longer cyclohexane bridge maintains the advantage of

stabilising the maleimide group, while offering better spatial separation of CpG from the antibody. This may improve access of conjugated CpG to TLR9 in the endosome.

For the conventional conjugates, we have shown that binding to human HER2 is impaired as a result of conjugations CpG, but not smaller molecules such as cysteine. Using cross-linkers with longer spacers may lead to conjugates with superior HER2 binding affinity. To fully explore the degree of separation between the functional groups of the cross-linker that leads to Trastuzumab-CpG conventional conjugates with better HER2 binding, SM(PEG)n (Fig. S3 C) linkers could be used. These linkers consist of an NHS ester and a maleimide separated by polyethylene glycol (PEG) spacers of 2-24 ethylene glycol units, with lengths varying from 17.6 to 95.2 angstroms (Bidast et al. 2020; Shukla et al. 2015). In addition to the benefit of longer spacers, PEG-containing reagents have been shown to provide additional advantages including better solubility, lesser potential for precipitation, and may mask the conjugate from enzymatic degradation, which is why PEGylation is widely used to improve the properties of various protein therapies such as PEG-interferon (Gupta et al. 2019). The availability of anti-PEG antibodies opens additional avenues for detection of conjugates in assays (Kozma et al. 2020). While using PEG-containing linkers is expected to improve the therapeutic potential of Trastuzumab-CpG conjugates, whether generated using conventional biochemical conjugation, or THIOMAB technology, the expected disadvantage is that these linkers may render the maleimide group, and therefore the conjugate, less stable in serum.

In summary, different cross-linkers, such as LC-SMCC or SM(PEG)n can be explored to further optimise the therapeutic potential of Trastuzumab-CpG conjugates.

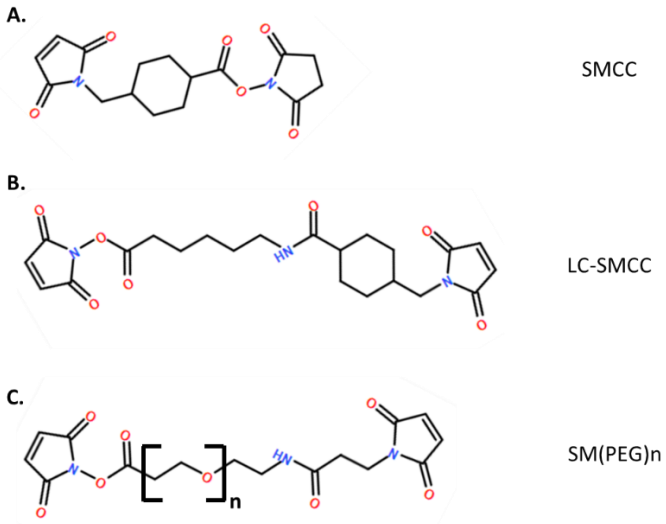


**Fig. S3.** Chemical formulas of: **A.** SMCC, **B.** LC-SMCC, **C.** SM(PEG)n, n=2-24.

**References:**

Bidast, S., A. Golchin, A. Baybordi, A. Zamani, and R. Naidu. 2020. 'The effects of non-stabilised and Na-carboxymethylcellulose-stabilised iron oxide nanoparticles on remediation of Co-contaminated soils', *Chemosphere*, 261: 128123.

Botos, I., D. M. Segal, and D. R. Davies. 2011. 'The structural biology of Toll-like receptors', *Structure*, 19: 447-59.

Brinkley, M. 1992. 'A brief survey of methods for preparing protein conjugates with dyes, haptens, and cross-linking reagents', *Bioconjug Chem*, 3: 2-13.

Brinkmann, M. M., E. Spooner, K. Hoebe, B. Beutler, H. L. Ploegh, and Y. M. Kim. 2007. 'The interaction between the ER membrane protein UNC93B and TLR3, 7, and 9 is crucial for TLR signaling', *J Cell Biol*, 177: 265-75.

Dummer, R., M. Urosevic, W. Kempf, K. Hoek, J. Hafner, and G. Burg. 2003. 'Imiquimod in basal cell carcinoma: how does it work?', *Br J Dermatol*, 149 Suppl 66: 57-8.

Gay, N. J., and M. Gangloff. 2007. 'Structure and function of Toll receptors and their ligands', *Annu Rev Biochem*, 76: 141-65.

Geisse, J., I. Caro, J. Lindholm, L. Golitz, P. Stampone, and M. Owens. 2004. 'Imiquimod 5% cream for the treatment of superficial basal cell carcinoma: results from two phase III, randomized, vehicle-controlled studies', *J Am Acad Dermatol*, 50: 722-33.

Guallar-Garrido, S., and E. Julian. 2020. 'Bacillus Calmette-Guerin (BCG) Therapy for Bladder Cancer: An Update', *Immunotargets Ther*, 9: 1-11.

Gupta, V., S. Bhavanasi, M. Quadir, K. Singh, G. Ghosh, K. Vasamreddy, A. Ghosh, T. J. Siahaan, S. Banerjee, and S. K. Banerjee. 2019. 'Protein PEGylation for cancer therapy: bench to bedside', *J Cell Commun Signal*, 13: 319-30.

Iwasaki, A., and R. Medzhitov. 2015. 'Control of adaptive immunity by the innate immune system', *Nat Immunol*, 16: 343-53.

Jin, M. S., and J. O. Lee. 2008. 'Structures of the toll-like receptor family and its ligand complexes', *Immunity*, 29: 182-91.

Kozma, G. T., T. Shimizu, T. Ishida, and J. Szebeni. 2020. 'Anti-PEG antibodies: Properties, formation, testing and role in adverse immune reactions to PEGylated nano-biopharmaceuticals', *Adv Drug Deliv Rev*.

Lewis Phillips, G. D., G. Li, D. L. Dugger, L. M. Crocker, K. L. Parsons, E. Mai, W. A. Blattler, J. M. Lambert, R. V. Chari, R. J. Lutz, W. L. Wong, F. S. Jacobson, H. Koeppen, R. H. Schwall, S. R. Kenkare-Mitra, S. D. Spencer, and M. X. Sliwkowski. 2008. 'Targeting HER2-positive breast cancer with trastuzumab-DM1, an antibody-cytotoxic drug conjugate', *Cancer Res*, 68: 9280-90.

Liu, L., I. Botos, Y. Wang, J. N. Leonard, J. Shiloach, D. M. Segal, and D. R. Davies. 2008. 'Structural basis of toll-like receptor 3 signaling with double-stranded RNA', *Science*, 320: 379-81.

Love, W. E., J. D. Bernhard, and J. S. Bordeaux. 2009. 'Topical imiquimod or fluorouracil therapy for basal and squamous cell carcinoma: a systematic review', *Arch Dermatol*, 145: 1431-8.

Masuko, M. 2003. 'Hybridization of an immobilized PNA probe with its complementary oligodeoxyribonucleotide on the surface of silica glass', *Nucleic Acids Res Suppl*: 145-6.

Mattson, G., E. Conklin, S. Desai, G. Nielander, M. D. Savage, and S. Morgensen. 1993. 'A practical approach to crosslinking', *Mol Biol Rep*, 17: 167-83.

Medzhitov, R. 2007. 'Recognition of microorganisms and activation of the immune response', *Nature*, 449: 819-26.

Morales A, Eidinger D, Bruce AW. Intracavitary Bacillus Calmette-Guerin in the treatment of superficial bladder tumors. J Urol. 1976;116(2):180–183.

National Institute for Health and Care Excellence (NICE) Pathways. Managing melanoma. 2020.

O'Neill, L. A., and A. G. Bowie. 2007. 'The family of five: TIR-domain-containing adaptors in Toll-like receptor signaling', *Nat Rev Immunol*, 7: 353-64.

Ohto, U., T. Shibata, H. Tanji, H. Ishida, E. Krayukhina, S. Uchiyama, K. Miyake, and T. Shimizu. 2015. 'Structural basis of CpG and inhibitory DNA recognition by Toll-like receptor 9', *Nature*, 520: 702-5.

Scarfi, F., A. Patrizi, G. Veronesi, M. Lambertini, F. Tartari, M. Mussi, B. Melotti, and E. Dika. 2020. 'The role of topical imiquimod in melanoma cutaneous metastases: A critical review of the literature', *Dermatol Ther*: e14165.

Schon, M. P., and M. Schon. 2008. 'TLR7 and TLR8 as targets in cancer therapy', *Oncogene*, 27: 190-9.

Shukla, S., N. A. DiFranco, A. M. Wen, U. Commandeur, and N. F. Steinmetz. 2015. 'To Target or Not to Target: Active vs. Passive Tumor Homing of Filamentous Nanoparticles Based on Potato virus X', *Cell Mol Bioeng*, 8: 433-44.

Tanji, H., U. Ohto, T. Shibata, M. Taoka, Y. Yamauchi, T. Isobe, K. Miyake, and T. Shimizu. 2015. 'Toll-like receptor 8 senses degradation products of single-stranded RNA', *Nat Struct Mol Biol*, 22: 109-15.

Urosevic, M., T. Maier, B. Benninghoff, H. Slade, G. Burg, and R. Dummer. 2003. 'Mechanisms underlying imiquimod-induced regression of basal cell carcinoma in vivo', *Arch Dermatol*, 139: 1325-32.

Williams, H. C., F. Bath-Hextall, M. Ozolins, S. J. Armstrong, G. B. Colver, W. Perkins, P. S. J. Miller, Nodular Surgery Versus Imiquimod for, and Group Superficial Basal Cell Carcinoma Study. 2017. 'Surgery Versus 5% Imiquimod for Nodular and Superficial Basal Cell Carcinoma: 5-Year Results of the SINS Randomized Controlled Trial', *J Invest Dermatol*, 137: 614-19.

Zhang, Z., U. Ohto, T. Shibata, E. Krayukhina, M. Taoka, Y. Yamauchi, H. Tanji, T. Isobe, S. Uchiyama, K. Miyake, and T. Shimizu. 2016. 'Structural Analysis Reveals that Toll-like Receptor 7 Is a Dual Receptor for Guanosine and Single-Stranded RNA', *Immunity*, 45: 737-48.

Zhang, Z., U. Ohto, and T. Shimizu. 2017. 'Toward a structural understanding of nucleic acid-sensing Toll-like receptors in the innate immune system', *FEBS Lett*, 591: 3167-81.